DESIGN AND SYNTHESIS OF CONJUGATED POLYMERS FOR PHOTOVOLTAIC AND THIRD ORDER NONLINEAR OPTICAL APPLICATIONS

Thesis submitted to

Cochin University of Science and Technology

in partial fulfillment of the requirements
for the award of the degree of

Doctor of Philosophy

in

Chemistry

Under the Faculty of Science

by

Sowmya Xavier

Department of Applied Chemistry
Cochin University of Science and Technology
Kochi – 22

February 2018

Design and Synthesis of Conjugated Polymers for Photovoltaic and Third Order Nonlinear Optical Applications

Ph.D. Thesis under the Faculty of Science

By

Sowmya Xavier
Research Fellow
Department of Applied Chemistry
Cochin University of Science and Technology
Kochi, India 682022
Email: sowmya32x@gmail.com

Supervising Guide

Dr. K. Sreekumar
Professor
Department of Applied Chemistry
Cochin University of Science and Technology
Kochi, India 682022
Email: ksk@cusat.ac.in

Department of Applied Chemistry
Cochin University of Science and Technology
Kochi, India 682022

February 2018

DEPARTMENT OF APPLIED CHEMISTRY
COCHIN UNIVERSITY OF SCIENCE AND TECHNOLOGY
KOCHI - 682022, INDIA

Dr. K. Sreekumar	Ph: 9447121530
Professor	E-mail: ksk@cusat.ac.in

Date: 15/02/2018

Certificate

This is to certify that the thesis entitled **"Design and Synthesis of Conjugated Polymers for Photovoltaic and Third Order Nonlinear Optical Applications"** is an authentic record of research work carried out by Ms. Sowmya Xavier., under my supervision in partial fulfilment of the requirements for the award of the degree of Doctor of Philosophy in Chemistry under the Faculty of Science of Cochin University of Science and Technology, and further that no part thereof has been presented before for the award of any other degree. All the relevant corrections and modifications suggested by the audience and recommended by the doctoral committee of the candidate during the presynopsis seminar have been incorporated in the thesis.

Dr. K. Sreekumar
(Supervising Guide)

Declaration

I hereby declare that the thesis entitled **"Design and Synthesis of Conjugated Polymers for Photovoltaic and Third Order Nonlinear Optical Applications"** submitted for the award of the Ph. D. Degree, is based on the original research work done by me under the guidance of Dr. K. Sreekumar, Professor, Department of Applied Chemistry, Cochin University of Science and Technology, Cochin-22 and further that it has not previously formed the basis for the award of any other degree.

Kochi-22   **Sowmya Xavier**
15/02/2018

Acknowledgement

I would like to take this opportunity to acknowledge and extend my sincere thanks to all those who contributed to the success of this study and made it an unforgettable experience for me.

First and foremost, I wish to express my deep and sincere gratitude to my supervising guide Dr. K. Sreekumar, Professor, Department of Applied Chemistry, CUSAT for his inspiration, valuable suggestions, patience and constant support throughout my research work. I sincerely thank him for giving me an opportunity to be in his research group. He has continuously orienting me in the correct direction during my research and rightly guiding me during the documentation of this thesis even in the midst of his busy schedule. Without his guidance, this thesis would have been a distant possibility. I have been extremely lucky to have Dr. K. Sreekumar as my research guide. I express my sincere thanks to Dr. K. Girish Kumar, my Doctoral Committee member, Professor, Department of Applied Chemistry, CUSAT for all his support and help. I extend my gratitude to all the faculty members and non-teaching staff of the Department for their timely help and co-operation during my research work. I acknowledge DST & Cochin University of Science and Technology (CUSAT) for providing the financial assistance.

I whole heartedly thank Dr. K. P. Vijayakumar, Department of Physics, CUSAT and Dr. P. Predeep, Professor, NIT, Calicut for allowing me to do photovoltaic device fabrication and testing in their lab. I wish to express my sincere thanks to the Director, International School of Photonics, CUSAT for the Nonlinear Optical studies. My special thanks to Dr. K. Girish Kumar for the Cyclic Voltammetric studies provided in his lab.

I am very thankful to Dr. M. V. Mahesh Kumar for helping me in solving Computational Chemistry problems for designing suitable polymers. I whole heartedly thank Ms. R. Geethu, Department of Physics, CUSAT and Ms. Rosemary, NITC for the Photovoltaic studies of the polymers. Mr. S. Mathew and Ms. Ajina of Photonics

their support and inspiration. Special thanks to my amazing brother-in-laws and sister-in-law, they are always a source of love and energy.

Words are insufficient to express my thanks to my Dean chettan, my beloved husband, for his friendship, endless love and understanding. He has been a true and great supporter and I truly thank him for sticking by my side, even when I was irritable and depressed. Without his constant support and motivation, this Ph. D. thesis would never have been realized.

Thanks to my baby, whom I am eagerly waiting, for not giving me any difficulties, patiently staying within me during my thesis documentation. I am sorry for not giving you proper care.

Above all, I immensely thank The God Almighty, for His continuous blessings, throughout my life.

Sowmya Xavier

▐▌▌▌ **Preface** ▐▌▌▌

Organic electronics based on organic semiconducting polymers has been widely studied. The discovery of conducting conjugated polymers in the late 1970s became one of the most promising fields next to conventional inorganic (silicon) electronics era. To date, various organic electronic devices such as organic light-emitting devices (OLEDs), organic field-effect transistors (OFETs), organic solar cells (OSCs) and organic memory devices (OMDs) have been invented. The potential benefits such as low-cost fabrication of light weight/ flexible devices, mechanical stability and ease of processing made organic conducting polymers an emerging candidate for future technology. Such conjugated polymeric materials are used as active layers in optoelectronic devices. For instance, conjugated polymers and their doped forms were considered as potential alternatives for metals in the field of device fabrication. The major intention of the present study was to synthesize low band gap conjugated polymers which have the ability to absorb from the visible region and possessing both photovoltaic and nonlinear optical property.

Major objectives of the present study are:

- Theoretical designing of low bandgap conjugated polymers using Density Functional Theory (DFT) in the Periodic Boundary Condition (PBC).

- Synthesis of monomers and designed low band gap polymers using different synthetic strategies including Gilch Polymerization, Direct Arylation Polymerization and Suzuki Coupling Polymerization.

- Explore the third-order nonlinear optical properties of synthesized polymers.

- Explore the application of the conjugated polymers as active layer in photovoltaic devices and fabrication of solar cells using different configurations.

Summary of the thesis

The thesis is divided into six chapters

The **first chapter** gives a concise introduction to π-conjugated polymers and their application in different optoelectronic devices. The first section of the introduction chapter describes the fundamental concepts and structural aspects of conducting polymers. Various routes for the synthesis of conjugated polymers are discussed in the second section of this chapter. Third section deals with the concepts of theoretical designing of conjugated polymers. Fourth section illustrates the various technological aspects of device fabrication in organic photovoltaics and donor-acceptor concept in band gap modelling. The last section describes the fundamentals of nonlinear optical properties of conjugated polymers and their application in optical limiting devices.

The **second chapter** includes the theoretical design and synthesis of phenylene vinylene based copolymers. Monomers and D-A units were optimized using DFT/B3LYP/6-31G formalism. Polymers were optimized using DFT/HSE06/6-31G and DFT/B3LYP/6-31G methods. Band gap, oscillator strength and excitation energies were calculated using Time Dependent Density Functional Theory (TD-DFT) calculations. Four promising low band gap phenylene vinylene based alternate copolymers were designed and successfully synthesized via Gilch polymerisation. The polymers were characterized by different spectroscopic techniques including ^{1}H NMR and IR spectroscopy. GPC (Gel Permeation Chromatography) technique was used for finding the molecular weights of polymers. Absorption spectra were recorded for all the samples and from the onset value of absorption peak, optical band gaps were calculated. Emission spectra of copolymers were measured in different solvents and found to be in the visible range. Thermal stability of polymers were investigated by TG-DTG analysis and the polymers were found to be thermally stable up to 400 ^{o}C. The redox behavior of the copolymers were investigated using cyclic voltammetry. HOMO and LUMO energy values and electrochemical band gaps of

copolymers were calculated. The fluorescence lifetime of the polymers were monitored using TCSPC in $CHCl_3$. The change in the dipole moment was calculated both from solvatochromic shift method and on the basis of microscopic empirical solvent polarity parameter (E_T^N) and values are compared.

The **third chapter** includes the theoretical design and synthesis of bithiophene based copolymers. Polymers were optimized using DFT/HSE06/6-31G and DFT/B3LYP/6-31G methods. The designed polymers were synthesized through cost effective direct arylation reaction using palladium acetate as catalyst. The polymers were characterized by different spectroscopic techniques including ^{1}H NMR and IR spectroscopy. GPC technique was used for finding the molecular weights of polymers. Absorption spectra and emission spectra were recorded for the polymers and from the onset value of absorption peak, optical band gaps were calculated. Thermal stability of polymers were investigated by TG-DTG analysis and the polymers were found to have high thermal stability. Cyclic voltammetry studies were used to estimate the HOMO and LUMO energy values and electrochemical band gaps of copolymers. The fluorescence lifetimes of the polymers were monitored using TCSPC in $CHCl_3$.

Fourth chapter describes the theoretical design and synthesis of phenothiazine based copolymers. Polymers were optimized using DFT/HSE06/6-31G and DFT/B3LYP/6-31G methods. Band gap, oscillator strength and excitation energies were computed by applying Time Dependent Density Functional Theory (TD-DFT) calculations. The designed polymers were synthesized through Suzuki polycondensation reaction. The polymers were characterized by different spectroscopic techniques including ^{1}H NMR and IR spectroscopy. The molecular weight of the polymers were investigated using GPC technique. Absorption spectra and emission spectra of copolymers were measured in THF. From the onset value of absorption peak, optical band gaps were calculated. Thermal stability of polymers were investigated by TG-

DTG analysis and the polymers were found to be thermally stable. The redox behavior of the copolymers were investigated using cyclic voltammetry. The fluorescence lifetime of the polymers were monitored using TCSPC in CHCl$_3$.

In the **fifth chapter,** third-order nonlinear optical properties of the copolymers were investigated using Z-scan technique. The open aperture Z-scan traces of phenylene vinylene based copolymers gave saturable absorption type graphs. The other copolymers showed reverse saturable absorption type graphs. The open aperture Z-scan traces were fitted with the theoretical plot derived from the two photon absorption (TPA) theory. Nonlinear absorption coefficients of the polymers were in the order of 10^{-10} mW^{-1} and imaginary part of nonlinear susceptibility values were of the order of 10^{-11} esu, which implied that the polymers exhibited strong optical nonlinearity at 532 nm.

Photovoltaic performance of some of the copolymers were checked by constructing both conventional and inverted bulk heterojunction solar cells using polymer: PCBM blend as active layer. Bulk heterojunction photovoltaic cell with a conventional device structure was constructed with polymer MD-CA-PPV:PCBM blend as active layer, which gave a power conversion efficiency of 0.04 %. In inverted solar cells, ZnO was used as electron transport layer and cell configuration adopted was ITO/ZnO/Polymer:PCBM/Ag. Inverted solar cells were constructed using MD-CA-PPV:PCBM blend in 1:1 ratio as active layer, which gave a power conversion efficiency of 0.43 %. Bulk heterojunction photovoltaic cells with an inverted device structure were constructed using MD-FL-PPV as and gave maximum power conversion efficiency 0.51%. Inverted solar cells were constructed using MD-FL-PPV:PCBM blend in varying ratios and gave maximum power conversion efficiency 0.60 %.

The conclusions drawn from each part of the work and references are given to the end of each chapter. The summary and outlook of the work done are presented as the final chapter.

▓▓▓ Contents ▓▓▓

Chapter 2
DESIGN, SYNTHESIS AND CHARACTERIZATION OF PHENYLENE VINYLENE BASED COPOLYMERS BY GILCH POLYMERIZATION

55 - 105

Chapter 5

PHOTOVOLTAIC AND NONLINEAR OPTICAL
APPLICATIONS OF CONJUGATED POLYMERS   167 - 208

Chapter 6
SUMMARY   209 - 216

LIST OF PUBLICATIONS   217 - 218

▌▌▌ List of Abbreviations ▌▌▌

A	Acceptor
AN	9,10-bis(bromomethyl)anthracene
ANT	9,10-dibromoanthracene
Bu_4NPF_6	Tetrabutylammonium hexafluorophosphate
B3LYP	Becke, three parameter, Lee-Yang-Parr
BLA	Bond length alteration
CA	1,4-bis (bromomethyl)-2,3-bis(octyloxy) benzene
C60	Fullerene
C-C	Carbon-Carbon
CV	Cyclic Voltammetry
CZ	3,6-dibromo-N-octylcarbazole
D-A	Donor-Acceptor
DTG	Differential Thermogravimetry
DMSO	Dimethyl sulphoxide
DCM	Dicholoromethane
DFT	Density functional theory
D-A-D	Donor-Acceptor-Donor
Eg	Band gap
opt	Optical band gap
EA	Electron affinity
FL	2,7-bisbromomethyl-9,9-dioctyl-9H-fluorene
FLN	2,7-dibromo-9,9-dioctyl-9H-fluorene
FT-IR	Fourier Transform Infra-Red
GPC	Gel Permeation Chromatography
HOMO	Highest occupied molecular orbital
HSE06	Heyd-Scuseria-Ernzerhof
HPLC	High Performance Liquid Chromatography
h	Hour
^{1}H NMR	^{1}H Nuclear magnetic resonance
ICT	Intermolecular charge transfer
ITO	Indium tin oxide
$Im\chi^{(3)}$	Imaginary part of the third-order susceptibility

IP	Ionization potential
k	Wave vector
LUMO	Lowest unoccupied molecular orbital
L_{eff}	Effective thickness with linear absorption coefficient
OLEDs	Organic light emitting diodes
MD	1,4-bis-(bromomethyl)-2-decyloxy-5-methoxybenzene
M_n	Number average molecular weight
M_w	Weight average molecular weight
MeTH	2,5-dibromo-3-methylthiophene
NLO	Nonlinear optical
n_0	Linear refractive index of the polymer solution
NLR	Nonlinear refraction
n_2	Nonlinear refractive index
Nd:YAG	Neodymium-doped yttrium aluminium garnet
OPV	Organic photovoltaic
OA	Open-aperture
OFETs	Organic field-effect transistors
PC61BM	[6,6]-Phenyl C61 butyric acid methyl ester
PC71BM	[6,6]-Phenyl C71-butyric acid methyl ester
PBC	Periodic boundary condition
P(BT-ANT)	Poly(2,2′-Bithiophene-alt-anthracene)
P(BT-CZ)	Poly(2,2′-Bithiophene-alt- N-octylcarbazole)
P(BT-FLN)	Poly(2,2′-Bithiophene-alt-9,9-dioctyl-9H-fluorene)
P(BT-PH)	Poly(2,2′-Bithiophene-alt-10-octylphenothiazine)
P(BT-TPA)	Poly(2,2′-Bithiophene-alt-triphenylamine)
PDI	Poly dispersity index
PL	Photoluminescence spectrum
PH	3,7-dibromo-10-octylphenothiazine
P(PH)	Poly(phenothiazine)
PHENO	10-octyl-3,7-bis(4,4,5,5-tetramethyldioxaborolan-2-yl)-10H-phenothiazine
P(PHENO-TPA)	poly(N-octylphenothiazine-alt-triphenylamine)
P(PHENO-MeTH))	poly(N-octylphenothiazine-alt-methylthiophene)
PSC	Polymer solar cell
PT	3,7-bis(bromomethyl)-10-octyl-10H-phenothiazine

ProDOT	3,4-Propylenedioxythiophene
RSA	Reverse saturable absorber
Reχ (3)	Real part of $\chi^{(3)}$
SA	Saturable absorber
SHG	Second harmonic generation
TG	Thermogravimetry
TPA	Two photon absorption
TPA	4,4'-dibromotriphenylamine
TBAB	Tetrabutylammonium bromide
THF	Tetrahydrofuran
T(z)	Normalized transmittance
UV–Visible	Ultraviolet-Visible

Chapter 1

INTRODUCTION TO π-CONJUGATED POLYMERS AND THEIR APPLICATIONS

1.1 Introduction

As an interesting research topic, organic conjugated polymers has grown to maturity during the last two decades, since they may serve as candidates in optoelectronic devices and can fulfill the energy need of today's world. Conducting polymers were practically predicted in 1962 by John Pople and S.H. Walmsley; they introduced the concept of solitons in polyacetylene.[1] After that, a key discovery in the development of conducting polymer was observed by Gill et al. in 1977, that the inorganic polymer, polysulphur nitride exhibited room temperature conductivity and it could be enhanced by exposing to bromine and other similar oxidising agents.[2] The major breakthrough in the area of organic conducting polymer happened in

1977 when films of polyacetylene were found to exhibit profound increase in electrical conductivity when exposed to halogen vapour. In 2000, Alan Heeger, Alan MacDiarmid, and Hideki Shirakawa, founders of the conjugated conducting polymer chemistry won the Nobel Prize for their discovery of highly conducting polyacetylene.[3] The conjugated organic polymer showed interesting properties like solution processability, easy band gap alternation via structural modification, capability for flexible design, large area fabrication, low cost and flexibility.[4,5] It was used for applications such as solar cells (OPVs),[6-9] organic light emitting diodes (OLEDs),[10-13] organic field effect transistors (OFETs),[14,15] biosensors[16-18] and electrochromics.[19-22] In addition to this, organic polymers were used as active layers in electronic devices which led to the realistic promise of flexible electronics in the near future.[23,24]

The present chapter describes the fundamental concepts and terminology used in photovoltaic device technology and the third order nonlinear properties of the polymers. The chapter is divided into four sections. First is the introductory section, which illustrates the structural aspects of the conjugated polymers and explains the molecular design and band gap engineering of conjugated polymers. In the second section, concepts of theoretical investigation and use of quantum chemical tools for designing low band gap donor-acceptor conjugated polymers are discussed. Third section describes the common reaction pathways for the synthesis of conjugated polymers. Various strategies for the fabrication of photovoltaic devices and the molecular design of new electron-rich donor monomers for the development p-type D-A polymers are discussed in the fourth section.

The last section illustrates the concepts of nonlinear optical behaviour of copolymers and the application in optical limiting devices.

Band gap is a critical parameter determining electrical transport properties of a material.[26, 27] Tuning the band gap using quantum chemical tools and molecular engineering will be of utmost importance in order to design new conjugated polymers for optoelectronic devices. For the polyaromatic conjugated polymers such as polyphenylene, poly(phenylene vinylene) and polythiophene, there are two possible resonance structures for the ground state with nondegenerate energy. The first is called the aromatic form or the benzenoid form. In this, each thiophene or benzene unit retains its aromaticity with confined π-electrons. Delocalization of the π-electrons along the conjugated polymer chain converts double bonds into single bonds and vice versa, leading to a resonance structure mentioned as quinoid form. Quinoid structure involves destruction of the aromaticity which results loss in the stabilization energy and hence has a smaller band gap, obviously it is energetically less stable compared to the aromatic form. The geometrical parameter, bond length alternation (BLA), is used to represent the ratio of aromatic to quinoid population in the conjugated system.[28] Bond length alternation is defined as the average of the difference in length between adjacent carbon-carbon bonds in a polyene chain. When the quinoid contribution increases, the carbon-carbon double bond character between two adjacent rings increases, which results decrease in BLA. The HOMO-LUMO band gap is directly related to BLA and decreases linearly as a function of the increasing quinoid character. Reduction in aromaticity of the conjugated main chain permits a greater tendency to adopt the quinoid form through π-electron delocalization.[29] Schematic representation of aromatic and

quinoid resonance forms of poly(phenylene), poly(p-phenylene vinylene), polythiophene, and polyisothianaphthene are shown in the Figure 1.1.
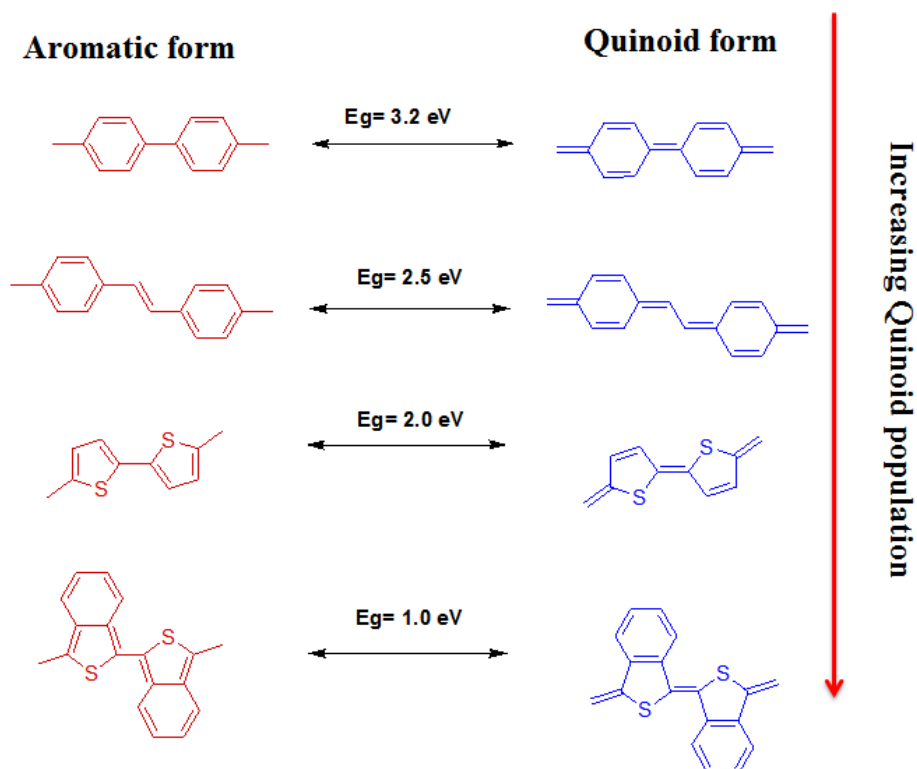
Figure 1.1: Aromatic and quinoid resonance forms of poly(phenylene), poly(p-phenylene vinylene), polythiophene and polyisothianaphthene

In the case of benzene ring, high degree of aromaticity results in larger band gap of 3.2 eV. Whereas, in poly(phenylene vinylene), number of double bond increases and reduces the aromaticity which results in small band gap of 2.4 eV compared to benzene ring. Furthermore, thiophene has an even lower aromaticity than benzene, so polythiophene can easily adopt a quinoid form, and has a lower band gap of 2.0 eV. The quinoid character of

polyisothianaphthene (PITN) is greater than polythiophene which tends to favor the quinoid form to selectively maintain the benzene aromaticity which results in a narrow band gap as low as 1 eV. [30-32]

Planarity between the adjacent aromatic units is also an important factor which affects the band gap. Planarization allows parallel p-orbital interactions to extend conjugation and facilitate delocalization. Heteroatom in heterocyclic systems and monomer aromaticity are responsible for the planarity. Roncali *et al.* reported that when 4H-Cyclopenta[2,1-b;3,4-b']dithiophene was bridged by the sp^3 carbon of a ketal group, it exhibited a remarkably low band gap of 1.2 eV.[33,34] Roncali *et al.* described that the extension from bithiophene to terthiophene decreased the band gap to 1.1 eV.[35] Generally, the HOMO and LUMO decreases as the length of conjugation increases. However, unlimited extension of the conjugation length results only in a limited reduction of the band gap, because, the number of monomer units attains a certain value where effective conjugation length is saturated.

Another important factor which affects the band gap is the presence of electron-donating or electron-withdrawing substituents directly on the aromatic unit. Usually, electron-withdrawing groups lower the LUMO energy, whereas, electron-donating groups raise the HOMO energy, resulting in a decreased band gap. For example, in poly[3,4-(propylenedioxy)thiophene] (A) the electron-donating alkoxy groups get directly attached and has a band gap of 1.76 eV, which is about 0.24 eV lower than that of the parent polythiophene.[36] The bithiophene attached with dual electron-donating amino groups and electron-withdrawing nitro groups (B) results in reduced band gap of 1.1 eV due to its high degree of zwitter ionic and quinoid character.[37]

(A)   (B)
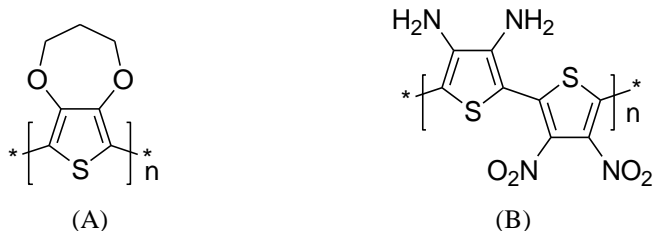
The intramolecular charge transfer correlated with the high lying HOMO of the donor unit and the low lying LUMO of the acceptor unit can also account for the reduced optical band gap. The copolymer with stronger donor of pyrrole and a stronger acceptor of benzothiadiazole, shows a very low band gap of 1.1 eV.[38,39] Such a low band gap of the polymer was attributed to the presence of intramolecular hydrogen bonding, which resulted in conformational planarization assisted by supramolecular interaction.
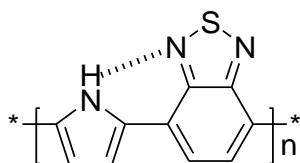
The major advantage of utilizing conjugated polymers for technological applications is the ability to tune the material properties at the molecular level through the synthetic modification of the monomeric units.

1.1.1 Band gap engineering in donor-acceptor polymers

The concept of donor-acceptor (D-A) approach to conjugated polymer design was first introduced in 1992 by Havinga and co-workers.[40,41] The combination of high-lying HOMO (residing on the donor units) and low-lying LUMO (residing on the acceptor units) is an important property which

results in an overall narrow band gap for the polymer.[42-44] Various molecular approaches have been recommended for modifying intrinsically low band gap conjugated polymers. The tunable nature of the D-A polymer is highly desirable. The choice of D-A units or more correctly on the basis of the difference in electron density between the donor and acceptor units is responsible for the structural variations in the polymer backbone which results in extensive exploration of these polymers with respect to optoelectronic applications such as OLED and PSC.[45-47]

In D-A hybridization, valence band maximum of the combination lies energetically near the HOMO of the donor while the conduction band minimum is formed in the region of the LUMO of the acceptor, thus narrowing the band gap through effective push-pull driving forces. Havinga *et al.* reported the combinations of different donor groups with different acceptors like croconic or squaric acid which resulted in a very low optical band gap of ~ 0.5 eV.[41] The band gap reduction in D-A copolymer is described by introducing the concept of hybridization. Based on the perturbation theory, in D-A copolymer, the HOMO of the donor unit will interact with the HOMO level of the acceptor unit and the LUMO level of the donor will interact with LUMO level of the acceptor to yield two new HOMOs and two new LUMOs. The redistribution of the electrons themselves occurs from their original non interacting orbitals to the new hybridized orbitals of the polymer, a high lying HOMO level and a low lying LUMO level are formed and leads to lowering of the band gap.[48] The hybridisation process of HOMOs and LUMOs of a D-A system are shown in Figure 1.2. Thakral *et al.* employed donor-acceptor strategy for designing low band gap heteroaromatic copolymers with the combination of pyrrole, thiophene and furan as donor

units with carbonyl and dicyanomethylene as acceptor groups.[49] The electronic properties of the donor and acceptor combinations have been compared using the band structure results derived from *ab initio* calculations. The result showed that the pyrrole-carbonyl donor-acceptor polymeric packaging was found to be most effective due to efficient push-pull effect in the polymer backbone.
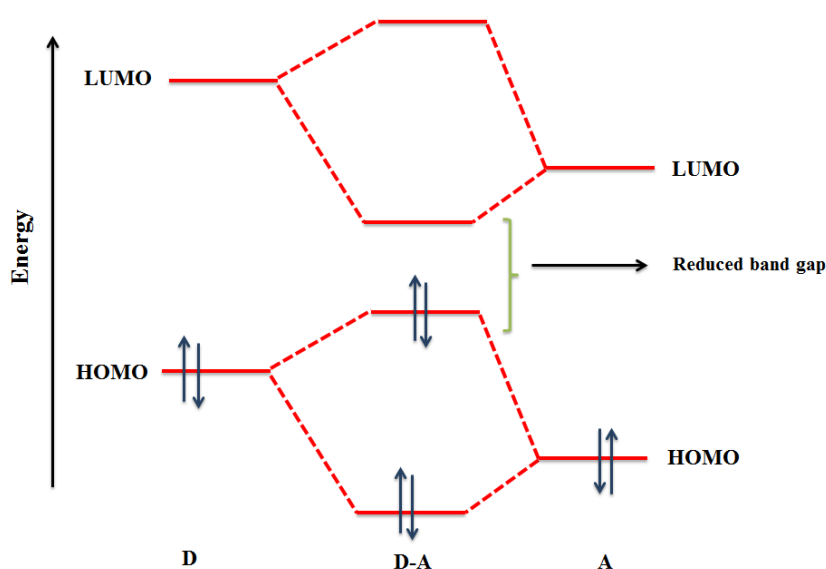
Figure 1.2: Orbital interactions of donor and acceptor units in D-A copolymer

1.2   Computational study of the electronic structure of conjugated polymers

Low band gap conjugated (co)polymers are a highly promising class of materials due to their low processing cost and applicability in optoelectronic devices. Generally, polymers are synthesized using appropriate methods and their properties are measured. Based on the results they are used for various applications. A significant challenge in the field of conjugated polymer research is to relate the chemical structure of these materials with their

morphology and dynamics, which in turn affect their charge transport characteristics. Facing these challenges, economically viable quantum chemical calculations are used to calculate the electronic structure of polymers and to eliminate unsuitable molecules before synthesis. The computational methods can be classified into four types: semiempirical, *ab initio*, density functional theory and molecular mechanics. Recently, the quantum chemical studies have been done on model compounds using *ab initio* and DFT methods. By comparing the results obtained from the two methods, it is clear that, the gradient-corrected DFT methods are more superior to *ab initio* methods. In DFT methods, the interaction of an electron is a functional of the electronic density.[50,51] Commonly employed hybrid DFT method is B3LYP (Becke, three parameter, Lee-Yang-Parr)[52-54] and HSE06 (Heyd-Scuseria-Ernzerhof functional).[55,56]

To identify the polymer excited state features (energies and oscillator strengths), the absolute position of the highest occupied molecular orbitals (HOMO) and lowest unoccupied molecular orbitals (LUMO) are required. Theoretical studies are more useful and help to identify the strategies for effective band gap control. There are two kinds of theoretical approaches available for the band gap calculation of conjugated polymers. The molecular or oligomer approach is the first method. In the past, number of researchers have used oligomers to determine the band gap of conjugated polymers.[57-59] In this method, the energy gap of increasing oligomer lengths was calculated by plotting the reciprocal oligomer length (1/n) as a function of the HOMO-LUMO gap (in eV). The main drawback of this approach was the need of repeated calculation until the convergence was reached. [60,61] The second method, Periodic Boundary Condition along with the Density Functional

Theory[62] is mainly focused to find out the optimized geometry and electronic states of the polymers in single calculation implemented in Gaussian 03[63] and Gaussian 09[64] quantum chemical codes. PBC has several advantages compared to the oligomer method. In PBC, polymer is treated as a one-dimensional unit cell and the lowest energy state and HOMO/ LUMO values are calculated. Calculation time could be saved in PBC approach, which required only one calculation, compared to the 1/n method which required multiple calculations. The band gap obtained by PBC/DFT methods support the experimental data.[65] PBC approach is based on the standard solid state methods, Born–Karman PBC, Bloch functions[66] and translational symmetry.[62] Gaussian type orbitals (GTOs)[67] are applied in G03 and G09 package. The periodic boundary condition of polymers is calculated by employing the Bloch functions to transform GTOs into crystal orbitals.[69-71]

Janesko *et al.* verified that the computational study of the band gap for periodic organic polymers using B3LYP resulted in good agreement with experimental band gaps.[72] Newly presented Heyd-Scuseria-Ernzerhof (HSE) functional incorporates a screened Hartree-Fock interaction, more computationally effective than traditional hybrid functionals like B3LYP. Band gaps obtained from both the methods, B3LYP and HSE06 gave comparable results.[73] M. Bouzzine *et al.* optimized the molecular geometries of Polythiophene (PTh) and its derivatives at B3LYP/6-31G level of theory.[74] The band gap calculated from the HOMO and LUMO levels were related to π-conjugation in the polymer back bone. DFT calculations were employed to investigate the stability of geometries and electrical properties. M. Bouzzine *et al.* came to a conclusion that substituted forms were stable with low E_g, and were in good agreement with the experimental observations. In the

present study, both B3LYP and HSE06 combined with 6-31G basis set were used to calculate the properties of the conjugated polymers.

1.3 General polymerization methods for conjugated copolymers

New approaches in the design of D-A combination permits the fine tuning of band gap of the hetero-aromatic copolymers to the desired magnitude for a variety of optical and optoelectronic technologies. Now-a-days, several polymerization techniques are available for the preparation of low band gap conjugated copolymers which include chemical oxidative polymerization,[75] electrochemical polymerization[76-78] and transition metal catalysed cross-coupling reactions.[79] The most commonly employed transition-metal catalysts are nickel or palladium based complexes. Palladium-catalysed cross-coupling reactions are often used for the synthesis of conjugated polymers with different organometallic nucleophiles such as Suzuki-Miyaura (boron reagents),[80] Stille (stannyl)[81] and Sonogashira (copper).[82] The organometallic reagents can be Grignard reagents for nickel catalysed Kumada-Corriu reaction.[83]

The cross-coupling reaction involves the formation of organo palladium species by the transition metal catalyzed oxidative addition reaction across the C-X bond of an electrophile. This is followed by the formation of an intermediate via transmetallation with a main group organometallic nucleophile, which is followed by reductive elimination of the desired product which restores the original palladium catalyst and completes the catalytic cycle.[84] The polymerization follows a step-growth mechanism, and is still the most suitable choice for the synthesis of conjugated copolymers. Catalytic cycle of transition metal catalyzed reactions is shown in Figure 1.3.
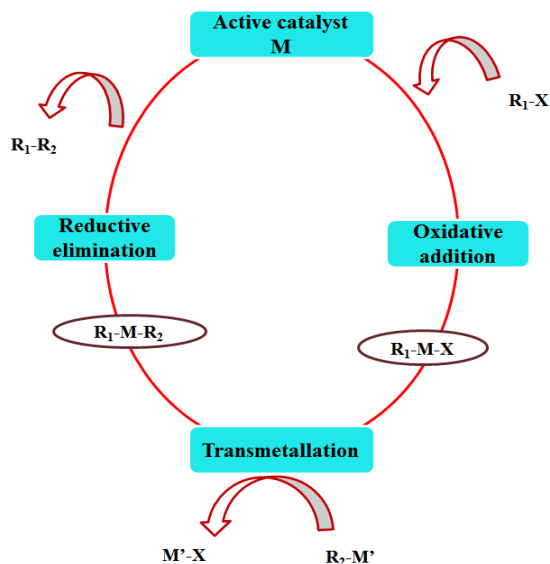
Figure 1.3: Catalytic cycle of transition-metal catalysed reaction

Some of the general routes for the synthesis of copolymers are explained with examples.

1.3.1 Suzuki-Miyaura coupling reaction

The impact of the Suzuki-Miyaura reaction of aryl halides with organoboronic acids and esters, on academic and industrial research as well as on production is immense. Palladium catalysed cross-coupling reaction in organic synthesis was first reported in 1979 by Akira Suzuki and won the Nobel Prize in Chemistry in 2010 which was shared with R. F. Heck and Ei-ichi Negishi.[85] The benefit of Suzuki reaction includes the mild conditions under which these are conducted, the commercial availability and stability of boronic acids to heat, oxygen and water, and the ease of handling and separation of boron-containing by-products from the reaction mixtures. These advantages make the Suzuki reaction an important tool in medicinal chemistry as well as in the large-scale synthesis of pharmaceuticals and fine

chemicals. As in other cross-coupling reactions, the mechanism involves transmetallation with a boronic acid and reductive-elimination from the resulting diarylpalladium complex affords the corresponding biaryl and regenerates the Pd(0) complex. K_3PO_4 and K_2CO_3 are the most commonly used base for this reaction which facilitate the slow transmetallation of the boronic acid by forming a more reactive boronate species.

Lee *et al.* utilised this method to synthesize poly(diketopyrrolopyrrole-alt-benzothiadiazole) (PDPPBT-Si) alternating D-A copolymers using highly soluble DPP with hybrid siloxane side chains and 4,7-diboronic ester-2,1,3-benzothiadiazole monomers (Scheme 1.1). The reaction was performed in the presence of either [Pd(PPh$_3$)$_4$] or [Pd$_2$(dba)$_3$]/P(o-tolyl)$_3$ as the catalyst in a mixture of toluene and basic aqueous solution (K_2CO_3 or K_3PO_4).[86] The annealed PDPPBT-Si films showed well balanced ambipolar charge transport with the maximum hole and electron mobilities of 0.18 and 0.13 cm^{2}V^{-1} s^{-1}, respectively.
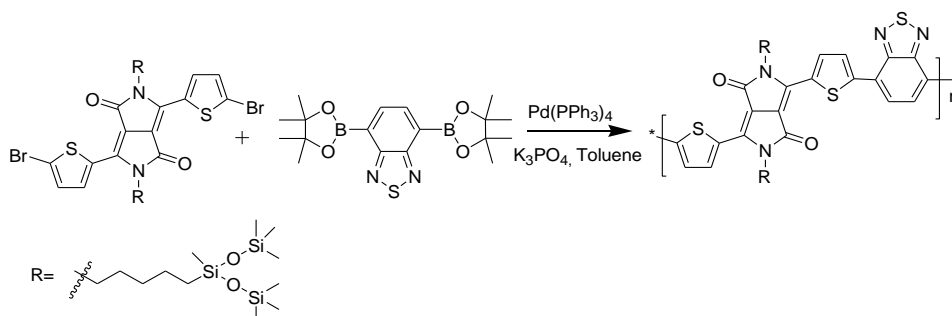
Scheme 1.1: Synthesis of DPP based D-A copolymers by Suzuki reaction

1.3.2 Heck coupling reaction

The palladium catalysed Mizoroki-Heck coupling reaction of aryl halide with vinyl benzene is one of the most successful routes for the vinylation of aryl/vinyl halides.
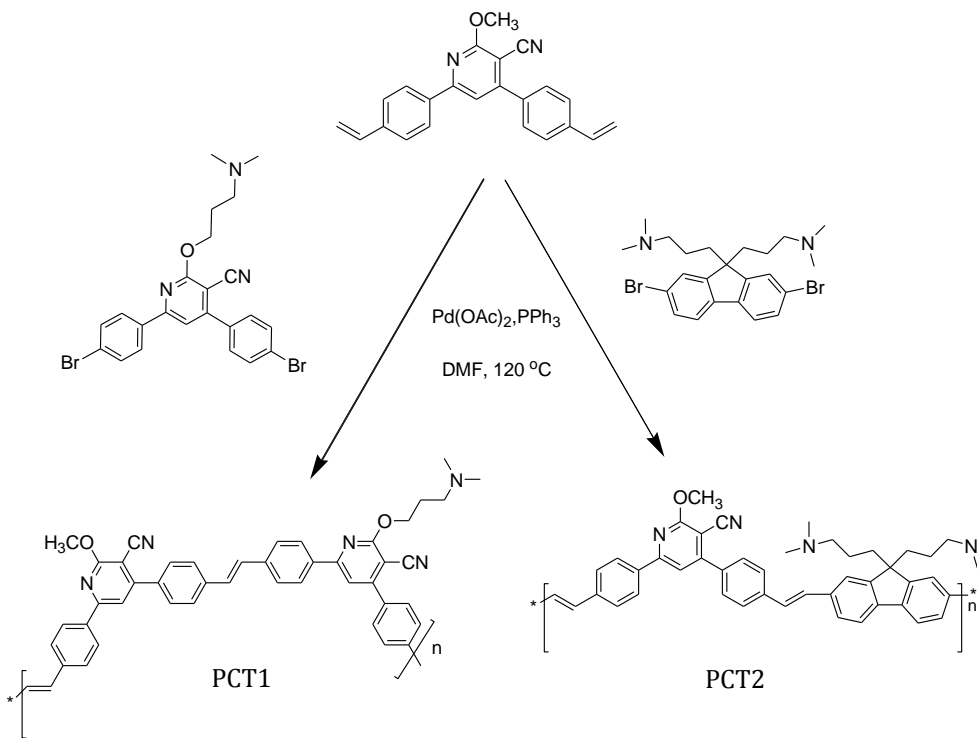
Scheme 1.2: Synthesis of cyanopyridine based D-A copolymers by Heck reaction

Hemavathi *et al.* successfully synthesized two polymers (PCT1 and PCT2) bearing cyanopyridinyl and phenylene or fluorenyl tethered with N,N-dimethylaminopropyl group (as side chain) via Heck polymerisation technique. Here, cyanopyridinyl acts as acceptor and phenylene or fluorenyl acts as donor unit. Fluorenyl moiety increased the thermal stability of PCT2 and lowered the optical band gap to 2.26 eV compared to the PCT1 having phenylene moiety (Scheme 1.2). Both the polymers showed optical transmittance spectra of polymer thin films coated on ITO substrate and revealed the transparency of 90 %, which was better compared to that of poly(3,4-ethylenedioxythiophene) film (80 % transparency).[87]

1.3.3 Stille cross-coupling reaction

The Stille cross-coupling reaction provides construction of molecules containing sp^2-sp^2 linkages between stannanes and halides or pseudohalides. It is a well-elaborated method for the formation of carbon–carbon bonds. Palladium catalysed Stille reaction has found applications in drug discovery, synthesis of natural products and materials chemistry. The main drawback includes the toxicity of organostannanes, difficulty in the removal of the tin by-products and their low polarity, which makes them poorly soluble in water.
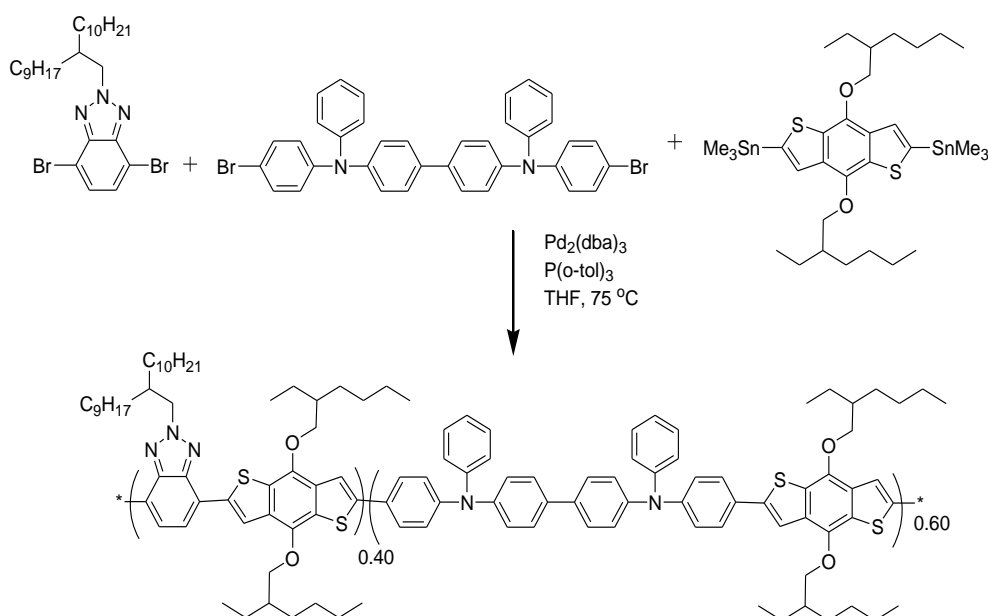
Scheme 1.3: Synthesis of triphenyamine and BTz-based random copolymers by Stille cross-coupling reaction

Donor-acceptor random copolymer comprising benzotriazole acceptor and bistriphenylamine and benzodithiophene donors, were successfully synthesized by Cetin *et al.* by means of the versatile Stille cross-coupling reaction.[88] Bulk heterojunction photovoltaic cell was constructed with

polymer: PCBM blend as active layer (1:2 ratio) in 3 % 1,2-dichlorobenzene solution, which gave a power conversion efficiency of 3.50 % (Scheme 1.3).

1.3.4 Sonogashira coupling reaction

Pd-catalyzed Sonogashira reaction is one of the straightforward methods for the coupling of vinyl or aryl halides with terminal alkynes to form conjugated enynes or aryl alkynes. The reaction presents the concept of utilizing a co-catalyst such as copper Iodide paired with palladium catalyst which allowed conjugated enynes and aryl alkynes to be produced at room temperature.
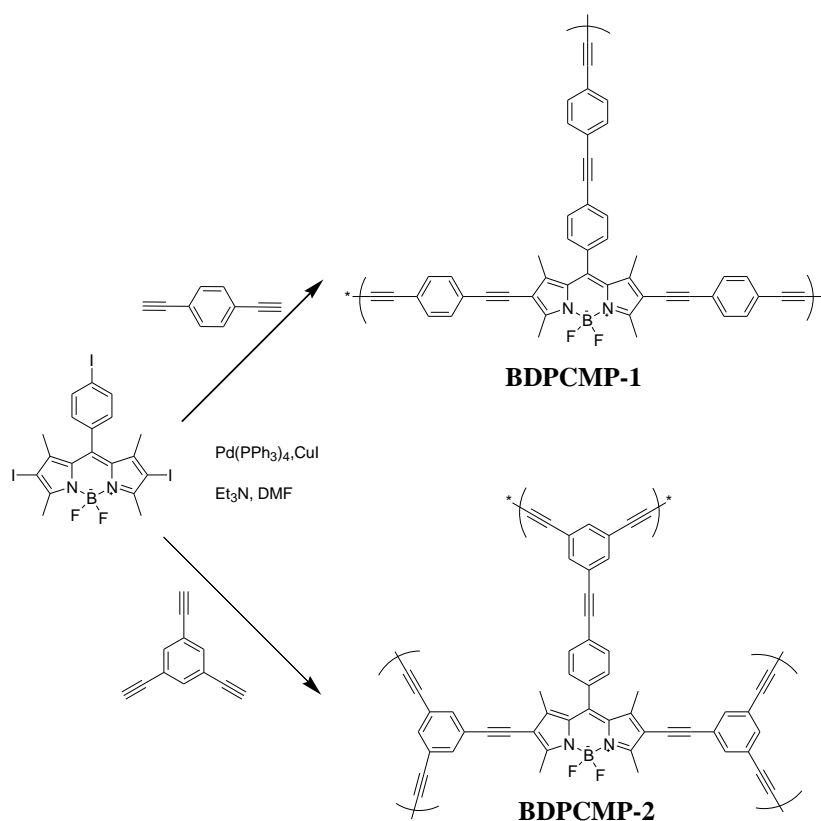
Scheme 1.4: Synthesis of BODIPY-functionalized microporous organic polymers by Sonogashira coupling reaction

Xu *et al.* synthesized a series of BODIPY-functionalized microporous organic polymers with triple polymerisable groups and a range of aryl–alkyne monomers via a Sonogashira cross-coupling reaction.[89] These polymers are promising candidates for potential applications in post-combustion CO_2 capture and sequestration technology (Scheme 1.4).

1.3.5 Gilch polymerisation reaction

Poly(p-phenylene vinylene) and its derivatives are synthesized via the Gilch reaction in which 1,4-bis(bromomethyl) or (chloromethyl) arenes undergo self-polymerisation with potassium tertiary butoxide in a non-hydroxylic solvent like THF. The concentration of the monomer, temperature of the reaction and speed of the base addition are the crucial conditions for getting high molecular weight and narrower PDI of PPV copolymer.
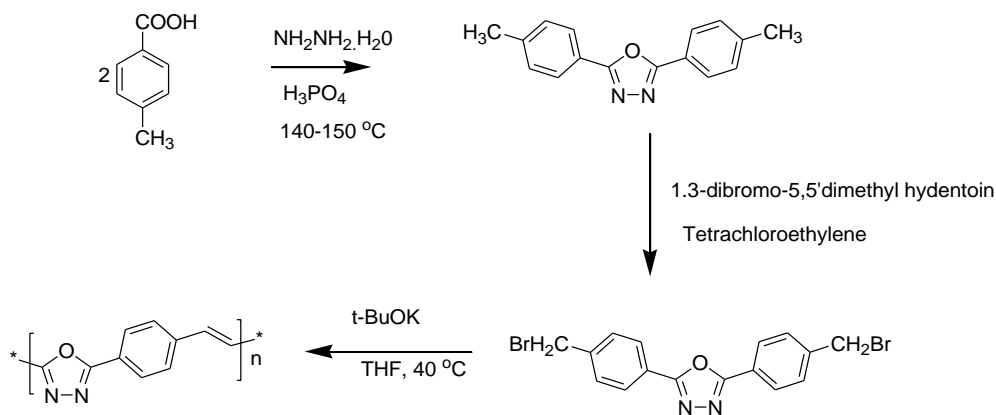
Scheme 1.5: Synthesis of PPV based homopolymers by Gilch polymerisation reaction

Nimisha *et al.* synthesized novel π-conjugated polymer, namely poly(p-phenylene vinylene-1,3,4-oxadiazole) (PPVO) with good solubility and processability via Gilch polymerisation reaction.[90] The PPVO polymer

showed attractive emission features in the blue-green region with high quantum yields and were used as electron transport materials in optoelectronic devices such as OLEDs (Scheme 1.5). In addition to homopolymer derivatives, the monomers undergo copolymerisation to improve efficiency, processability and stability.

R. Li *et al.* synthesized two groups of novel poly(p-phenylene vinylene) (PPV) derivatives with hyperbranched structure via a Gilch reaction in different monomer ratios.[91] The polymer was red-light-emitting material and was used as an efficient acceptor material in polymer solar cell (Scheme 1.6).
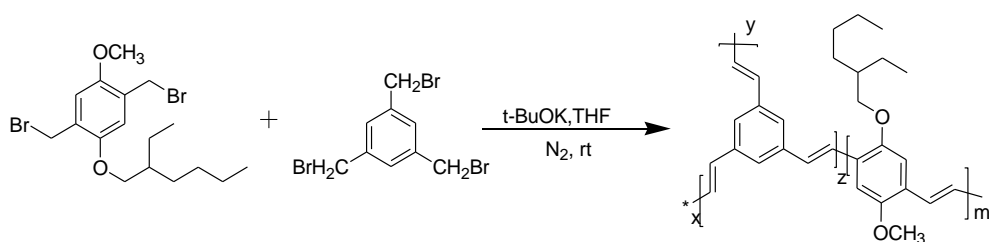
Scheme 1.6: Synthesis of PPV based copolymers by Gilch polymerisation reaction

1.3.6 Knoevenagel polycondensation reaction

The band gap of phenylene vinylene copolymers can be tuned by incorporating electronic substituents into the conjugated backbone. Salem *et al.* synthesized an anthracene based semiconducting polymer by introducing the cyano group (CN) into the π-conjugated system.[92] The incorporation of such electron-withdrawing groups increases the electron affinity and electroluminescence efficiency of the organic material due to the improved electron injection and transport (Scheme 1.7). The I–V characteristics of the

device in the configuration ITO/polymer/Al shows typical diode behaviour with relatively low turn-on voltages.
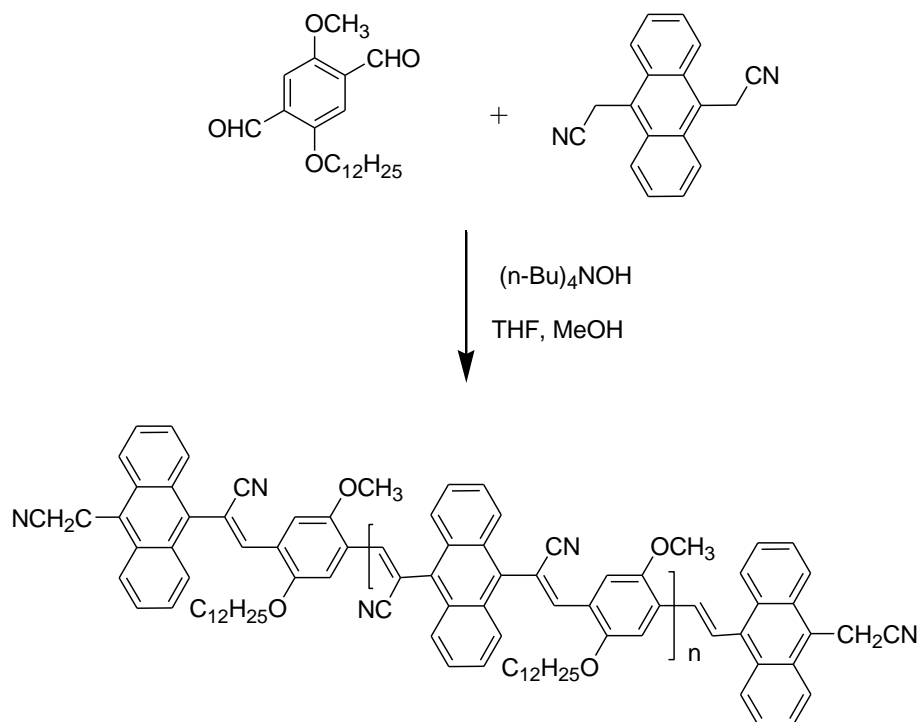
Scheme 1.7: Synthesis of An-CN-PPV based copolymers by Knoevenagel polycondensation reaction

1.3.7 Direct arylation reaction

Direct C−H arylation reaction is a powerful methodology for constructing Ar–Ar compounds and the heteroaryl analogues via C–H activation. Direct arylation by catalytic C–H activation is a more convenient process, because it avoids the preactivation steps.
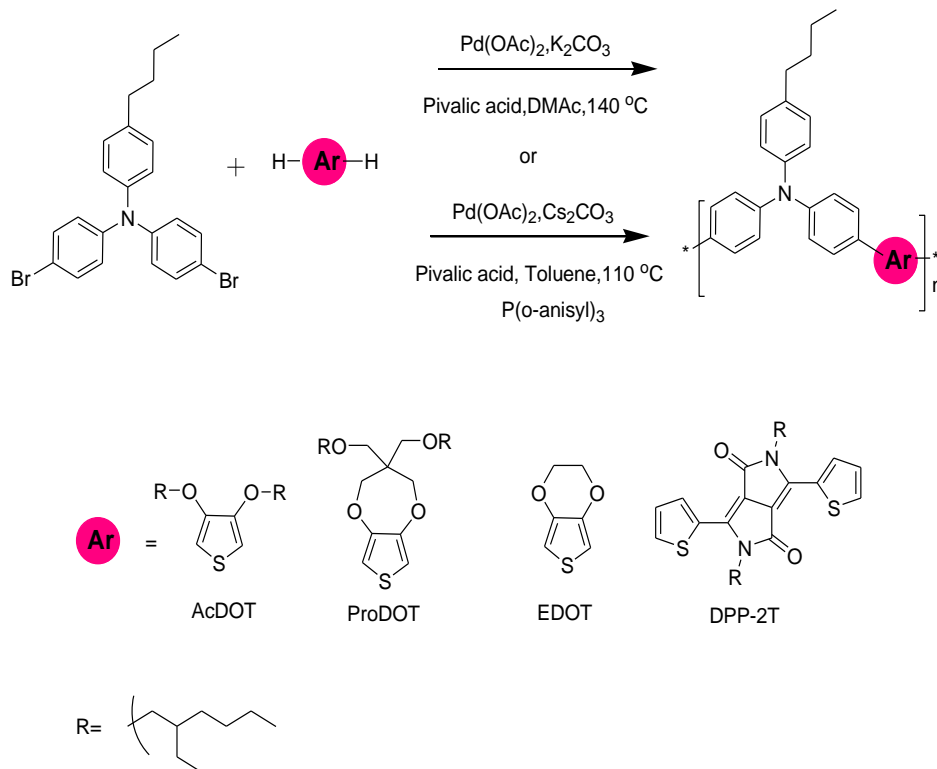
Scheme 1.8: Synthesis of triphenyl amine based organic polymers by direct arylation reaction

B. Schmatz *et al.* reported copolymerisation of twisted triphenylamine (TPA) and electron rich dioxythiophene (XDOT) monomers via direct (hetero) arylation polymerization.[93] Triphenyl amine based low band gap polymers when blended with PC71BM in conventional organic photovoltaic (OPV) devices can give a power conversion efficiencies up to 2.5% (Scheme 1.8).

1.4 Organic photovoltaic devices

French physicist Edmund Becquerel in 1839 first discovered the conversion of electromagnetic radiation energy into electricity. When

exposed to sunlight, AgCl electrode in an electrolyte solution generated direct current electricity and light induced voltage was observed.[94] Now-a-days, standard solar panels based on multicrystalline silicon have power conversion efficiencies around 15%. Conjugated polymers offer notable advantages over inorganic materials in photovoltaic technologies: such as solution processablility, ease of preparation, the ability to engineer the electronic structure at the molecular level and tuning essential parameters to improve device performance. Organic photovoltaics is classified into two types: devices based on organic small molecules and those based on polymer semiconductors. Small molecules are usually processed by vapour deposition, while the polymer is deposited from solution as thin films.

Four fundamental steps are involved in the mechanism of photon-to-electron conversion process in organic solar cell. First step, the conjugated polymer molecule (donor material) undergoes photoinduced excitation generating an electron in LUMO and a hole in HOMO. The photon absorption creates a Frenkel exciton (intra-molecular electron (e-) and hole (h+) pair).[95] Generally, conjugated polymers have high light absorption coefficients due to facile electrical polarization of delocalized π-electrons. Second, the bound electron and hole diffuse to the donor-acceptor (D-A) interfaces within the diffusion length to prevent recombining to the ground state. In the third step, exciton at a D-A interface undergoes charge-transfer process and are dissociated into free hole and electrons at the donor and acceptor interface. The dissociation efficiency of the exciton is relatively low due to the large excitonic binding energy in organic polymers. Therefore, electrical force must be applied to overcome the excitonic binding energies for dissociation in organic solar cells. Finally, as a result of the internal

electric field, the fully separated charge carriers are transported to the respective electrodes in the opposite direction which generate photocurrent and photovoltage. The process of conversion of light into electricity can be schematically described in the following Figure 1.4.
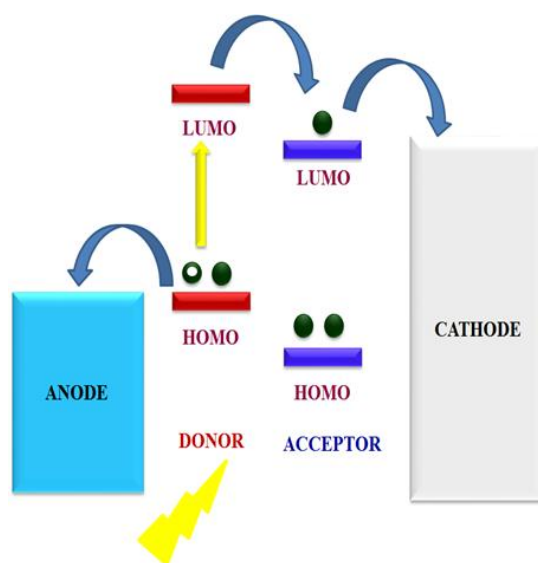
Figure 1.4: Energy conversion process in donor-acceptor organic solar cells

1.4.1 Organic solar cell (OSC) device architecture

A number of different device architectures have been developed to support the efficient photon to charge conversion. Most commonly used device architectures are single layer, bilayer heterojunction and bulk heterojunction. The single layer comprises of only one active material, whereas, bilayer and bulk heterojunction are based on electron donors (D) and electron acceptors (A). The difference of these architectures lays in the charge generation mechanism.

1.4.1.1 Single layer device

In this device structure, a thin layer of conducting polymer is sandwiched between transparent electrode (ITO) and aluminium. In 1994, Kim *et al.* constructed a single layer device structure using poly(phenylene vinylene) (PPV) sandwiched between an ITO and a low work-function cathode.[96] In a single layer device, there is only one place to dissociate excitons into free carriers, i.e., the interface between active layer and a cathode, which decreases the carrier generation efficiency. Schematic representation of single layer device structure is shown in Figure 1.5.
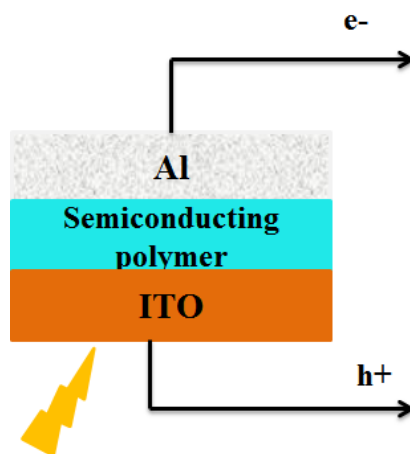
Figure 1.5: Schematic representation of single layer device architecture

1.4.1.2 Bilayer heterojunction device

Bilayer heterojunction architecture, containing p-type layer for hole transport and n- type layer for electron transport, was first fabricated by C.W. Tang in 1986 with 1 % polymer solar cell efficiency.[97] In a bilayer device, the p-n type semiconductors are stacked on top of each other to improve the photocurrent of the photovoltaic device. The first step in the fabrication of

bilayer device is the deposition of donor and acceptor layer on the ITO coated glass plate. Using vacuum evaporation technique, the metal electrode is coated on the top of the photoactive layer. The bilayer heterojunction device structure is shown in the Figure 1.6.
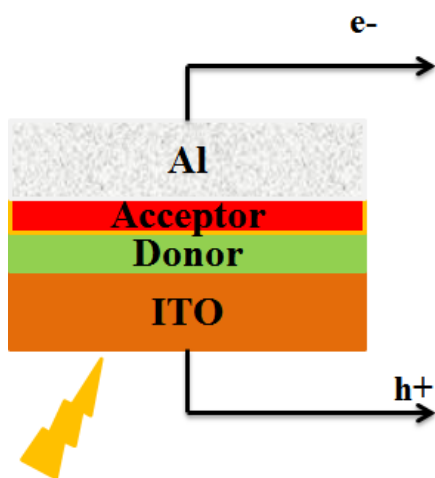
Figure 1.6: Schematic representation of bilayer heterojunction device

However, the bilayer device is still reported to have lower power conversion efficiency compared with the inorganic devices. This is because, the separated layer of donor and acceptor has small interfacial area which limits the dissociation of excitons into free carriers. The diffusion length of exciton is normally much less than the optical absorption length and this decreases the quantum efficiency of such devices. The thickness of the donor and acceptor layer should be similar to the penetration length of the incident light, which is typically 80-200 nm. In this architecture, directional photo-induced charge transfer takes place across the interface. Since charge carriers travel to their respective electrodes, the chances for recombination losses are significantly reduced. Thus both the exciton diffusion length and

the poor shunt resistance can be improved.[98-101] J. J. M. Halls *et al.* described a solution to this problem in 1995, i.e., instead of using two layers, the donor and acceptor materials are deposited into a single mixed layer.[102] Organic solar cells utilizing these types of blends are known as bulk heterojunctions.

1.4.1.3 Bulk heterojunction (BHJ) device

Bulk heterojunction organic solar cell device is a thin film comprised of mixture of donor and acceptor materials that are sandwiched between a pair of asymmetric electrodes, in which the interfacial area between the donor and acceptor is increased.[103,104] The blend morphology enables charge carrier transport in the two different phases and enhances the quantum efficiency of charge separation. The formation of continuous network creates two channels i.e., the donor material (polymer or small molecules) forms a hole-transporting path to the anode, while the acceptor material (fullerenes or inorganic material) forms the electron-transporting path to the cathode resulting in efficient charge collection. In bulk heterojunction device, only a single thin film is used as photoactive layer to create an internal donor-acceptor heterojunction which eliminates the interfacial erosion problems which bilayer configuration faced. The major advantage of the bulk heterojunction device is that the interface distance should be in the order of the exciton diffusion length and the excitons can be dissociated anywhere in the active layer. Although absorption coefficient is very high above 10^5 cm^{-1}, by combining donor and acceptor materials in a single layer, where it creates p-n junctions throughout bulk materials and ensures that photogenerated exciton regardless of the thickness layer. Polymer-

fullerene solar cells were among the first to utilize this bulk heterojunction principle. Shaheen *et al.* fabricated organic solar cell, with notable power conversion efficiencies (close to 3 %) obtained with a bulk heterojunction device using a MDMO-PPV as the donor and a soluble PCBM as the acceptor.[105] Figure 1.7 illustrates the schematic representation of bulk heterojunction. The bulk heterojunction photovoltaic devices fabricated using the blend of polymer and fullerene derivative act as photoactive layer in which hole-transporting conjugated polymers act as donors and electron transporting fullerene derivatives act as acceptors.
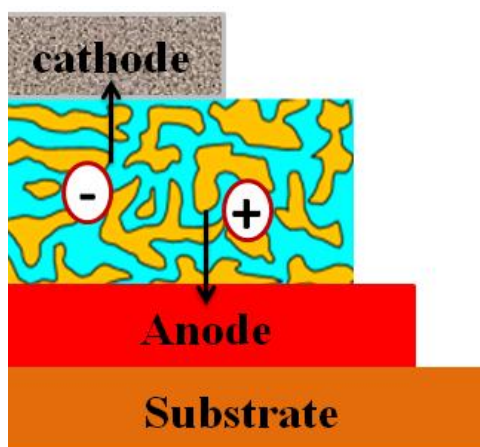
Figure 1.7: Schematic representation of bulk heterojunction (BHJ) device

1.4.2 p- Type donor-acceptor copolymer semiconductors

In recent years, low band gap donor-acceptor copolymers have been broadly applied in organic optoelectronics. The properties of donor-acceptor copolymers, like solubility, electrochemical properties, device performance, molecular weight and film morphology can simply be improved by tuning the structures of donor, acceptor and side chains. Also, the intra and

intermolecular "push-drag" effect between donor-acceptor units could effectively modify the packing mode in thin film of polymers affording close and orderly π-π arrangements of polymer chains which could produce high device performance. Mullen *et al.* in 2007 studied a D-A copolymer of benzothiadiazole (BD) and cyclopenta[2,1-b:3,4-b']dithiophene (CDT) and the thin films resulted in very low mobility. By using dip coating method, the organisation was improved and resulted better hole mobility.[106] In 2011 Mullen *et al.* further modified the polymer by tuning the molecular weight, side alkyl chain and morphology of the thin film which resulted in improved mobility of 3.3 $cm^2 V^{-1} s^{-1}$ which was considered to be the best for p-type thin film at that time.

The position of the HOMO and LUMO energy levels and the band gap are the major factors for determining the optical and electrochemical properties of the conjugated copolymers which in turn affect the photovoltaic performance. The initial step in the photovoltaic mechanism involves the conversion of light energy to electrical energy in a device by absorbing the light by the photoactive material. The wavelength of the photon flux density of the solar spectrum is ~700 nm corresponding to a low energy of 1.77 eV.[107] To exploit the unlimited source of solar energy, the absorption spectrum of a polymer should cover both the red and near infrared regions to match the larger part of the solar spectrum and hence produce the maximum photon flux. While designing the copolymer for organic photovoltaic devices, various factors are to be taken into account such as (1) broad and strong absorption in visible and near IR region through narrowing their optical band gap, (2) suitable LUMO and HOMO energy levels to maintain energy offset for exciton dissociation at D-A interface, (3) high

hole mobility for donor and electron mobility for acceptor to enhance the charge transport and (4) optimum morphology of D-A within active layer. The optical property related with light harvesting does not only depend on the properties of p-type polymers, but also the properties of the n-type material used. The open-circuit voltage in polymer solar cells with ohmic contacts is linearly dependent on the magnitude of the built-in potential i.e., the difference between the LUMO level of an n-type material and HOMO level of a p-type polymer. The lower HOMO level of the donor results in better theoretically attainable V_{oc} and LUMO level of donor has to be at atleast 0.3 eV higher than that level of the acceptor to guarantee the formation of a downhill driving force for the energetically favourable electron transfer and overcome the binding energy of the intra-chain exciton. To achieve narrow band gap by lowering the LUMO level of the polymer, this may result eventually in lower LUMO level than that of the acceptor and hence hampering the efficient electron transfer. [108-110] The design and synthesis of new p-type copolymers for photovoltaic devices is not only directed to pursuing low band gaps, but also in adjusting the band gap by modulating the HOMO-LUMO levels. Bulk-heterojunction photovoltaic device based on fullerene-polymer combinations have been established over 15 years. Theoretical computational study has revealed that, over 10 % power conversion efficiency (PCE) of a BHJ solar cell is attainable using an ideal p-type conjugated polymer if it is prepared with all essential properties. The properties required for ideal p-type conjugated polymers are: solution processability, miscibility with n-type materials, low optical band gap for the broad absorption spectrum to capture more solar energy and high hole mobility and suitable HOMO and LUMO energies to ensure a large V_{oc}. In

this connection, molecular design of new electron-rich donor monomers is central to the development of p-type donor–acceptor polymers.

J. Hu *et al.* synthesized two D-A conjugated polymers based on 5H-dithieno [3,2-b:20,30-d]pyran (DTPa) with thiophene bridged benzo[d][1,2,3]triazole (BTA) or di-fluorinated benzo[d][1,2,3] triazole (ffBTA).[111] They have constructed polymer solar cells using PDTPa-TBTA as donor and [6,6]-phenyl-C71-butyric acid methyl ester (PC71BM) as an acceptor which exhibited power conversion efficiencies (PCE) of 2.22 % (Scheme 1.9). The introduction of fluorine substituents on the BTA unit obviously influenced the optical and photovoltaic properties. The solar cell constructed using PDTPa-TffBTA showed a decreased V_{oc} of 0.52 V in solar cells and the efficiency was improved by nearly 55 %, and reached 3.43 %. The result showed that the introduction of fluorine on the BTA unit was also effective in improving the photovoltaic performance.
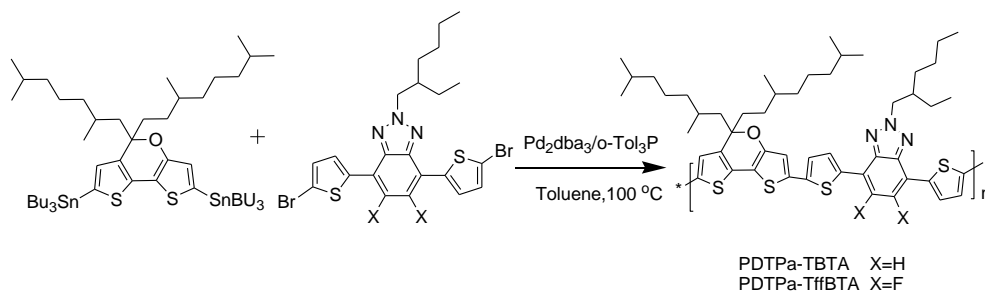
Scheme 1.9: Synthesis of PDTPa-TBTA and PDTPa-TffBTA

1.5 Nonlinear optics

Nonlinear optics is the branch of optics that occurs as a consequence of the modification of the optical properties of a material system by the presence of light. Franken *et al.* in 1961 performed the very first nonlinear

optical experiment, a ruby laser radiation with a wavelength of 694.2 nm was used to generate the second harmonic in a quartz crystal at the wavelength of 347.1 nm.[112] Davydov *et al.* in 1970, reported the SHG in organic molecules which led to a new concept of molecular engineering, i.e., to synthesize new organic materials for NLO studies.[113] The search for materials with high optical nonlinearities is gaining interest both in the research as well as in industry. Some classes of nonlinear optical effects were known long before the invention of the laser, examples of such phenomena include Pockels and Kerr electrooptic effects,[114] light-induced resonant absorption saturation, described by Vavilov etc.[115,116] Since the advent of the laser in the 1960s, the systematic studies of optical nonlinearities and the observation of vast catalog of spectacular nonlinear optical phenomena have become readily accessible. The main focus on the NLO research includes the second and third-order properties. Of which, nonlinear optical properties of donor-acceptor conjugated copolymers are the current areas of interest. The criteria required for organic NLO materials to act as an ideal NLO material are fast optical response, synthetic flexibility for molecular design and morphology, processability into crystals or thin films, ease of fabrication, nontoxicity, optical transparency and high mechanical and thermal stability.[117] Optical nonlinearity is mainly due to the strong D-A interactions in π-bonding sequence and the conjugation length of organic polymer.[118] The nonlinear optical response can occur in an optical system when there is suitable intense illumination. Whenever strong electric field is applied to the NLO material, in the presence of intense laser light, the charge distribution in a medium gets modified and the medium gets polarized.[119] In nonlinear optics, the nonlinear optical effects can be described within the

general framework of macroscopic Maxwell equations by expressing the dipole moment per unit volume, or polarization density $(\vec{\rho})$ of a material, as a power series in the electric field '$\vec{E}$':

$$(\vec{\rho}) = \epsilon_0 (\chi^{(1)} \vec{E}_1 + \chi^{(2)} \vec{E}_2 + \chi^{(3)} \vec{E}_3 + \ldots\ldots) \ldots\ldots\ldots\ldots\ldots (1.1)$$

Here, $\chi^{(1)}$ is the linear susceptibility representing the linear absorption and linear refractive index, $\chi^{(n)}$ are called the nth order nonlinear susceptibilities.

Recently, organic materials have drawn significant attention as third order NLO materials, because of their potential applications in optical switching,[120,121] optical limiting,[122-127] three dimensional (3D) lithographic microfabrication,[128,129] 3D fluorescence imaging[130] and 3D optical data storage. M. S. Bahae *et al.* in 1989, designed and developed a simple single beam Z-scan technique to measure the sign as well as magnitude of both nonlinear absorption and nonlinear refraction coefficients.[131,132] When a high intensity laser beam propagates through a material, along the propagation path of a Gaussian beam in Z-direction using an aperture or without an aperture, induced refractive index changes lead to self-focusing or defocusing of the laser beam. This enables to determine the third-order nonlinear optical properties of various materials in liquid, thin film or crystal forms.

1.5.1 Nonlinear absorption (NLA)

Nonlinear absorption refers to the change in absorption of the medium as a function of intensity or fluence. Nonlinear absorption is the key phenomenon in nonlinear spectroscopy. At high input optical intensities, the

chances for a material to absorb more than a single photon can be increased before relaxing down to the ground state.[133-135] The major applications of nonlinear absorption are:

- Use of nonlinear absorbers for light-intensity dependent attenuation of a laser beam (e.g., power limiting applications)

- Use of nonlinear absorbers for initiation of a photochemical reaction, (e.g., two-photon induced photopolymerization)

- Use of nonlinear absorbers for generation of luminescence through a nonlinear absorption process followed by emission of light.

In the case of solids, nonlinear absorption may be due to direct multiphoton absorption, saturation of the single photon absorption or free carrier absorption. Near atomic resonance, the absorption processes can be strongly nonlinear. Introduction of multi-photon absorption at high intensity levels, nonlinear absorption increases, whereas, saturating the absorption line with high intensity light, it decreases. The nonlinear absorption can be expressed as a function of intensity i.e.,

$$\alpha(I) = \alpha_o + \alpha_1 I + \alpha_2 I^2 + \dots \dots \dots \dots \dots \dots \dots (1.2)$$

Where α_o represents linear absorption, α_1 represents two-photon absorption, α_2 represents three-photon absorption, etc. [133] The optical nonlinear absorption can take the form of either reverse saturable absorption or saturable absorption depending on the incident wavelength, fluence, material concentration, and pulse duration.

1.5.2 Saturable absorption (SA)

At high input laser intensities, the absorption of a material decreases and the transmission will show saturable absorption characteristics. SA is vital for use of Q-switching, mode locking to produce short and ultrashort laser pulses, nonlinear filtering outside laser resonators, which can clean up pulse shapes. Saturable absorption is particularly strong in semiconductor lasers at wavelengths just above the band edge. Most of the organic materials show saturable absorption (Figure 1.8), but often only at very high optical intensities. Saturable absorption enhances the peak and suppresses the valley which shows negative type of absorption nonlinearity. At sufficiently high incident light intensity, when excited state absorption is lower than the ground state absorption, atoms in the ground state of a material become excited into an upper energy state in such a way that there is insufficient time for them to decay back to the ground state before the ground state becomes depleted, and the absorption subsequently saturates.[136]
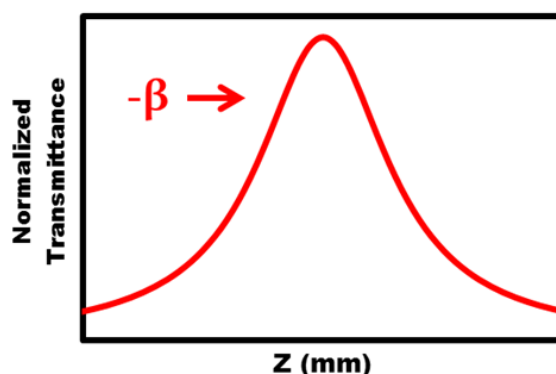
Figure 1.8: Open aperture Z-scan traces in saturable absorption

1.5.3 Reverse saturable absorption

In reverse saturable absorption, the excited state absorption cross section was found to be larger than the ground state absorption cross section and exhibited a decrease in transmittance with intensity of the copolymer sample. The two-photon absorption (TPA), multiphoton absorption, excited state absorption and free carrier absorption, where the absorption increases with input intensity, can cause reverse saturable absorption (Figure 1.9). Reverse saturable absorbers were widely used as optical power limiters and molecular spatial light modulators. Reverse saturable absorption enhances the valley and suppresses the peak which shows positive type of absorption nonlinearity.[136]
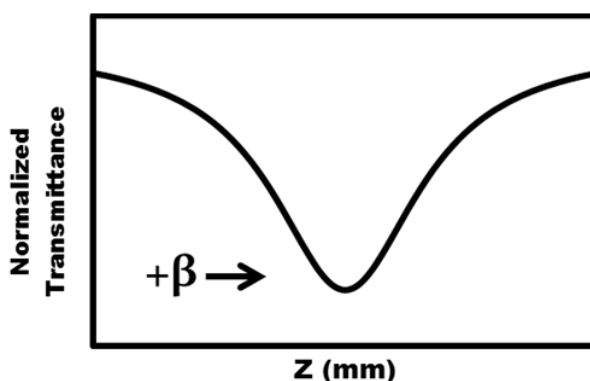
Figure 1.9: Open aperture Z-scan traces reverse saturable absorption

The organic polymer materials can perform either as saturable absorbers or as reverse saturable absorbers depending predominantly on the excitation wavelength. A transition from reverse saturable absorption to saturable absorption or vice versa may be observed when experimental parameters such as intensity of light, concentration of the materials and morphology of the films etc. are changed. There are various reports of such

behaviour in dyes and metals, metal doped semiconductors, dye doped polymer films etc. Srinivas *et al.* investigated nonlinear absorption of Rhodamine B dye in methanol and water using an open aperture Z-scan technique with nanosecond pulses.[137] Reverse saturable absorption was observed at 435 nm in both the solvents, and a transition from SA to RSA at 600 nm in methanol whereas a transition from RSA to SA with an increase in concentration at 600 nm with water as the solvent was observed.

1.5.4 Two photon absorption

Two-photon absorption is the absorption process by which the energy gap between two real states is bridged by the simultaneous absorption of two photons from the incident radiation, not necessarily at the same frequency.[136] In Two-photon absorption, the atomic transition rate depends on the square of the light intensity which it is differs from linear absorption and is shown in equation (1.3):

$$\frac{dl}{dz} = -\alpha l - \beta l^2 \dots\dots\dots\dots\dots\dots\dots\dots\dots\dots\dots\dots\dots\dots\dots\dots (1.3)$$

Here, 'α' and 'β' are the linear absorption coefficient and two photon absorption coefficient, respectively

In organic materials, TPA is normally transparent in the spectral range, because both photons are lacking in energy to complete the transition alone. Figure 1.10 represents the energy scheme of the two photon excitation process. When the photons are present together for an instant of time, an optical transition can take place. Quantum mechanically, the first photon making a virtual transition to imaginary state and second photon

appears within the virtual lifetime of that state, the absorption sequence to the upper state can be completed. If not, the virtual transition collapses back to the ground state and no absorption takes place. Because the virtual lifetime is so short, photon fluxes must be high and therefore power levels from laser beams are required. The efficiency of TPA is affected by the proximity of the input photons to a real state of the system. At the same time, there must be an allowed optical transition linking the initial state and this real state. TPA has important practical effects in semiconductors and dielectrics which enhance or degrade optical switching performance in semiconductor devices leading to optical damage in laser window materials.
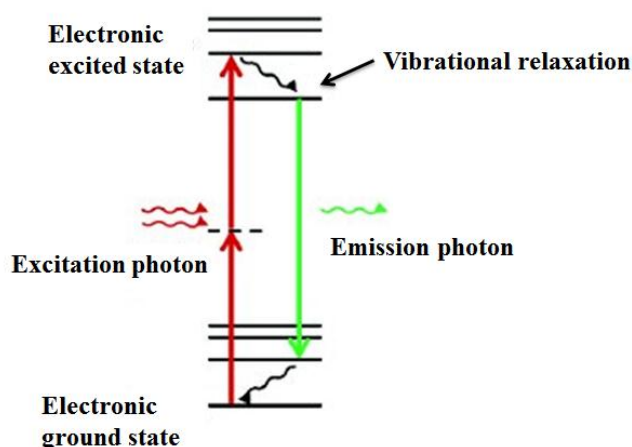
Figure 1.10: Energy scheme of two photon excitation process

1.5.5 Multiphoton absorption

Multiphoton absorption process involve the simultaneous absorption of 'n' photons by the transition of an absorbing molecule from a lower energy level to higher energy level.[136] The absorption of (n+1) photons from a single optical beam is defined as:

$$\frac{dl}{dz} = -\left(\alpha + \gamma^{(n+1)} I^n\right) I \quad \text{..(1.4)}$$

here, $\gamma^{(n+1)}$ is the (n+1) photon absorption coefficient.

Multiphoton absorption has the potential application of protecting sensitive detectors and eyes from high power lasers.

1.5.6 Free carrier absorption

It is one of the important optical properties in semiconductors in which an intraband optical absorption takes place i.e., the excited carrier is already in an excited band, such as an electron in the conduction band or a hole in the valence band, where it is free to move . Free carrier absorption explains the scattering mechanisms of carriers and in determining the optical absorption. It is a two-step process in which the electron absorbs a photon and is transferred to an intermediate state where it interacts with lattice vibrations and reaches a final state.[136] The excited state electron relaxes to the conduction band and it will recombine with an excited hole in the valence band after a characteristic recombination time. Whereas, excited state electron is retained in the conduction band, it can absorb another photon, if the intensity is sufficiently high. It is called free carrier absorption.

1.5.7 Optical power limiting

Leite *et al.* in 1967 introduced first optical power limiter based on thermal mechanism with a continuous wave laser using 488 nm Ar ion laser beam as incident light and nitrobenzene as the linearly absorbing medium with an aperture in front of the detector.[137] An optical limiter is a device

which exhibits linear transmittance at low powers, but it becomes slightly opaque at high input fluence (Figure 1.11). Ideally, an optical limiter is designed to keep the power, irradiance and energy transmitted by an optical system below some specified maximum value irrespective of the magnitude of the input. The potential application of optical limiters is protection of sensitive optical sensors, laser power regulation and restoration of signal levels in logic systems.[138,139] The intensity dependent optical nonlinear processes such as nonlinear absorption, nonlinear refraction and nonlinear scattering lead to optical limiting effect. Various materials are studied for optical limiting purposes based on different processes. Nonlinear optical materials with more sensitivity and less linear loss are being developed to incorporate them into optical systems. The experimental set-up of optical limiting is very similar to the Z-scan geometry.
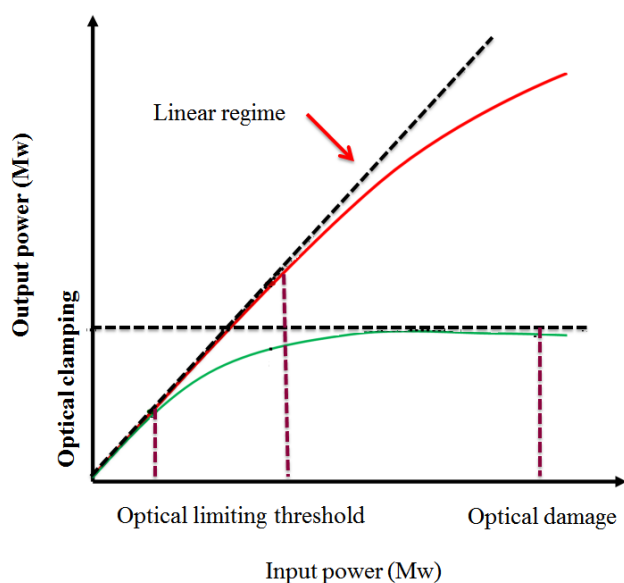
Figure 1.11: Schematic diagram of ideal optical limiter

1.5.8 Nonlinear refraction (NLR)

Nonlinear refraction of a material is explained using the third order term in the series of expansion of polarisation

$$\text{P} = \epsilon_0(\chi^{(1)} + \chi^{(2)}E + \chi^{(3)}E^2 + \cdots)E \quad \text{...............................} (1.5)$$

Where E is the electric field strength. According to this the relation between nonlinear refraction and intensity of illumination is shown in equation.[133]

$$n = n_0 + n_2I \quad \text{...} (1.6)$$

Here, n_0 is the linear refractive index and n_2 is the nonlinear refraction coefficient.

The effects like molecular reorientation, optical Kerr effect, excitation of free carriers, photorefraction or optically-induced heating may result in nonlinear refraction property of an organic material. It is the change in intensity dependent index of refraction of a medium when a material is exposed to electromagnetic radiation of suitable frequency. In the case of homogeneous material, the nonlinear refraction arises from a four-wave interaction and the third-order nonlinearity is mainly field dependent. This property of the material has been employed in several applications such as optical switching, logic gates, communication systems, data processing, nonlinear spectroscopy and optical limiting devices.[133]

1.5.9 Z-scan technique

Z-scan is the most popular method for the characterization of the sign and magnitude of third-order nonlinear refraction coefficient (n_2) and nonlinear absorption coefficient (β), via the closed and open aperture

methods. Principle used in this technique is spatial beam distortion. It can work, even if the thickness of the material is smaller than the beam's waist length. It offers high simplicity and sensitivity compared to nonlinear interferometry, degenerate four wave mixing, ellipse rotation and beam distortion measurements. Using this technique, the third-order NLO properties of solids, liquids and liquid crystals can be determined. The simplicity of Z-scan theory occasionally affects the accuracy, when the laser induced nonlinear response at a certain point of the medium is not solely determined by the laser intensity at that point, but also depends on the laser intensity in the surrounding regions, it will be called a nonlocal nonlinear optical response. Usually, a variety of mechanisms may contribute to the nonlinearity, some of which may be nonlocal. [131,132]

The experimental setup for single beam Z-scan is shown in Fig. 1.12. The closed-aperture Z-scan setup is used for measuring the real part of the nonlinear refractive index. In this set up, a lens focuses the laser to a certain point, and after this point the beam obviously defocusses. After a further distance, an aperture is placed with a detector behind it. The aperture allows only the central portion of the cone of light reach into the detector and the transmitted light is measured through this finite aperture. The open-aperture Z-scan setup is used for determining the imaginary part of the nonlinear refractive index, or the nonlinear absorption coefficient. In this measurement, the far-field aperture allows the whole signal and is measured by the detector.[132]
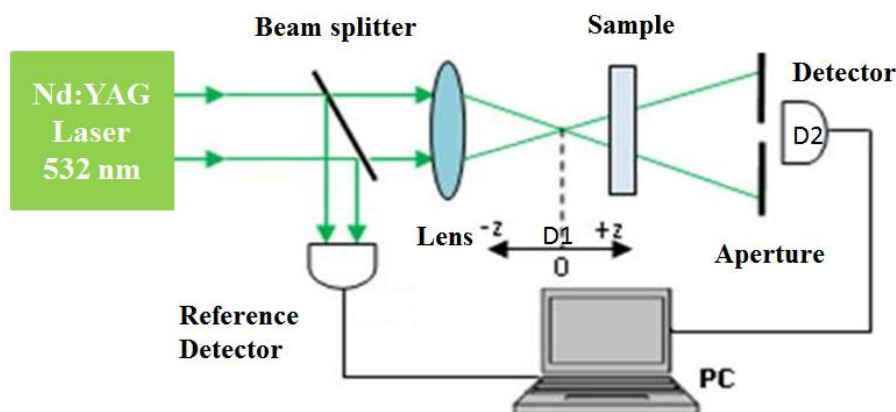
Figure 1.12: Schematic diagram of the experimental set up for Z-scan technique

1.5.9.1 Open aperture (OA) Z-scan

When a laser beam is incident on a nonlinear material, it makes intense changes in the optical properties of the material. By performing the open aperture Z-scan experiment, the nonlinear absorption of the material is measured. OA Z-scan experiments is insensitive to nonlinear refraction. The Z-scan traces obtained with no aperture is estimated to be symmetric in respect of the focus where the transmittance is minimum. The material is made to travel across one end to the other end through the focus. At the farfield, the intensity is low and hence linear absorption occurs. If the material is exhibiting two photon absorption, and the transmission is minimum at focal region, it behave as reverse saturable absorber.

Zidan *et al.* investigated the third-order nonlinear optical properties of C60/poly (dimethylacetylendicarboxylate) by Z-scan technique using a CW diode laser at 635 nm wavelength.[140] The OA Z-scan traces gave a reverse saturable absorption graph with a positive nonlinear absorption coefficient. The OA Z-scan curve fitted well with the graph derived from two photon

absorption. The theoretical fitting confirmed that two photon absorption mechanism was involved in the optical absorption.

1.5.9.2 Closed aperture (CA) Z-scan

Closed aperture Z-scan experiment is performed to measure the nonlinear refractive index and it is based on the self-refraction and self-modulation effects. When a laser beam is passed through the material, along the beam path, the effective focal length of the material changes due to the change in input intensity. The amount of light transmitting through the aperture depends on the sample location on the z-axis and on the sign of n_2. If the material has negative refractive index and it is far from the focus, the intensity of the beam is not strong enough to cause any nonlinearity within the sample and the measured power on the detector remains approximately constant. When the material moves towards focus, the nonlinear absorption and refraction enhances and deviates the beam passing through it and a small amount of light will fall on the detector, resulting in an increase in the measured transmittance. When the material is at focus, the sample will not have any effect on the beam. As the sample moves away from the focus, the strength of the refraction decreases due to lower intensity. The sign of the nonlinear refractive index is directly clear from the shape of the graph, but it is not easily obtained in other techniques. The sensitivity of nonlinear refraction is entirely due to the aperture, and removal of aperture totally reduces the effect.[132] A wide variety of materials including organic molecules, organic dyes, fullerene derivatives, and polymer systems, display nonlinear optical properties which have found use in variety of applications.

Rubi *et al.* performed Z-scan nonlinear analysis in copolymer films of 3-hexylthiophene and thiophene functionalized with azobenzene derivative, poly(3-HT-co-TDR1) obtaining a negative nonlinear refractive index at very low optical powers.[141] Observance of self-defocusing effects at very low laser intensities projects the strong presence of nonlinear properties in these samples. Real part of third-order nonlinear susceptibility could also be measured. Rubi et al. reported that optical limiting with these materials could be implemented even at very low powers.

1.6 Scope of the present study

- Design of donor-acceptor low band gap conjugated polymers using Density Functional Theory in the Periodic Boundary Condition (PBC) formalism.

- Synthesis of the polymers adopting appropriate synthetic strategies.

- Exploring the application of the synthesized polymers as active layer in the conventional and inverted bulk heterojunction device using ZnO and LiF as the electron transport layers and MoO_3 as hole transport material.

- Exploring the application of the fluorescent conjugated polymers in third-order nonlinear optical devices.

1.7 Instrumentation

^{1}H Nuclear magnetic resonance (^{1}H NMR) spectra of the polymers were recorded with a Bruker Avance III (400 MHz) spectrometer, and chemical shifts were recorded in δ units downfield of TMS as the internal standard using

CDCl$_3$ solvent (SAIF, CUSAT). Fourier Transform Infra-Red (FT-IR) spectra were recorded on a Perkin Elmer Spectrum 100, FT-IR Spectrometer by the KBr pellet method. All the electrochemical experiments were performed using BAS Epsilon Electrochemical analyser with a quiet time of 2 s and a scan rate of 100 mVs^{-1} in dry acetonitrile with Bu$_4$NPF$_6$ (the supporting electrolyte). UV-Visible absorption and emission spectra were measured using a Thermo Scientific, Evolution 201, UV-Visible Spectrophotometer and an Ocean Optics Inc SD 2000, UV-Vis-NIR Ocean Optics Spectrophotometer, respectively. Molecular weight and polydispersity index of the copolymers were determined by Gel Permeation Chromatography (GPC) analysis using Waters GPC with polystyrene standard calibration using THF solvent (SCTIMST, Thiruvananthapuram). Thermogravimetric measurements (TG & DTG) were performed under nitrogen atmosphere at a heating rate of 10 ^{o}C/min with TA Instrument Q 50 thermogravimetric analyser (PS&RT, CUSAT). Fluorescence lifetime measurements were performed using a Horiba Fluorolog-3 fluorescence spectrometer.

References

1.   J. A. Pople, S. H. Walmsley, *Mol. Phys.,* 1962, **5,** 15

2.   W. D. Gill, W. Bludau, R. H. Geiss, P.M. Grant, R. L. Greene, J. J. Mayerle, G. B. Street, *Phys. Rev. Lett.,* 1977, **38**, 1305.

3.   H. Shirakawa, E.J. Louis, A.G. MacDiarmid, C. K. Chiang, A. J. Heeger, *J. Chem. Soc. Chem. Commun.,* 1977, **474**, 578.

4.   A. L. Dyer, M. R. Craig, J. E. Babiarz, K. Kiyak, J. R. Reynolds, *Macromolecules*, 2010, **43**, 4460.

5.   S. O. Hacioglu, S. Toksabay, M. Sendur, L. Toppare, *J. Polym. Sci., Part A: Polym. Chem.,* 2013, **52**, 537.

6. T. Ameri, N. Li, C. J. Brabec, *Energy Environ. Sci.,* 2013, **6**, 2390.

7. J. H. Seo, A. Gutacker, Y. Sun, H. Wu, F. Huang, Y. Cao, U. Scherf, A. J. Heeger, G. C. Bazan, *J. Am. Chem. Soc.,* 2011, **133**, 8416.

8. S. C. Price, A. C. Stuart, W. You, *Macromolecules*, 2010, **43**, 4609.

9. W. Li, R. Qin, Y. Zhou, M. Andersson, F. Li, C. Zhang, B. Li, Z. Liu, Z. Bo, F. Zhang, *Polymer,* 2010, **51,** 3031.

10. J. H. Burroughes, D. D. C. Bradley, A. R. Brown, R. N. Marks, K. Mackay, R. H.Friend, P. L. Burns, A. B. Holmes, *Nature*, 1990, **347**, 539.

11. K. T. Kamtekar, H. L. Vaughan, B. P. Lyons, A. P. Monkman, S. U. Pandya, M. R. Bryce, *Macromolecules*, 2010, **43**, 4481.

12. A. Cirpan, L. Ding, F. E. Karasz, *Polymer*, 2005, **46**, 811.

13. A. Cirpan, L. Ding, F. E. Karasz, *Synth. Met.,* 2005, **150,** 195.

14. N. Stutzmann, R. H. Friend, H. Sirringhaus, *Science*, 2003, **299**, 1881.

15. R. Mondal, H. A. Becerril, E. Verploegen, D. Kim, J. E. Norton, S. Ko, N. Miyaki, S. Lee, M. F. Toney, J. L. Bredas, M. D. McGehee, Z. Bao, *J. Mater. Chem.,* 2010, **20**, 5823.

16. D. T. McQuade, A. E. Pullen, T. M. Swager, *Chem. Rev.,* 2000,**100**, 2537.

17. J. Turan, M. Kesik, S. Soylemez, S. Goker, M. Kolb, M. Bahadir, L. Toppare, *J. Electroanal. Chem.,* 2014, **735**, 43.

18. C. Lete, S. Lupu, B. Lakard, J. Y. Hihn, F. J. Campo, *J. Electroanal. Chem.,* 2015, **744**, 53.

19. A. A. Argun, A. Cirpan, J. R. Reynolds, *Adv. Mater.,* 2003, **15**, 1338.

20. A. Bolduc, S. Dufresne, W. G. Skene, *J. Mater. Chem.,* 2010, **20**, 4820.

21. A. Pennisi, F. Simone, G. Barlette, G.D. Marco, M. Lanza, *Electrochim. Acta.,* 1999, 44, 3237.

22. G. Inzelt, M. Pineri, J.W. Schultze, M.A. Vorotyntsev, *Electrochim. Acta.,* 2000,**45**, 2403.

23. S. Logothetidisa, A. Laskarakis, *Eur. Phys. J. Appl. Phys*., 2009, **46**, 12502.

24. T. Sekitani, T. Someya, *Adv. Mater.*, 2010, **22,** 2228.

25. S. C. Rasmussen, K. Ogawa, S. D. Rothstein, *Handbook of Organic Electronics and Photonics,* H. S. Nalwa, Ed., American Scientific Publishers: Stevenson Ranch, CA, 2008.

26. H. A. M. van Mullekom, J. A. J. M. Vekemans, E. E. Havinga, E. W. Meijer, *Mater. Sci. Eng.,* R 2001, **32**, 1.

27. J. Roncali, *Macromol. Rapid Commun.,* 2007, **28**, 1761.

28. J. L. Bredas, *J. Chem. Phys.,* 1985, **82**, 3808.

29. Y. J. Cheng, S. H. Yang, C. S. Hsu, *Chem. Rev.,* 2009, **109**, 5868.

30. F. Wudl, M. Kobayashi, A. J. Heeger, *J. Org. Chem.,* 1984, **49**, 3382.

31. J. L. Bredas, A. J. Heeger, F. Wudl, *J. Phys. Chem.,* 1986, **85**, 4673.

32. I. Hoogmartens, P. Adriaensens, D. Vanderzande, J. Gelan, C. Quattrocchi, R. Lazzaroni, J. L. Bredas, *Macromolecules,* 1992, **25**, 7347.

33. H. Brisset, C. Thobie-Gautier, A. Gorgues, M. Jubault, J. Roncali, *J. Chem. Soc.Chem. Commum.,* 1994, **130**, 5.

34. E. Orti, M. J. Sanchis, P. M. Viruela, R. Vituela, *Synth. Met.,* 1999,**101**, 602.

35. J. Roncali, C. T. Gautier, *Adv. Mater.,* 1994, **6**, 846.

36. Q. Pei, G. Zuccarello, M. Ahlskog, O. Inganas, *Polymer,* 1994, **35,** 1347.

37. Q.T. Zhang, J. M. Tour, *J. Am. Chem. Soc.,* 1998, **120**, 5355.

38. G. Brocks, A. Tol, *J. Phys. Chem.,* 1996, **100**, 1838.

39. H. A. M. van Mullekom, J. A. J. M. Vekemans, E. W. Meijer, *Chem. Commun.,* 1996, **21**,63.

40. E. Havinga, W. ten Hoeve, H. Wynberg, *Polym. Bull.,* 1992, **29**,119.

41. E. Havinga, W. ten Hoeve, H. Wynberg, *Synth. Met.,* 1993, **55**, 299.

42. X. Guo, M. D. Watson, *Macromolecules,* 2011, **44**, 6711.

43. E. Wang, Z. Ma, Z. Zhang, K. Vandewal, P. Henriksson, O. Inganaas, F. Zhang, M. R. Andersson, *J. Am. Chem. Soc.,* 2011, **133,** 14244.

44. B. Burkhart, P. Khlyabich, T. Canak, T. LaJoie, B.C. Thompson, *Macromolecules* 2011, **44**, 1242.

45. G. Öktem, A. Balan, D. Baran, L. Toppare, *Chem. Commun.,* 2011, **47**, 3933.

46. A. W. Hains, Z. Liang, M. A. Woodhouse, B. A. Gregg, *Chem. Rev.,* 2010, **110**, 6689.

47. P. M. Beaujuge, J. Subbiah, K. R. Choudhury, S. Ellinger, T. D. McCarley, F. So, J. R. Reynolds, *Chem. Mater.,* 2010, **22**, 2093.

48. G. Brocks, A. Tol, *J. Phys. Chem.,* 1996, **100**, 1838.

49. P. Thakrala, A. K. Bakhshia, *Indian J. Chem.,* 2015, **54A**, 9.

50. F. Jensen, *Introduction to Computational Chemistry*, 2nd ed., John Wiley & Sons, England, 2007.

51. J. B. Foresman, A. Frisch, *Exploring Chemistry With Electronic Structure Methods* 2nd ed., Gaussian, Pittsburgh, PA,1996.

52. A. D. Becke, *J. Chem. Phys.*,1993, **98**, 5648.

53. C. Lee, W. Yang, R. G. Parr, *Phys. Rev. B.,* 1994, **37**, 785.

54. K. Burke, J. P. Perdew, Y. Wang, J. F. Dobson, G. Vignale, M. P. Das, *Electronic Density Functional Theory: Recent Progress and New Directions*, Plenum Press, New York, 1998.

55. J. Heyd, G. E. Scuseria, M. Ernzerhof, *J. Chem. Phys.,* 2003, **118**, 8207.

56. A. V. Krukau, O. A. Vydrov, A. F. Izmaylov, G. E. Scuseria, *J. Chem. Phys.,* 2006, **125**, 224106.

57. S. M. Cassemiro, C. Zanlorenzi, T. D. Z. Atvars, G. Santos, F. J. Fonseca, L. Akcelrud, *J. Lumin.,* 2013, **134**, 670.

58. S. S. Zade, N. Zamoshchik, M. Bendikov, *Acc. Chem. Res.,* 2011, **44**, 14.

59. L. Zhang, Q. Zhang, H. Ren, H. Yan, J. Zhang, H. Zhang, J. Gu, *Sol. Energy Mater. Sol. Cells,* 2008, **92**, 581.

60. C. S. Ra, S. Yim, G. Park, *Bull. Korean Chem. Soc.,* 2008, **29**, 891.

61. U. Salzner, J. B. Lagowski, P. G. Pickup, R. A. Poirier, *Synth. Met.,* 1998, **96**, 177.

62. T. E. Cheatham, J. H. Miller, T. Fox, P. A. Darden, P. A. Kollman, *J. Am. Chem. Soc.,* 1995, **117**, 4193.

63. M. J. Frisch, G. W. Trucks, H. B. Schlegel, G. E. Scuseria, M. A. Robb, J. R. Cheeseman, J. A. Montgomery, Jr. T. Vreven, K. N. Kudin, J. C. Burant, J. M. Millam, S. Iyengar, J. Tomasi, V. Barone, B. Mennucci, M. Cossi, G. Scalmani, N. Rega, G. A. Petersson, H. Nakatsuji, M. Hada, M. Ehara, K. Toyota, R. Fukuda, J. Hasegawa, M. Ishida, T. Nakajima, Y. Honda, O. Kitao, H. Nakai, M. Klene, X. Li, J. E. Knox, H. P. Hratchian, J. B. Cross, V. Bakken, C. Adamo, J. Jaramillo, R. Gomperts, R. E. Stratmann, O. Yazyev, A. J. Austin, R. Cammi, C. Pomelli, J. W. Ochterski, P. Y. Ayala, K. Morokuma, G. A. Voth, P. Salvador, J. J. Dannenberg, V. G. Zakrzewski, S. Dapprich, A. D. Daniels, M. C. Strain, O. Farkas, D. K. Malick, A. D. Rabuck, K. Raghavachari, J. B. Foresman, J. V. Ortiz, Q. Cui, A. G. Baboul, S. Clifford, J. Cioslowski, B. B. Stefanov, G. Liu, A. Liashenko, P. Piskorz, I. Komaromi, R. L. Martin, D. J. Fox, T. Keith, M. A. Al-Laham, C. Y. Peng, A. Nanayakkara, M. Challacombe, P. M. W. Gill, B. Johnson, W. Chen, M. W. Wong, C. Gonzalez, J. A. Pople, Gaussian 03, Revision C.02, Gaussian, Inc., Wallingford CT, 2004.

64. Gaussian 09, Revision B02, M. J. Frisch, G. W. Trucks, H. B. Schlegel, G. E. Scuseria, M. A. Robb, J. R. Cheeseman, G. Scalmani, V. Barone, B. Mennucci, G. A. Petersson, H. Nakatsuji, M. Caricato, X. Li, H. P. Hratchian, A. F. Izmaylov, J. Bloino, G. Zheng, J. L. Sonnenberg, M. Hada, M. Ehara, K. Toyota, R. Fukuda, J. Hasegawa, M. Ishida, T. Nakajima, Y. Honda, O. Kitao, H. Nakai, T. Vreven, Jr. J. A. Montgomery, J. E. Peralta, F. Ogliaro, M. Bearpark, J. J. Heyd, E. Brothers, K. N. Kudin, V. N. Staroverov, R. Kobayashi, J. Normand, K. Raghavachari, A. Rendell, J. C. Burant, S. S. Iyengar, J. Tomasi, M. Cossi, N. Rega, N. J. Millam, M. Klene, J. E. Knox, J. B. Cross, V. Bakken, C. Adamo, J. Jaramillo, R. Gomperts, R. E. Stratmann, O. Yazyev, A. J. Austin, R. Cammi, C. Pomelli, J. W. Ochterski, R. L. Martin, K. Morokuma, V. G. Zakrzewski, G. A. Voth, P. Salvador, J. J. Dannenberg, S. Dapprich, A. D. Daniels, Ö. Farkas, J. B. Foresman, J. V. Ortiz, J. Cioslowski, D. J. Fox, Gaussian, Inc., Wallingford CT, 2009.

65. C. Y. David, *Computational Chemistry: A Practical Guide for Applying Techniques to Real-World Problems*, John Wiley & Sons, Inc, New York, 2001.

66. C. Pisani, *Lecture Notes in Chemistry*, Springer-Verlag, Heidelberg, 1996.

67. K.N. Kudin, G. E. Scuseria, *Phy. Rev. B.,* 2000, **61**, 16440

68. P. J. Feibelman, *Phys. Rev. B.,* 1987, **35**, 2626.

69. J. E. Jaffe, A. C. Hess, *J. Chem. Phys.,* 1996, **105**, 10983.

70. S. Hirata, S. Iwata, *J. Chem. Phys.,* 1997, **107**, 10075.

71. J. Q. Sun, R. J. Bartlett, *J. Chem. Phys.,* 1998, **109**, 4209.

72. B. G. Janesko, *J. Chem. Phys.,* 2011, **134**, 184105.

73. B. M. Wong, J. G. Cordaro, *J. Phys. Chem. C.,* 2011, **115**, 18333.

74. M. Bouzzine, G. Salgado-Morán, M. Hamidi, M. Bouachrine, A. G. Pacheco, D. Glossman-Mitnik, *J. Chem.,* 2015, **2015**, ID 296386.

75. N. Toshima, S. Hara, *Prog. Polym. Sci.,* 1995, **20,** 155.

76. S. Sadki, P. Schottland, N. Brodie, G. Sabouraud, *Chem. Soc.Rev.,* 2000, **29**, 283.

77. G. A. Sotzing, J. R. Reynolds, P. Steel, *J. Adv Mater.,* 2004, **9**, 795.

78. R. J. Waltman, J. Bargon, *Can. J. Chem.,* 1986, **64**, 76.

79. Cheng, Y. J.; Luh, T. Y. *J. Organomet. Chem.,* 2004, **689,** 4137.

80. (a) N. Miyaura, K. Yamada, A. Suzuki, *Tetrahedron Lett.,* 1979, **20**, 3437.

(b) N. Miyaura, A. Suzuki, *J. Chem. Soc. Chem. Commun.,* 1979, **8,** 66 .

(c) A. Suzuki, *J. Organomet. Chem.,* 1999, **576,** 147.

(d) N. Miyaura, T. Yanagi, A. Suzuki, *Synth.Commun.,* 1981, **11**, 513.

81. D. Milstein, J. K. Stille, *J. Am. Chem. Soc.,* 1978, **100**, 3636.

82. K. J. Sonogashira, *Organomet. Chem.,* 2002, **653**, 46.

83. K. Tamao, M. J. Kumada, *J. Am. Chem. Soc.,* 1972, **94**, 4374.

84. R. Bates, *Organic Synthesis Using Transition Metals*, 2nd ed., John Wiley & Sons Ltd., 2012.

85. Nobelprize.org., The Nobel Prize in Chemistry 2010. Nobel Prize Foundation. Retrieved 2013-10-25.

86. J. Lee, A. R. Han, S. Myeon Lee, D. Yoo, J. Hak Oh, C. Yang, *.Angew. Chem. Int. Ed.* 2015, **54,** 4657

87. B. Hemavathi, B. R. Geetha, T.N. Ahipa, *Eur. Polym. J.,* 2017, **95**, 1.

88. A. Cetin, C. Istanbulluoglu, S. O. Hacioglu, S. C. Cevher, L. Toppare, A. Cirpan, *J. Polym. Sci. A. Polym. Chem.,* 2017, **55**, 3705.

89. Y. Xu, D. Chang, S. Feng, C. Zhang, J. Jiang, *New. J. Chem.,* 2016, **40,** 9415.

90. K. Nimisha, G. Unnikrishnan, *Polym. Int.,* 2016, **65**, 1221.

91. R. Li , Y. Mo, R. Shi, P. Li, C. Li, Z. Wang , X. Wang, S. Li, *Monatsh Chem.,* 2014, **145**, 85.

92. B. B. Salem, K. Hriz, N. Jaballah, D. Kreher, M. Majdoub, *Opt. Mater.,* 2015, **50,**114.

93. B. Schmatz, J. F. Ponder, J. R. Reynolds, *J. Polym. Sci. A. Polym. Chem.,* 2018, **56**, 147.

94. A. E. Becquerel, *Comptes Rendus,* 1839, **9,** 561.

95. Pope, M.; Swenberg, C. E. *Electronic Processes in Organic Crystals and Polymers*, Oxford Univ., UK, 1999.

96. M. Kim, M. G. Kang, L. J. Guo, J. Kim. *Understanding organic photovoltaic cells: Electrode. Nanostructure, Reliability, and Performance,* Ph. D Thesis, 2009.

97. C. W. Tang, *Appl. Phys. Lett.,* 1986, **48,** 183.

98. S. R. Scully, M. D. McGehee, *J. Appl. Phys.,* 2006, **100**, 034907.

99. J. Brédas, J. E. Norton, J. Cornil, V. Coropceanu, *Acc Chem. Res.,* 2009, **42,** 1691.

100. V. D. Mihailetchi, J. Wildeman, P. W. M. Blom, *Phys. Rev. Lett.,* 2005, **94,** 126602.

101. L. G. Shrotriya, V. Yao, Y. Huang, J. Yang, *J. Mater. Chem.,* 2007, **17**, 3126.

102. J. J. M. Halls, C. A. Walsh, N. C. Greenham, E. A. Marseglia, R. H Friend, S. C . Moratti, A. B. Holmes, *Nature*, 1995, **376**, 498.

103. M. Hiramoto, H. Fujiwara, M. Yokoyama, *J. Appl. Phys.,* 1992, **72**, 3781.

104. T. Taima, M. Chikamatsu, Y. Yoshida, K. Saito, K. Yase, *Appl. Phys. Lett.,* 2004, **85**, 6412.

105. S. E. Shaheen, C. J. Brabec, N. S. Sariciftci, F. Padinger, T. Fromherz, J. C. Hummelen, *Appl. Phys. Lett.,* 2001, **78**, 841.

106. K. Müllen, M. Zhang, H. N. Tsao, W. Pisula, C. Yang, A. K.Mishra*, J. Am. Chem. Soc.,* 2007, **129**, 3472.

107. The data of Solar Spectral Irradiance (air mass 1.5) was obtained from the Web site http://rredc.nrel.gov/solar/spectra/am1.5.

108. C. J. Brabec, C. Winder, N. S. Sariciftic, J. C. Hummelen, A. Dhanabalan P. A. van Hal, R. A. Janssen, *J. Adv. Funct. Mater.,* 2002, **12**, 709.

109. J. J. M. Halls, J. Cornil, D. A. dos Santos, R. Silbey, D. H. Hwang, A. B. Holmes, J. L. Bredas, R. H. Friend, *Phys. Rev. B.,* 1999, **60,** 5721.

110. L. J. A. Koster, V. D. Mihailetchi, P. W. M. Blom, *Appl. Phys. Lett.,* 2006, **88,** 093511.

111. J. Hu, X. Wang, F. Chen, B. Xiao, A. Tang, E. Zhou, *Polymers,* 2017, **9**, 516.

112. P. A. Franken, A. E. Hill, C. W. Peters, G. Weinrich, *Phys. Rev. Lett.,*1961*,* **7,** 118.

113. B. L. Davydov, L. D. Derkacheva, V. V. Dunina, M. E. Zhabotinskil, V. K. Zolin, L. D. Kreneva, M. A. Samokhina, *JEPT Lett.,* 1970, **12**, 16.

114. R. W. Boyd, *Nonlinear Optics,* 2nd edn., Academic, San Diego, 2003.

115. S. I. Wawilov, W. L. Lewschin, *Z. Phys.* 1926, **35**, 920.

116. S. I. Vavilov, *Microstructure of Light*, USSR Acad. Sci., Moscow, 1950.

117. Y. Zhang, J. Etxebarria, *Ferroelectric Liquid Crystals for Nonlinear Optical Applications, in Liquid Crystals Beyond Displays: Chemistry, Physics, and Applications* (ed Q. Li), John Wiley & Sons, Inc., Hoboken, NJ, USA, 2012.

118. G. Sreekumar, P. G. L. Frobel, C. I. Muneera, K. Sathiyamoorthy, C. Vijayan, C. Mukherjee, *J. Opt. A: Pure Appl. Opt.,* 2009, **11**, 125204.

119. P. Yeh, *Introduction to Photorefractive Nonlinear Optics*, 1st ed., John Wiley & Sons, Inc., New York, 1993.

120. S. Sun, L. R. Dalton, *Introduction to Organic Electronic and Optoelectronic Materials and Devices*, CRC Press, Taylor & Francis Group, Boca Raton, FL, 2008

121. L. V. Interrante, M. J. Hampden-Smith, *Chemistry of Advanced Materials: An Overview*, Wiley-VCH, New York, 1998.

122. C. Q. Tang, Q. D. Zheng, H. M. Zhu, L. X. Wang, S. C. Chen, E. Ma, X. Y. Chen, *J. Mater. Chem. C.,* 2013, **1**, 1771.

123. J. M. Hales, S. Zheng, S. Barlow, S. R. Marder, J. W. Perry, *J. Am. Chem. Soc.,* 2006, **128**, 11362.

124. R. Zieba, C. Desroches, F. Chaput, M. Carlsson, B. Eliasson, C. Lopes, M. Lindgren, S. Parola, *Adv. Funct. Mater.,* 2009, **19**, 235.

125. T. C. Lin, Y. F. Chen, C. L. Hu, C. S. Hsu, *J. Mater. Chem.,* 2009, **19**, 7075.

126. T. C. Lin, G. S. He, Q. D. Zheng, P. N. Prasad, *J. Mater. Chem.,* 2006, **16**, 2490.

127. L. Kamath, K. B. Manjunatha, S. Shettigar, G. Umesh, B. Narayana, S. Samshuddin, B. K. Sarojini, *Opt. Laser Technol.,* 2014, **56**, 425.

128. L. D. Zarzar, B. S. Swartzentruber, J. C. Harper, D. R. Dunphy, C. J. Brinker, J. Aizenberg, B. Kaehr, *J. Am. Chem. Soc.,* 2012, **134**, 4007.

129. B. H. Cumpston, S. P. Ananthavel, S. Barlow, *Nature*, 1991, **398**, 51.

130. W. Denk, J. H. Strickler, W. W. Webb, *Science,* 1990, **248,** 73.

131. M. S. Bahae, A. A. Said, T. H Wei, D. J. Hagan, E. W. Van Stryland, *IEEE J. Quantum Electron.,* 1990, **26**, 760.

132. M. S. Bahae, A. A. Said, E. W. Van Stryland, *Opt. Lett.,* 1989, **14**, 955.

133. R. L. Sutherland, *Hand Book of Nonlinear Optics*, 2nd ed., Eastern Hemisphere Distribution, Marcel Dekker. Inc., USA, 2003.

134. N. K. M. N. Srinivas, S. V. Rao, D. N. Rao, *J. Opt. Soc. Am. B: Opt. Phys.,* 2003, **20**, 2470.

135. U. Kurum, M. Yuksek, H. G. Yagliolu, A. Elmali, A. Ates, M. Karabutlut, G. M. Mamedov, *J. Appl. Phys.,* 2010, **108**, 063102.

136. L. Irimpan, *Spectral and Nonlinear Optical Characterisation of ZnO Nanocomposites,* Ph.D Thesis, Cochin University of Science and Technology, 2008.

137. R.C.C. Leite, S.P.S. Porto, T.C. Damen, *Appl. Phys. Lett.,* 1967, **10**, 100.

138. C. Zhang, Y. L. Song, Y. Xu, H. K. Fun, G. Y. Fang, Y. X. Wang, X. Q. Xin, *J. Chem. Soc. Dalton Trans.,* 2823, 2000.

139. E. I. Stiefel, K. Matsumoto, *Transition Metal Sulfur Chemistry: Biological and Industrial Significance,* American Chemical Society, Washington, DC, 1996.

140. M. D. Zidan, A. Allahham, *Acta Phys. Pol. A.,* 2015, **128,** 25.

141. R. M. A. G. Rubí, M. G. Rodríguez, D. M. Cruz, M. A. B. Pensado, J. A. G. Álvarez, G. R. Ortiz, M. Rodríguez, J. L. Maldonado, *Opt. Mater.,* 2015, **46,** 366.

Chapter **2**

DESIGN, SYNTHESIS AND CHARACTERIZATION OF PHENYLENE VINYLENE BASED COPOLYMERS BY GILCH POLYMERIZATION

In this chapter, a series of low band gap phenylene vinylene based copolymers were synthesized through Gilch polymerization route using potassium t-butoxide as base in dry THF at room temperature. The band structures of the four polymers were determined by quantum mechanical calculation employing Density Functional Theory (DFT) in the Periodic Boundary Condition (PBC) using HSE06/6-31G basis set. The polymers were characterized using ^{1}H NMR, FT-IR, GPC, UV-Vis and cyclic voltammetry. The four polymers have energy gap below 2.30 eV and have broad absorption in the visible region. The experimental results support the theoretical prediction. The fluorescence lifetime of the polymers, MD-CA-PPV, MD-FL-PPV, MD-PT-PPV and MD-AN-PPV were monitored using Time-Correlated Single Photon Counting technique (TCSPC) in CHCl$_3$. The absorption and emission spectra of phenylene vinylene based copolymers have been recorded at room temperature in toluene/acetonitrile mixtures of different polarities. The change in the dipole moment (Δμ) was calculated both from solvatochromic shift method and on the basis of microscopic empirical solvent polarity parameter (E_T^N) and values were compared.

2.1 Introduction

Due to their spectacular electroluminescent (EL) and optoelectronic properties, conjugated polymers such as poly (phenylene ethynylene) (PPE)[1] and poly(p-phenylene vinylene) (PPV)[2] have attracted great attention during recent years.[3,4] Poly(p-phenylene vinylene) (PPV) and its derivatives are well studied semiconducting polymers. Their potential as semiconductors was utilised in electro-optic devices such as thin film transistors,[5,6] organic light emitting diodes (OLEDs)[7-9] and organic photovoltaic devices (OPVs). [10-12] The drawback of PPV is that it has the tendency for aggregation which leads to formation of excitons in the solid state, fluorescence quenching, and also decreases electroluminescence efficiency.[13-14] Modified PPVs containing electron withdrawing groups not only improve the charge capacity, but also can enhance the electronic properties of conjugated polymers, increase the interaction between charges, improve energy transfer, the quenching efficiency and can be used as efficient active layer in photovoltaic devices.[15] In order to reduce the band gap of the PPV polymers effectively, strong electron withdrawing groups have been incorporated into the main skeleton to form a donor-acceptor (D-A) bridge. Alkoxy substituted PPV based polymers have been widely used in several optoelectronic devices, due to their strong electron donor effect of alkoxy group. The soluble phenylene vinylene based polymers such as, poly[2-(2-ethylhexyloxy)-5-methoxy-1,4-phenylene vinylene] (MEH–PPV),[16,17] poly[2-butoxy-5-(2-ethylhexyloxy)phenylene vinylene] (BEHPPV),[17] and poly[2-(2,7-dimethyloctyloxyl)-5-methoxy-1,4-phenylene vinylene] (OC1C10–PPV)[18,19] were extensively investigated.

Four PPV based copolymers MD-CA-PPV, MD-FL-PPV, MD-PT-PPV and MD-AN-PPV have been synthesized via Gilch polymerisation

method. Because of the broad absorption and the low band gap of the Gilch copolymers, these materials have the potential to be used in thin film electronics, mainly, photovoltaic (PV) devices. The photochemical and electronic properties of the π-conjugated copolymers can be tuned to some extent by varying the size, structure and electronic properties of the side chain substituents. The copolymers MD-CA-PPV, MD-FL-PPV, MD-PT-PPV and MD-AN-PPV are highly soluble in common organic solvents such as chloroform, tetrahydrofuran, dichlorobenzene and toluene through the introduction of flexible side chains.

The fluorescence emission of the copolymers was measured as a function of time after excitation by a laser pulse using Time-Correlated Single Photon Counting technique (TCSPC) in $CHCl_3$. Fluorescence lifetimes were obtained with nanosecond time resolution and were seen to fit to bi-exponential decay. The phenylene vinylene based copolymers showed high fluorescence quantum yields, which could make them suitable candidates for light emitting applications.

The solvatochromic method is based on the shift of absorption and emission maxima in solvents of varying polarity. A number of researchers have investigated experimental and theoretical studies on ground state (μ_g) and excited state (μ_e) dipole moments using different techniques in variety of organic fluorescent compounds like indoles, purines, and fluorescein and in some laser dyes etc.[20-26] A number of direct methods are available for the determination of the excited state dipole moment such as electronic polarization of fluorescence,[27] electric dichroism,[28] Stark splitting of rotational levels[29,30] and microwave conductivity.[31] These are considered to be more accurate, but they are restricted to relatively small molecules.

Experimentally much simpler and the most common method based on the analysis of solvatochromism of the absorption and fluorescence maxima have been used, because it does not use any external field.[32,33] Solvatochromic behaviour of MD-CA-PPV, MD-FL-PPV, MD-PT-PPV and MD-AN-PPV have been studied extensively in toluene/acetonitrile mixtures of varying polarity at room temperature. The ground and excited state dipole moments were estimated from Bakhshiev's and Kawski-Chamma-Viallet's equations using the variation of Stoke's shift with the solvent dielectric constant and refractive index. Onsager radius determined from *ab initio* calculation was used in the determination of dipole moments. Further, the change in the dipole moment ($\Delta\mu$) was measured both from solvatochromic shift method and on the basis of E_T^N parameter and values were compared. The present aim was to develop a viable method for determining the second order polarizability parameter (β) adopting the two level model using the values of the change in dipole moment ($\Delta\mu$), oscillator strength (f) and the transition dipolemoment (μ_{eg}). But due to the errors in the determination of the value transition dipole moment, the attempt to determine β was not successful.

In this chapter, four promising low band gap phenylene vinylene based alternate copolymers were designed and successfully synthesized via Gilch polymerisation. Monomers and D-A units were optimized using DFT/B3LYP/6-31G formalism. Polymers were optimized using DFT/HSE06/6-31G and DFT/B3LYP/6-31G methods. Their thermal, optical and electrochemical properties have been investigated. The experimental results agree with the theoretical prediction obtained by HSE06/6-31G method compared to the B3LYP/6-31G method. The

fluorescence measurements of all the polymers were measured with life time resolution, high life time accuracy with multi exponential decay function using TCSPC in CHCl$_3$. The effects of solvent on absorption and emission spectra, and the experimental study of dipole moments of PPV copolymers by solvatochromic shift method have also been reported.

2.2 Results and discussion
2.2.1 Theoretical calculation

The electronic structure and properties of the phenylene vinylene based copolymers MD-CA-PPV, MD-FL-PPV, MD-PT-PPV and MD-AN-PPV were studied using quantum chemical calculations, based on density functional theory (DFT) methods. [34-38] The DFT calculations at two different energy levels were carried out with both B3LYP and HSEh1PBE referred to as HSE06 (full Heyd–Scuseria–Ernzerh functional) using 6-31G basis set as implemented in Gaussian 09 package. Before proceeding to evaluate the electronic structure of the polymers, the ground state geometries of monomers and oligomers were optimized. Here, the ground state geometries of oligomers were optimized by means of DFT at the B3LYP (Becke, three parameter, Lee–Yang–Parr) level of theory using 6-31G basis set,[39-43] which enabled elimination of unsuitable materials before synthesis. Since the electronic properties of the polymers depended on their constituent monomers, the properties of bromomethylated monomers 1,4-bis-(bromomethyl)-2-decyloxy-5-methoxybenzene (MD), 1,4-bis (bromomethyl)-2,3-bis(octyloxy) benzene (CA), 2,7-bis(bromomethyl)-9,9-dioctyl-9H-fluorene (FL), 3,7-bis(bromomethyl)-10-octyl-10H-phenothiazine (PT) and 9,10-bis(bromomethyl)anthracene (AN) and their corresponding oligomer units were studied first (Figure 2.1).
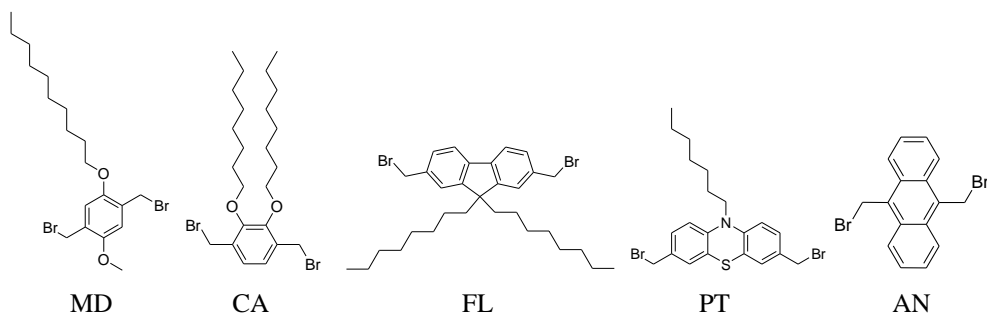
Figure 2.1: Structure of model compounds

       To evaluate the excited-state vertical transition energies and oscillator strengths, time-dependent DFT/ (TD-DFT) calculations were used. The properties are shown in Table 2.1.

Table 2.1: Values of $E_{activation}$ (eV), Oscillator strength and λ_{max} (nm) of the monomer units obtained by TD-DFT/B3LYP/6-31G

Monomer	Optimized Geometries of Monomers[a]	$E_{activation}$[b] (eV)	Oscillator strength[b]	λmax[b] (nm)
1,4-bis-(bromomethyl)-2-decyloxy-5-methoxy benzene (MD)		4.87	0.058	255
1,4-bis-(bromomethyl)-2,3-bis(octyloxy)benzene (CA)		6.23	0.004	199
2,7-bis(bromomethyl)-9,9-dioctyl-9H-fluorene (FL)		4.68	0.216	293
3,7-bis(bromomethyl)-10-octyl-10H-phenothiazine (PT)		3.93	0.012	317
9,10-bis(bromomethyl) anthracene (AN)		3.27	0.098	379

[a] Estimated from DFT/B3LYP/6-31G calculation
[b] Estimated from TD-DFT/B3LYP/6-31G calculation

Figure 2.2 compares the highest occupied molecular orbital (HOMO), lowest unoccupied molecular orbital (LUMO) energy levels and band gap of monomer units, D-A units and tetramers using Density Functional Theory (DFT) at the B3LYP/6-31G method.
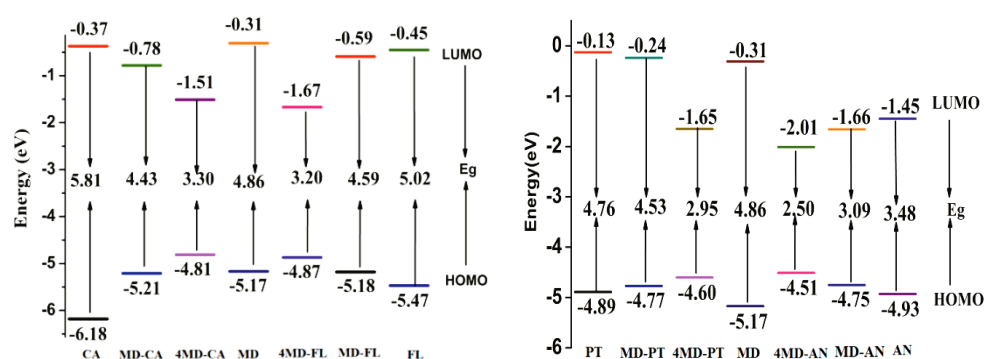
Figure 2.2: Energy levels of monomers D-A units and tetramer units of MD-CA-PPV, MD-FL-PPV, MD-PT-PPV and MD-AN-PPV copolymers

As shown in the energy level diagram, the LUMO levels of MD, CA, FL, PT and AN were found to be -0.31, -0.37, -0.45, -0.13 and -1.45 eV respectively. The LUMO levels of MD-CA, MD-FL, MD-PT and MD-AN were obtained to be -0.78, -0.59, -0.24, -1.66 eV respectively. The HOMO/LUMO energy levels describe electron or hole transporting capacity. In the case of MD-CA, MD-FL and MD-AN, MD acts as donor unit and CA, FL and AN act as acceptors, whereas in MD-PT, donor unit is PT. From this data, it is clear that where MD is coupled with bromomethylated monomer units such as CA, FL and AN, HOMOs are elevated, and the LUMOs are lowered, which facilitate electron and hole transport. The reduction in band gap of copolymers is due to the intramolecular charge transfer

between the donor and acceptor, which results in the decrease of the bond length alternation (BLA)[44,45] of phenylene vinylene type monomers. This can be visualized from the frontier orbital distribution of the model compounds (Figure 2.3).

LUMO

HOMO
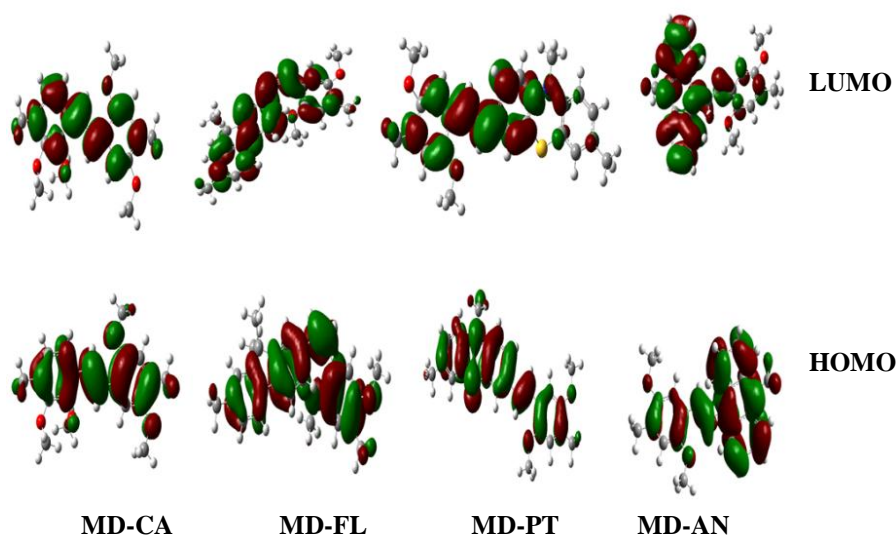
MD-CA **MD-FL** **MD-PT** **MD-AN**

Figure 2.3: Frontier molecular orbital distribution of monomeric units of MD-CA, MD- FL, MD-PT and MD-AN by DFT/B3LYP/6-31G method

2.2.2 Band structure of the polymers

The electronic properties of the PPV based copolymers were studied using PBC-DFT encoded in Gaussian 09 quantum chemical codes.[46] Periodic boundary condition (PBC) calculation is more computationally cost effective than the oligomer approach, because, in PBC calculation, polymer molecule of infinite chain length is optimized using translational symmetry. In addition to this, PBC allows the calculation of band structure in the positive region of the first Brillouin zone (between k=0 and k=π/a). The electronic structure of the copolymers were computed by applying two

levels of theory *i.e.*, DFT/PBC/HSE06/6-31G and DFT/ PBC/B3LYP/6-31G. DFT/PBC/HSE06/6-31G is a good method to consistently predict the band gap of conjugated polymers compared to DFT/ PBC/B3LYP/6-31G. Band structures in the positive region of the first Brillouin zone were calculated along the k-vector of one dimensional copolymers with 32 k-points after the optimization. The lowest four unoccupied and highest four occupied bands in the positive region of the first Brillouin zone were plotted. The band structure of the copolymers, MD-CA-PPV, MD-FL-PPV, MD-PT-PPV and MD-AN-PPV copolymers calculated through HSE06/6-31G level is shown in Fig. 2.4. The band gap was obtained from the difference between maximum point of the highest occupied molecular orbital and the minimum point of the lowest unoccupied molecular orbitals, respectively at constant k. It is clear from Figure 2.4 that lowest band gap occur at k=0, suggesting that all the polymers are direct band gap polymers.

The starting unit cell geometries for the PBC was calculated using HSE06/6-31G theory. The optimized unit cell for the Periodic Boundary Condition of the phenylene vinylene copolymers are shown in the Figure 2.5. The horizontal red line represents the translational vector. The starting unit cell geometries were taken from the central portion of the optimized tetramer by assuming that the unit cell was repeated identically an infinite number of times along the translational vector. The length of the translational vector for MD-CA-PPV, MD-FL-PPV, MD-PT-PPV and MD-AN-PPV were found to be 29.02, 36.62, 33.59 and 29.10 Å respectively.
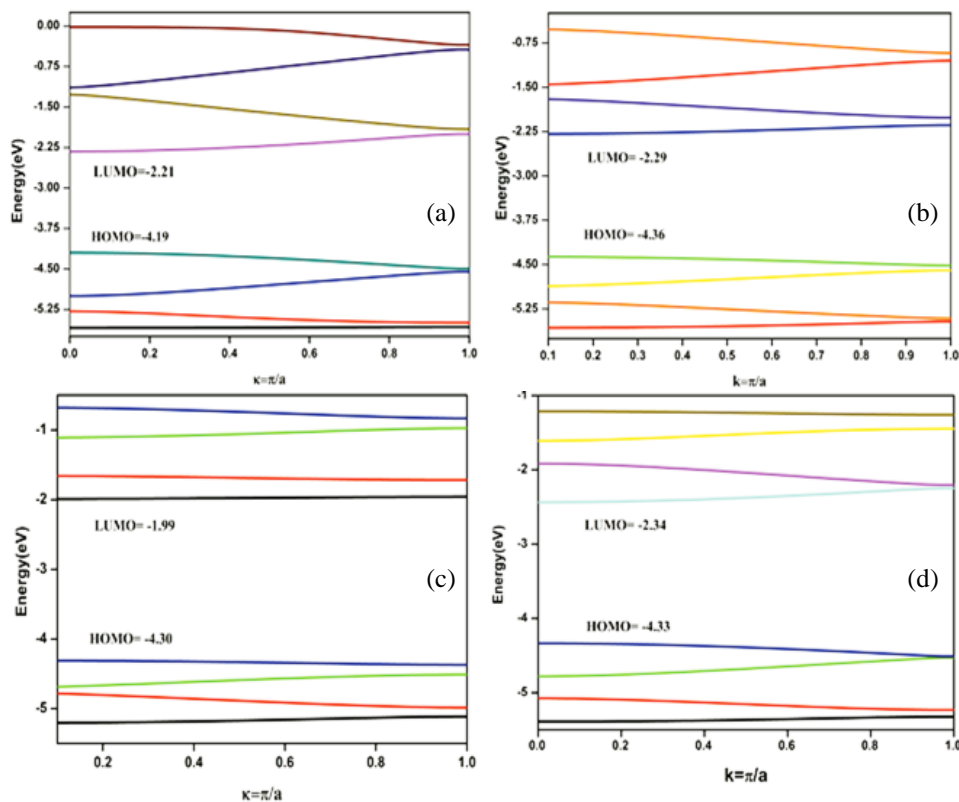
Figure 2.4: Band structure of (a) MD-CA-PPV, (b) MD-FL-PPV, (c) MD-PT-PPV and (d) MD-AN-PPV by HSE06/6-31G method
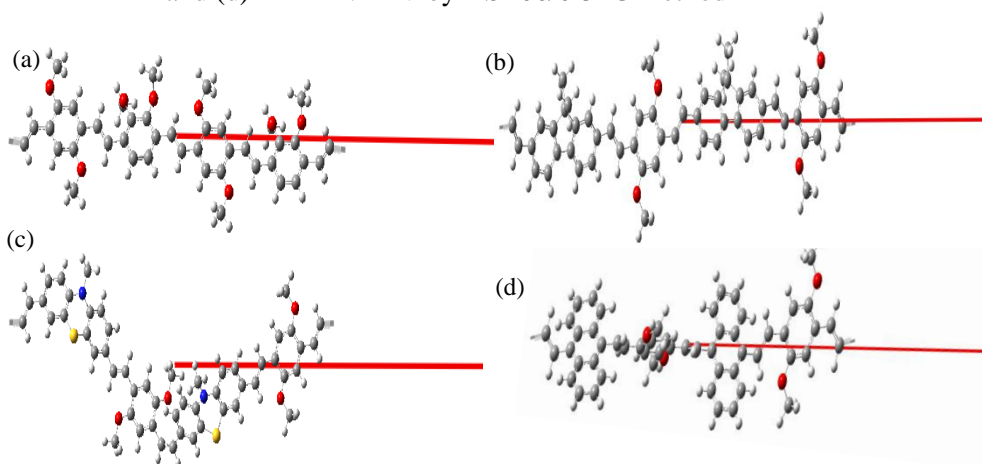
Figure 2.5: Unit cell of (a) MD-CA-PPV, (b) MD-FL-PPV, (c) MD-PT-PPV and (d) MD-AN-PPV for the PBC/HSE06/6-31G calculation. The red line represents the translational vector

The band structure data, ionization potential and electron affinity of the copolymers are summarized in Table 2.2.

Table 2.2: Computational data of MD-CA-PPV, MD-FL-PPV, MD-PT-PPV and MD-AN-PPV with DFT/HSE06/6-31G[a] and DFT/B3LYP/6-31G[b] methods

Polymer	HOMO (eV)	IP (eV)	LUMO (eV)	EA (eV)	Eg (eV)
MD-CA-PPV	-4.19[a]	4.19	-2.21	2.21	1.98
	-4.31[b]	4.31	-2.03	2.03	2.28
MD-FL-PPV	-4.36[a]	4.36	-2.29	2.29	2.07
	-4.48[b]	4.48	-2.00	2.00	2.47
MD-PT-PPV	-4.30[a]	4.30	-1.99	1.99	2.31
	-4.44[b]	4.44	-1.71	1.71	2.73
MD-AN-PPV	-4.33[a]	4.33	-2.34	2.34	1.99
	-4.47[b]	4.47	-2.12	2.12	2.34

[a] Estimated from DFT/HSE06/6-31G calculation.
[b] Estimated from DFT/B3LYP/6-31G calculation.

The band gap of the copolymers MD-CA-PPV, MD-FL-PPV, MD-PT-PPV and MD-AN-PPV were obtained to be 1.98, 2.07, 2.31 and 1.99 eV respectively using DFT/HSE06 and 2.28, 2.47, 2.73 and 2.34 eV using DFT/B3LYP methods. A noteworthy difference was observed between the band gap values obtained from these two methods. In order to improve computational efficiency, the first method, HSE06, which used an error function screened coulomb potential to calculate the exchange portion of the energy was fixed.[31] This screened-hybrid functionals such as the HSE approach reduces self-interaction errors in systems possessing both localized and delocalized orbitals and could be applied to both finite and extended systems reported by Marom *et al.*[47,48] The Ionization potential

(negative of HOMO energy) and the electron affinity (negative of LUMO energy) were also calculated and summarized in Table 2.2.

2.2.3 Synthesis of monomers and polymers

2.2.3.1 Monomer synthesis

Synthetic route for the synthesis of key monomers are summarized in scheme 2.1. 1,4-bis-(bromomethyl)-2-decyloxy-5-methoxybenzene (MD) was synthesized through the alkylation of 4-methoxyphenol using 1-bromooctane followed by bromomethylation gave the product as off white powder in 92 % yield. The precursor monomer 1,4-bis-(bromomethyl)-2,3-bis(octyloxy)benzene (CA) was synthesized in two steps starting from catechol. First step involved alkylation of catechol followed by bromomethylation using paraformaldehyde and 33 % HBr in glacial acetic acid. Starting from 9,9-di-n-octylflourene, 2,7-bis(bromomethyl)-9,9-dioctyl-9H-fluorene (FL) was prepared by bromomethylation using paraformaldehyde and 33 % HBr in glacial acetic acid. To obtain 3,7-bis(bromomethyl)-10-octyl-10H-phenothiazine (PT), phenothiazine was treated with 1-bromooctane followed by bromomethylation which gave the product as a green powder in 74 % yield. 9,10-bis(bromomethyl)anthracene (AN) was synthesized from anthracene by bromomethylating it with paraformaldehyde and 33 % HBr in glacial acetic acid. The structure of the monomers were confirmed by ^{1}H NMR spectrum and are depicted in Figure 2.6.
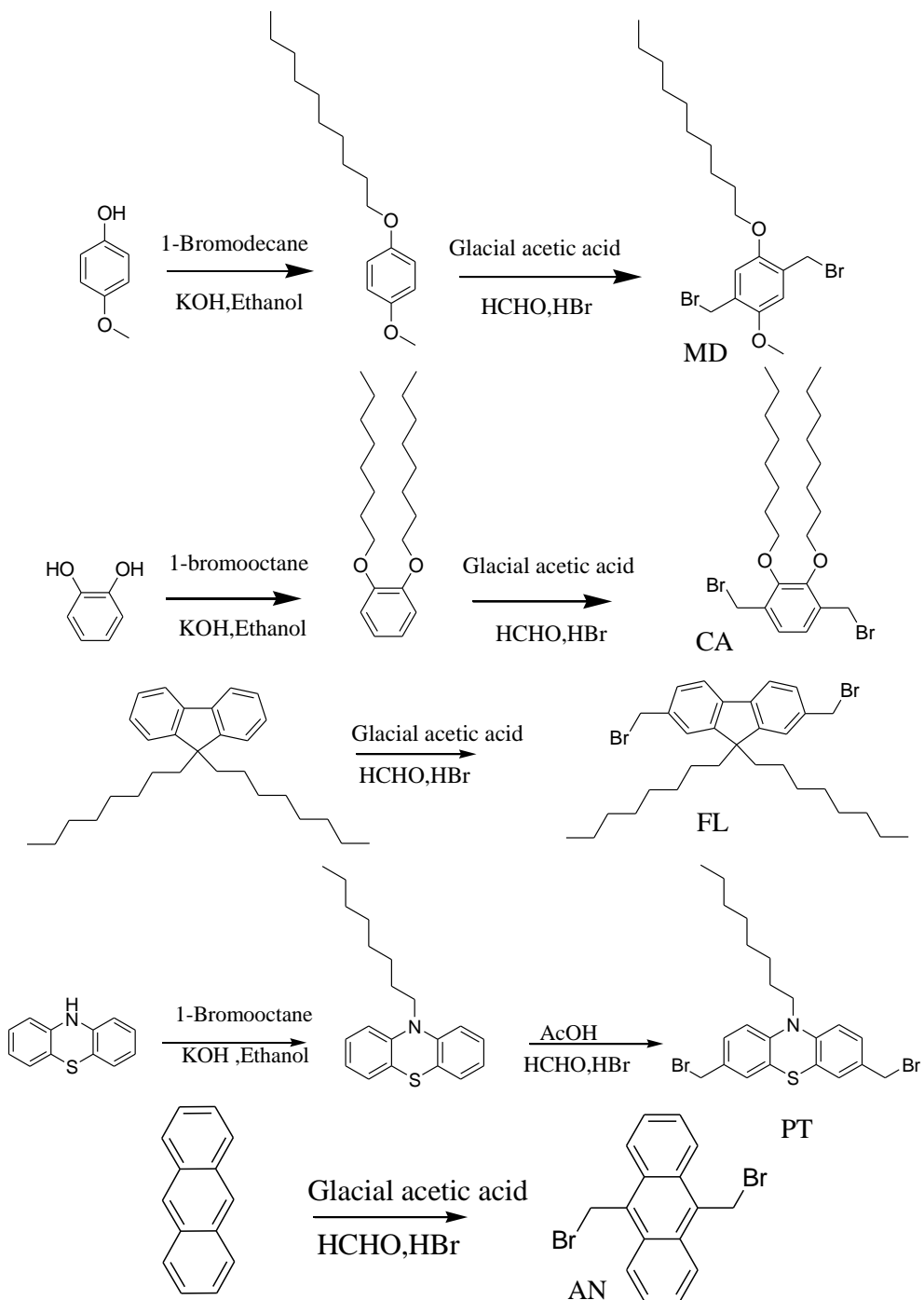
Scheme 2.1: Synthesis of monomers
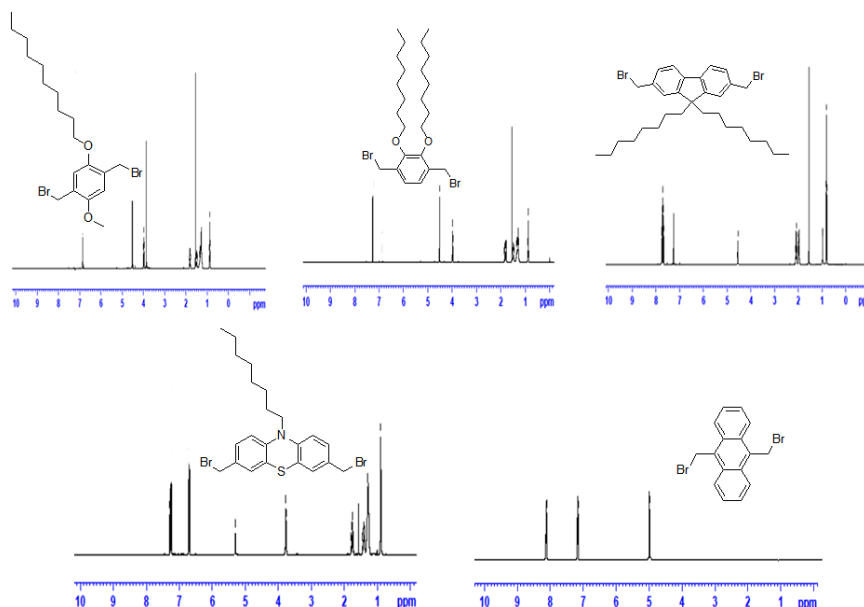
Figure 2.6: ^{1}H NMR spectra of monomers

2.2.3.2 Polymer synthesis

The synthesis of copolymers were carried out by Gilch polymerisation method using potassium t-butoxide as base in dry THF at room temperature. The PPV based copolymers attained satisfactory yield by following the synthetic routes outlined in Scheme 2.2. The copolymers MD-CA-PPV, MD-FL-PPV, MD-PT-PPV and MD-AN-PPV were synthesized through copolymerisation of 1,4-bis-(bromomethyl)-2-decyloxy-5-methoxybenzene (MD) with 1,4-bis-(bromomethyl)-2,3-bis(octyloxy)benzene (CA), 2,7-bis (bromomethyl)-9,9-dioctyl-9H-fluorene (FL), 3,7-Bis-(bromomethyl)-10-octyl-10H-phenothiazine (PT) and 9,10-bis-(bromomethyl)anthracene (AN) respectively. The resulting copolymers were purified by precipitating in methanol. The precipitate was filtered followed by soxhlet extraction using methanol and hexane to remove the oligomers. All the copolymers were readily

soluble in common organic solvents such as chloroform, tetrahydrofuran and toluene.

The copolymer structures were confirmed by ^{1}H NMR, FT-IR and GPC analysis. The number average and weight average molecular weights ($\overline{\text{Mn}}$ and $\overline{\text{Mw}}$) of the copolymers were determined by GPC analysis. The copolymers showed $\overline{\text{Mn}}$ in the range of 30000-40000 g/mol and $\overline{\text{Mw}}$ in the range of 50000-80000 g/mol with a polydispersity index of 1.6-1.9 using THF as eluent and polystyrene as the standard. Molecular weight and yield of the copolymers are given in Table 2.3. The ^{1}H NMR spectra of the copolymers showed broad peaks between 8.5 and 6.3 ppm which were assigned to aromatic and vinylic protons (Fig. 2.7). The -OCH$_2$ groups appeared between 4.1 and 3.5 ppm. The aliphatic protons showed a broad peak between 1.7 and 0.9 ppm. All other peaks exhibited good correspondence with the chemical structure of the copolymers. The copolymer MD-PT-PPV was only slightly soluble in CDCl$_3$ which resulted in less intense peaks.

TIR data for MD-CA-PPV, MD-FL-PPV, MD-PT-PPV and MD-AN-PPV showed (KBr pellet, cm^{-1}): 3000-3100 (alkenyl C–H), 2950-2990 (asymmetric C–H stretch in CH$_3$ group), 2900-2930 (asymmetric C–H stretch in CH$_2$ group), 2800-2860 (symmetric C–H stretch in CH$_2$ group), 1600-1630 (C=C stretch), 1500-1525 (C–C ring stretch), 1455 (asymmetric C–H bending in CH$_3$ group), 1400-1420 (Ring stretch and C–H deformation), 1300-1350 (C–C stretch and C–H deformation), 1230-1250 (aryl–alkyl ether (C–O–C) asymmetric stretch), 1200-1210 (ring stretch and C–H deformation), 1010-1040 (aryl–alkyl ether (C–O–C) symmetric stretch). In the copolymers, the bands showed the presence of both Z (700-810 cm^{-1}) and E (910-990 cm^{-1}) vinylic absorptions.
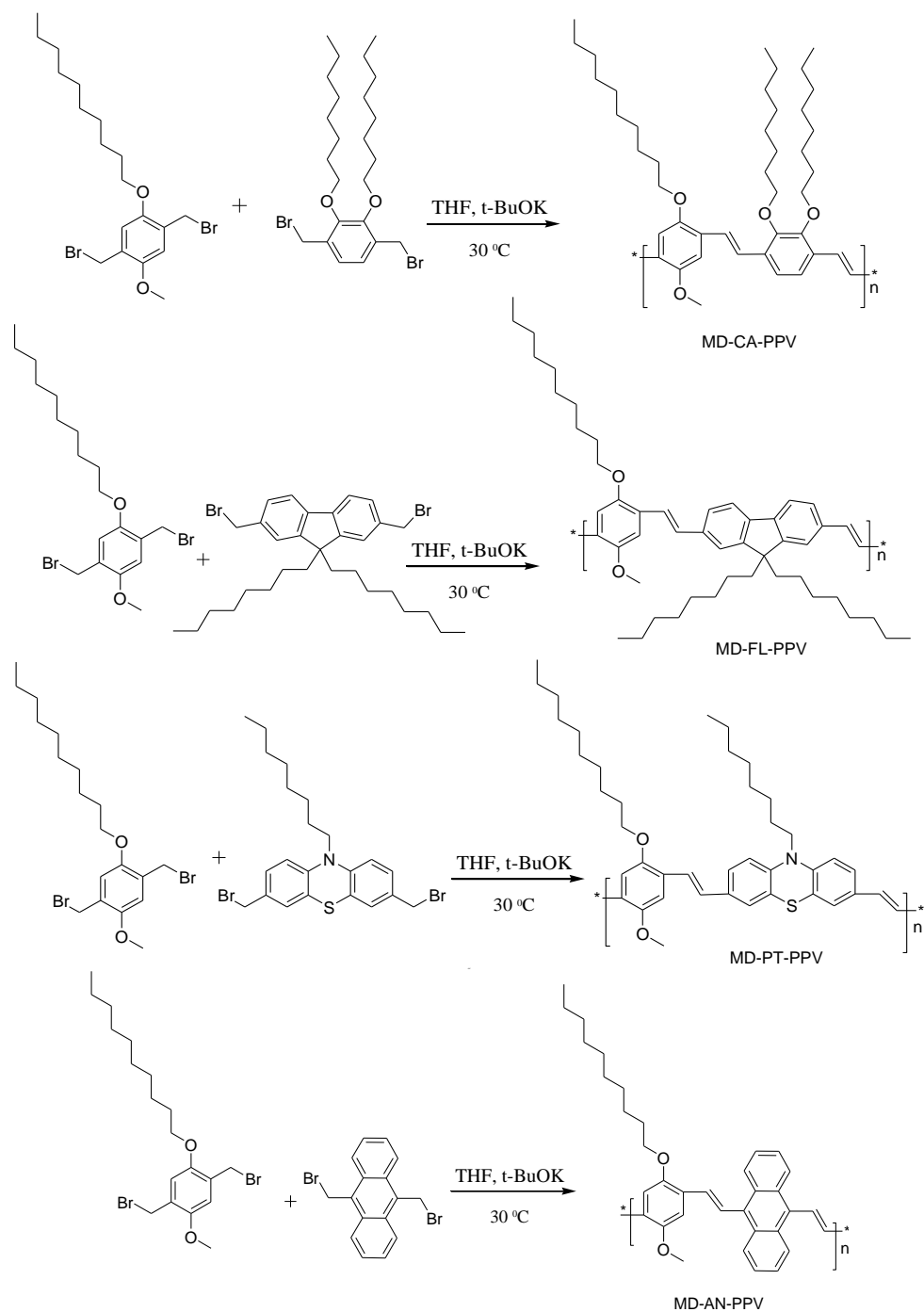
Scheme 2.2: Synthesis of polymers
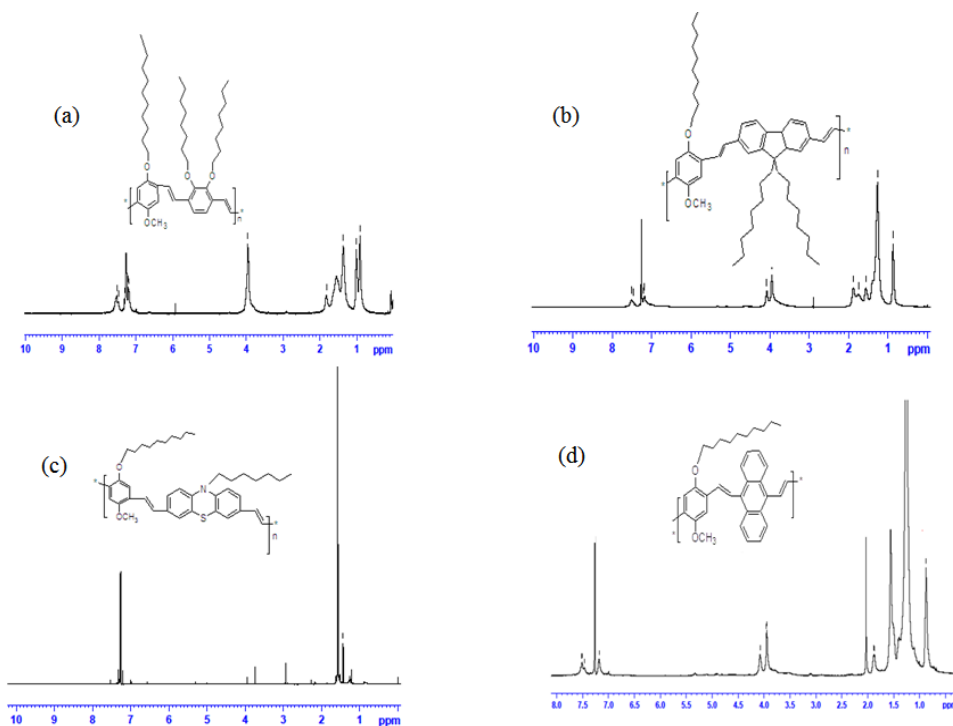
Figure 2.7: ^{1}H NMR Spectra of (a) MD-CA-PPV (b) MD-FL-PPV(c) MD-PT-PPV and (d) MD-AN-PPV

Table 2.3: Results of polymerization

Copolymer	$M_n{}^a$	$M_w{}^a$	PDI	Yield (%)
MD-CA-PPV	45682	87413	1.91	86
MD-FL-PPV	33916	56908	1.68	84
MD-PT-PPV	45742	73382	1.60	79
MD-AN-PPV	82679	83907	1.80	88

[a] Determined by GPC in THF based on polystyrene standards

2.2.4 Thermal properties

The onset degradation and the degradation temperature were determined by thermogravimetric analysis (TGA) in nitrogen atmosphere at a heating rate of 10 °C/min. From the TG curves of the synthesized copolymers, it was clear that the polymer showed single degradation pattern (Figure 2.8). The

copolymers exhibited high thermal stability as shown in the TG curves. The onset of weight loss temperature of MD-CA-PPV, MD-FL-PPV, MD-PT-PPV and MD-AN-PPV were 391, 420, 389 and 409 ^{o}C respectively. DTG traces showed that the onset of degradation and the degradation temperature of MD-CA-PPV were found to be around 350 ^{o}C and 435 ^{o}C with 5 % weight loss as the onset loss point. In MD-FL-PPV, the onset of degradation was around 335 ^{o}C and the degradation temperature was 429 °C with about 6 % weight loss. In the case of MD-PT-PPV and MD-AN-PPV the onset of degradation was around 373 ^{o}C, 343 ^{o}C and the degradation temperature was 416 ^{o}C, 445 ^{o}C respectively with 12 % and 5 % weight loss at the onset loss point.
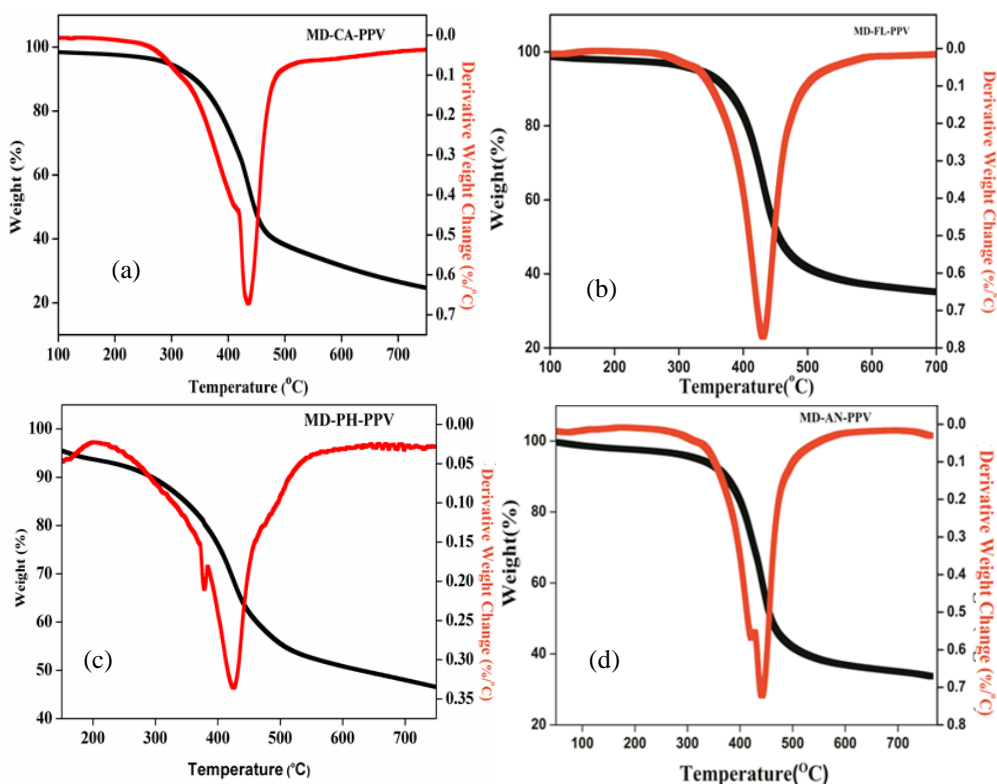
Figure 2.8: TG-DTG traces of the copolymers (a) MD-CA-PPV (b) MD-FL-PPV (c) MD-PT-PPV and (d) MD-AN-PPV

The TGA result showed that the copolymers have excellent thermal stability, much higher than those of MEHPPV and cyclohexyl or phenyl silyl-substituted PPVs.[49] This higher degradation temperature of the copolymers in comparison to MEHPPV may be due to the more closely packed structure of PPV chains upon the incorporation of flourene, phenothiazine, or anthracene monomer units. The high thermal stability of the copolymers could prevent the deformation and degradation of the active layer during the high temperature sealing procedures in device fabrication.

2.2.5 Optical properties

To study the optical absorption, the UV–Vis absorption spectra of PPV polymers in the range of 300–700 nm were recorded in THF and are shown in Fig. 2.9. The absorption of polymers ranged from 400 to 650 nm. The onset edge of the lower energy peak of the polymer in THF solution was obtained from the UV–Vis absorption data which was found to be 631, 610, 617 and 625 nm for MD-CA-PPV, MD-FL-PPV, MD-PT-PPV and MD-AN-PPV respectively. The optical band gap of copolymers was determined from the onset of absorption using Tauc's equation.[50] The band gap of the copolymers, MD-CA-PPV, MD-FL-PPV, MD-PT-PPV and MD-AN-PPV were calculated to be 1.96, 2.03, 2.01 and 1.98 eV respectively. The strong absorption of the PPV copolymers in the visible region was attributed to the enhanced HOMO-LUMO overlap, resulting from the delocalized molecular orbital density for both HOMO and LUMO wave functions of the polymers.
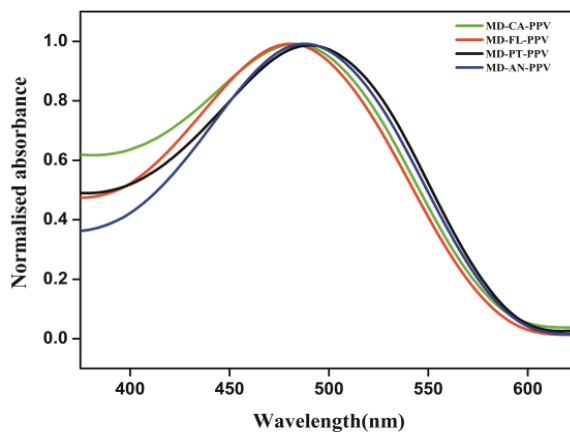
Figure 2.9: Absorption spectra of MD-CA-PPV, MD-FL-PPV, MD-PT-PPV and MD-AN-PPV in THF solution

Figure 2.10 presents the emission spectra of MD-CA-PPV, MD-FL-PPV, MD-PT-PPV and MD-AN-PPV in THF medium and excitation wavelength 370 nm. The emission peaks of the copolymers were observed at the wavelength of 550–590 nm respectively. The optical properties of the polymers are listed in Table 2.4.
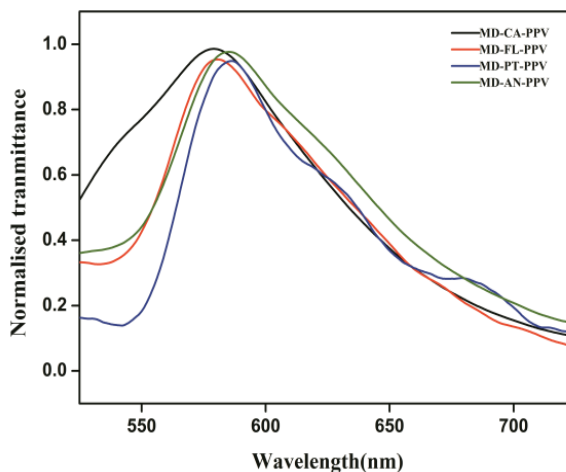
Figure 2.10: Emission spectra of MD-CA-PPV, MD-FL-PPV, MD-PT-PPV and MD-AN-PPV in THF solution at excitation wavelength 370 nm

Table 2.4: Optical properties of polymers in THF solution

Polymer	Absorption λ_{max} (nm)	Absorption onset (nm)	Emission λ_{max} (nm)	E_g (Optical) (eV)
MD-CA-PPV	483	631	580	1.96
MD-FL-PPV	480	610	577	2.03
MD-PT-PPV	490	617	587	2.01
MD-AN-PPV	487	625	584	1.98

2.2.6 Electrochemical studies

To determine the highest occupied molecular orbital (HOMO) and lowest unoccupied molecular orbital (LUMO) level of the PPV polymers, which are important for the construction of photovoltaic devices, Cyclic Voltammetry (CV) was carried out. The electrochemical process probed by cyclic voltammetry was performed with a solution of tetrabutylammonium hexafluoroborate (Bu_4NBF_6, 0.10 M) (supporting electrolyte) in anhydrous acetonitrile at a scan rate of 100 mV/s at room temperature under nitrogen atmosphere. Platinum electrode coated with the thin polymer film was used as the working electrode, Pt wire and Ag/Ag+ electrode were used as the counter and reference electrodes, respectively. The redox behaviour of the copolymers is summarized in Table 2.5. The HOMO and LUMO energy levels of four copolymers were measured from the onset potentials for oxidation and reduction according to the equation proposed by Bredas.[51] The onset oxidation potential of MD-CA-PPV, MD-FL-PPV, MD-PT-PPV and MD-AN-PPV were 0.27, 0.69, 0.29 and 0.26 eV respectively. The onset reduction potential was calculated to be -1.24, -0.75, -0.93 and -0.78 eV, for MD-CA-PPV, MD-FL-PPV, MD-PH-PPV and MD-AN-PPV, respectively. The HOMO and LUMO levels were calculated using the empirical formula.

HOMO (IP; ionization potential) = - (4.71 +E_{ox}^{onset}) .... (2.1)

LUMO (EA; electron affinity)   = - (4.71 +E_{red}^{onset}) .... (2.2)

The electrochemical band gap of the copolymers were calculated and found to be 1.50, 1.44, 1.22 and 1.04 eV for MD-CA-PPV, MD-FL-PPV, MD-PT-PPV and MD-AN-PPV respectively. The deviation of electrochemical band gap compared to optical and theoretical band gap is due to the difference in the mechanism of optical excitation and electrochemical oxidation and reduction processes. In the former process, excitation creates excitons (bound electrons and hole pair) and the latter process creates ions. The low energy of excitons compared to the ions and solvation of the ions in the electrochemical experiment were reflected in the observed electrochemical band gap.

Table 2.5: Redox properties of MD-CA-PPV, MD-FL-PPV, MD-PT-PPV and MD-AN-PPV

Polymer	E_{ox} (V)	HOMO (eV)	E_{red} (V)	LUMO (eV)	Band Gap (eV)
MD-CA-PPV	0.27	-4.98	-1.24	-3.48	1.50
MD-FL-PPV	0.69	-5.40	-0.75	-3.97	1.44
MD-PT-PPV	0.29	-5.00	-0.93	-3.79	1.22
MD-AN-PPV	0.26	-4.97	-0.78	-3.93	1.04

2.2.7 Time resolved fluorescence measurements

A time correlated single photon counting (TCSPC) setup was used to measure the fluorescence decay of PPV based copolymers. In the time resolved fluorescence decay experiment, the polymer was excited by a laser

pulse; it began with high intensity and then decayed, rapidly. TCSPC is a sensitive method for determining very low emission from a sample on nanosecond time scale and longer. A fluorescence decay curve from the appropriate fitted functions obtained from the TCSPC measurement is used to extract type of decay, fluorescence lifetime and amplitudes of the copolymer. The copolymers MD-CA-PPV, MD-FL-PPV, MD-PT-PPV and MD-AN-PPV in $CHCl_3$ were excited at 340 nm. The observed decay could not fit well with the single exponential fit. In the case of PPV polymers, the fluorescence decay curve was obtained using bi-exponential fitting due to the existence of different fluorescing moieties with distinct lifetimes. The τ_1 and τ_2 are the lifetimes, and the α_1 and α_2 are the pre-exponential factors. The average lifetime of MD-CA-PPV, MD-FL-PPV, MD-PT-PPV and MD-AN-PPV was obtained to be 4.73, 3.97, 3.91 and 3.76 ns respectively. The bi-exponential fitted decay curves of copolymers in $CHCl_3$ solution are shown in Fig. 2.11. The magnitude of the decay times of the phenylene vinylene based copolymers across the emission wavelength and quantum yields are summarized in the Table 2.6. PPV derivatives have displayed promising properties in the development of photovoltaic devices as donor moieties due to their chemical stability together with stabilized photoexcited state by charge delocalization in the aryl substituents. Zhou *et al.* reported that the introduction of benzimidazole derivatives in the phenyl ring of the triphenylamine core increased the molar extinction coefficients due to the increased π-conjugation, and photovoltaic performance was improved when compared to the unsubstituted counterpart.[52] In general, electron-donating groups induce an increase in the molar absorption coefficient and enhance the fluorescence efficiency.[53, 54]
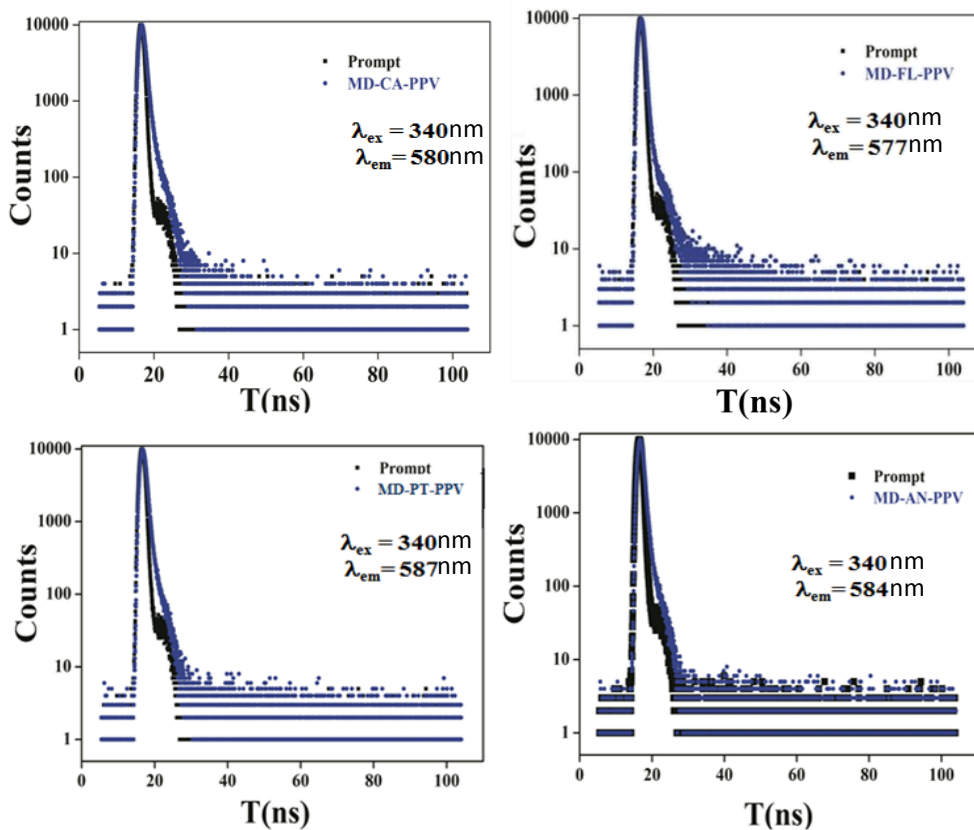
Figure 2.11: Bi-exponential fitted decay curves of MD-CA-PPV, MD-FL-PPV, MD-PT-PPV and MD-AN-PPV in $CHCl_3$ at 340 nm excitation

The quantum yield (ϕ^d) of the polymer is the ratio between the number of photons emitted and the number of photons absorbed under optical excitation. It is one of the major parameters characterizing fluorescent organic materials. The quantum yield of the copolymers measured with the same excitation wavelength were obtained to be 0.59, 0.69, 0.65 and 0.71 for MD-CA-PPV, MD-FL-PPV, MD-PT-PPV and MD-AN-PPV respectively. All the PPV polymers showed high quantum efficiency; which revealed the suitability of the copolymers to be used as active components in optical

devices. The "absolute" method was used for the accurate ϕ determination; it was based on collecting the whole spatially distributed fluorescence emission.[55]

Table 2.6: Fluorescence lifetimes, pre-exponential factor and quantum yield of MD-CA-PPV, MD-FL-PPV, MD-PT-PPV and MD-AN-PPV in CHCl$_3$ at 340 nm excitation

Polymer	χ^2	τ_1 (ns)	α_1 %	τ_2 (ns)	α_2 %	τ_{av} (ns)	ϕ^d
MD-CA-PPV	1.33	0.41	82.29	1.63	17.71	4.73	0.59
MD-FL-PPV	1.08	0.25	77.87	0.86	20.37	3.97	0.69
MD-PT-PPV	1.10	0.33	79.21	1.26	20.79	3.91	0.65
MD-AN-PPV	1.06	0.32	78.37	1.14	21.63	3.76	0.71

2.2.8 Solvatochromic effect

The study of the effect of solvents on the absorption and fluorescence spectra of π-conjugated polymers reveals information on the electronic and geometric structure of the polymers in the excited state. The solvatochromic method is based on a linear correlation between the wave numbers of the absorption and fluorescence maxima with solvent polarity function which involves dielectric constant (ε) and refractive index (n) of the medium. The experimental determination of the ground and excited state dipole moments is based on the analysis of solvatochromism. The dipole moment of the excited organic polymers is useful in the extraction of parameters like molecular polarizability in nonlinear optical materials [56] using electrooptic methods and also in the design of new molecules. In the present study, the absorption and fluorescence maxima of the copolymers MD-CA-PPV, MD-FL-PPV, MD-PT-PPV and MD-AN-PPV were measured in toluene /

acetonitrile mixtures of varying polarity. The following two solvatochromic methods were used to determine the ground and excited state dipole moments of the PPV based copolymers.

2.2.9 Evaluation of ground state and excited state dipole moments

2.2.9.1 Method 1

The two independent equations used for the estimation of excited state dipole moments of the PPV polymers are as follows:

Bakshiev's equation [57]

$$\left(v_a - v_f\right) = m_1\, f(\varepsilon,n) + constant \quad \text{...(2.3)}$$

Kawski-Chamma-Viallet's equation [58,59]

$$\left(v_a + v_f\right) = m_2\, f_1(\varepsilon,n) + constant \quad \text{....................................(2.4)}$$

Where v_a and v_f are absorption and fluorescence wavelength maxima of the copolymers in solvents of varying polarity respectively. The expressions for f(ε,n) [Bakshiev's polarity equation] and f$_1$(ε,n) [Kawski-Chamma-Viallet's polarity equation] are given as :

$$f(\varepsilon,n) = \left[\frac{\varepsilon-1}{\varepsilon+1} - \frac{n^2-1}{n^2+2}\right]\left(\frac{2n^2+1}{n^2+2}\right) \quad \text{..(2.5)}$$

$$f_1(\varepsilon,n) = \frac{2n^2+1}{2(n^2+2)}\left[\frac{\varepsilon-1}{\varepsilon+1} - \frac{n^2-1}{n^2+2}\right] + \frac{3(n^4-1)}{2(n^2+2)^2} \quad \text{.............................(2.6)}$$

The symbols ε and n are dielectric constant and refractive index of toluene and acetonitrile mixtures of varying polarity respectively.

From Eqs. 2.5 & 2.6, it follows that $\left(\nu_a - \nu_f\right)$ versus f(ε,n) and $\left(\nu_a + \nu_f\right)$ versus f_1(ε,n) should give linear graphs with slopes m_1 and m_2 respectively and are given as

$$m_1 = \frac{2(\mu_e - \mu_g)^2}{hca^3}$$ .... (2.7)

$$m_2 = \frac{2(\mu_e^2 - \mu_g^2)}{hca^3}$$ .... (2.8)

Where μ_g and μ_e are the ground and excited state dipole moments of the copolymers. '*h*' being Planck's constant , 'c' is the velocity of light in vacuum and 'a' is the Onsager radius of the solute molecule. The Onsager radius can be calculated using the density (d) and the molecular weight (M) of the polymer using the relation:[60]

$$a^3 = \frac{3M}{4\pi d N_A}$$ ....(2.9)

Assuming that the ground and excited states are parallel, [61] the values of μ_g and μ_e calculated from eqns. (2.7) and (2.8) can be given as,

$$\mu_g = \frac{m_2 - m_1}{2}\left[\frac{hca^3}{2m_1}\right]^{\frac{1}{2}}$$ ....(2.10)

$$\mu_e = \frac{m_2 + m_1}{2}\left[\frac{hca^3}{2m_1}\right]^{\frac{1}{2}}$$ ....(2.11)

The parameters m_1 and m_2 can be determined from the slopes occurring for the difference $\left(\nu_a - \nu_f\right)$ and the sum $\left(\nu_a + \nu_f\right)$ of the wave-numbers

which are linear functions of the solvent polarity parameters f (ε, n) and f_1 (ε, n). Even small errors in the estimated value of the Onsager cavity radius results in large errors as the value enters as cubed in the above equations.

2.2.9.2 Method 2

In the second method, the solvatochromic measurements are based on the microscopic dimensionless solvent polarity parameter E_T^N proposed by Reichardt,[62] which is given by equation 2.12.

$$E_T^N = \frac{E_T(solvent) - 30.7}{32.4}$$ .... (2.12)

Where,

$$E_T(solvent) = \frac{28591}{\lambda_{max}}$$ .... (2.13)

Here, λ_{max} corresponds to the absorption maxima of the molecule 2,6-diphenyl-4-(2,4,6-triphenyl-N-pyridino)phenolate[34] also called Reichardt's dye which shows a large solvatochromic effect. The absorption maxima of the Reichardt's dye in toluene/acetonitrile mixtures of varying polarity were experimentally determined and used for the calculation of empirical polarity parameter E_T^N. The second method gave better results rather than the traditionally used bulk solvent polarity functions involving dielectric constant (ε) and refractive index (n). Using the Molecular-Microscopic solvent polarity parameter (E_T^N), the error in the estimation of the Onsager cavity radius has been minimized; it also includes intermolecular solute/solvent hydrogen bond donor/acceptor interactions along with solvent polarity.

For the determination of change in dipole moment ($\Delta\mu$), the Stoke's shift ($\nu_a - \nu_f$) was calculated from the absorption and fluorescence spectra of the copolymers in toluene/acetonitrile mixtures of varying polarity. The theoretical basis for the correlation of the spectral band shift was developed by Ravi *et al.*[63] according to Eq. (2.14).

$$\nu_a - \nu_f = 11307.6 \left(\frac{\Delta\mu^2 \, a_D^3}{\Delta\mu_D^2 \, a^3}\right) E_T^N + constant \quad ....(2.14)$$

Here, $\Delta\mu$ is the difference between the ground and excited state dipole moments of the polymer being studied and 'a' is the Onsagar radius of the polymer calculated using the equation (2.9). $\Delta\mu_D$ (9D) and a_D (6.2Å) are the change in dipole moment and Onsager radius of Reichardt's dye.

The change in dipole moment of the copolymer can be evaluated from the slope (m) of the Stokes shift versus E_T^N plot and is given by the equation

$$\Delta\mu = \sqrt{\frac{m \times 81}{\left(\frac{6.2}{a}\right)^3 \times 11307.6}} \quad ....(2.15)$$

The solvent polarity function values E_T^N, f (ε, n) and f_1 (ε, n) for toluene/acetonitrile mixtures of varying polarity are presented in Table 2.7 respectively.

Table 2.7: Calculated values of polarity functions for Reichardt's dye in toluene/ acetonitrile mixtures of varying polarity

Fraction of acetonitrile (%)	ε	n	E_T^N	f(ε,n)	f_1(ε,n)
100	37.50	1.344	0.483	0.863	1.331
90	35.68	1.359	0.467	0.854	1.343
80	33.65	1.374	0.455	0.844	1.353
70	31.39	1.389	0.438	0.832	1.362
60	28.83	1.404	0.422	0.818	1.368
50	25.92	1.420	0.397	0.801	1.371
40	22.59	1.435	0.389	0.778	1.368
30	18.74	1.450	0.358	0.744	1.354
20	14.22	1.465	0.318	0.687	1.317
10	8.85	1.480	0.284	0.564	1.214
0	2.38	1.496	0.136	0.029	0.699

2.2.9.3 Solvatochromic measurements

The absorption and emission spectra of the copolymers in solvents of varying polarity were needed for the analysis. The present study used a binary solvent mixture comprising of polar solvent acetonitrile and the nonpolar solvent toluene to get gradual variation of polarity of solvent.[64] For the analysis of data, only solvent mixtures showing linear variation of the polarity parameters were used. The absorption and fluorescence spectra of the copolymers MD-CA-PPV, MD-FL-PPV, MD-PT-PPV and MD-AN-PPV in toluene/ acetonitrile mixtures of varying polarity are shown in Fig. 2.12.
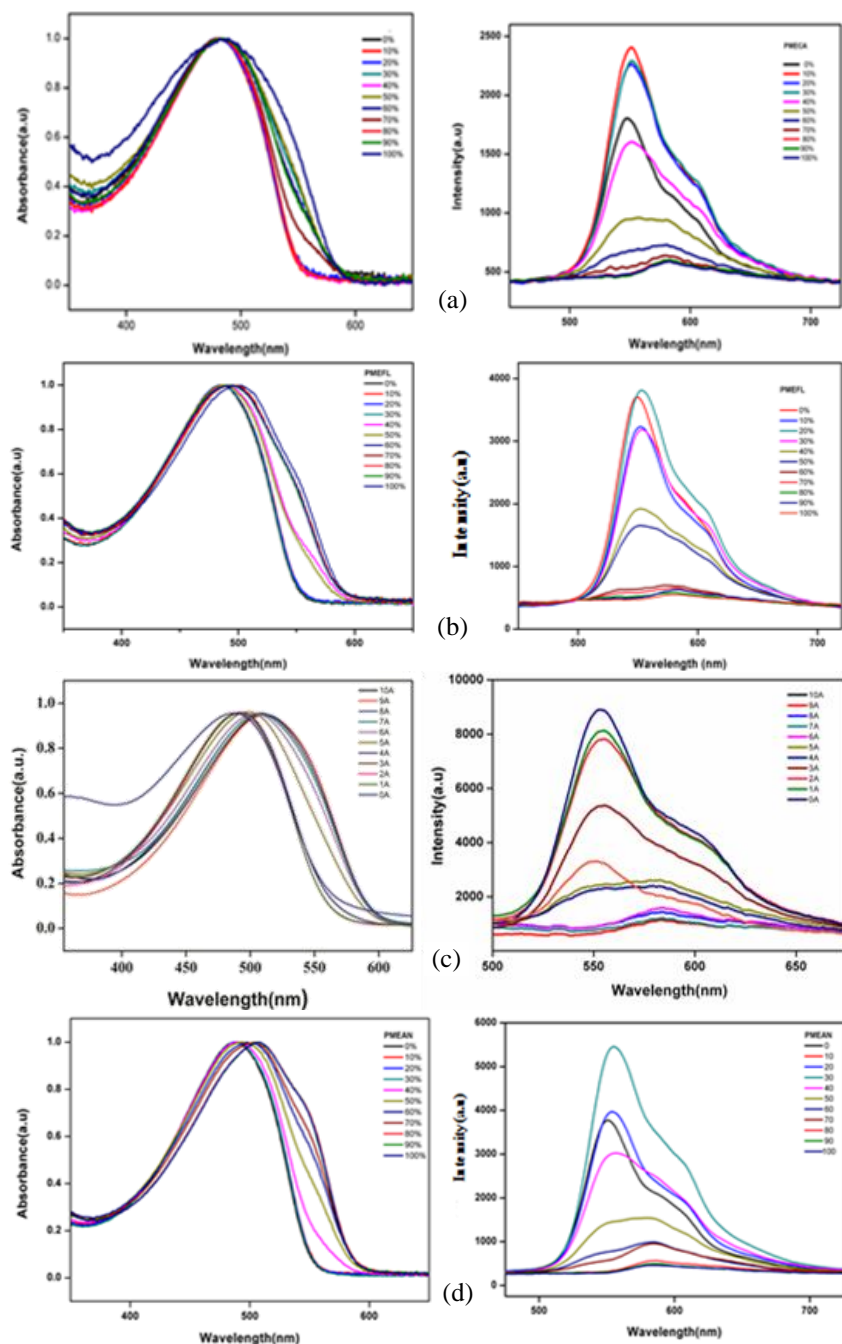
Figure 2.12: The absorption and fluorescence spectra of (a) MD-CA-PPV, (b) MD-FL-PPV, (c) MD-PT-PPV and (d) MD-AN-PPV in toluene/ acetonitrile mixtures of varying Polarity

The solvatochromic data of the copolymers are summarized in the Table 2.8-2.11. Eleven ratios of toluene/ acetonitrile mixtures with dielectric constants varying from 2.38 to 37.50 were used.

Table 2.8: Solvatochromic data of MD-CA-PPV in toluene/acetonitrile mixtures of varying polarity

Weight fraction of acetonitrile (%)	Abs max (nm)	$\bar{\nu}_a$ (cm^{-1})	Emission max (nm)	$\bar{\nu}_f$ (cm^{-1})	$\bar{\nu}_a - \bar{\nu}_f$ (cm^{-1})	$\bar{\nu}_a + \bar{\nu}_f$ (cm^{-1})
100	490	20408	583.7	17131	3276	37539
90	485	20618	583.3	17143	3474	37762
80	484	20661	582.0	17180	3480	37842
70	484	20661	580.7	17218	3442	37879
60	484	20661	579.5	17255	3405	37917
50	483	20703	557.0	17951	2752	38655
40	482	20746	551.9	18116	2629	38863
30	482	20746	551.9	18116	2629	38863
20	482	20746	550.6	18159	2587	38905
10	481	20790	550.2	18172	2617	38962
0	480	20833	546.8	18286	2547	39119

Table 2.9: Solvatochromic data of MD-FL-PPV in toluene/acetonitrile mixtures of varying polarity

Weight fraction of acetonitrile (%)	Abs max (nm)	$\bar{\nu}_{ab}$ (cm^{-1})	Emission max (nm)	$\bar{\nu}_f$ (cm^{-1})	$\bar{\nu}_a - \bar{\nu}_f$ (cm^{-1})	$\bar{\nu}_a + \bar{\nu}_f$ (cm^{-1})
100	503	19880	583.3	17143	2736	37024
90	496	20161	582.4	17168	2992	37329
80	496	20161	579.0	17268	2892	37430
70	492	20325	578.6	17281	3043	37606
60	490	20408	571.9	17485	2922	37893
50	488	20491	552.8	18089	2402	38580
40	486	20576	551.9	18116	2459	38693
30	487	20533	552.8	18089	2444	38622
20	486	20576	551.9	18116	2459	38693
10	484	20661	551.5	18131	2530	38792
0	483	20703	549.8	18187	2516	38891

Table 2.10: Solvatochromic data of MD-PT-PPV in toluene/acetonitrile mixtures of varying polarity

Weight fraction of acetonitrile (%)	Abs max (nm)	$\bar{\nu}_{ab}$ (cm^{-1})	Emission max (nm)	$\bar{\nu}_f$ (cm^{-1})	$\bar{\nu}_a - \bar{\nu}_f$ (cm^{-1})	$\bar{\nu}_a + \bar{\nu}_f$ (cm^{-1})
100	508	19685	585.8	17069	2615	36754
90	506	19762	584.5	17106	2656	36869
80	505	19801	584.5	17106	2695	36908
70	503	19880	584.5	17106	2774	36987
60	498	20080	583.7	17131	2948	37211
50	493	20283	580.7	17218	3065	37502
40	488	20491	557.0	17951	2540	38442
30	488	20491	555.3	18006	2485	38497
20	488	20491	553.6	18061	2430	38553
10	488	20491	553.6	18061	2430	38553
0	488	20491	550.6	18159	2332	38650

Table 2.11: Solvatochromic data of MD-AN-PPV in toluene/acetonitrile mixtures of varying polarity

Weight fraction of acetonitrile (%)	Abs max (nm)	$\bar{\nu}_{ab}$ (cm^{-1})	Emission max (nm)	$\bar{\nu}_f$ (cm^{-1})	$\bar{\nu}_a - \bar{\nu}_f$ (cm^{-1})	$\bar{\nu}_a + \bar{\nu}_f$ (cm^{-1})
100	513	19493	584.1	17118	2374	36612
90	513	19493	583.7	17131	2361	36624
80	511	19569	583.7	17131	2437	36700
70	508	19685	583.7	17131	2553	36816
60	506	19762	582.4	17168	2594	36931
50	505	19801	579.5	17255	2546	37057
40	496	20161	555.3	18006	2155	38167
30	494	20242	555.3	18006	2236	38248
20	493	20283	555.3	18006	2277	38289
10	493	20283	552.8	18089	2194	38373
0	492	20325	551.5	18131	2194	38456

Figs. 2.13-2.16 show the graphs of E_T^N versus $(v_a - v_f)$, $f(\varepsilon, n)$ versus $(v_a - v_f)$ and $f_1(\varepsilon, n)$ versus $(v_a + v_f)$ for MD-CA-PPV, MD-FL-PPV, MD-PT-PPV and MD-AN-PPV respectively. A linear progression was done and the data were fit to a straight line, corresponding values of the slopes were measured (Table 12). In all cases, the correlation coefficients were larger than 0.95 which indicated a good linearity for the curves with slopes m, m_1 and m_2 with selected number of Stokes shift data points.
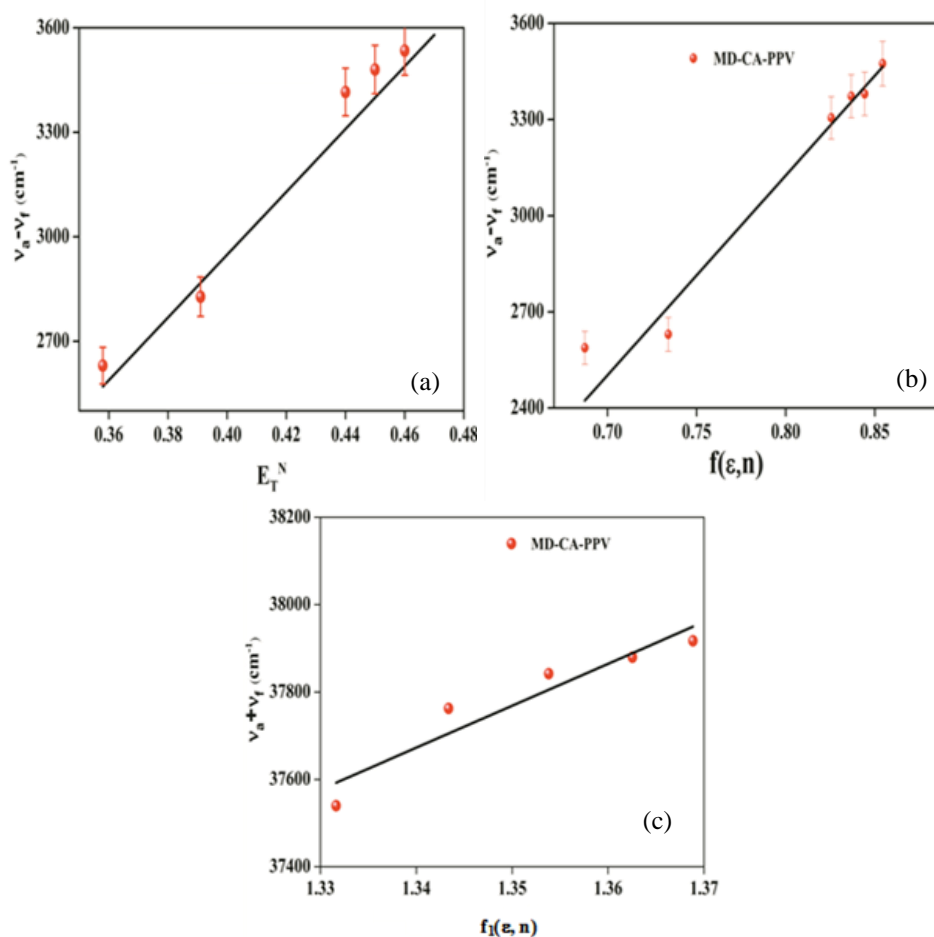
Figure 2.13: The variation of Stoke's shift with (a) E_N^T, (b) $f(\varepsilon, n)$ and (c) arithmetic mean of Stoke's shift $f_1(\varepsilon, n)$ for MD-CA-PPV
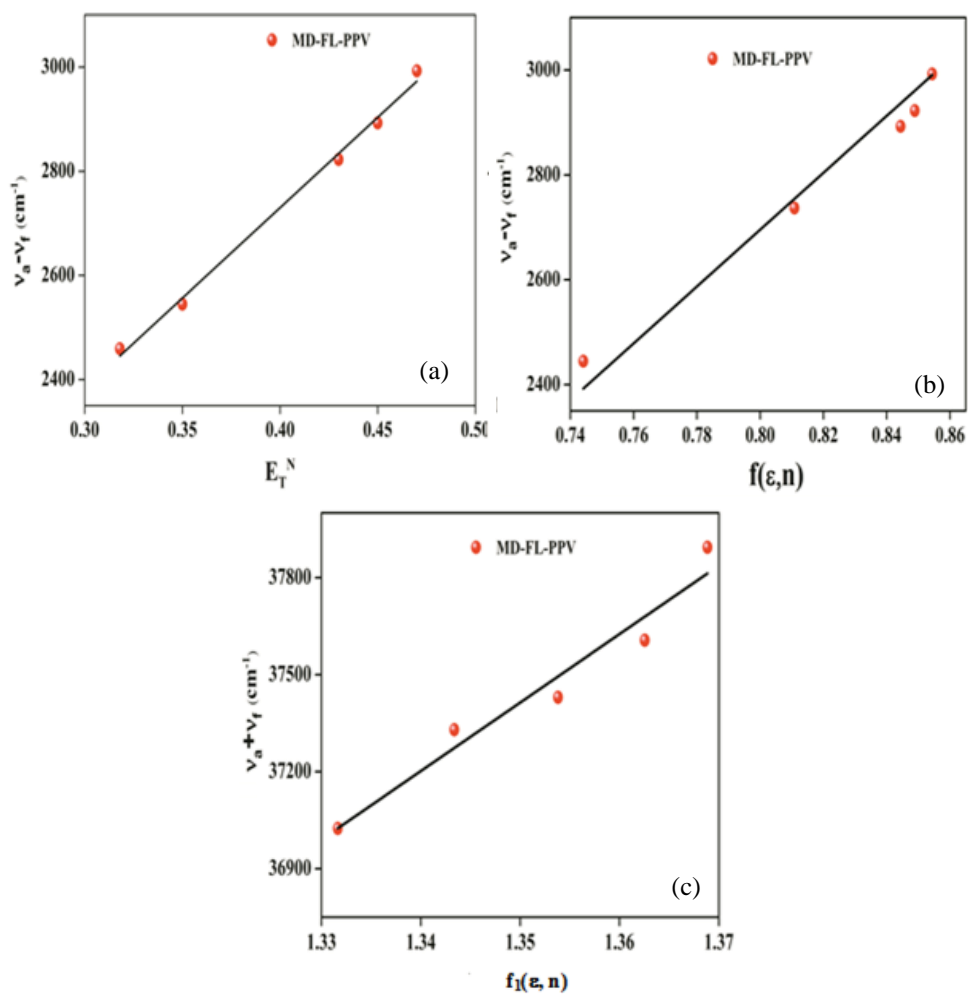
Figure 2.14: The variation of Stoke's shift with (a) E_N^T, (b) f(ε, n) and (c) arithmetic mean of Stoke's shift $f_1(\varepsilon, n)$ for MD-FL-PPV
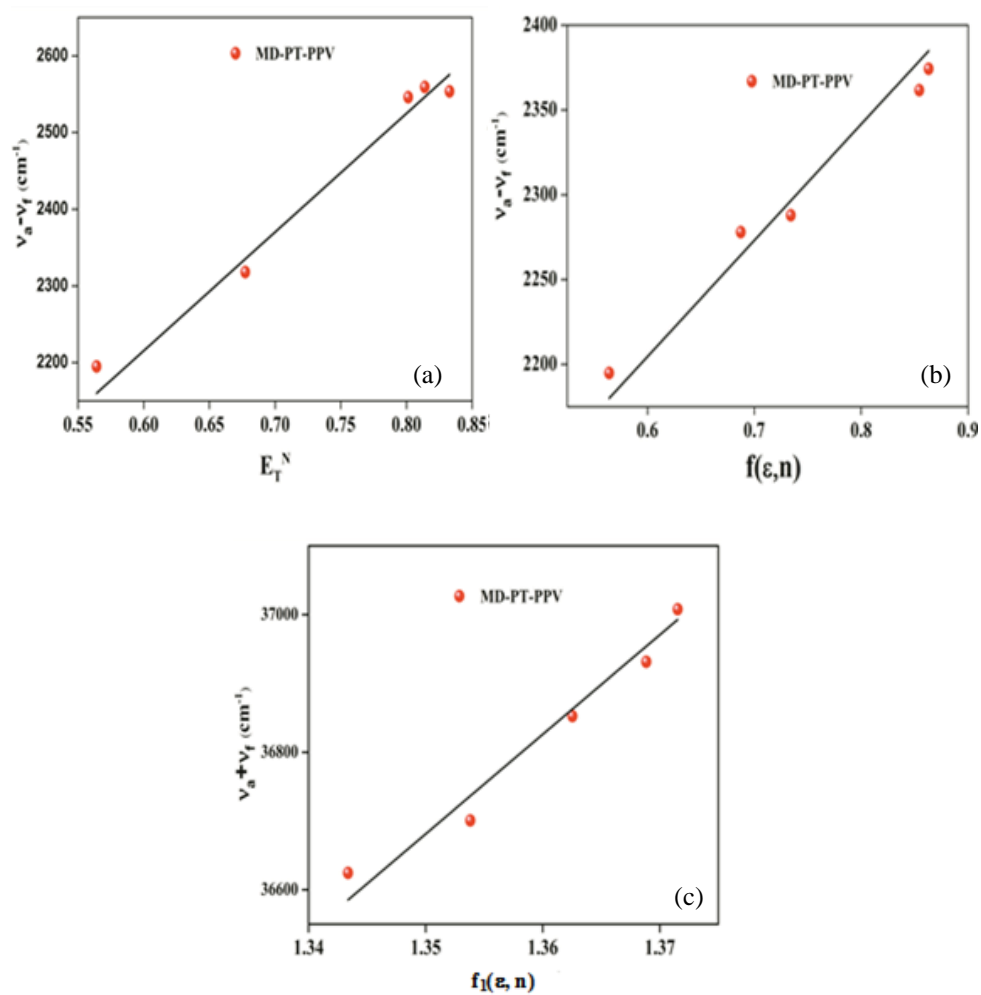
Figure 2.15: The variation of Stoke's shift with (a) E_N^T, (b) $f(\varepsilon, n)$ and (c) arithmetic mean of Stoke's shift $f_1(\varepsilon, n)$ for MD-PT-PPV
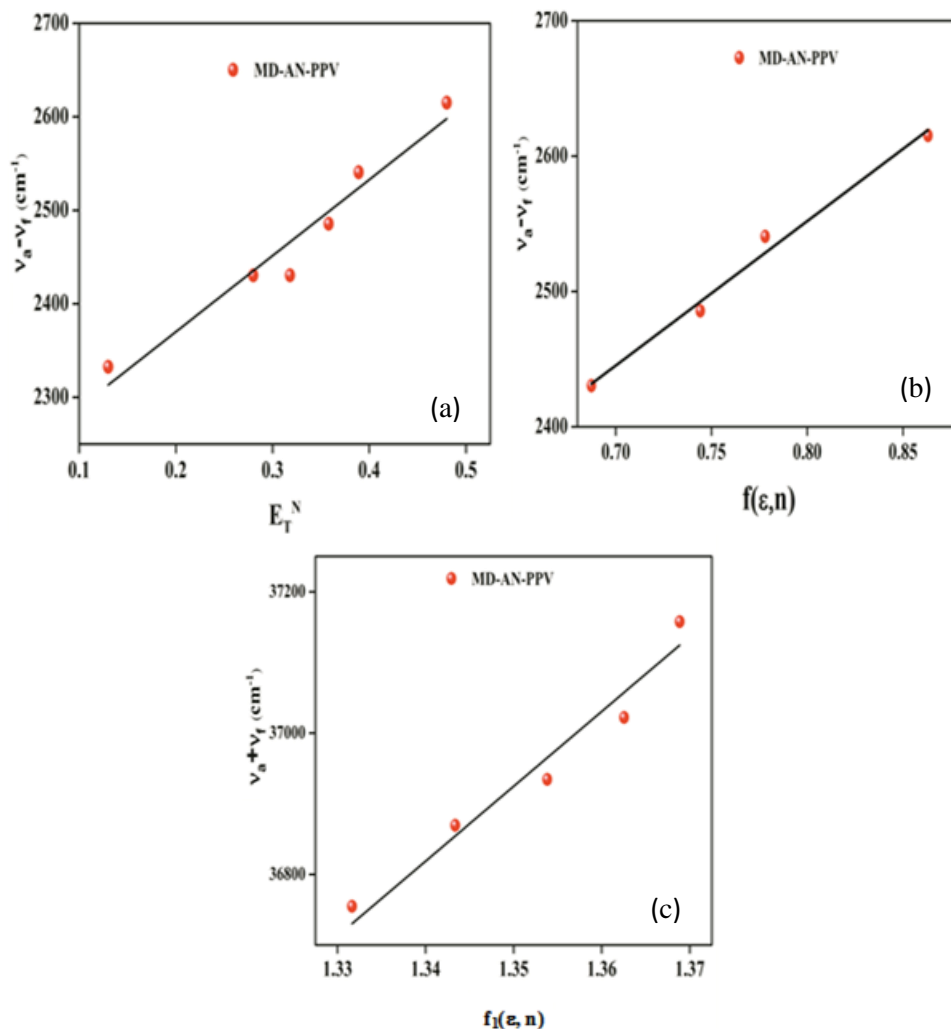
Figure 2.16: The variation of Stoke's shift with (a) E_N^T, (b) $f(\varepsilon, n)$ and (c) arithmetic mean of Stoke's shift $f_1(\varepsilon, n)$ for MD-AN-PPV

The ground state and excited state dipole moment values were calculated from equation 2.10 and 2.11. The value of Onsager cavity radius for the PPV was calculated using the equation 2.9. Statistical treatment of data are given in Table 2.12. Results of the calculation are given in Table 2.13.

Table 2.12: Statistical treatment of the correlation of (a) MD-CA-PPV, (b) MD-FL-PPV, (c) MD-PT-PPV and (d) MD-AN-PPV in toluene/acetonitrile mixtures of varying polarity

Polymer	Slope with correlation co-efficient 'R'		
	E_T^N	Bakshiev's	Chamma-Viallet's
MD-CA-PPV	8262 (0.99)	5606 (0.99)	9599 (0.97)
MD-FL-PPV	3467 (0.99)	5423 (0.98)	17992 (0.95)
MD-PT-PPV	610 (0.97)	578 (0.99)	11912 (0.95)
MD-AN-PPV	808 (0.99)	1067 (0.98)	7156 (0.96)

In the case of MD-CA-PPV, the ground (μ_g) and excited (μ_e) state dipole moments calculated from the solvatochromic shift method were 4.7 D and 17.9 D respectively. The large variation of the dipole moment value between the ground state and the excited state suggested that fluorescence originated from highly polar excited state. In the excited state, the charge separation was increased, resulting in a large dipole moment than in the ground state.[65]

Table 2.13: Ground and excited state dipole moments of (a) MD-CA-PPV, (b) MD-FL-PPV, (c) MD-PT-PPV and (d) MD-AN-PPV in toluene/acetonitrile mixtures of varying polarity

Polymer	a^1 (Å)	$\mu_g{}^2$ (D)	$\mu_e{}^3$ (D)	$\Delta\mu^4$ (D)	$\Delta\mu^5$ (D)
MD-CA-PPV	6.8	4.7	17.9	13.2	8.83
MD-FL-PPV	6.78	15	26.5	11.5	5.72
MD-PT-PPV	6.40	37.9	41.8	3.9	2.19
MD-AN-PPV	6.27	13.5	18.2	4.7	5.92

[1]Calulated from equation 2.9
[2]The ground state dipole moment calculated using Eq. 2.10.
[3]The excited state dipole moment calculated from Eq. 2.11.
[4]The change in dipole moment for $\mu_g{}^2$ and $\mu_e{}^3$
[5]The change in dipole moment calculated from Eq. 2.15.

The attempt to calculate the first hyperpolarizability parameter (β) from the solvatochromic data was not successful because of the errors that

originated in the determinations of oscillator strength and transition dipole moment.

2.3 Conclusion

A series of novel poly (phenylene vinylene) derivatives MD-CA-PPV, MD-FL-PPV, MD-PT-PPV and MD-AN-PPV have been designed and synthesized by Gilch polymerisation method. Monomers, D-A and tetramer units were optimized using DFT/B3LYP/6-31G formalism. Both optical and electrochemical results support the theoretical prediction obtained by HSE06/6-31G method compared to the B3LYP/6-31G method. The polymers were soluble in common organic solvents such as chloroform, tetrahydrofuran etc. and could be easily spin coated to make films, with high thermal stability. The fluorescence lifetime of the phenylene vinylene copolymers were determined using TCSPC in CHCl$_3$ and all the copolymers fitted well with bi-exponential decay due to the presence of different fluorescing moieties. The photophysical behaviour of the copolymers MD-CA-PPV, MD-FL-PPV, MD-PT-PPV and MD-AN-PPV were studied. It was found that excited state dipole moments of the copolymers were larger than ground state dipole moment. The increase in dipole moment in the excited state ranged from 4 to 13 D. This demonstrated that the molecule was more polar in the excited state than in the ground state for all the solvents studied. It might be noted that there was significant difference in the change in dipole moments ($\Delta\mu$) of the copolymers obtained by the two methods i.e., solvatochromic shift method and on the basis of microscopic empirical solvent polarity parameter (E_T^N). The discrepancies observed may be due to the different approximations made in both the methods to estimate $\Delta\mu$ of the copolymers.

2.4 Experimental section

2.4.1 Synthesis of 1-decyloxy-4-methoxybenzene

A mixture of 4-methoxyphenol (0.08 mol) and KOH (0.16 mol) in ethanol (40 mL) was refluxed for 1 h at 80 °C under nitrogen atmosphere. After cooling to room temperature, 1-bromodecane (0.08 mol) was added drop wise and further refluxed for 24 h. When the brownish solution was turned to yellow, the reaction mixture was poured into 200 mL of distilled water and the brown liquid was extracted with diethyl ether. The crude product was washed several times with aqueous sodium carbonate solution and water. It was recrystallized from hexane.

Yield	:	87 %.
^{1}H NMR (CDCl$_3$, 400 MHz)	:	δ 6.71 (m, 4H), 3.80 (t, 2H), 3.62 (s, 3H),
		1.76 (m, 2H), 1.42-1.28 (m, 12H),
		0.90 (t, 3H).
GCMS	:	m/z = 264.

2.4.2 Synthesis of 1,4-bis-(bromomethyl)-2-decyloxy-5-methoxybenzene (MD)

A three necked flask containing 1-Decyloxy-4-methoxybenzene (0.01 mol), paraformaldehyde (0.035 mol), and glacial acetic acid (40 mL) was placed in an ice bath. 33% HBr in glacial acetic acid (20 mL) was carefully added drop wise into this flask, and the mixture was stirred for 24 h at 60 °C. The mixture was poured into 200 mL of saturated NaHCO$_3$ after being cooled to room temperature and extracted with DCM. The crude product was washed several times with brine solution and water and

recrystallized from hexane twice to obtain the compound as a white crystal.

Yield	: 82 %.
^{1}H NMR (CDCl$_3$, 400 MHz) :	δ 7.00 (s, 2H), 4.72 (s, 4H), 4.06 (t, 2H), 3.84 (s, 3H), 1.80-1.64 (m, 2H), 1.38-1.25 (m, 12H), 0.90 (t, 3H).
LCMS	: m/z = 450

2.4.3 Synthesis of 1, 2 -bis(octyloxy)benzene[66]

A solution of catechol (0.25 mol) in 100 mL of ethanol was slowly added to a stirred solution of KOH (0.63 mol) in 35 mL of ethanol at room temperature. The reaction mixture was stirred for 1 h. A solution of 1-bromooctane (0.75 mol) in 50 mL of ethanol was added drop wise. The reaction mixture was refluxed overnight. Ethanol was removed by rotary vacuum evaporation and the reaction mixture was partitioned between ethyl acetate and sodium carbonate solution. After drying over sodium sulfate, the product was obtained by distillation under reduced pressure to get 1, 2-bis (octyloxy) benzene.

Yield	: 72 %.
^{1}H NMR (CDCl$_3$, 400 MHz) :	δ 6.91 (s, 4H), 4.05–4.02 (t, 4H), 1.76 (m, 4H), 1.42-1.28 (m, 20H), 0.90 (t, 6H).
GCMS	: m/z = 335

2.4.4 Synthesis of 1, 4-bis(bromomethyl)-2,3-bis(octyloxy)benzene (CA)

A three necked flask containing 1,2-bis(octyloxy)benzene (0.01 mol), paraformaldehyde (0.035 mol), and glacial acetic acid (40 mL) was placed in

an ice bath. 33% HBr in glacial acetic acid (20 mL) was carefully added drop wise into this flask, and the mixture was stirred for 24 h at 80 °C. The mixture was poured into 200 mL of saturated $NaHCO_3$ after being cooled to room temperature and extracted with DCM. The solvent was removed using rotary vacuum evaporator, the residue was purified by column chromatography using a mixture of hexane and CH_2Cl_2 (8:1) to offer 1,4-bis-(bromomethyl)-2,3-bis(octyloxy)benzene.

Yield	:	77 %.
^{1}H NMR (CDCl$_3$, 400 MHz)	:	δ 7.08 (s, 2H), 4.00–3.97 (t, 4H), 1.86–1.83 (m, 2H), 1.74–1.69 (m, 4H), 0.99–0.97(m,12H).
LCMS	:	m/z = 520

2.4.5 Synthesis of 2, 7-bis(bromomethyl)-9, 9-dioctyl-9H-fluorene (FL)

A three necked flask containing 9, 9-di-n-octylflourene (0.01 mol), paraformaldehyde (0.035 mol), and glacial acetic acid (40 mL) was placed in an ice bath. 33% HBr in glacial acetic acid (20 mL) was carefully added drop wise into this flask, and the mixture was stirred for 24 h at 80 °C. The mixture was poured into 200 mL of saturated $NaHCO_3$ after being cooled to room temperature and extracted with DCM. The crude product was washed with brine solution and water and recrystallized from hexane to obtain the compound as a white crystal.

Yield	:	82%.
^{1}H NMR (CDCl$_3$, 400 MHz)	:	δ 7.00-7.8 (m, 6H), 4.6 (s, 4H), 1.2 -1.9 (m, 24H), 0.90 (t, 6H).
LCMS	:	m/z = 574

2.4.6 Synthesis of 10-n-Octylphenothiazine

Phenothiazine (10 g, 50 mmol), potassium hydroxide (20.0 g, 500 mmol), and DMSO (100 mL) were placed in a 250 mL two-necked flask. The mixture was stirred for half an hour. Octyl bromide (7.7 mL, 55 mmol) was added drop wise to the reaction mixture in 20 min and this mixture was stirred for 24 h at room temperature. The reaction mixture was poured into water, extracted with methylene chloride, and dried with $MgSO_4$. The resulting liquid was purified by column chromatography using petroleum ether as eluent which gave colourless liquid.

Yield : 93 %.

^{1}H NMR (CDCl$_3$, 400 MHz) : δ 0.87 (t, 3H), 1.24-1.43 (m, 10H), 1.77 (m, 2H), 3.80-3.84 (t, 2H), 6.83-6.91 (m, 4H), 7.11-7.15 (m, 4H).

GCMS : m/z = 311

2.4.7 Synthesis 3,7-bis(bromomethyl)-10-octyl-10H-phenothiazine (PT)

A three necked flask containing 10-n-Octylphenothiazine (0.01 mol), paraformaldehyde (0.035 mol), and glacial acetic acid (40 mL) was placed in an ice bath, 33% HBr in glacial acetic acid was carefully added drop wise into this flask, and the mixture was stirred for 24 h at 80 °C. The mixture was poured into 200 mL of saturated NaHCO$_3$ after being cooled to room temperature and extracted with DCM. The solvent was removed using rotary vacuum evaporator, the residue was purified by column chromatography using a mixture of hexane and CH$_2$Cl$_2$ (8:1) to offer 3,7-bis(bromomethyl)-10-octylphenothiazine.

Yield   : 79 %.

^{1}H NMR (CDCl$_3$, 400 MHz) : δ 6.4-6.8 (m, 6H), 4.4(s, 4H), 3.17(t,2H),

1.4–1.29 (m, 12H), 0.92 (t, 3H)

LCMS   : m/z = 497

2.4.8 Synthesis 9, 10-bis(bromomethyl)anthracene (AN)

A three necked flask containing anthracene (0.01 mol), paraformaldehyde (0.035 mol), and glacial acetic acid (40 mL) was placed in an ice bath. 33% HBr in glacial acetic acid (20mL) was carefully added drop wise into this flask, and the mixture was stirred for 24 h at 60°C. The mixture was poured into 200 mL of saturated NaHCO$_3$ after being cooled to room temperature and extracted with DCM. The crude product was washed with brine solution and water and recrystallized from hexane to obtain the compound as a light yellow powder.

Yield   : 67 %.

^{1}H NMR (CDCl$_3$, 400 MHz) : δ 7.32-7.38 (d, 4H), 5 (s, 4H),

7.90-7.95 (s, 4H).

GCMS   : m/z = 364

2.4.9 General procedure for polymerization through Gilch polymerization

To a solution of bromomethylated monomer (3 mmol) in 20 mL of anhydrous THF was added drop wise a solution of 95% potassium tertiarybutoxide (18 mmol) in 80 mL of THF at 30 ^{o}C with stirring for 20 h. The solution was poured into cold methanol. The precipitate was filtered and washed with methanol. The polymer was further purified by soxhlet extraction with acetone and methanol.

2.4.9.1 Synthesis of MD-CA-PPV

1,4-Bis-(bromomethyl)-2-decyloxy-5-methoxybenzene (3 mmol), 1,4-bis-(bromomethyl)-2,3-bis(octyloxy)benzene (3 mmol), 95 % Potassium tertiarybutoxide (18 mmol) and THF (100 mL). Red solid.

Yield	:	86 %
UV-Visible (THF) λmax	:	483 nm
GPC	:	Mn = 45682, PDI =1.91
Td (^{o}C)	:	435
^{1}H NMR (400 MHz, CDCl$_3$)	:	δ 7.43 (s, 2H, Ar-H), 7.15 (s, 2H, -CH=CH-), 7.79(d, 2H, Ar-H), 3.97 (b, - OCH$_2$- and - OCH$_3$), 1.9-0.8 (m, 49H, aliphatic-H).

2.4.9.2 Synthesis of MD-FL-PPV

1,4-Bis-(bromomethyl)-2-decyloxy-5-methoxybenzene (3mmol), 2,7-bis-(bromomethyl) 9,9-dioctyl-9H-fluorene (3 mmol), 95 % Potassium tertiarybutoxide (18 mmol) and THF (100 mL). Brownish red solid.

Yield	:	84 %
UV-Visible (THF) λmax	:	480 nm
GPC	:	Mn = 33916, PDI =1.68
Td (^{o}C)	:	429
^{1}H NMR (400 MHz, CDCl$_3$)	:	δ 7.39 (s, 2H, Ar-H), 7.10 (s, 2H, -CH=CH-), 7.4-7.6 (d, 4H, Ar-H), 7.7 (s, 2H, Ar-H), 3.99- 4.05 (b, -OCH$_2$- and – OCH$_3$), 1.9-0.8 (m, 49H, aliphatic-H).

2.4.9.3 Synthesis of MD-PT-PPV

1,4-bis-(bromomethyl)-2-decyloxy-5-methoxybenzene (3 mmol) , 3,7-bis-(bromomethyl)-10-octyl-10H-phenothiazine (3 mmol), 95 % Potassium tertiarybutoxide (18 mmol) and THF (100 mL). Dark Red solid.

Yield	:	79 %
UV-Visible (THF) λmax	:	490 nm
GPC	:	M_n = 45742, PDI =1.60
Td (^{o}C)	:	416
^{1}H NMR (400 MHz, CDCl$_3$)	:	δ 7.22 (s, 2H, Ar-H), 7.12 (s, 2H, -CH=CH-), 7.15- 7.18 (dd, 2H), 7.20 (d, 2H), 3.77- 4.01 (b, -OCH$_2$- and – OCH$_3$), 1.14-1.51 (m, 28 H, aliphatic- H), δ 0.92 (t, 6H).

2.4.9.4 Synthesis of MD-AN-PPV

1,4-bis-(bromomethyl)-2-decyloxy-5-methoxybenzene (3 mmol) , 9,10-bis-(bromomethyl)anthracene (3 mmol), 95 % Potassium tertiarybutoxide (18 mmol) and THF (100 mL). Red solid.

Yield	:	88 %
UV-Visible (THF) λmax	:	487 nm
GPC	:	M_n = 82679, PDI =1.80
Td (^{o}C)	:	445
^{1}H NMR (400 MHz, CDCl$_3$)	:	δ 7.50 (s, 2H, Ar-H), 7.21 (s, 2H, -CH=CH-), 7.78-7.85 (dd, 5H, Ar-H), 7.36 (dd, 4H, Ar-H), 7.79(d, 2H, Ar-H), 3.98 (b, -OCH$_2$- and -OCH$_3$), 1.7-0.8 (m, 15H, aliphatic-H).

References

1. U. H. Bunz, *Macromol. Rapid. Commun.,* 2009, **30,**772.

2. A. Kraft, A.C. Grimsdale, A. B. Holmes, *Angew. Chem. Int. End. Eng.,* 1998, **37**, 402.

3. X. Zhao, X. Zhan, *Chem. Soc. Rev.,* 2011, **40**, 3728.

4. M. Dominic, M. Christopher, B. Kerstin, H. F. B. Uwe, *ACS. Macro. Lett.,* 2014, **3**, 415.

5. S. Cataldo, B. Pignataro, *Materials*, 2013, **6**, 1159.

6. J. Lee, D. H. Kim, J. Y. Kim, B. Yoo, J. W. Chung, J. I. Park, S. Im, *Adv. Mater.,* 2013, **25**, 5886.

7. C. R. Paula, D. F. Bruno, B. M. T. Bruno, S. S. Washington, C. F. Gregorio, T. B. Debora, M. F. Roberto, A. Leni, *J. Appl. Polym. Sci.,* 2015, **132**, 42579.

8. J. F. De Deus, G. C. Faria, E. T. Iamazaki, R. M. Faria, T. D. Atvars, L. Akcelrud, *Org. Electron.,* 2011, **12**, 1493.

9. Y. M. Liao, H. M. Shih, K. H. Hsu, C. S. Hsu, Y. C. Chao, S. C. Lin, H. F. Meng, *Polymer*, 2011, **52,** 3717.

10. Y. J. Cheng, S. H. Yang, C. S. Hsu, *Chem. Rev.,* 2009, **109**, 5868.

11. K. Nakabayashi, H. Mori, *Materials.,* 2014, **7**, 3274.

12. H. K. Ji, E. S. Chang, U. K. Hee, N. K. In, S. S. Won, J. P. Moo, H. H. Do, *J. Polym. Sci. A. Polym. Chem.,* 2013, **51**, 4136.

13. H. Y. Chu, D. H. Hwang, L. M. Do, J. H. Chang, H. K. Shim, A. B. Holmes, T. Zyung, *Synth. Metals.,* 1999, **101**, 216.

14. Z. Peng, J. Zhang, B. Xu, *Macromolecules.,* 1999, **32**, 5162.

15. R. Li ,Y. Mo , R. Shi , P. Li , C. Li , Z. Wang , X. Wang , S. Li, *Monatsh Chem.,* 2014, **145**, 85.

16. J. Z. Jian, G. Ge, D. Wei, C. Z. Da, Q. L. Feng, *Polym. Int.,* 2008, **57**, 921.

17. T. T. Cuong, S. Geoff, R. P. Matthew, P. N. Thien, H. H. Chun, C. Ala, *Polym. Int.,* 2008, **57**, 496.

18.   H. Roex, P. Adriaensens, D. Vanderzande, J. Gelan, *Macromolecules.,* 2003, **36**, 5613.

19.   S. Hameed, P. Predeep, M. R. Baiju., *Rev. Adv. Mater. Sci.,* 2010, **26**, 30.

20.   M. Raveendra Melavanki, N. R. Patil, S. B. Kapatkar, N. H. Ayachit, S. Umapathy, J. Thipperudrappa, A. R. Nataraju, *J. Mol. Liquids.,* 2011, **158**, 105.

21.   M. Raveendra Melavanki, H. D. Patil, S. Umapathy, J. S. Kadadevaramath, *J. Fluoresc.,* 2012, **22**, 137.

22.   C. Parkanyi, M. R. Stem-Beren, O. R. Martinez, J. J. Aaron, M. B. Macnair, A. F. Arietta, *Spectrochim. Acta. Part A.*, 2004, **60**, 1805.

23.   M. S. Zakerhamidi, S. Ahmadi- Kanjani, M. Mohadam, E. Ortyl, S. Kucharski, *J. Mol. Struct.,*2011, **996** , 95.

24.   S. Joshi, D. D. Pant, *J. Mol. Liquids.,* 2012, **172**, 125.

25.   M. K. Saroj, N. Sharma, R. C. Rastogi, *J. Mol. Struct.,* 2012, **1012**,73.

26.   A. Kawski, *Acta. Phys. Polon*, 1966, **29**, 507.

27.   A. Kawski, J.F. Rabek (Eds.), *Progress in Photochemistry and Photophysics*, vol. 5, 350 CRC Press, Boca Raton, 1992.

28.   W. Liptay, E.C. Lim (Eds.), *Excited States,* vol. 1, Academic Press, New York, 1974.

29.   J. R. Lombardi, *J. Am. Chem. Soc.,* 1970, **92,** 1831.

30.   W. Baumann, B. W. Rossiter, J. F. Hamilton (Eds.), *Physical Methods of Chemistry,* Vol. 38, John Wiley and Sons, New York, 1989.

31.   J. Czekella, *Z. Elektrochem.,* 1960, **64,** 1221.

32.   C. Párkányi, J. J. Aaron, *Theor. Org. Chem.,,* 1998, **5**, 233.

33.   C. Reichardt, *Chem. Rev.*, 1994, **94**, 2319.

34.   R. G. Parr, W. Yang, *Density-Functional Theory of Atoms and Molecules*: Oxford University Press, New York, 1989.

35. K. Kornobis, N. Kumar, P. Lodowski, M. Jaworska, P. Piecuch, J. J. Lutz, P.M. Kozlowski, *J. Chem. Theory. Comput.,* 2013, **34**, 987.

36. N. Kumar, M. Alfonso-Prieto, C. Rovira, P. Lodowski, M. Jaworska, P. M. Kozlowski, *J. Chem. Theory. Comput.,* 2011, **7**, 1541.

37. M. W. Bryan, P. Manuel, D. S. Fabio, *Phys. Chem. Chem. Phys.,* 2009, **11**, 4498.

38. M. W. Bryan, *J. Phys. Chem. C.,* 2009, **113**, 21921.

39. C. Lee, W. Yang, R. G. Parr, *Phys. Rev. B.,* 1988, **37**, 785.

40. K. Kim, K. D. Jordan, *J. Phys. Chem.,* 1994, **98**, 10089.

41. S. H. Vosko, L. Wilk, M. Nusair. *Can. J. Phys.,* 1980, **58**, 1200.

42. F. J. Devlin, J. W. Finley, P. J. Stephens, M. J. Frisch, *J. Phys. Chem.,* 1995, **99**,16883.

43. J. F. Dobson, G. Vignale, M. P. Das. *Electronic Density Functional Theory: Recent Progress and New Directions.* Springer Science & Business Media; 2013.

44. C. L. Pai, C. L. Liu, W. C. Chen, S. A. Jenekhe, *Polymer.,* 2006, **47,** 699.

45. N. Sona, P. R. Sreejesh, M. Sebastian, M. V. Mahesh Kumar, A. Anshad, K. Sreekumar, C. SudhaKartha, J. Rani, *Eur. Polym. J.,* 2015, **64,** 157.

46. Gaussian 09, Revision B02, M. J. Frisch, G. W. Trucks, H. B. Schlegel, G. E. Scuseria, M. A. Robb, J. R. Cheeseman, G. Scalmani, V. Barone, B. Mennucci, G. A. Petersson, H. Nakatsuji, M. Caricato, X. Li, H. P. Hratchian, A. F. Izmaylov, J. Bloino, G. Zheng, J. L. Sonnenberg, M. Hada, M. Ehara, K. Toyota, R. Fukuda, J. Hasegawa, M. Ishida, T. Nakajima, Y. Honda, O. Kitao, H. Nakai, T. Vreven, Jr. J. A. Montgomery, J. E. Peralta, F. Ogliaro, M. Bearpark, J. J. Heyd, E. Brothers, K. N. Kudin, V. N. Staroverov, R. Kobayashi, J. Normand, K. Raghavachari, A. Rendell, J. C. Burant, S. S. Iyengar, J. Tomasi, M. Cossi, N. Rega, N. J. Millam, M. Klene, J. E. Knox, J. B. Cross, V. Bakken, C. Adamo, J. Jaramillo, R. Gomperts, R. E. Stratmann, O. Yazyev, A. J. Austin, R. Cammi, C. Pomelli, J. W. Ochterski, R. L. Martin, K. Morokuma, V. G. Zakrzewski, G. A. Voth, P. Salvador, J. J. Dannenberg, S. Dapprich, A. D. Daniels, Ö. Farkas, J. B. Foresman, J. V. Ortiz, J. Cioslowski, D. J. Fox, *Gaussian, Inc.,* Wallingford CT, 2009.

47. N. Marom, A. Tkatchenko, M. Rossi, V. V. Gobre, O. Hod, M. Scheffler, L. Kronik*, J. Chem. Theory. Comput.,* 2011, **7**, 3944.

48. J. Heyd, G. E. Scuseria, M. Ernzerhof, *J. Chem. Phys.,* 2003, **118**, 8207.

49. T. Ahn, *Trans. Electr. Electron. Mater.,* 2013, **14**, 263.

50. M. A. Abdullah, Al-Hussam, J. J. Salah Abdul, *J. Assn. Arab. Univ. Basic. Appl. Sci.,* 2012, **11**, 27.

51. J. L. Bredas, R. Silbey, D. X. Boudreux, R. R. Chance, *J. Am. Chem. Soc.,* 1983, **105**, 6555.

52. L. Zhou, C. Jia, Z. Wan, Z. Li, J. Bai, L. Zhang, J. Zhang, X. Yao, *Dyes. Pigm.,* 2012, **95,** 743.

53. B. Valeur, *Molecular Fluorescence: Principles and Applications*; Wiley-VCH, Weinheim, 2002.

54. R. M. F. Batista, S. P. G. Costa, M. M. M. Raposo, J. O. Pina , J. S. Seixas de Melo, *J. Org. Chem.,* 2013, **78**, 11389.

55. R. Zhao, X. Ji, S. Jiang, L. Liu, B. L. Weeks, Z. Zhang*, Green. Chem.,* 2011, **13**, 1891

56. D. S. Chemla, J. Zyss, *Nonlinear Optical Properties of Organic Molecules and Crystals*, Academic Press, New York, 1987.

57. N.G. Bakhshiev, *Opt. Spektrosk*., 1964, **16** , 821.

58. A. Chamma, P. Viallet, C. R. Acad, *Sci. Paris, Ser.,* 1970, **C270**, 1901.

59. L. Bilot, A. Kawski, Z. *Naturforsch., A: Phys. Sci.,* 1963, **18a**, 256.

60. P. Suppan, *Chem. Phys. Lett.,* 1983, **94**, 272.

61. L. Bilot, A. Kawski, Z. *Naturforsch., A: Phys. Sci*., 1962, **17a**, 621.

62. C. Reichradt, *Solvents and Solvent Effect in Organic Chemistry,* 3rd edn. Wiley-VCH. Verlag. GmbH and Co. 2004

63. M. Ravi, T. Soujanya, A. Samanta, T. P. Radhakrishnan, *J. Chem. Soc. Faraday. Trans*.,1995, **91**, 2739.

64. V. C. Kishore, R. Dhanya, K. Sreekumar, R. Joseph, and C. S. Kartha, *Spectrochimica Acta Part A: Molecular and Biomolecular Spectroscopy*, 2008, **71**, 1355.

65. S. Joshi , S. Kumari, R. Bhattacharjee, R. Sakhuja, D. D. Pant, *J. Mol. Liq. Part B*, 2014, **200**, 115.

66. C. Huang, C. G. Zhen, S. P. Su, C. Vijila, B. Balakrisnan, M. D. J. Auch, Z. K. Chen, *Polymer* 2006, **47**, 1820.

DONOR-ACCEPTOR TYPE BITHIOPHENE BASED COPOLYMERS BY DIRECT ARYLATION REACTION: THEORY, SYNTHESIS AND CHARACTERIZATION

In this chapter, electronic structure calculation and synthesis of five Donor-Acceptor (D-A) π-conjugated copolymers are described. The copolymers of bithiophene with 3,7-dibromo-10-octylphenothiazine, 3,6-dibromo-N-octylcarbazole, 2,7-dibromo-9,9-dioctyl-9H-fluorene, 4,4'-dibromotriphenylamine and 9,10-dibromoanthracene were synthesized using palladium catalysed direct arylation reaction in good yields. Structural characterization was performed by FT-IR, ^{1}H NMR and GPC etc. The polymers showed good solubility in common organic solvents like chloroform, tetrahydrofuran, toluene etc. The fluorescence lifetime of the polymers, P(BT-PH), P(BT-CZ), P(BT-FLN), P(BT-ANT) and P(BT-TPA) were observed using Time-Correlated Single Photon Counting technique (TCSPC) in $CHCl_3$. The absorption and emission spectra of P(BT-CZ) have been recorded at room temperature in binary solvent mixtures of varying polarities. The ground state (μ_g) and exited state (μ_e) dipole moments were estimated from Bakhshiev's and Kawski-Chamma-Viallet's equations using the variation of Stoke's shift with the solvent dielectric constant and refractive index. Further, change in dipole moment ($\Delta\mu$) was calculated both from solvatochromic shift method and on the basis of microscopic solvent polarity parameter (E_T^N) and the values are compared.

3.1 Introduction

Organic conducting polymers containing heteroatoms such as oxygen (O), nitrogen (N) or sulphur (S) have been extensively used because of their extraordinary electronic, magnetic and optical properties. Recently, donor-acceptor (D-A) type semiconducting polymers with tunable optoelectronic properties, mechanical flexibility, solution processability were largely focused in the fabrication of optoelectronic devices. Among these, polythiophene and its derivatives have been extensively studied due to their promising low band gaps and good environmental stability.[1-4] To explore the full potential applications of polythiophene, materials have been made by the structure modification by copolymerisation of thiophene unit with other conjugated building blocks into the polymer chain.[5-11] Moreover, thiophene can be a good candidate for copolymerisation with monomers such as furan,[12-14] pyrrole,[15] phenothiazine,[16] benzanthrone [17] and benzothiophene.[18] In the current work, the monomers with electron-rich sulphur or nitrogen heteroatoms, such as phenothiazine, carbazole and triphenylamine were incorporated with bithiophene moiety.

Conventionally, transition metal catalysed cross-coupling reactions (e.g., Kumada, Negishi, Stille, and Suzuki type) were commonly employed in the synthesis of π-conjugated polymers.[19-23] These polycondensation reactions often require tedious preactivation of C–H bonds using bifunctional organometallic reagents as monomers. These reagents are flammable (e.g. butyl lithium), nonstable and they produce stoichiometric amount of toxic by-products (organotins). To overcome these synthetic issues, facile direct coupling of arylhalides with heteroaryls without the need of

preactivating the sp^2 C–H bonds have been actively investigated.[24-27] Figure 3.1 depicts the graphical representation of polycondensation using traditional cross-coupling and direct C-H/ C-X arylation reaction.
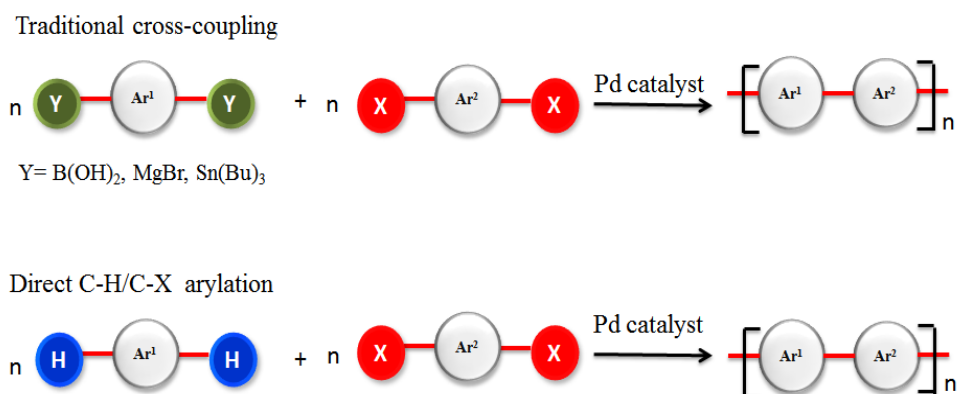
Figure 3.1: Schematic representation of polycondensation using traditional cross-coupling and direct C-H/ C-X arylation reaction
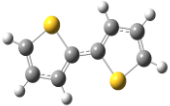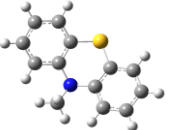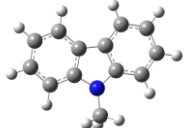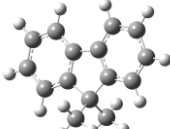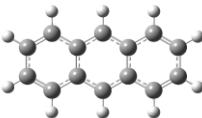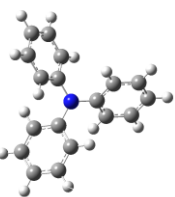
In this chapter, electronic structure properties and synthesis of five copolymers composed of bithiophene donor and 3,7-Dibromo-10-octylphenothiazine, 3,6-Dibromo-N-octylcarbazole, 2,7-Dibromo-9,9-dioctyl-9H-fluorene, 4,4'-dibromotriphenylamine and 9,10-dibromoanthracene as acceptors were investigated. Low band gap Donor-Acceptor (D-A) type conducting polymers were synthesized via palladium catalysed direct arylation. Polymers were optimized using DFT/HSE06/6-31G and DFT/B3LYP/6-31G methods. Their electrochemistry, optical and thermal properties were studied. The fluorescence lifetime of the polymers were monitored using TCSPC in CHCl$_3$. Effects of solvents on absorption and emission spectra, and estimation of ground and excited state dipole moments of P(BT-CZ) by solvatochromic shift method were also studied.

3.2 Results and discussion

3.2.1 Theoretical calculation

The versatile and popular quantum chemical method, Density Functional Theory (DFT)[28-31] was used to investigate the electronic structure and properties of the bithiophene based copolymers. DFT calculations using the Gaussian 09 suite of codes [32,33] at two different energy levels, B3LYP [34-36] and HSEh1PBE referred to as HSE06 (full Heyd–Scuseria–Ernzerh of functional) [37,38] using 6-31G basis set were carried out to obtain band gaps of the conjugated polymers. Quantum chemical calculations have been carried out to examine the interaction between the monomer units linked in copolymer chain. The electronic properties of the polymers depended on their constituent monomers. The properties of constituents, 2,2′-Bithiophene (BT), 3,7-dibromo-10-octylphenothiazine (PH), 3,6-dibromo-N-octyl carbazole (CZ), 2,7-dibromo-9,9-dioctyl-9H-fluorene (FLN), 9,10-dibromoanthracene (ANT) and 4,4'-dibromotriphenylamine (TPA) were studied. The ground state geometries of monomers and oligomers were optimised using DFT at the B3LYP (Becke, three parameter, Lee-Yang-Parr) level of theory using 6-31G basis set. The excited state vertical transition energies, oscillator strengths and absorption maximum of the designed monomers were computed by Time-Dependent DFT/ (TD-DFT) calculations and are shown in Table 3.1.

Table 3.1: Values of $E_{activation}$ (eV), Oscillator strength and λ_{max} (nm) of the monomer units obtained by TD-DFT/B3LYP/6-31G method

Monomer	Optimized geometries of monomers[a]	$E_{activation}$[b] (eV)	Oscillator strength[b]	λmax[b] (nm)
2,2′-Bithiophene (BT)		3.98	0.431	312
3,7-dibromo-10-octylphenothiazine (PH)		3.96	0.007	315
3,6-dibromo-N-octylcarbazole (CZ)		4.09	0.035	303
2, 7-dibromo-9,9-dioctyl-9H-fluorene (FLN)		4.81	0.171	257
9,10-dibromoanthracene (ANT)		3.35	0.068	370
4,4'-dibromotriphenyl amine (TPA)		3.94	0.015	310

[a] Estimated from DFT/B3LYP/6-31G calculation
[b] Estimated from TD-DFT/B3LYP/6-31G calculation

B3LYP/6-31G method was employed to predict the energy levels of monomers and oligomers. The results are summarized in Fig. 3.2.
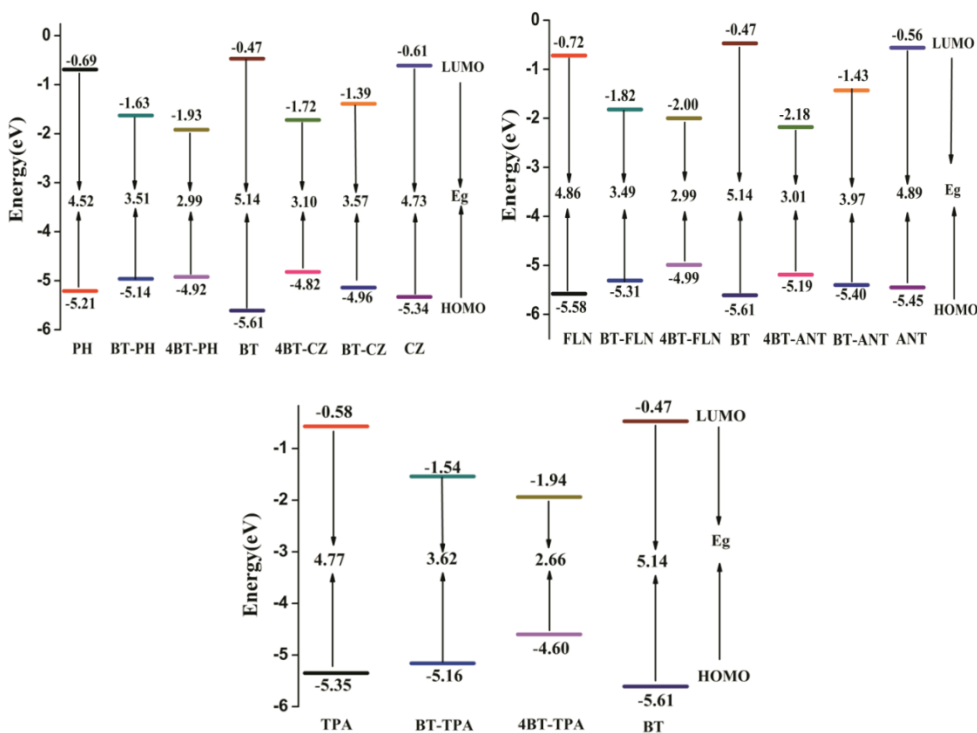
Figure 3.2: Energy levels of monomers, D-A, tetramer units of P(BT-PH), P(BT-CZ), P(BT-FLN), P(BT-ANT) and P(BT-TPA) copolymers

From this data, the LUMO levels of BT, PH, CZ, FLN, ANT and TPA were found to be -0.47, -0.69, -0.61, -0.72, -0.56 and -0.58 eV respectively. The band gap of the polymer depended on the acceptor strength. Acceptor strength increased with decreasing LUMO energy level. Hence the acceptor strength of the monomer followed the order: FLN > PH > CZ >TPA >ANT. As shown in the energy level diagram, the LUMO level of BT-PH, BT-CZ, BT-FLN, BT-ANT and BT-TPA were obtained to be -1.63,-1.39, -1.82,

-1.43 and -1.54 eV respectively. It is clear that by introducing, PH, CZ, FLN, ANT and TPA into the BT back bone, HOMO energy levels are being raised and the LUMO levels are being reduced. The band gap of compounds, followed the order, BT-FLN >BT-PH >BT-CZ >BT-TPA >BT-ANT. Both the acceptor strength and geometry have played a major role in band gap reduction. This band gap reduction is mainly due to the intramolecular charge transfer between donor, BT and acceptor, PH, CZ, FLN, ANT and TPA, which improved the π-electron delocalization and thus decreased the bond length alternation (BLA) of D-A type units.[39] This can be visualized from the frontier orbital distribution of the model compounds (Fig.3.3).

BT-PH   BT-CZ   BT-FLN   BT-ANT   BT-TPA
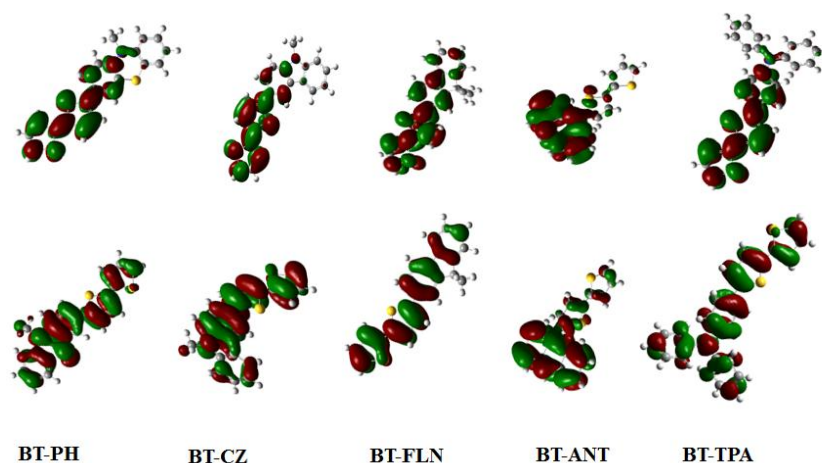
Figure 3.3: Frontier molecular orbital distribution of repeating unit of BT-PH, BT-CZ, BT-FLN, BT- ANT and BT-TPA

3.2.2 Band structure of the polymers

Polymers were optimized using DFT/HSE06/6-31G and DFT/B3LYP/6-31G methods. The computational data of the D-A copolymers are shown in Table 3.2. The band gap of the copolymers P(BT-PH), P(BT-CZ), P(BT-FLN), P(BT-ANT) and P(BT-TPA) were obtained to be 2.52 , 2.68, 2.48,

2.94 and 2.24 eV respectively using DFT/HSE06 and 2.91, 3.05, 2.52, 3.39, 2.87 eV using DFT/B3LYP methods. DFT/PBC/HSE06/6-31G is a better method compared to DFT/PBC/B3LYP/6-31G due to its reliability to predict the band gap of conjugated polymers. HSE06 exchange correlation functional approach reduces self-interaction errors in systems by using an error function screened coulomb potential to calculate the exchange portion of the energy in order to improve computational efficiency.[37,40]

Table 3.2: Computational data of P(BT-PH), P(BT-CZ), P(BT-FLN), P(BT-ANT) and P(BT-TPA) with DFT/HSE06/6-31G[a] and DFT/ B3LYP/6-31G[b] methods

Polymer	HOMO (eV)	IP (eV)	LUMO (eV)	EA (eV)	Eg (eV)
P(BT-PH)	-4.54[a]	4.54	-2.02	2.02	2.52
	-4.67[b]	4.67	-1.76	1.76	2.91
P(BT-CZ)	-4.46[a]	4.46	-1.78	1.78	2.68
	-4.58[b]	4.58	-1.53	1.53	3.05
P(BT-FLN)	-4.75[a]	4.75	-2.27	2.27	2.48
	-4.82[b]	4.82	-2.30	2.30	2.52
P(BT-ANT)	-5.18[a]	5.18	-2.24	2.24	2.94
	-5.36[b]	5.36	-1.96	1.96	3.39
P(BT-TPA)	-4.52[a]	4.52	-2.28	2.28	2.24
	-4.61[b]	4.61	-1.74	1.74	2.87

[a] Estimated from DFT/HSE06/6-31G calculation.
[b] Estimated from DFT/B3LYP/6-31G calculation.

The ground state unit cell geometries for the Periodic Boundary Condition (PBC) was calculated using HSE06/6-31G theory. The starting unit cell for the PBC/DFT calculations were taken from the central portion of the optimized tetramer by assuming that the unit cell was repeated identically an infinite number of times along the translational vector and the calculation was done using G09 suite of codes on IBM power servers. The optimized unit cell for the PBC/HSE06 is given in Fig.3.4. The length of the

translational vector for P(BT-PH), P(BT-CZ), P(BT-FLN), P(BT-ANT) and P(BT-TPA) were found to be 28.38, 22.31, 31.58, 24.08, and 29.60 Å respectively. PBC permitted the calculation of band structure in the positive region of the first Brillouin zone (between k=0 and k=π/a). After the optimization using the HSE06 level of theory, band structures in the positive region were calculated along the k-vector of these one dimensional polymers with 32 k-points. [34,35,41]

(a)

(b)

(c)

(d)

(e)
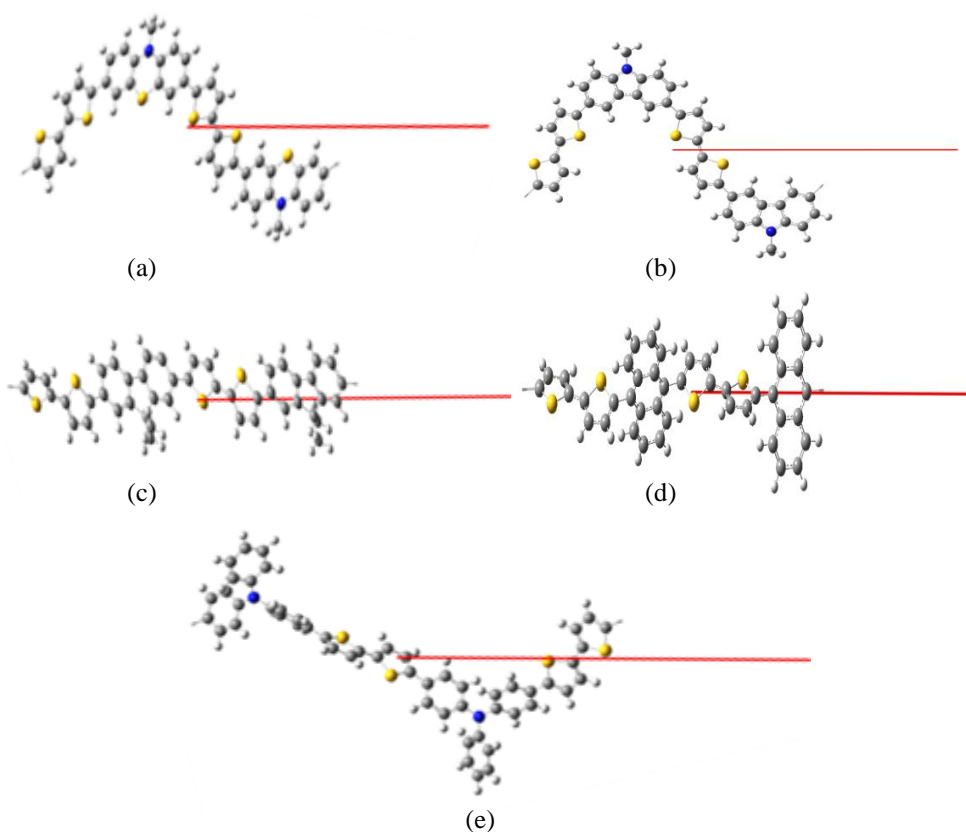
Figure 3.4: Unit cell of (a) P(BT-PH), (b) P(BT-CZ), (c) P(BT-FLN), (d) P(BT-ANT) and (e) P(BT-TPA) for the PBC/HSE06/6-31G calculation. The red line represents the translational vector

The band structure of the copolymers, P(BT-PH), P(BT-CZ), P(BT-FLN), P(BT-ANT) and P(BT-TPA) are shown in Fig.3.5. From the data, it is clear that the lowest band gap occur at k=0 i.e., all the copolymers are direct band gap polymers. By the introduction of the acceptor units, the energy levels of the bithiophene have been tuned and made them suitable for photovoltaic application.
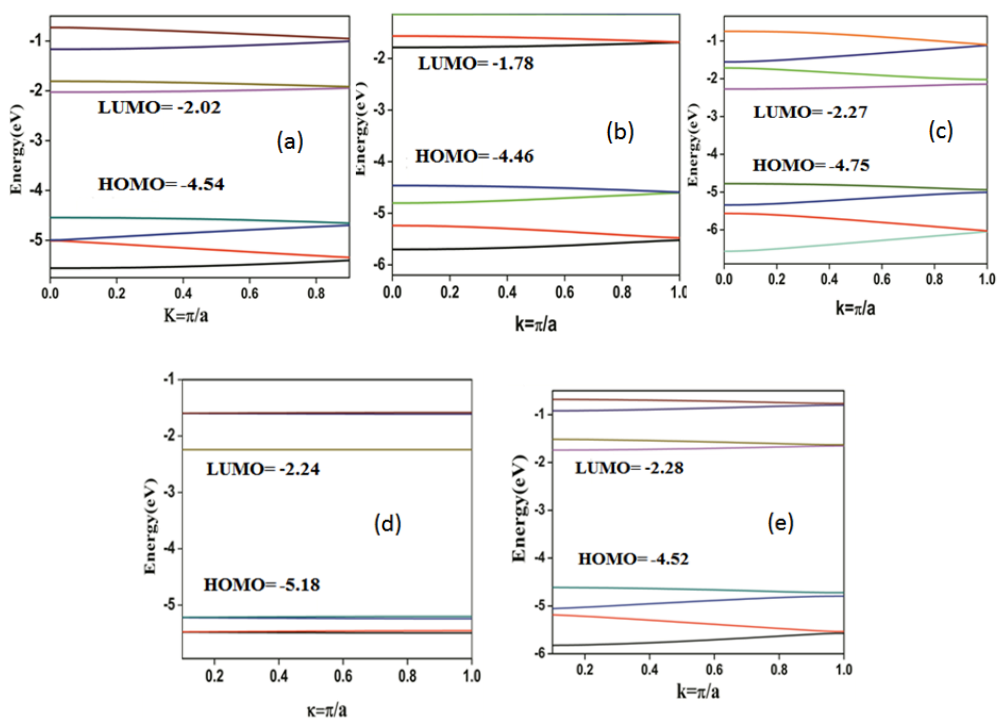
Figure 3.5: Band structure of (a) P(BT-PH), (b) P(BT-CZ), (c) P(BT-FLN), (d) P(BT-ANT) and (e) P(BT-TPA)

3.2.3 Synthesis of monomers and polymers
3.2.3.1 Monomer synthesis

Scheme 3.1 summarizes the synthesis of key monomers.
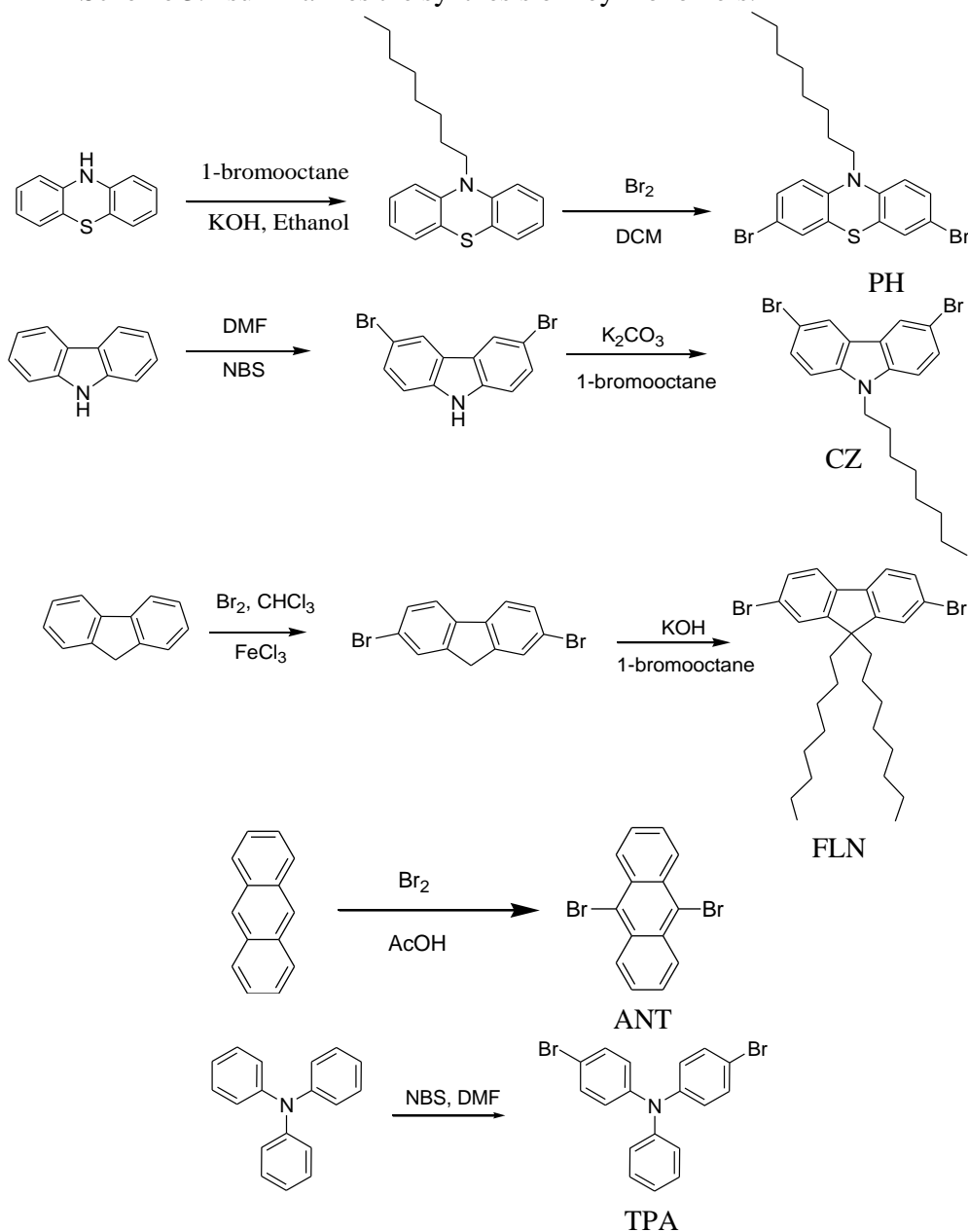
Scheme 3.1: Synthesis of monomers

The precursor monomer 3,7-dibromo-10-octylphenothiazine was synthesized in two steps starting from phenothiazine. First step involved alkylation of phenothiazine using 1-bromooctane followed by bromination in 47 % HBr. Starting from carbazole, 3,6-dibromo-N-octylcarbazole was prepared by bromination using NBS followed by alkylation. To obtain 2,7-dibromo-9,9-dioctyl-9H-fluorene, 9H-fluorene was treated with iron (III) chloride in CHCl$_3$ and bromine was added drop by drop followed by alkylation. The precursor monomers 4,4'-dibromotriphenylamine and 9,10-dibromoanthracene were synthesized by the bromination of triphenylamine and anthracene respectively. The structure of the monomers were confirmed by ^{1}H NMR spectra and are depicted in Figure 3.6.
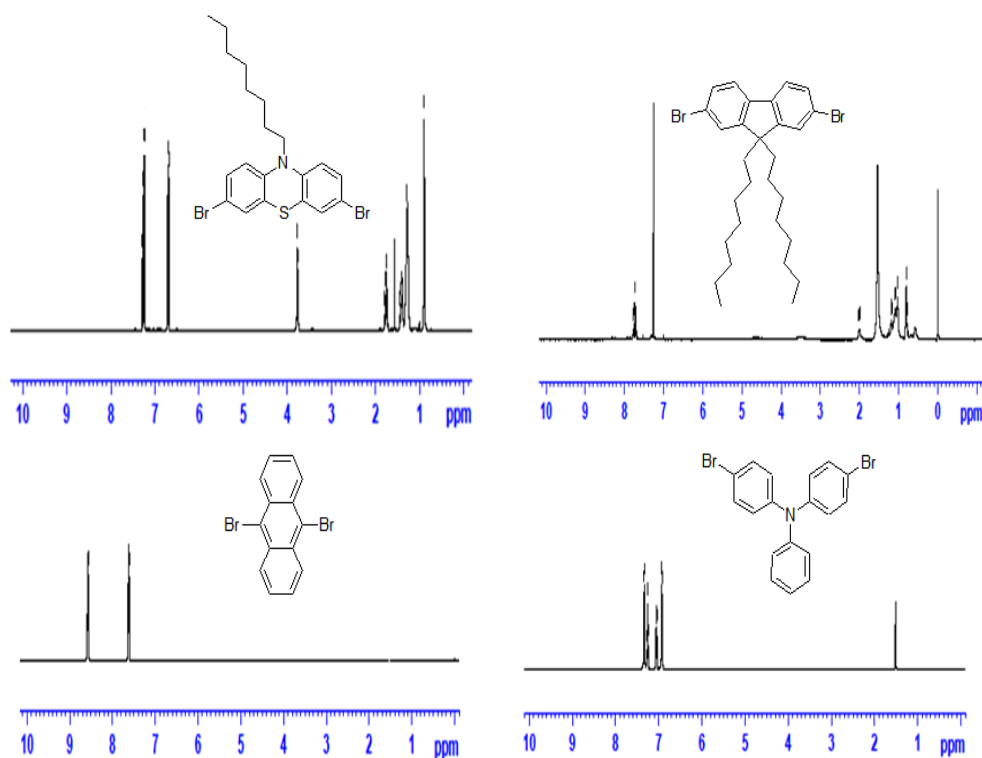
Figure 3.6: ^{1}H NMR spectra of monomers

3.2.3.2 Polymer synthesis

An efficient and simple method, palladium catalysed direct arylation was developed successfully to obtain the bithiophene based alternating copolymers P(BT-PH), P(BT-CZ), P(BT-FLN), P(BT-ANT) and P(BT-TPA). In addition to the benefit of reducing toxic by-products, the direct arylation proceeded with a small amount of Pd catalyst (0.012 mmol) in a short reaction time (12 h) compared to conventional polycondensation based on cross-coupling reactions. The synthetic route to bithiophene based copolymers is shown in scheme 3.2. 3,7-dibromo-10-octylphenothiazine (PH), 3,6-dibromo-N-octylcarbazole (CZ), 2, 7-dibromo-9,9-dioctyl-9H-fluorene (FLN), 9,10-dibromoanthracene (ANT) and 4,4'-dibromotriphenylamine (TPA) were reacted with 2, 2'-bithiophene to obtain P(BT-PH), P(BT-CZ), P(BT-FLN), P(BT-ANT) and P(BT-TPA) respectively. Here, $Pd(OAc)_2$ was used as the catalyst, K_2CO_3 as the base, and N-methylpyrrolidone as the solvent at 80 ^{o}C for 12 h. The crude copolymers were purified by precipitating in methanol. The precipitate was filtered followed by soxhlet extraction using methanol and acetone. The polymers were soluble in common organic solvents such as chloroform, chlorobenzene, tetrahydrofuran and toluene. The reaction in N-methylpyrrolidone (NMP) afforded the polymers in around 70 % yield.

The ^{1}H NMR spectrum of P(BT-PH), P(BT-CZ) and P(BT-FLN) showed multiplets at δ 0.8-2.1 region due to alkyl protons. In P(BT-PH) and P(BT-CZ) the peaks corresponding to –NCH_2- protons were observed at δ 3.8 - 4.1 as triplet. All the copolymers have peaks corresponding to aromatic protons and are observed at δ 6.9 -7.8 as multiplets. P(BT-FLN) was slightly

soluble in $CDCl_3$ and showed less intense peaks (Figure 3.7). The FT-IR spectrum of the copolymers showed characteristic peaks in the range 1400-1550 cm^{-1} (C=C stretching vibration) and 1210-1280 cm^{-1} (C-S stretching vibration) which were attributed to bithiophene unit. FTIR data for P(BT-PH) (KBr pellet, cm^{-1}) showed intense bands at 1575 and 1546 and are attributed to the aromatic C=C stretching and the bands at 2935 and 2860 are indications of alkylated phenothiazine unit. P(BT-CZ) showed peaks at 3100 cm^{-1} (alkenyl C–H), 2965 cm^{-1} (asymmetric C–H stretch in CH_3 group), 2900 cm^{-1} (asymmetric C–H stretch in CH_2 group), 1630 cm^{-1} (C=C stretch). P(BT-FLN) exhibited intense peaks at 2921 and 1370 cm^{-1} and are characteristic of aliphatic C-H stretching and bending vibration of fluorene (FLN) moiety, respectively. The peaks at 809, 851 and 917 cm^{-1} were attributed to the C-H out-of-plane vibration and the peak at 1064 cm^{-1} was due to C-H in-plane vibration of the phenyl ring of FLN unit. In P(BT-ANT) and P(BT-TPA), the FT-IR spectrum showed aromatic C-H bands centered at 3015-3020 cm^{-1} along with C=C aromatic ring vibrations at 1620-1625 and 1540-1545 cm^{-1}.

The number average and weight average molecular weights ($\overline{Mn}$ and $\overline{Mw}$) of the copolymers were determined by GPC analysis using THF as the eluent and polystyrene as the standard. Molecular weight and yield of the copolymers are given in Table 3.3.
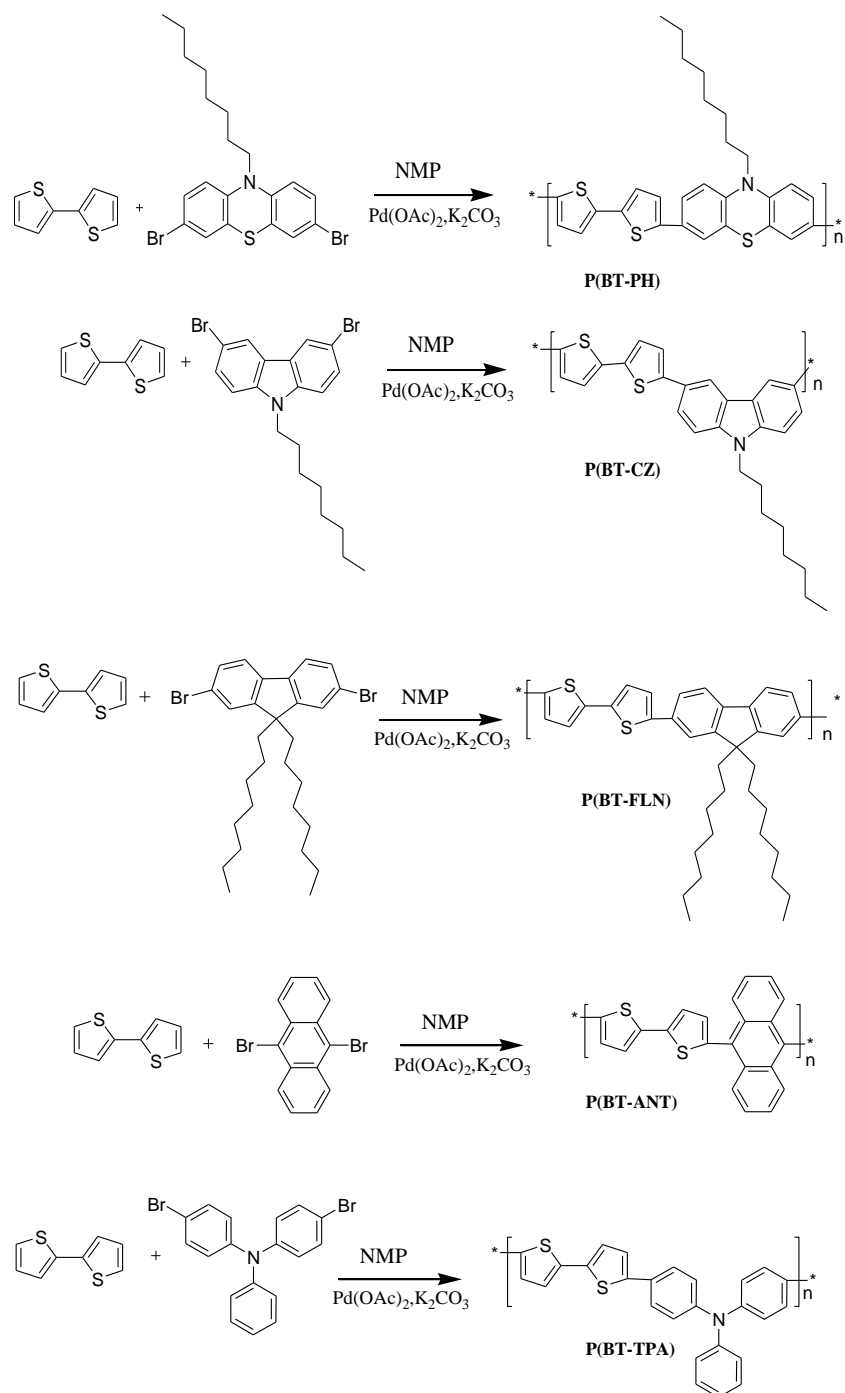
Scheme 3.2: Synthesis of polymers
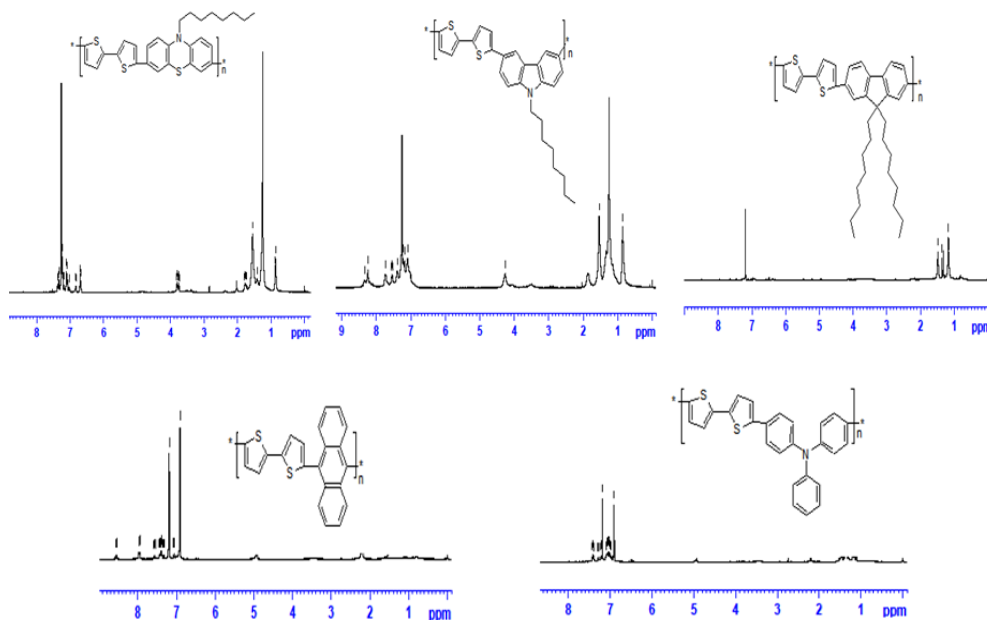
Figure 3.7: ^{1}H NMR spectra of polymers

Table 3.3: Results of direct arylation polymerization

Copolymer	M_n^a	M_w^a	PDI	Yield (%)
P(BT-PH)	3350	4590	1.37	75
P(BT-CZ)	6175	10189	1.65	81
P(BT-FLN)	8534	13139	1.53	79
P(BT-ANT)	5132	9237	1.79	72
P(BT-TPA)	5586	6926	1.23	74

[a]Determined by GPC in THF based on polystyrene standards

3.2.4 Thermal properties

The thermal properties of the bithiophene based copolymers were determined by thermogravimetric analysis (TGA) in nitrogen atmosphere at a heating rate of 10 °C/min. It is clear, that the polymers, P(BT-PH), P(BT-CZ), P(BT-FLN), P(BT-ANT) and P(BT-TPA) showed single step degradation pattern. The copolymers exhibited good thermal stability as shown in the

TGA curves in Fig. 3.8. The onset of weight loss temperatures of P(BT-PH), P(BT-CZ), P(BT-FLN), P(BT-ANT) and P(BT-TPA) are 300 $^{\circ}$C, 425 $^{\circ}$C, 451 $^{\circ}$C, 363 $^{\circ}$C and 427 $^{\circ}$C respectively.
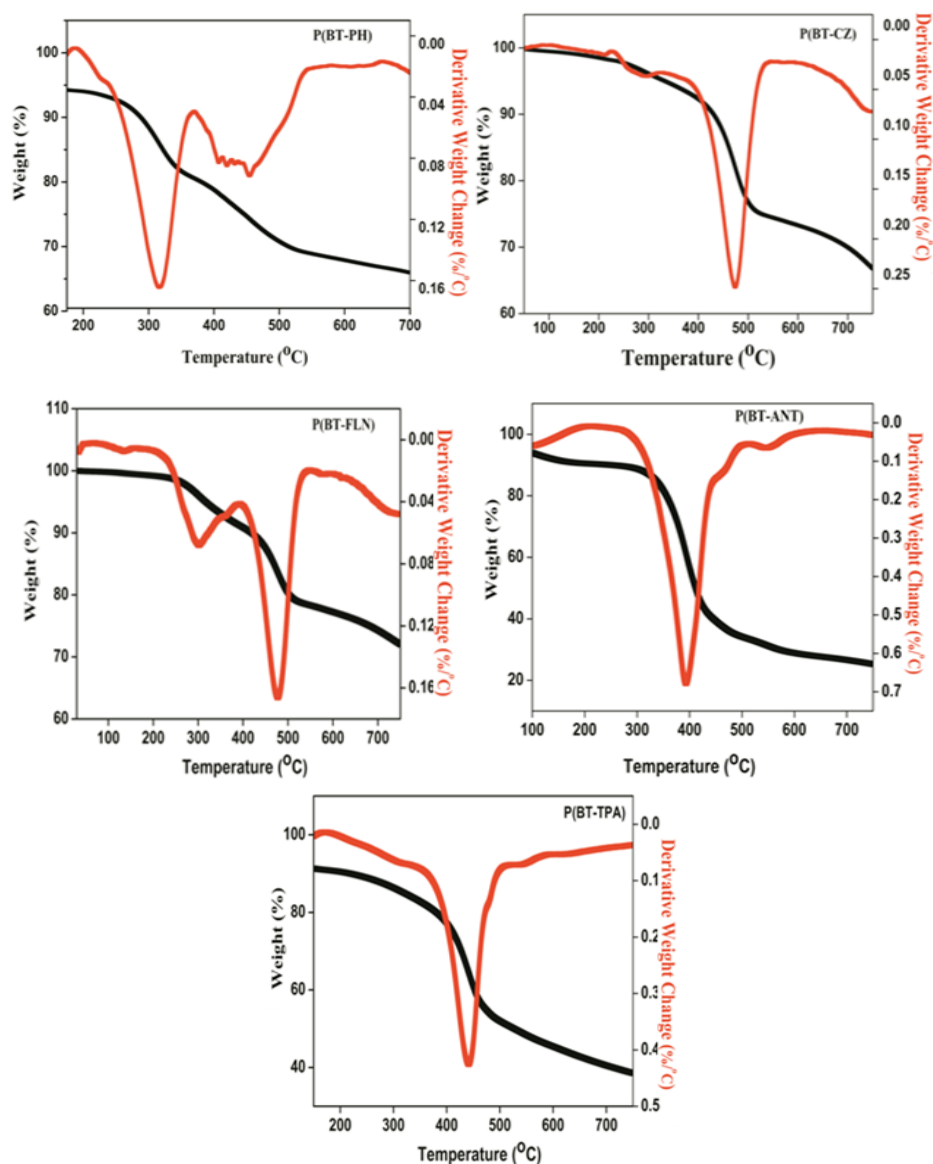
Figure 3.8: TG-DTG traces of the copolymers P(BT-PH), P(BT-CZ), P(BT-FLN), P(BT-ANT) and P(BT-TPA)

DTG traces showed that the onset of degradation and the degradation temperature of P(BT-PH) were found to be 259 and 317 ^{o}C with 4 % weight loss as the onset loss point. In P(BT-CZ), the onset of degradation was around 409 ^{o}C and the degradation temperature was 475 °C with about 6 % weight loss. In the case of P(BT-FLN), P(BT-ANT) and P(BT-TPA) the onset of degradation was around 430 ^{o}C, 312 ^{o}C and 381 ^{o}C and the degradation temperature was 476 ^{o}C, 395 ^{o}C and 441 ^{o}C respectively with 7 %, 4 % and 5 % weight loss at the onset loss point. Bithiophene based polymers have thermal stability much higher than those of homopolymer of phenothiazine,[42] carbazole [43] and flourene.[44]

3.2.5 Optical properties

The optical absorption and fluorescence emission spectra of copolymers P(BT-PH), P(BT-CZ), P(BT-FLN), P(BT-ANT) and P(BT-TPA) were recorded at room temperature in THF solution (Figure 3.9). The homopolymer, poly(phenothiazine),[42] poly(carbazole),[43] poly(fluorene)[44] and poly(anthracene)[45] have low absorption maxima compared to bithiophene containing copolymers. The insertion of bithiophene moiety in the polymer backbone has a pronounced influence on the spectroscopic properties of the polymers. The increasing wavelength of the absorption maxima indicate that the polymers are more conjugated as more thiophene units are added to the structure. Their photophysical properties are summarized in Table 3.4. The optical band gap of copolymers was determined from the absorption edge using Tauc's equation.[46] The band gap of the copolymers, P(BT-PH), P(BT-CZ), P(BT-FLN), P(BT-ANT) and P(BT-TPA) were calculated to be 2.09, 2.14, 2.12, 2.15 and 2.11 eV respectively. Fig 3.9 b represents the emission spectra of P(BT-PH), P(BT-CZ), P(BT-FLN), P(BT-ANT) and P(BT-TPA) in THF

medium. The emission peaks of the copolymers are observed at the wavelength range of 515–535 nm.
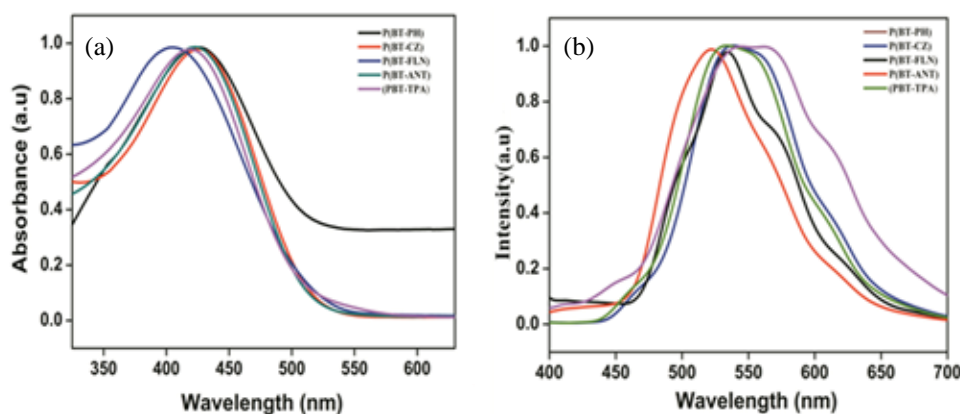
Figure 3.9: (a) UV–Visible absorption Spectra (b) Emission Spectra of P(BT-PH), P(BT-CZ), P(BT-FLN), P(BT-ANT) and P(BT-TPA)

Table 3.4: Optical properties of polymers in THF solution

Polymer	Absorption λ_{max} (nm)	Absorption onset (nm)	Emission λ_{max} (nm)	E_g (Optical) (eV)
P(BT-PH)	428	592	534	2.09
P(BT-CZ)	422	579	532	2.14
P(BT-FLN)	411	585	517	2.12
P(BT-ANT)	423	577	530	2.15
P(BT-TPA)	421	587	525	2.11

3.2.6 Electrochemical studies

The electrochemical behaviour of the bithiophene based copolymers were investigated by Cyclic Voltammetry (CV). The results of the electrochemical measurements observed from the cyclic voltammograms

which estimate the HOMO, LUMO levels and band gap of the copolymers P(BT-PH), P(BT-CZ), P(BT-FLN), P(BT-ANT) and P(BT-TPA) are presented in Table 3.5. The process was carried out for the copolymer films on Pt electrode in 0.1 M tetrabutylammonium hexafluoroborate (Bu_4NBF_6) solution in anhydrous acetonitrile at a scan rate of 100 mV/s at room temperature under nitrogen atmosphere. The onset oxidation and the onset reduction potentials of the copolymers estimated the HOMO and LUMO energy levels using the following equation proposed by Bredas.[47]

HOMO (IP; ionization potential) = - $(4.71 + E_{ox}^{onset})$

LUMO (EA; electron affinity)   = - $(4.71 + E_{red}^{onset})$

The onset oxidation potential of P(BT-PH), P(BT-CZ), P(BT-FLN), P(BT-ANT) and P(BT-TPA) were 0.32, 0.86, 0.19, 0.27 and 0.22 eV respectively. The onset reduction potential was obtained to be -1.23, -1.02, -1.07, -1.09 and -1.29 eV, for P(BT-PH), P(BT-CZ), P(BT-FLN), P(BT-ANT) and P(BT-TPA) respectively. The band gap was calculated to be 1.55, 1.87, 1.25, 1.36 and 1.50 eV respectively for P(BT-PH), P(BT-CZ), P(BT-FLN), P(BT-ANT) and P(BT-TPA). The experimental value has distinct deviation from the theoretical calculated values. It is because, the predicted band gaps are for the isolated gas phase chains and also, the solid state effects such as polarization effects and intermolecular packing forces are neglected.[48,49] The lower band gap of the bithiophene based copolymers is due to the higher acceptor strength of PH, CZ, FLN, ANT and TPA units which enhances the charge transfer from donor.

Table 3.5: Redox properties of for P(BT-PH), P(BT-CZ), P(BT-FLN), P(BT-ANT) and P(BT-TPA)

Polymer	E_{ox} (V)	HOMO (eV)	E_{red} (V)	LUMO (eV)	Band Gap (eV)
P(BT-PH)	0.32	-5.03	-1.23	-3.47	1.55
P(BT-CZ)	0.86	-5.56	-1.02	-3.68	1.87
P(BT-FLN)	0.19	-4.89	-1.07	-3.64	1.25
P(BT-ANT)	0.27	-4.98	-1.09	-3.62	1.36
P(BT-TPA)	0.22	-4.93	-1.29	-3.41	1.50

3.2.7 Time resolved fluorescence measurements

The lifetime measurement was performed on the bithiophene based copolymers using Time-Correlated Single Photon Counting technique (TCSPC). The fluorescence of a sample is monitored as a function of time after excitation by a laser pulse. The copolymers in $CHCl_3$ were excited at 340 nm. The observed decay could not fit well with the single exponential fit. The fluorescence decay curve was obtained using bi-exponential fitting due to existence of different fluorescing moieties with distinct lifetimes. The τ_1 and τ_2 are the lifetimes, and the α_1 and α_2 are the pre-exponential factors. The average lifetime of P(BT-PH), P(BT-CZ), P(BT-FLN), P(BT-ANT) and P(BT-TPA) were calculated to be 8.70, 7.02, 6.22, 4.43 and 2.38 ns respectively. The bi-exponentially fitted decay curves of copolymers in $CHCl_3$ solution monitored at 340 nm are shown in Fig. 3.10.
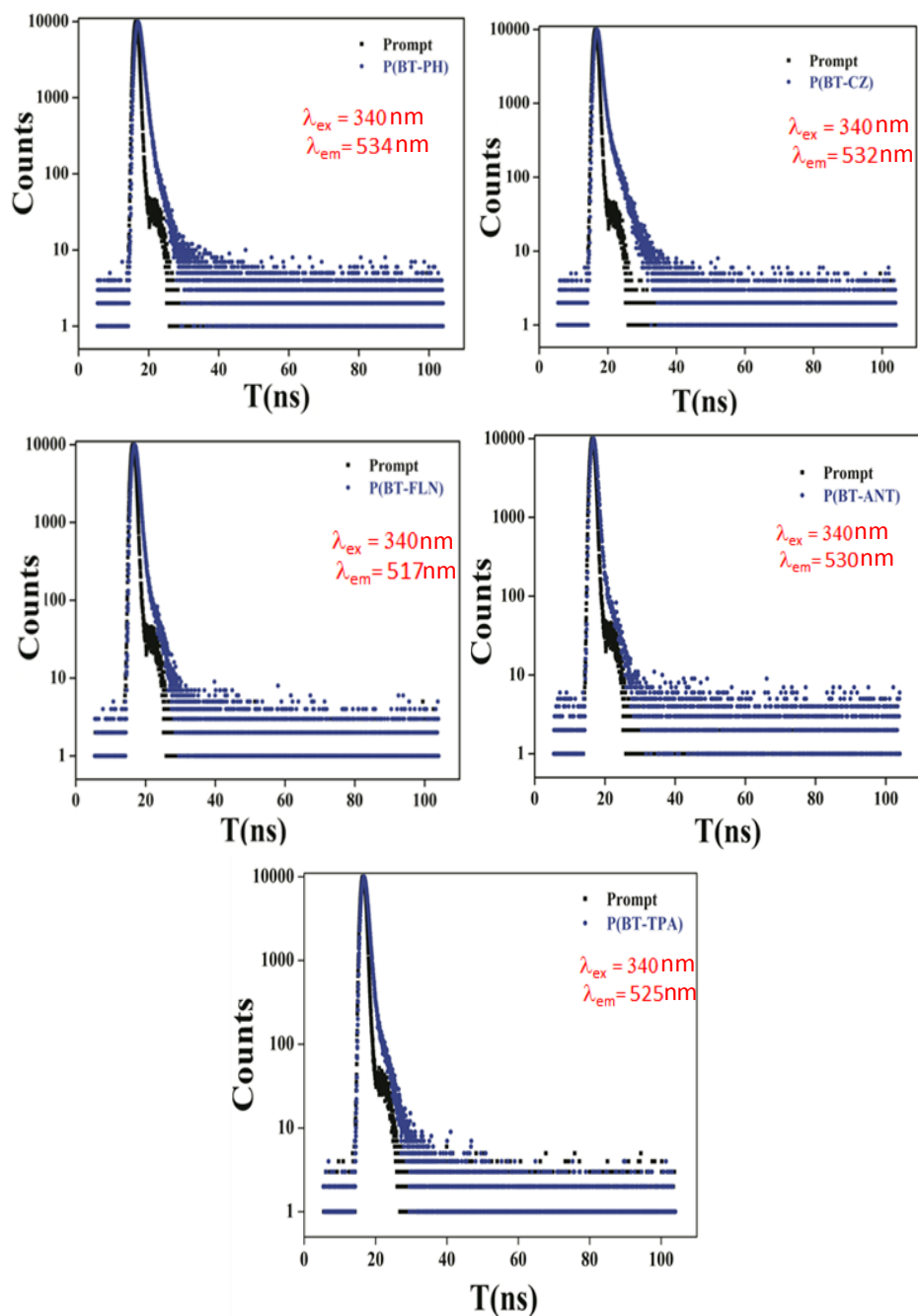
Figure 3.10: Bi-exponential fitted decay curves of P(BT-PH), P(BT-CZ), P(BT-FLN), P(BT-ANT) and P(BT-TPA) in CHCl$_3$ at 340 nm excitation

Quantum yield of fluorescence ϕ^d is one of the major parameters characterizing fluorescent materials. It is used to quantify the efficiency of the emission process; it determines the suitability of such materials for applications in chemical sensing, bioanalysis and fluorescence imaging as well as for the active components in optical devices. For accurate ϕ determination, different methods were developed. Here, the "absolute" method was used that was based on collecting the whole spatially distributed fluorescence emission.[50] The quantum yield (ϕ^d) of the copolymers was measured with the same excitation wavelength, 340 nm. The magnitude of the decay times of the bithiophene based copolymers across the emission wavelength and quantum yields are summarized in the Table 3.6.

Table 3.6: Fluorescence lifetimes, pre-exponential factors and quantum yield of P(BT-PH), P(BT-CZ), P(BT-FLN), P(BT-ANT) and P(BT-TPA) in CHCl$_3$ at 340 nm excitation

Polymer	χ^2	τ_1 (ns)	α_1 %	τ_2 (ns)	α_2 %	τ_{av} (ns)	ϕ^d
P(BT-PH)	1.16	0.85	96.78	3.26	3.22	8.70	0.43
P(BT-CZ)	1.24	0.63	86.05	2.83	13.95	7.02	0.39
P(BT-FLN)	1.19	0.31	74.14	7.83	25.86	6.22	0.49
P(BT-ANT)	1.11	0.42	95.75	2.41	4.25	4.43	0.45
P(BT-TPA)	0.91	0.12	40.15	0.69	59.85	2.38	0.37

3.2.8 Solvatochromic measurements

The absorption and emission spectra of P(BT-CZ) have been recorded at room temperature in Toluene/acetonitrile mixtures of different polarities. The change in the dipole moment ($\Delta\mu$) was calculated both from solvatochromic shift method and on the basis of microscopic empirical solvent polarity parameter (E_T^N) and values are compared. The values of the polarity parameter were obtained from Table 2.7. given in section 2.2.9. The

solvatochromic data of the copolymers are summarised in the Table 3.7. Eleven ratios of toluene/ acetonitrile mixtures with dielectric constants varying from 2.38 to 37.50 were used.

Table 3.7: Solvatochromic data of P(BT-CZ) in in toluene/acetonitrile mixtures of varying polarity

Weight fraction of acetonitrile (%)	Abs max (nm)	Emission max (nm)	$\bar{\nu}_a - \bar{\nu}_f$ (cm^{-1})	$\bar{\nu}_a + \bar{\nu}_f$ (cm^{-1})
100	416	534.0	5313	42762
90	416	534.0	5313	42762
80	415	532.7	5326	42865
70	414	531.5	5339	42969
60	414	531.5	5339	42969
50	413	532.9	5450	42975
40	412	531.6	5463	43080
30	411	525.5	2629	38863
20	410	520.3	2587	38905
10	409	514.7	2617	38962
0	404	498.0	2547	39119

E_T^N versus $(\nu_a - \nu_f)$, $f(\varepsilon, n)$ versus $(\nu_a - \nu_f)$ and $f_1(\varepsilon,n)$ versus $(\nu_a + \nu_f)$ for P(BT-CZ) was plotted. For the analysis of data, only solvent mixtures showing linear variation of the polarity parameters were used. A linear progression was done and the data were fit to a straight line, corresponding values of the slopes were calculated (Table 3.8). The correlation coefficient was larger than 0.95 which indicated a good linearity for the slopes m, m_1 and m_2 with selected number of Stokes shift data points.

Table 3.8: Statistical treatment of the correlations of P(BT-CZ) in toluene/acetonitrile mixtures of varying polarity

Polymer	Slope with correlation co-efficient 'R'		
	E_T^N	Bakshiev's	Chamma-Viallet's
P(BT-CZ)	2849 (0.98)	5665 (0.96)	1760 (0.98)

The ground state and excited state dipole moment values were calculated from equation 2.10 and 2.11. The value of Onsager cavity radius (a) for P(BT-CZ) was calculated using the equation 2.9. given in section 2.2.9. Results of the calculation are given in Table 3.9.

Table 3.9: Ground and excited state dipole moments of P(BT-CZ) in toluene/ acetonitrile mixtures of varying polarity

Polymer	a^1 (Å)	$\mu_g{}^2$ (D)	$\mu_e{}^3$ (D)	$\Delta\mu^4$ (D)	$\Delta\mu^5$ (D)
P(BT-CZ)	6.13	7.02	13.36	6.34	4.44

[1]Caluated from equation 2.9
[2]The ground state dipole moment calculated using Eq. 2.10.
[3]The excited state dipole moment calculated from Eq. 2.11.
[4] The change in dipole moment for μ_g and μ_e
[5]The change in dipole moment calculated from Eq. 2.15.

3.3 Conclusion

In conclusion, it was shown theoretically that the introduction of 3,7-dibromo-10-octylphenothiazine, 3,6-dibromo-N-octylcarbazole, 2,7-dibromo-9,9-dioctyl-9H-fluorene, 4,4'-dibromotriphenylamine and 9,10-dibromoanthracene units to the bithiophene unit effectively reduced the band gap of the conjugated polymers in accordance with the donor-acceptor concept. The band gap reduction depended on the acceptor strength of the PH, CZ, FLN, ANT and TPA which facilitated the charge transfer from donor to acceptor units. The polymers were synthesized by direct arylation reaction and characterized by electrochemical and photophysical methods. Time-resolved fluorescence techniques were applied to P(BT-PH), P(BT-CZ), P(BT-FLN), P(BT-ANT) and P(BT-TPA) in CHCl$_3$. The absorption, emission and fluorescence decay were measured at room temperature. The solvatochromic properties of the copolymer P(BT-CZ) were studied. There was significant difference observed in the change in dipole moment of the

copolymer obtained by the two methods i.e., solvatochromic shift method and on the basis of microscopic empirical solvent polarity parameter(E_T^N). The discrepancies observed may be due to the different approximations adopted in both methods to estimate $\Delta\mu$ of the copolymer.

3.4 Experimental section

3.4.1 10-n-octylphenothiazine [51]

Phenothiazine (10 g, 50 mmol) and potassium hydroxide (20 g, 500 mmol) were dissolved in DMSO (100 mL) placed in a 250 mL two-necked flask. The mixture was stirred for half an hour. Octyl bromide (7.7 mL, 55 mmol) was added drop wise into the reaction mixture in 20 min and this mixture was stirred for 24 h at room temperature. The reaction mixture was poured into water, extracted with dichloromethane and dried with MgSO₄. The resulting liquid was purified by column chromatography using petroleum ether as eluent which gave colourless liquid.

Yield	:	93 %
^{1}H NMR (400MHz, CDCl₃)	:	δ 0.87 (t, *J=6.8* Hz, 3H), 1.24-1.43 (m, 10H), 1.77 (m, 2H), 3.80-3.84 (t, *J=7.2* Hz, 2H), 6.83-6.91 (m, 4H), 7.11-7.15 (m, 4H).
GCMS	:	m/z = 311

3.4.2 3,7-dibromo-10-octylphenothiazine [51]

10-n-Octylphenothiazine (7.5 g, 0.024 mol) was dissolved in 50 mL of dichloromethane and bromine (8.0 g, 0.05 mol) was injected into the solution using a syringe and stirred for 4 h at room temperature. Dilute

aqueous sodium hydroxide (20 mL) was added to the reaction mixture and kept for 30 min. The reaction mixture was extracted three times using dichloromethane and brine, and the organic layer was separated and concentrated. The crude product was purified using column chromatography using hexane as the eluent which gave yellow oil.

Yield	:	79 %
^{1}H NMR (400MHz, CDCl$_3$)	:	δ 0.86 (t, 3H), 1.14-1.51 (m, 10 H), 1.74 (m, 2H), 3.72 (t, 2H), 6.66 (d, 2H), 7.18-7.20 (dd, 2H), 7.24 (d, 2H).
LCMS	:	m/z = 470

3.4.3 3,6-dibromocarbazole

Carbazole (16.7 g, 100 mmol) was dissolved in DMF (150 mL) at 0 ^{o}C with stirring, followed by the addition of a solution of NBS (36.3 g, 200 mmol) in 100 mL of DMF. The resulting mixture was stirred at room temperature for 2 h, and the solution was poured into 500 mL of water, filtered, and washed with water. The crude product was recrystallized from ethanol.

Yield	:	88 %
^{1}H NMR (400MHz, CDCl$_3$)	:	δ 8.14 (s, 2H), 8.11 (s, 1H), 7.53 (d, 2H), 7.33 (d, 2H).
GCMS	:	m/z = 322.89

3.4.4 3,6-dibromo-N-octylcarbazole

3,6-dibromocarbazole (6.5 g, 20 mmol) was dissolved in 50 mL of anhydrous DMF and potassium carbonate (5.5 g, 40 mmol) was added to it. The mixture was allowed to stir for 1 h, after which 1-bromooctane (5.8 g,

30 mmol) was added drop wise. The reaction mixture was allowed to reflux for 2 days. It was cooled, the mixture was poured into water and extracted with chloroform three times and the combined organic layer was dried over anhydrous $MgSO_4$. The solvent and the unreacted 1-bromooctane were removed under reduced pressure and the residue was purified by column chromatography with hexane and ethyl acetate (9:1) to afford the compound as a waxy solid.

Yield	:	80 %.
^{1}H NMR (400MHz, CDCl$_3$)	:	δ 8.17 (s, 2H), 7.60-7.52 (d, 2H), 7.30-7.23 (d, 2H), 4.15-4.09 (m, 2H), 2.01-1.97 (m, 1H), 1.35-1.25 (m, 8H), 0.96-0.85 (m, 6H).
LCMS	:	m/z = 435.02

3.4.5 2,7-dibromofluorene [52]

To a solution of 9H-fluorene (6 g, 36 mmol), iron (III) chloride (92 mg, 1.6 mmol) in CHCl$_3$ (100 mL) at 0 ^{o}C and 4 mL bromine was added drop by drop. The mixture was stirred for 12 h. After the reaction, it was poured into 50 mL water. The precipitate was washed with NaHCO$_3$ and NaHSO$_3$ solution. The organic layer was extracted with CHCl$_3$ and was dried over anhydrous $MgSO_4$. After filtration, the solvent was removed using rotary vacuum evaporator, and the residue was recrystallized from ethanol resulting in white crystalline product.

Yield	:	75 %.
^{1}H NMR (400MHz, CDCl$_3$)	:	δ 7.66 (s, 2H), 7.60-7.59 (d, 2H), 7.51-7.49 (d, 2H)
GCMS	:	m/z = 321.90

3.4.6 2, 7-dibromo-9,9-dioctyl-9H-fluorene

KOH solution (10 mL, 50 %) and 1-Bromooctane (5.60 g, 29.0 mmol) was added drop wise to a mixture of 2,7-dibromo-9H-fluorene (3.88 g, 12.0 mmol), tetrabutylammonium bromide (0.0225 g, 0.0975 mmol) in DMSO (50.0 mL) under N_2 atmosphere. The reaction mixture was stirred at 80 ^oC for 2 days. The mixture was poured into H_2O (500 mL). The organic layer was extracted with dichloromethane. The combined organic layer was dried over anhydrous $MgSO_4$. The solvent was removed under reduced pressure. The crude product was purified by recrystallization from hexane to yield colourless crystals.

Yield	: 89 %.
^{1}H NMR (400MHz, $CDCl_3$)	: δ 7.51 (s, 2H), 7.45 (m, 4H), 1.90 (m, 4H), 1.25-0.86 (m, 24H), 0.83 (t, 6H).
LCMS	: m/z = 546.15

3.4.7 9,10-dibromoanthracene

Bromine (17.9 g, 0.112 mol) in acetic acid (50 mL) was added drop wise over a period of 5 minutes to a mixture of anthracene (10.0 g, 0.056 mol) in acetic acid (300 mL) at room temperature. The reaction was left to stir for 30 minutes during which a canary yellow precipitate was formed. Water (300 mL) was added, the suspension was left to stir for 10 minutes, filtered and washed with water. The yellow solid was dried under vacuum for 24 h to give the title compound.

Yield	: 94 %.
^{1}H NMR (400MHz, $CDCl_3$)	: δ 8.10 (4H, d), 7.35 (4H,d).
GCMS	: m/z = 336.25

3.4.8 4,4'-dibromotriphenylamine [53]

To a mixture of triphenylamine (2.43 g, 10 mmol) in DMF (50 mL), NBS (3.56 g,10 mmol) in small portions were added. When the colour of the solution was changed from colourless to light yellow, 100 mL dichloromethane was added to the reaction mixture and stirred at room temperature for 24h. After the reaction was complete, the mixture was washed with water; the organic layer was separated and dried over $MgSO_4$. The solvent was evaporated using rotary vacuum evaporator. The crude product was purified by column chromatography over silica gel (Hexane: dichloromethane at 5:1) and a curdy white powder was obtained.

Yield	:	72 %.
^{1}H NMR (400MHz, $CDCl_3$)	:	δ 6.93 (d, 4H), 7.05 (d, 2H), 7.17 (m, 1H), 7.25 (m, 2H), 7.37 (d, 4H).
LCMS	:	m/z = 402.78

3.4.9 General procedure for polymerization through direct arylation reaction

To a stirred solution of bithiophene (0.124 mmol) in 1.25 mL of N-methylpyrrolidone in a 10 mL Schlenk tube was added, dibromomonomer (0.124 mmol), $Pd(OAc)_2$ (0.012 mmol) and K_2CO_3 (0.31 mmol). The solution was purged with nitrogen gas for 5 minutes; the mixture was stirred at 80 ^{o}C for 12 h. The reaction mixture was cooled to room temperature and poured in to methanol. The precipitate was filtered and washed with methanol. The polymer was purified by soxhlet extraction using acetone and methanol for 24 h. The residue was dissolved in minimum amount of toluene and precipitated from methanol and dried in vacuum.

3.4.9.1 Synthesis of P(BT-PH)

Bithiophene (0.124 mmol), 3,7-dibromo-10-octylphenothiazine (0.124 mmol), $Pd(OAc)_2$ (0.012 mmol), K_2CO_3 (0.31 mmol), NMP (1.25 mL) were used. Dark green solid.

Yield	: 75 %
UV-Visible (THF) λmax	: 428 nm
GPC	: M_n = 3350, PDI = 1.37
Td (^{o}C)	: 317
^{1}H NMR (400 MHz, CDCl$_3$)	: δ 7-7.21 (m, 5H of bithiophene), 6.72-7.15 (m, ~6H of phenothiazine), 3.82 (t, 2H, -NCH$_2$-), 1.92-1.18 (m, ~12H, aliphatic-H), 0.96 (t, ~3H, -CH$_3$)

3.4.9.2 Synthesis of P(BT-CZ)

Bithiophene (0.124 mmol), 3,6-Dibromo-N-octylcarbazole (0.124 mmol), $Pd(OAc)_2$ (0.012 mmol), K_2CO_3 (0.31 mmol), NMP (1.25 mL) were used. Dark brown solid.

Yield	: 81 %
UV-Visible (THF) λmax	: 422 nm
GPC	: M_n = 6175, PDI = 1.65
Td (^{o}C)	: 475
^{1}H NMR (400 MHz, CDCl$_3$)	: δ 7-7.21 (m, 5H of bithiophene), 7.12 - 8.5 (m, 6H of carbazole), 4.2 (m, 2H, -NCH$_2$-), 1-1.99 (m, ~12H, aliphatic-H), 0.98 (t, ~3H, -CH$_3$)

3.4.9.3 Synthesis of P(BT-FLN)

Bithiophene (0.124 mmol), 2, 7-Dibromo-9,9-dioctyl-9H-fluorene (0.124 mmol), Pd(OAc)$_2$ (0.012 mmol), K$_2$CO$_3$ (0.31 mmol), NMP (1.25 mL) were used. Brown solid.

Yield	: 79 %
UV-Visible (THF) λmax	: 411 nm
GPC	: M$_n$ = 8534, PDI = 1.53
Td (^{o}C)	: 476
^{1}H NMR (400 MHz, CDCl$_3$):	δ 7-7.21 (m, 5H of bithiophene), 7.38 – 7.40 (3d, 6H of fluorene), 1.84-1.90 (m, 4H), 1.10- 1.20 (m, 20H, aliphatic-H), 0.92 (t, 6H, -CH$_3$-)

3.4.9.4 Synthesis of P(BT-ANT)

Bithiophene (0.124 mmol), 9,10-dibromoanthracene (0.124 mmol), Pd(OAc)$_2$ (0.012 mmol), K$_2$CO$_3$ (0.31 mmol), NMP (1.25 mL) were used. Yellow solid.

Yield	: 72 %
UV-Visible (THF) λmax	: 423 nm
GPC	: M$_n$ = 5132, PDI = 1.79
Td (^{o}C)	: 395
^{1}H NMR (400 MHz, CDCl$_3$):	δ 7-7.21 (m, 5H of bithiophene), 7.00 -8.35 (d, 8H of anthracene)

3.4.9.5 Synthesis of P(BT-TPA)

Bithiophene (0.124 mmol), 4,4'-dibromotriphenylamine (0.124 mmol), $Pd(OAc)_2$ (0.012 mmol), K_2CO_3 (0.31 mmol), NMP (1.25 mL) were used. Brown solid.

Yield	:	74 %
UV-Visible (THF) λmax	:	421 nm
GPC	:	M_n = 5586, PDI = 1.23
Td (^{o}C)	:	441
^{1}H NMR (400 MHz, CDCl$_3$):		δ 7-7.21 (m, 5H of bithiophene),
		δ 6.90-7.35 (d, 10H), 7.15-7.30 (m, 3H).

References

1. J. Hou, Z. Tan, Y. Yan, Y. He, C. Yang, Y. Li, *J. Am. Chem. Soc.,* 2006, **128**, 4911.

2. J. Roncali, *Macromol. Rapid. Commun.,* 2007, **28**, 1761.

3. S. Gunes, H. Neugebauer, N. S. Sariciftci, *Chem. Rev.,* 2007, **107**, 1324.

4. P. L. T. Boudreault, A. Najari, M. Leclerc, *Chem. Mater.,* 2011, **23**, 456.

5. Q. Wang, R. Takita, Y. Kikuzaki, F. Ozawa, *J. Am. Chem. Soc.,* 2010, **132**, 11420.

6. S. Tamba, K. Shono, A. Suige, A. Mori, *J. Am. Chem. Soc.,* 2011, **133**, 9700.

7. S. Bernier, S. Garreau, M. Bera-Aberem, C. Gravel, M. Leclerc, *J. Am. Chem. Soc.,* 2002, **124**, 12463.

8. Y. Zhu, R. D. Champion, S. A. Jenekhe, *Macromolecules.,* 2006, **39**, 8712.

9. R. Yang, R. Tian, Q. Hou, Y. Zhang, Y. Li, W. Yang, C. Zhang, Y. Cao, *J. Polym. Sci Part A: Polym. Chem.,* 2005, **43**, 823.

10. E. Lim, B. J. Jung, H. K. Shim, *J. Polym. Sci. Part A: Polym. Chem.,* 2006, **44**, 243.

11. Y. K. Jung, J. Lee, S. K. Lee, H. J. Cho, H. K. Shim, *J. Polym. Sci. Part. A: Polym. Chem.,* 2006, **44**, 4611.

12. Y. J. Wang, M. Huang, Z. Wang, Y. Wu, Y. Wu, *J. Org. Chem.*, 2014, **79,** 2890.

13. F. Alakhras, R. Holze, *Synth. Met.,* 2007,**157**, 109.

14. F. Alakhras, R. Holze*, Electrochim. Acta.,* 2007, **52**, 5896.

15. T. Yohannes, J. C. Carlberg, O. Inganas, T. Solomon, *Synth.Met*., 1997, **8**, 15.

16. W. Tang, T. Kietzke, P. Vemulamada, Z. Kuan Chen, *J. Polym. Sci.,: Part A: Polym. Chem.,* 2007, **45**, 5266.

17. R. R. Yue, J. K. Xu, B.Y. Lu, C. C. Liu, Z. J. Zhu, Z. Zhang, *Chin. J. Polym. Sci.,* 2010, **28**, 771.

18. B. Ustamehmetoglu, F. Demir, E. Sezer, *Prog. Org. Coat.,* 2013, 76, 1515.

19. (a) T. Yamamoto*, Bull. Chem. Soc. Jpn.,* 2010, **83**, 431.

    (b) J. Sakamoto, M. Rehahn, G. Wegner, A. D. Schlüter, *Macromol. Rapid. Commun.,* 2009, **30**, 653.

20. B. Carsten, F. He, H. J. Son, T. Xu, L. Yu, *Chem. Rev.,* 2011, **111**, 1493.

21. T. Yokozawa,Y. Nanashima, Y. Ohta, *ACS Macro Lett.,* 2012, **1**, 862.

22. M. J. Robb, S. Y. Ku, C. J. Hawker, *Adv. Mater*., 2013, **25**, 5686.

23. Z. J. Bryan, A. J. McNeil, *Macromolecules* 2013, **46**, 8395.

24. A. Mori, *J. Synth. Org. Chem., Jpn.,* 2011, **69**, 1202.

25. N. Kuhl, M. N. Hopkinson, J. Wencel Delord, F. Glorius, *Angew. Chem. Int. Ed.* 2012, **51**, 10236.

26. F. Shibahara, T. Murai, *Asian J. Org. Chem.,* 2013, **2**, 624.

27. L. Ackermann, *Acc. Chem. Res.,* 2014, **47,** 281.

28. K. Kornobis, N. Kumar, P. Lodowski, M. Jaworska, P. Piecuch, J. J. Lutz, P. M. Kozlowsk, *J. Chem. Theory Comput.,* 2013,**34**, 987.

29. N. Kumar, M. Alfonso-Prieto, C. Rovira, P. Lodowski, M. Jaworska, P. M. Kozlowski, *J. Chem. Theory Comput.,* 2011, **7,** 1541.

30. M. W. Bryan, P. Manuel, D. S. Fabio, *Phys. Chem. Chem. Phys.,*2009, **11**, 4498.

31. R. G. Parr, W. Yang, *Density-Functional Theory of Atoms and Molecules*, Oxford University Press, New York, 1989.

32. (a) W. J. Hehre, D. R, J. A. Pople, *J. Chem. Phys.,* 1972, **56**, 2257

    (b) P. C. Harihara, J. A. Pople, *Theor. Chim.Acta.,* 1973, **28**, 213.

33. M. J. Frisch, G. W. Trucks, H. B. Schlegel, G. E. Scuseria, M. A. Robb, J. R. Cheeseman, G. Scalmani, V. Barone, B. Mennucci, G. A. Petersson, H. Nakatsuji, M. Caricato, X. Li, H. P. Hratchian, *Gaussian 09 Revision B.01*, Gaussian, Inc., Wallingford, CT, 2010.

34. A. D. Becke, *J. Chem. Phys.,* 1993, **98**, 5648.

35. C. Lee, W. Yang, R. G. Parr, *Phys. Rev. B.,* 1994, **37**, 785.

36. K. Burke, J. P. Perdew, Y. Wang, J. F. Dobson, V. G. Das, *Electronic Density Functional Theory: Recent Progress and New Direction,* NewYork, Plenum Press, 1998.

37. J. Heyd, G. E. Scuseria, M. Ernzerhof, *J. Chem. Phys.,* 2003,**118**, 8207.

38. A. V. Krukau, O. A. Vydrov, A. F. Izmaylov, G. E. Scuseria, *J. Chem. Phys.,* 2006, **125**, 224106.

39. C. L. Pai, C. L. Liu, W. C. Chen, S. A. Jenekhe, *Polymer.,* 2006, **47**, 699.

40. N. Marom, A. Tkatchenko, M. Rossi, V. V. Gobre, O. Hod, M. Scheffler, *J. Chem. Theory. Comput.,* 2011, **7**, 3944.

41. P. J. Stephens, F. J. Devlin, C. F. Chabalowski, M. J. Frisch, *J. Phys. Chem.,* 1994, **98**, 11623.

42. M. M. Alam, S. A. Jenekhe, *Chem. Mater.,* 2002, **14,** 4775.

43. I. L.Vesque, P. O. Bertrand, N. Blouin, M. Leclerc, S. Zecchin, G. Zotti, C. I. Ratcliffe, D. D. Klug, X. Gao, F. Gao, J. S. Tse, *Chem. Mater.,* 2007, **19**, 2128.

44. B. Liu, W. L. Yu, Y. H. Lai, W. Huang, B. Liu, *Opt. Mater*., 2002, **21**, 125.

45. K. Rameshbabu, Y. Kim, T. Kwon, J. Yoo, E. Kim, *Tetrahedron Lett.,* 2007, **48,** 4755.

46. M. A. Abdullah, Al-Hussam, J. J. Salah Abdul, *J. Assn. Arab. Univ. Basic. Appl. Sci.,* 2012, **11**, 27.

47. J. L. Bredas, R. Silbey, D. X. Boudreux, R. R. Chance, *J. Am. Chem. Soc.,* 1983, **105**, 6555.

48. P. Puschnig, C. Ambrosch-Draxl, G. Heimel, E. Zojer, R. Resel, G. Leising, M. Kriechbaum, W. Graupner, *Synthetic Met.,* 2001, **116**, 327.

49. V. J. Eaton, D. Steele, *J. Chem. Soc., Faraday Trans.,* 1973, **2**, 1601.

50. R. Zhao, X. Ji, S. Jiang, L. Liu, B. L. Weeks, Z. Zhang, *Green. Chem.,* 2011, 13, 1891

51. S. Guangyi, Z. Yingping, L. Yongfang, *J. Phys. Chem. C.,* 2008, **112**, 12058.

52. A. P. Demchenko, *Introduction to Fluorescence Sensing, Second Edition,* Springer, Switzerland, 2015.

53. Y. Zhu, A. R. Rabindranath, T. Beyerlein, B. Tieke, *Macromolecules*, 2007, **40**, 6981.

DESIGN, SYNTHESIS AND CHARACTERIZATION OF PHENOTHIAZINE BASED COPOLYMERS BY SUZUKI POLYCONDENSATION REACTION

Contents

In chapter four, the synthesis of theoretically designed phenothiazine based polymers by means of palladium catalysed Suzuki polycondensation reaction is discussed. The electronic properties of the two copolymers, poly(N-octylphenothiazine-alt-triphenylamine) (P(PHENO-TPA)) and poly(N-octylphenothiazine-alt-3-methylthiophene) (P(PHENO-MeTH)) were calculated by employing Density Functional Theory (DFT) in the Periodic Boundary Condition (PBC) formalism. The band gap was experimentally determined using Cyclic Voltammetric studies and optical measurement. The experimental results support the theoretical prediction. The polymers were characterized using ^1H NMR, UV-Visible spectroscopy, Cyclic Voltammetry, TG/DTG and GPC etc. The copolymer showed good solubility in common organic solvents like chloroform, tetrahydrofuran, chlorobenzene and toluene. The fluorescence lifetime of the polymers, P(PHENO-TPA) and P(PHENO-MeTH) were measured using Time-Correlated Single Photon Counting technique (TCSPC) in CHCl$_3$ at excitation wavelength 340 nm.

4.1 Introduction

Synthesis and investigation of π-conjugated polymers with donor-acceptor architectures are essential, because, they have built in intramolecular charge transfer which can manipulate the energy levels of the materials, leading to a small band gap polymer with enhanced optical properties. In the present chapter, focus was given for the design and synthesis of phenothiazine based copolymers considering the following: (1) heterocyclic phenothiazine unit contain both electron-rich sulfur and nitrogen heteroatoms, and enhance the intramolecular charge transfer in polymers,[1] (2) the butterfly nonplanar structure of phenothiazine inhibits π-stacking aggregation and intermolecular excimer formation, resulting in various optoelectronic applications,[2-6] (3) phenothiazine is cheap and commercially available and it can be easily tailored by attaching solubilizing alkyl groups to the N atom to improve solubility. As a result, these phenothiazine based polymers are widely used as dyes, antioxidants, pharmaceuticals etc.[7,8] π-conjugated organic polymers are potential candidates for use in electronics and optoelectronics,[9-15] including light-emitting diodes,[16-18] photovoltaic devices,[19-22] thin film transistors,[23] electrochromic cells,[24] organic field effect transistors[25,26] etc. The low band gap polymers have emerged as promising candidates due to their fast response time, large third-order susceptibility and processability.[27,28] Recently, large number of donor-acceptor copolymers of phenothiazine with various applications were reported. Chao *et al*. synthesized six thiophene-substituted phenothiazine based polymers, via the Suzuki coupling reaction which were efficient photosensitizers.[29] Ali *et al.* have synthesized phenothiazine-functionalized polymers with different alkyl spacer lengths and have explained whether the spacer has played a key role

for tuning the redox stability, which was closely related to self-discharge behaviour of copolymers.[30]

In this chapter, electronic structures of two copolymers composed of phenothiazine acceptor and 4,4'-dibromotriphenylamine (TPA) and 2,5-dibromo-3-methylthiophene (MeTH) as donors were investigated theoretically. The copolymers poly(N-octylphenothiazine-alt-triphenylamine) (P(PHENO-TPA)) and poly(N-octylphenothiazine-alt-3-methylthiophene) (P(PHENO-MeTH)) were synthesized via transition metal catalysed Suzuki cross-coupling reaction. Their electrochemical, optical and thermal properties are discussed.

4.2 Results and discussion

4.2.1 Theoretical calculation

Quantum chemical calculations were used to investigate the ground state geometries and electronic properties of the monomers and oligomers. On the basis of the data obtained, the polymers were designed and evaluated using Density Functional Theory (DFT) calculations. [31-35] The calculation described in this chapter was done using G09 suite of codes[36] on IBM power servers. The electronic structure of the monomers were optimized by means of the DFT/B3LYP level of theory using 6-31G basis set.[37,38] These are computationally cost effective methods to calculate the electronic structure of various monomers with a good approximation and enable elimination of unsuitable materials before synthesis of polymers. Time-dependent DFT/(TD-DFT) calculations were also performed to assess the excited state vertical transition energies, oscillator strengths and excitation wavelength on the optimized molecular geometries of the monomers (Table 4.1). In the

present work, HSE06[37,38] and B3LYP[39-41] combined with 6-31G basis set were used to study the electronic structure and properties of P(PHENO-TPA) and P(PHENO-MeTH) copolymers. The investigation started with studying the properties of monomers, 10-octyl-3,7-bis(4,4,5,5-tetramethyldioxaborolan-2-yl)-10H-phenothiazine (PHENO), 4,4'-dibromotriphenylamine (TPA) and 2,5-dibromo-3-methylthiophene (MeTH) (Figure 4.1).
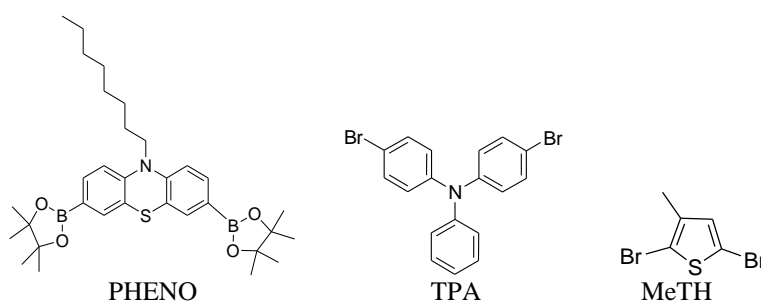
Figure 4.1: Structure of model compounds

Table 4.1: Values of $E_{activation}$ (eV), Oscillator strength and λ_{max} (nm) of the monomer units obtained by TD-DFT/B3LYP/6-31G

Monomer	Optimized geometries of monomers[a]	$E_{activation}$[b] (eV)	Oscillator strength[b]	λmax[b] (nm)
10-octyl-3,7-bis(4,4,5,5-tetramethyldioxaborolan-2-yl)-10H-phenothiazine (PHENO)		4.00	0.058	312
4,4'-dibromotriphenylamine (TPA)		3.96	0.004	315
2,5-Dibromo-3-methylthiophene (MeTH)		3.94	0.216	310

[a] Estimated from DFT/B3LYP/6-31G calculation
[b] Estimated from TD-DFT/B3LYP/6-31G calculation

The HOMO and LUMO energy levels and band gap of monomer units, D-A and tetramer units using Density Functional Theory (DFT) at the B3LYP/6-31G method are shown in Figure 4.2.
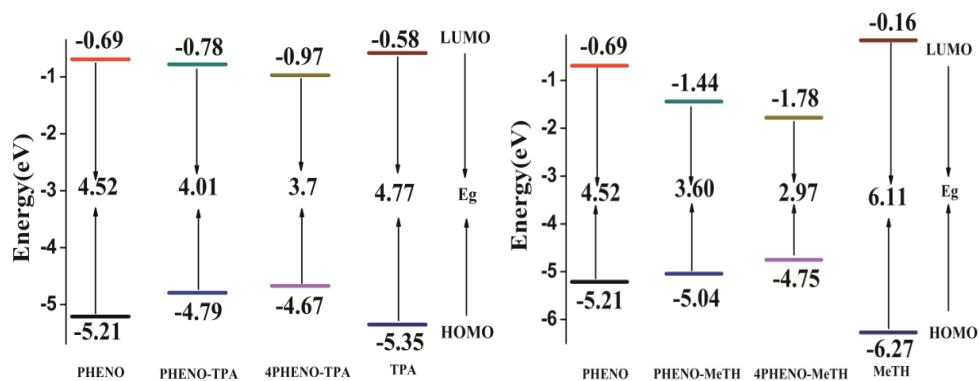
Figure 4.2: Energy levels of monomers, D-A units and tetramer units of P(PHENO-TPA) and P(PHENO-MeTH) copolymers

From the energy level diagram, the LUMO levels of PHENO, TPA and MeTH were found to be -0.69, -0.58 and -0.16 eV respectively. The LUMO level of tetramer units of PHENO-TPA and PHENO-MeTH were obtained to be -0.97 and -1.78 eV respectively. In both the polymers PHENO acted as acceptor unit and TPA and MeTH acted as donor units. When PHENO was coupled with TPA and MeTH, HOMO energy levels were raised and LUMO energy levels were lowered which resulted in reduction in band gap. The reduction in band gap was due to the intramolecular charge transfer between PHENO, the acceptor and TPA and MeTH donor units, which resulted in the decrease of the Bond Length Alternation (BLA)[42,43] of phenothiazine based monomers. This can be visualized from the frontier orbital distribution of the model compounds (Figure 4.3).
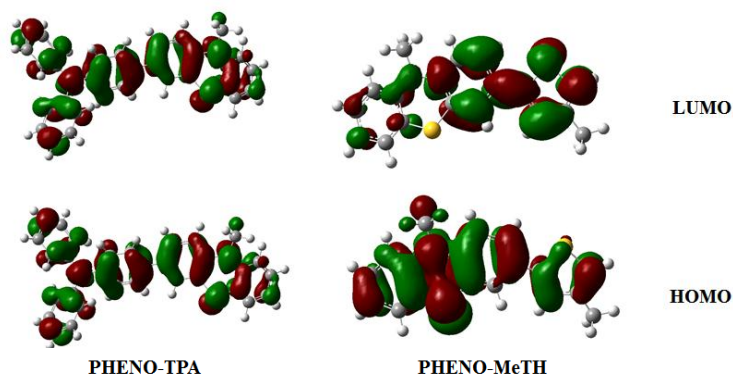
Figure 4.3: Frontier molecular orbital distribution of monomeric units of PHENO-TPA and PHENO-MeTH by DFT/B3LYP/6-31G method

4.2.2 Band structure of the polymers

The electronic properties of the P(PHENO-TPA) and P(PHENO-MeTH) copolymers were investigated by PBC calculation at two different energy levels, B3LYP/6-31G and HSE06/6-31G; the values are summarised in the Table 4.2. The band structure obtained by HSE06/6-31G level is plotted in Fig. 4.4. Periodic Boundary Condition (PBC) was computationally cost effective than oligomer approach. In PBC, translational symmetry was used to optimise the copolymers of infinite chain length. After the optimization, band structures in the positive region of the first Brillouin zone (between k=0 and k=π/a) were calculated along the k-vector of one dimensional copolymers with 32 k-points. The energy levels of the HOMO and LUMO were determined from the maximum point of the highest occupied molecular orbital level and the minimum point of the lowest unoccupied molecular orbital level respectively. The band gap was calculated from the lowest energy difference between the HOMO and LUMO energies at constant k. The band structure of the copolymers revealed that that lowest band gap occur at k=0, suggesting that the polymers were direct band gap

polymers. Band gap of the polymers, P(PHENO), P(PHENO-TPA) and P(PHENO-MeTH) are 3.37, 3.04 and 2.43 eV respectively.

Comparing the band structure data of P(PHENO) with P(PHENO-TPA) and P(PHENO-MeTH), it is clear that the incorporation of donor units into the phenothiazine moiety has resulted in the reduction in band gap by a factor 0.33 eV in the case of P(PHENO-TPA) and reduced by 0.94 eV for P(PHENO-MeTH). The band gap of the copolymers P(PHENO-TPA) and P(PHENO-MeTH) were obtained to be 3.04 and 2.43 eV respectively using PBC/DFT/HSE06/6-31G and 3.09 and 3.07 eV using PBC/DFT/B3LYP/6-31G methods. This screened-hybrid functionals such as the HSE approach reduces self-interaction errors in systems possessing both localized and delocalized orbitals and could be applied to both finite and extended systems which improves the computational efficiency reported by Marom *et al.*[44] The ionization potential (negative of HOMO energy) and the electron affinity (negative of LUMO energy) are also calculated and summarized in Table 4.2.
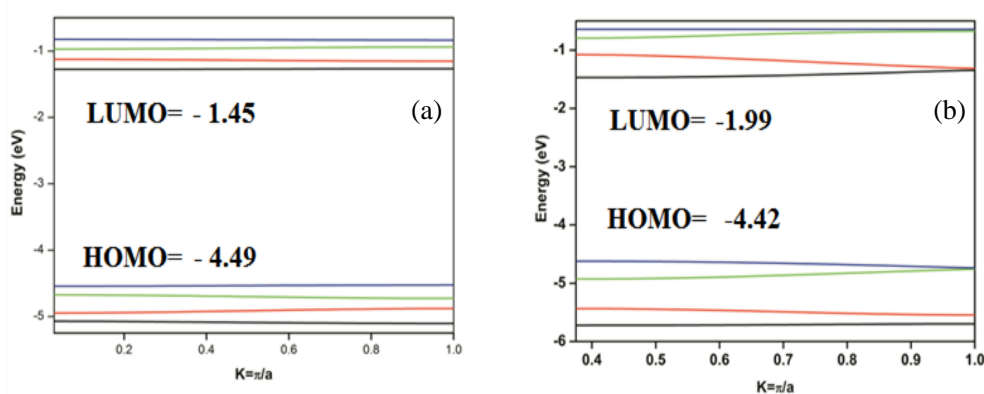
Figure 4.4: Band structure of (a) P(PHENO-TPA) (b) P(PHENO-MeTH)

Table 4.2: Computational data of P(PHENO-TPA) and P(PHENO-MeTH) with DFT/HSE06/6-31G[a] and DFT/ B3LYP/6-31G[b] methods

Polymer	HOMO (eV)	IP (eV)	LUMO (eV)	EA (eV)	Eg (eV)
P(PHENO)	-4.75[a]	4.75	-1.38	1.38	3.37
P(PHENO-TPA)	-4.49[a]	4.49	-1.45	1.45	3.04
	-4.62[b]	4.62	-1.53	1.53	3.09
P(PHENO-MeTH)	-4.42[a]	4.42	-1.99	1.99	2.43
	-4.59[b]	4.59	-1.52	1.52	3.07

[a] Obtained by the DFT/HSE06/6-31G method.
[b] Obtained by the DFT/B3LYP/6-31G method.

The starting unit cell geometries for the PBC/DFT/HSE06/631G calculation were taken from the central portion of the optimized tetramer units by assuming that the unit cell was repeated identically an infinite number of times along the translational vector. The optimized unit cell of P(PHENO-TPA) and P(PHENO-MeTH) are shown in the Figure 4.5. The red line represents the translational vector. The length of the translational vector for P(PHENO-TPA) and P(PHENO-MeTH) were found to be 24.28 and 28.42 Å respectively.

(a)   (b)
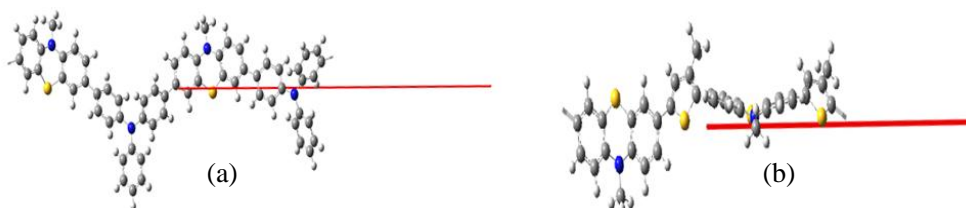
Figure 4.5: Unit cell of (a) P(PHENO-TPA) and (b) P(PHENO-MeTH) for the PBC/DFT/HSE06/631G calculation. The red line represents the translational vector

4.2.3 Synthesis of monomers and polymers

4.2.3.1 Monomer synthesis

Scheme of synthesis of monomer 4,4'-dibromotriphenylamine (TPA) was depicted in chapter 3. The monomer 2,5-Dibromo-3-methylthiophene (MeTH) was purchased from Sigma Aldrich and used as received. The precursor

monomer, 10-octyl-3,7-bis(4,4,5,5-tetramethyldioxaborolan-2-yl)-10H-phenothiazine was synthesized in three steps starting from phenothiazine (Scheme 4.1). First step involved alkylation of phenothiazine followed by bromination which gave 3,7-dibromo-10-octylphenothiazine. It was converted to 3,7-bis(4,4,5,5-tetramethyldioxaborolan)-10H-phenothiazine (PHENO) by reaction with bis(pinacolato)diboron in the presence of potassium acetate in anhydrous 1,4-dioxane at 80 °C for 20 h. The product was obtained as off white powder in 72 % yield. The ^{1}H NMR spectrum of 3,7-bis(4,4,5,5-tetramethyldioxaborolan)-10H-phenothiazine is depicted in Figure 4.6. The ^{1}H NMR spectrum of the monomer showed multiplets at δ 0.74-1.9 due to alkyl protons and a triplet at δ 3.75 due to –NCH$_2$-protons. It showed multiplets at δ 6.71-7.52 due to aromatic protons.
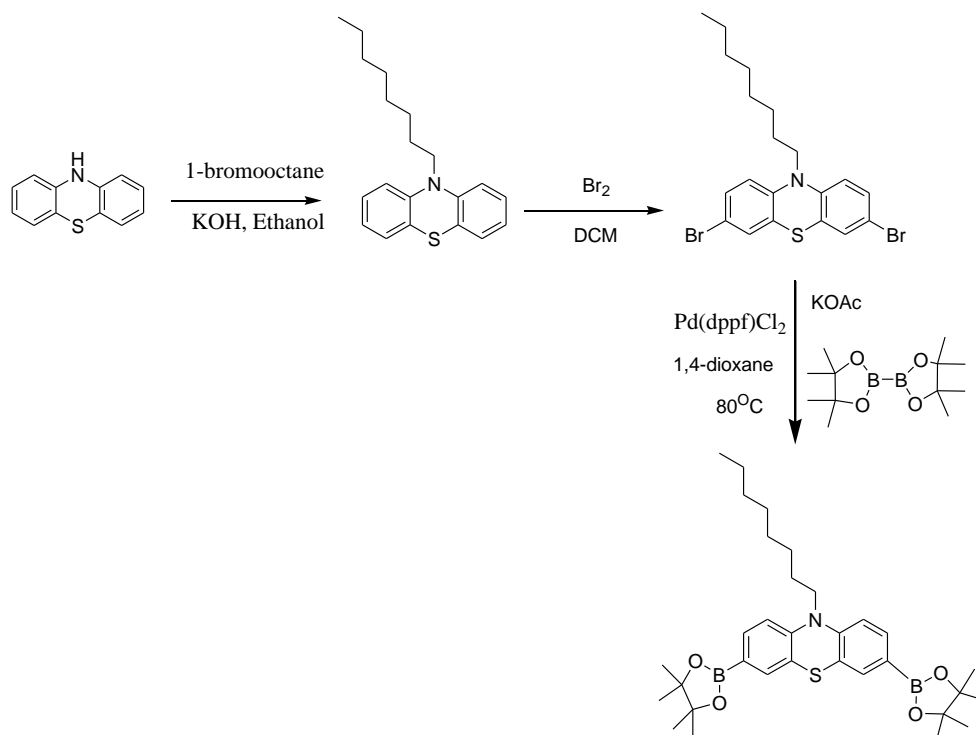
Scheme 4.1: Synthesis of PHENO
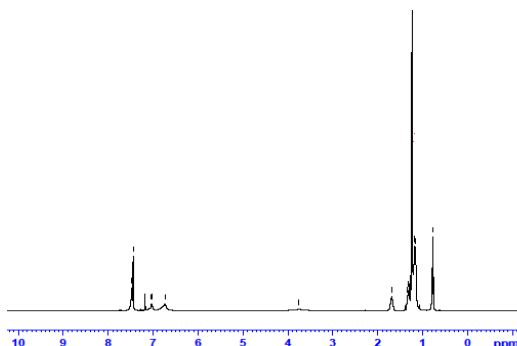
Figure 4.6: ^{1}H NMR spectra of PHENO

4.2.3.2 Polymer synthesis

Standard Suzuki polycondensation reaction was carried out to synthesize the phenothiazine based copolymers (Scheme 4.2). The polymers P(PHENO-TPA) and P(PHENO-MeTH) were synthesized through the copolymerisation of diboronate ester of phenothiazine with TPA and MeTH using freshly prepared palladium triphenylphosphene as the catalyst, which gave the polymers in 77 % and 72 % yields respectively. The crude product was purified by precipitating in methanol, filtered and followed by soxhlet extraction using methanol and hexane to remove oligomers. The copolymers were dissolved in small amounts of chloroform and reprecipitated from methanol and dried under vacuum to offer the pure polymer. Both the polymers were soluble in tetrahydrofuran, chloroform, chlorobenzene, toluene etc. The polymers were characterized using ^{1}H NMR, FT-IR, GPC, TG-DTG, UV-Visible spectroscopy and cyclic voltammetry etc. The molecular weights of the polymers were investigated using Gel Permeation Chromatography (GPC) in THF referring to polystyrene standards and the results are summarized in Table 4.3. The number average molecular weight of the copolymers, P(PHENO-TPA) and P(PHENO-MeTH) were found to be 4586 and 3167 with Poly Dispersity Index 1.46 and 1.93 respectively.

Table 4.3: Results of polymerization of copolymers

Polymer	M_n	M_w	PDI	Yield (%)
P(PHENO-TPA)	4586	6705	1.46	77
P(PHENO-MeTH)	3167	5106	1.93	72

[a]Determined by GPC in THF based on polystyrene standards

The ^{1}H NMR spectra of the polymers are shown in Figure 4.7. The ^{1}H NMR spectrum of P(PHENO-TPA) and P(PHENO-MeTH) showed multiplets at δ 0.8-2.1 region due to alkyl protons. The peaks corresponding to –NCH$_2$- protons are observed at δ 3.8-3.9 as triplet. It could be seen that in both the polymers, aromatic region is highly populated and the peaks corresponding to aromatic protons are observed at δ 6.8-7.7 as multiplets.

P(PHENO-TPA)
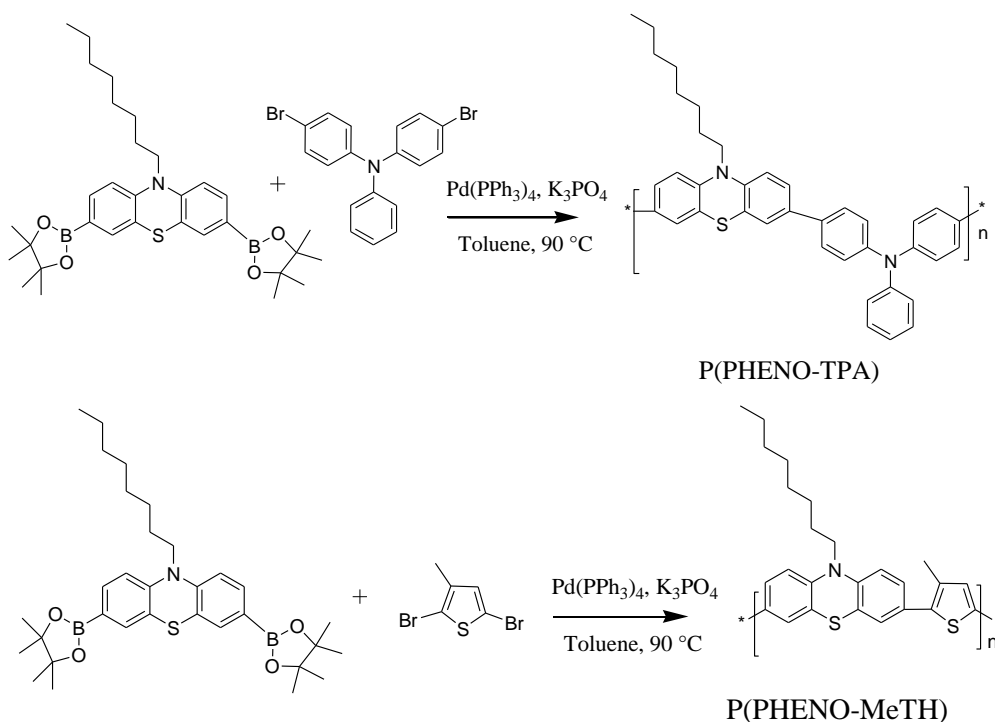
P(PHENO-MeTH)

Scheme 4.2: Synthesis of polymers
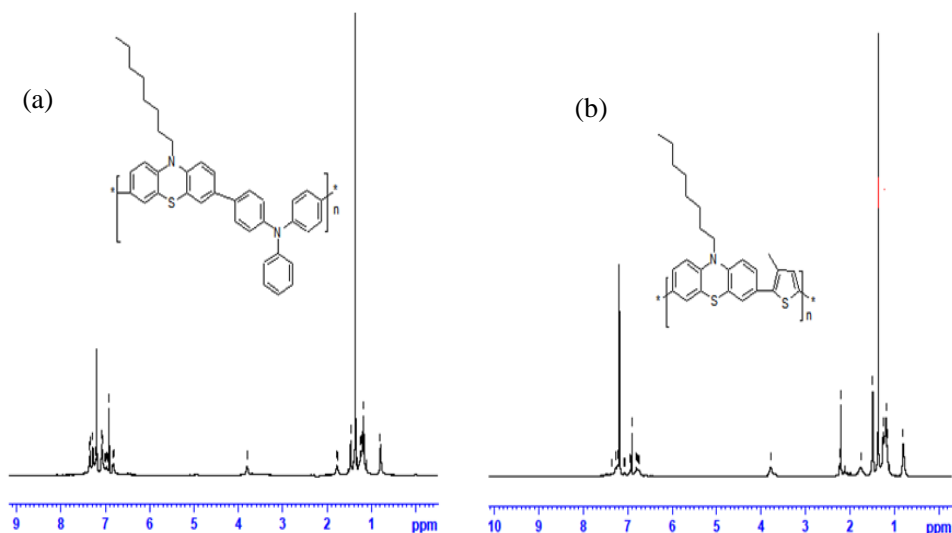
Figure 4.7: ^{1}H NMR Spectra of (a) P(PHENO-TPA) and (b) P(PHENO-MeTH)

4.2.4 Thermal Properties

The thermal properties of the polymers were investigated by thermogravimetric analysis (TGA) in nitrogen atmosphere at a heating rate of 10 ^{o}C/min. TG curve revealed that both the copolymers showed single step degradation pattern. The onset weight loss temperature was measured from TG curve and it was found to be 375 ^{o}C and 300 ^{o}C for P(PHENO-TPA) and P(PHENO-MeTH) respectively. The peak decomposition temperature is defined as the first inflection point in the thermogravimetric curve, corresponding to peak in the first derivative of thermogravimetric data. In P(PHENO-TPA), DTG traces showed that the onset of degradation was around 392 ^{o}C and the degradation temperature was 416 ^{o}C with around 4 % weight loss. In P(PHENO-MeTH), DTG traces showed that the onset of degradation was around 272 ^{o}C and the degradation temperature was 320 ^{o}C with around 7 % weight loss. TG-DTG traces of the polymers are shown in the Figure 4.8.
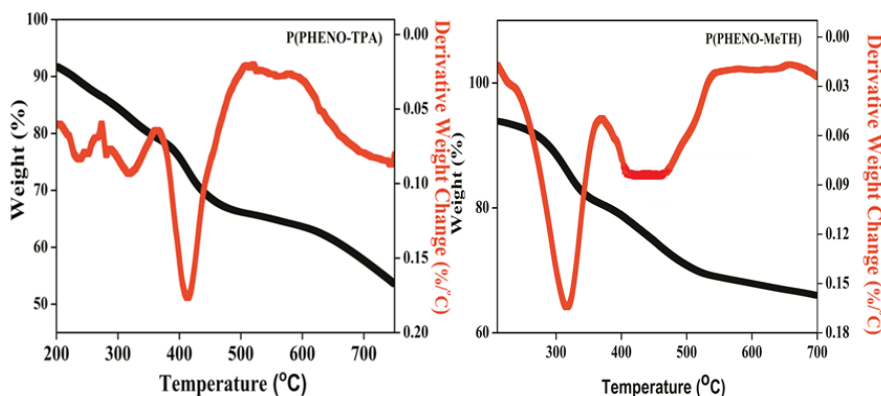
Figure 4.8: TG-DTG traces of the copolymers P(PHENO-TPA) and P(PHENO-MeTH)

4.2.5 Optical properties

To study the photophysical characteristics of the copolymers, UV-Visible absorption and emission spectra were recorded in THF. Absorption spectra of phenothiazine based copolymers were recorded in the range of 300–700 nm. P(PHENO-TPA) showed absorption maximum at 410 nm, while P(PHENO-MeTH) showed maximum at 501 nm which could be attributed to the intramolecular charge transfer between the donor and acceptor unit. The onset of absorption at 576 and 619 nm were used to calculate the optical band gap of the polymers P(PHENO-TPA) and P(PHENO-MeTH) respectively using Tauc's equation.[45] The band gap of the copolymers, P(PHENO-TPA) and P(PHENO-MeTH) were calculated to be 2.15 and 2.06 eV respectively. Both the copolymers showed low band gap compared to homopolymer, poly(phenothiazine) (2.76 eV)[6] due to better charge transfer between the units. Even if the optical band gap of copolymers support the theoretical prediction (DFT/HSE06/6-31G), some deviation still exists. This is because of the negligence of solid-state effects (polarization effects and intermolecular

forces) and environmental effects in theoretical prediction.[46,47] The absorption spectra of the copolymers are shown in Figure 4.9. The optical properties of the copolymers are listed in Table 4.4.
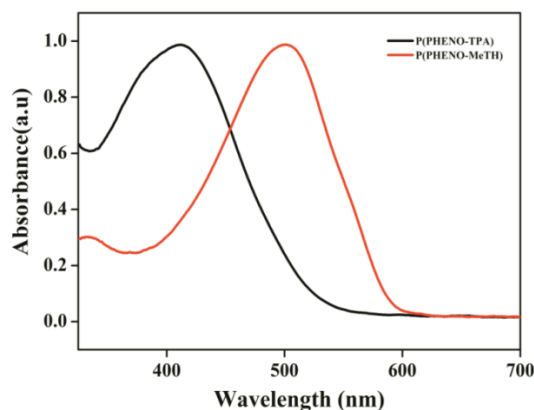
Figure 4.9: Absorption spectrum of P(PHENO-TPA) and P(PHENO-MeTH) in THF solution

The emission spectra of the polymers are shown in Figure 4.10. The wavelength corresponding to the absorption maximum of each polymer was used as excitation wavelength. The emission maximum of the P(PHENO-TPA) and P(PHENO-MeTH) occur at 483 nm and 525 nm respectively.
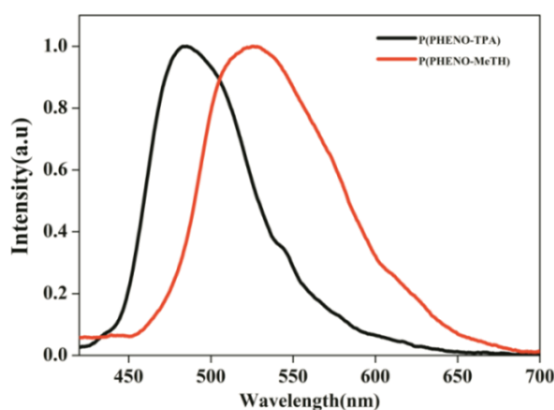
Figure 4.10: Emission spectra of P(PHENO-TPA) and P(PHENO-MeTH) in THF solution

Table 4.4: Optical properties of polymers in THF solution

Polymer	Absorption λ_{max} (nm)	Absorption onset (nm)	Emission λ_{max} (nm)	E_g (eV)
P(PHENO-TPA)	410	576	483	2.15
P(PHENO-MeTH)	501	619	525	2.06

4.2.6 Electrochemical studies

The electronic states of the conjugated polymers were investigated using Cyclic Voltammetry (CV). To assess the HOMO, LUMO energy levels and band gap of the copolymers, CV was carried out in thin polymer film which was coated on Pt electrode in a solution of tetrabutylammonium hexafluoroborate (Bu_4NBF_6, 0.10 M) electrolyte in acetonitrile. The measurement was carried out at a scan rate of 100 mV/s at room temperature under nitrogen atmosphere. Here, a platinum electrode coated with a thin polymer film was used as the working electrode, Pt wire and Ag/Ag+ electrode were used as the counter and reference electrodes, respectively. The electrochemical data of the phenothiazine based copolymers are summarized in Table 4.5. The HOMO and LUMO energy levels of the copolymers were measured from the onset potentials for oxidation and reduction according to the equation proposed by Bredas.[48] The onset oxidation potential of P(PHENO-TPA) and P(PHENO-MeTH) were found to be 0.42 and 0.37 eV respectively. The onset reduction potential was calculated to be -1.21 and -1.31 eV, for P(PHENO-TPA) and P(PHENO-MeTH) respectively. From the onset of oxidation, the HOMO levels of P(PHENO-TPA) and P(PHENO-MeTH) were calculated to be -5.13 eV and -5.08 eV respectively based on the equation, HOMO= $-(4.71+E_{ox}^{onset})$. The LUMO levels estimated

using the equation LUMO= -(4.71+ E_{red}^{onset}) were -3.50 eV and -3.41 eV for P(PHENO-TPA) and P(PHENO-MeTH) respectively. The HOMO level of P(PHENO) was reported to be -5.0 eV.[6] The HOMO level of the copolymer P(PHENO-TPA) was lowered by 0.13 eV and for P(PHENO-MeTH) HOMO level was lowered by 0.08 eV. The band gap was calculated to be 1.63 and 1.68 eV for P(PHENO-TPA) and P(PHENO-MeTH) respectively. Both the polymers showed good reversibility towards the oxidation and reduction processes, pointing out good chemical stability of the polymers.

The electrochemical band gap showed deviations of the order of 0.38-0.6 eV from the optical band gap. In the former process, (optical) excitation creates excitons (bound electrons and hole pair) and the latter process (electrochemical) creates ions. The low energy of excitons compared to the ions and solvation of the ions in the electrochemical experiment were reflected in the observed electrochemical band gap.

Table 4.5: Redox properties of P(PHENO-TPA) and P(PHENO-MeTH)

Polymer	E_{ox} (V)	HOMO (eV)	E_{red} (V)	LUMO (eV)	Band Gap (eV)
P(PHENO-TPA)	0.42	-5.13	-1.21	-3.50	1.63
P(PHENO-MeTH)	0.37	-5.08	-1.31	-3.41	1.68

4.2.7 Time resolved fluorescence measurements

A time correlated single photon counting setup was used for the fluorescence lifetime measurements of phenothiazine based copolymers. The time resolved fluorescence decay of the copolymers was measured as a function of time after excitation by a laser pulse. The experiment was carried out to determine even very low emission from the copolymers on

nanosecond time scale. The copolymers P(PHENO-TPA) and P(PHENO-MeTH) in CHCl$_3$ was excited at 340 nm. Both the copolymers showed bi-exponential decay due to the presence of different fluorescence moieties with distinct lifetimes. The τ_1 and τ_2 are the lifetimes, and α_1 and α_2 are the pre-exponential factors. The average lifetime of P(PHENO-TPA) and P(PHENO-MeTH) was obtained to be 1.52 and 7.89 ns respectively. The bi-exponential fitted decay curves of copolymers in CHCl$_3$ solution are shown in Fig. 4.11. The decay times of the phenothiazine based copolymers across the emission wavelength and quantum yields are summarized in the Table 4.6.

The quantum yield of the copolymers was measured with the same excitation wavelength and obtained to be 0.38 and 0.42 for P(PHENO-TPA) and P(PHENO-MeTH) respectively. The copolymers showed high quantum efficiency; which revealed the suitability of the copolymers to be used as the active components in optical devices. For the accurate determination of the quantum yield, 'absolute method' was used,[49] it was based on collecting the whole spatially distributed fluorescence emission.
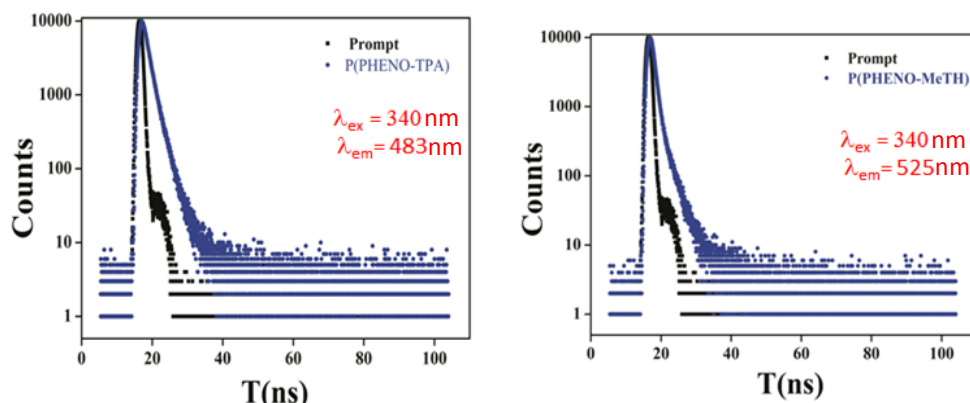
Figure 4.11: Bi-exponential fitted decay curves of P(PHENO-TPA) and P(PHENO-MeTH) in CHCl$_3$ at 340 nm excitation

Table 4.6: Fluorescence lifetimes, pre-exponential factors and quantum yield of P(PHENO-TPA) and P(PHENO-MeTH) in $CHCl_3$ at 340 nm excitation

Polymer	χ^2	τ_1 (ns)	α_1 %	τ_2 (ns)	α_2 %	τ_{av} (ns)	ϕ^d
P(PHENO-TPA)	1.13	0.14	86.20	3.24	13.80	1.52	0.38
P(PHENO-MeTH)	1.22	0.79	88.24	3.04	11.76	7.89	0.42

4.3 Conclusion

The phenothiazine based copolymers P(PHENO-TPA) and P(PHENO-MeTH) have been designed and synthesized by palladium catalysed Suzuki polycondensation reaction. Monomers, D-A and tetramer units were optimized using DFT/B3LYP/6-31G formalism. Both optical and electrochemical results support the theoretical prediction obtained by HSE06/6-31G method compared to the B3LYP/6-31G method. They are soluble in common organic solvents such as chloroform, tetrahydrofuran etc. The fluorescence lifetime of the copolymers were checked using TCSPC in $CHCl_3$ and all the copolymers fitted well with bi-exponential decay due to the presence of different fluorescence moieties.

4.4 Experimental section

The reaction sequence towards the synthesis of 4,4'-dibromo triphenylamine (TPA) and 3,7-dibromo-10-octylphenothiazine were depicted in Chapter 3.

4.4.1 Synthesis of 10-octyl-3,7-bis(4,4,5,5-tetramethyldioxaborolan-2-yl)-10H-phenothiazine (PHENO)

A mixture of 3,7-dibromo-10-octylphenothiazine (4.13 g, 9.5 mmol), bis(pinacolato)diboron (5.34 g, 21.0 mmol), Pd(dppf)Cl$_2$ (0.72 g, 0.97 mmol), and potassium acetate (5.49 g, 55.94 mmol) were dissolved in anhydrous

1,4-dioxane (40 mL). The mixture was stirred at room temperature for 30 min before it was stirred at 80 ^{o}C for 20 h. A portion of 20 mL of water was added into the reaction mixture and extracted with diethyl ether. After the organic extract was dried over $MgSO_4$ and filtered, the solvent was removed using a rotary vacuum evaporator. The crude product was purified by column chromatography using 3 % ethylacetate in hexane as eluent to afford the compound as off white solid.

Yield   : 72 %.

^{1}H NMR (CDCl$_3$, 400 MHz) : δ 0.74 (t, *J=6.3* Hz, 3 H), 1.49-1.9 (m, 34 H), 3.75 (t, *J=7.2* Hz 2 H), 6.71 (m, 2 H), 7.52 (m, 2 H), 7.41 (m, 2H).

LCMS   : m/z = 563.21

4.4.2 General procedure for polymerization through Suzuki polycondensation reaction

Suzuki cross-coupling reaction was used to synthesize phenothiazine based copolymers, P(PHENO-TPA) and P(PHENO-MeTH). Dry toluene (20 mL) was added to a flask charged with 10 mol % palladium acetate (0.0036 g, 0.016 mmol) and 20 mol % PPh$_3$ (0.0086 g, 0.032 mmol) and stirred for 30 min. To the reaction mixture of dibromo monomer (0.164 mmol) and 10-octyl-3,7-bis(4,4,5,5-tetramethyldioxaborolan-2-yl)-phenothiazine (0.18 mmol), K$_3$PO$_4$ (0.07 g, 2 equ) was added and stirred at 80-90 ^{o}C for 72 hours. Copolymer was precipitated from the reaction mixture by adding large amount of methanol. Repeated purification by soxhlet extraction was performed using methanol and hexane. The copolymers were dissolved in small amounts of chloroform and reprecipitated from methanol and dried under vacuum to offer the pure polymer.

4.4.2.1 Synthesis of P(PHENO-TPA)

10-octyl-3,7-bis(4,4,5,5-tetramethyldioxaborolan-2-yl)-phenothiazine (0.1g, 0.18mmol), 4,4'-dibromotriphenylamine (0.164 mmol), dry toluene (20 mL), 10 mol % palladium acetate (0.0036 g, 0.016 mmol), 20 mol % PPh_3 (0.0086 g, 0.032 mmol) and K_3PO_4 (0.07 g, 2 equ) were used. Green powder.

Yield	:	77 %
UV-Visible (THF) λmax	:	410 nm
GPC	:	Mn = 4586, PDI = 1.46
Td (^{o}C)	:	416
^{1}H NMR (400 MHz, CDCl$_3$):		δ 0.92 (m, 3H, -CH$_3$), 1.20-1.99 (m, 12H, aliphatic-H), 3.83-3.9 (t, 2H, -NCH$_2$-), 6.9-7.6 (m, Ar-H of Phenothiazine and triphenylamine)

4.4.2.2 Synthesis of P(PHENO-MeTH)

10-octyl-3,7-bis(4,4,5,5-tetramethyldioxaborolan-2-yl)-phenothiazine (0.1g, 0.18 mmol), 2,5-Dibromo-3-methylthiophene (0.164 mmol), dry toluene (20 mL), 10 mol % palladium acetate (0.0036 g, 0.016 mmol), 20 mol % PPh_3 (0.0086 g, 0.032 mmol) and K_3PO_4 (0.07 g, 2 equ) were used. Yellowish Green powder.

Yield	:	72 %
UV-Visible (THF) λmax	:	501 nm
GPC	:	Mn = 3167, PDI = 1.93
Td (^{o}C)	:	320
^{1}H NMR (400 MHz, CDCl$_3$):		δ 0.90 (m, 3H, -CH$_3$), 1.20-1.99 (m, 12H, aliphatic-H), 2.23 (s,3H), 3.83-3.9 (t, 2H, -NCH$_2$-), 6.7-7.4 (m, Ar-H of phenothiazine and 3-methyl-thiophene)

References

1. G. Kim, H. R. Yeom, S. Cho, J. H. Seo, J. Y. Kim, C. Yang, *Macromolecules,* 2012, **45**, 1847.

2. H. Padhy, J. H. Huang, D. Sahu, D. Patra, D. Kekuda, C. W. Chu, H.C. Lin, *J. Polym. Sci. Part A: Polym. Chem,.* 2010, **48**, 4823.

3. G. Y. Sang, Y. P. Zou, Y. F. Li, *J. Phys. Chem. C*, 2008, **112**, 12058.

4. Y. Liu, H. Cao, J. Li, Z. Chen, S. Cao, L. Xiao, S. Xu, Q. Gong, *J. Polym. Sci., Part A: Polym. Chem.*, 2007, **45**, 4867.

5. N. S. Cho, J. H. Park, S. K. Lee, J. Lee, H. K. Shim, M. J. Park, D. H. Hwang, B. J. Jung, *Macromolecules*, 2006, **39**, 177.

6. X. X. Kong, A. P. Kulkarni, S. A. Jenekhe, *Macromolecules*, 2003, **36**, 8992.

7. C. Garcia, R. Oyola, L. E. Pinero, R. Arce, J. Silva, V. Sanchez, *J. Phys. Chem. A,* 2005, **109**, 3360.

8. M. Hauck, J. Schonhaber, A. J. Zucchero, K. I. Hardcastle, T. J. J. Muller, U. H. F. Bunz, *J. Org. Chem.,* 2007, **72**, 6714.

9. (a) A. Heeger, *Angew. Chem., Int. Ed.*, 2001, **40**, 2591.
   (b) A. G. MacDiarmid, *Angew. Chem., Int. Ed.* 2001, **40**, 2581.

10. (a) X. Zhang, S. A. Jenekhe, *Macromolecules*, 2000, **33**, 2069.
    (b) M. M. Alam, S. A. Jenekhe, *Chem. Mater.* 2002, **14**, 4775.

11. A. C. Arias, J. D. MacKenzie, R. Stevenson, J. J. M. Halls, M. Inbasekaran, E. P. Woo, D. Richards, R. H. Friend, *Macromolecules*, 2001, **34**, 6005.

12. S. A. Jenekhe, S. Yi, *Appl. Phys. Lett.*, 2000, **77**, 2635.

13. A. Babel, S. A. Jenekhe, *Adv. Mater.* 2002, **14**, 371.

14. A. Babel, S. A. Jenekhe, *J. Phys. Chem. B*, 2003, **107**, 1749.

15. A. Babel, S. A. Jenekhe, *Macromolecules,* 2003, **36**, 7759.

16. S. A. Elkassih, P. Sista, H. D. Magurudeniya, A. Papadimitratos, A. A. Zakhidov, M. C. Biewer, M. C. Stefan, *Macromol. Chem. Phys.*, 2013, **214**,572.

17. A. P. Kulkarni, X. Kong, S. A. Jenekhe, *Macromolecules*, 2006, **39**, 8699.

18. B. Kim, J. Lee, Y. Park, C. Lee, J. W. Park, *J. Nanosci. Nanotechn.,* 2014, **14**, 6404.

19. Q. Tan, X. Yang, M. Cheng, H. Wang, X. Wang, L. Sun, *J. Phys. Chem. C*, 2014, **118**, 16851.

20. J. H. Huang, K. C. Lee, *Appl. Mater. Interfaces*, 2014, **6**, 7680.

21. G. D. Sharma, M. A. Reddy, D. V. Ramana, M. Chandrasekharam, *RSC Adv.,* 2014, **4**, 33279.

22. W. Jang, F. Lyu, H. Park, Q. B. Meng, S. H. Lee, Y. S. Lee, *Chem. Phys. Lett.,* 2013, **584**, 119.

23. A. Babel, S. A. Jenekhe, *J. Phys. Chem. B*, 2002, **106**, 6129.

24. F. Fungo, S. A. Jenekhe, A. Bard, *J. Chem. Mater.* 2003, **15**, 1264.

25. J. H. Kim, Y. H. Seo, W. H. Lee, Y. Hong, S. K. Lee, W. S. Shin, S. J. Moon, I. N. Kang, *Synth. Met.,* 2011, **161**, 72.

26. S. K. Son, Y. S. Choi, W. H. Lee, Y. Hong, J. R. Kim, W. S. Shin, S. J. Moon, D. H. Hwang, I. N. Kang, *J. Polym. Sci., Part A: Polym.Chem.,* 2010, **48**, 635.

27. P. N. Prasad, D. J. Williams, *Introduction to Nonlinear Optical Effects in Molecules and Polymers,* Wiley, New York, 1992.

28. H. S. Nalwa, S. Miyata, *Nonlinear Optics of Organic Molecules and Polymers*, CRC Press, Boca Raton, Florida, 1996.

29. P. Chaoa, R. Gub, X. Mab, T. Wang, Y. Zhaod*, Polym. Chem.,* 2016,**7**, 5147.

30. A. G. Ali, T. Suga, H. Nishide, R. Berger, J. S. Gutmannb, *RSC Adv.,* 2015,**5**, 22947.

31. R. G. Parr, W. Yang, *Density-Functional Theory of Atoms and Molecules*, Oxford University Press, New York, 1989.

32. K. Kornobis, N. Kumar, P. Lodowski, M. Jaworska, P. Piecuch, J.J. Lutz, P.M. Kozlowski, *J. Chem. Theory Comput.,* 2013, **34**, 987.

33. N. Kumar, M. Alfonso-Prieto, C. Rovira, P. Lodowski, M. Jaworska, P. M. Kozlowski. *J. Chem. Theor. Comput.,* 2011, **7**, 1541.

34. M.W. Bryan, P. Manuel, D.S. Fabio, *Phys. Chem. Chem. Phys.,* 2009, **11**, 4498.

35. M.W. Bryan, *J. Phys. Chem. C.,* 2009, **113**, 21921.

36. M. J. Frisch, G. W. Trucks, H. B. Schlegel, G. E. Scuseria, M. A. Robb, J.R. Cheeseman, Gaussian 03, revision E.01. Pittsburgh, PA: Gaussian, Inc, 2003.

37. J. Heyd, G. E. Scuseria, M. J. Ernzerhof, *Chem. Phys.* 2003, **118**, 8207.

38. A. V. Krukau, O. A. Vydrov, A. F. Izmaylov, G. E. Scuseria, *J. Chem. Phys.,* 2006, **125**, 224106.

39. A. D. Becke, *J. Chem. Phys.,* 1993, **98**, 5648.

40. C. Lee, W. Yang, R. G. Parr, *Phys. Rev. B.,* 1994, **37**, 785.

41. K. Burke, J. P. Perdew, Y. Wang, J. F. Dobson, G. Vignale, M. P. Das, *Electronic Density Functional Theory: Recent Progress and New Directions,* Plenum Press, New York, 1998.

42. C. L. Pai, C. L. Liu, W. C. Chen, S. A. Jenekhe, *Polymer*, 2006, **47**, 699.

43. N. Sona, P. R. Sreejesh, M. Sebastian, M.V. Mahesh Kumar, A. Anshad, K. Sreekumar, C. Sudha Kartha, J. Rani. *Eur. Polym. J.,* 2015, **64**, 157.

44. N. Marom, A. Tkatchenko, M. Rossi, V.V. Gobre, O. Hod, M. Scheffler, L. Kronik, *J. Chem. Theory. Comput.,* 2011, **7**, 3944.

45. M. A. Abdullah, Al-Hussam, J.J. Salah Abdul. *J. Assn. Arab. Univ. Basic. Appl. Sci.,* 2012, **11**, 27.

46. P. Puschning, C. Ambrosch-Draxl, G. Heimel, E. Zojer, R. Resel, G. Leising, M. Kriechbaum, W. Graupner, *Synth. Met.,* 2001, **116**, 327.

47. V. J. Eaton, D. J. Steele, *Chem Soc; Faraday Trans*, 1973, **2**, 1601.

48. J. L. Bredas, R. Silbey, D. X. Boudreux, R. R. Chance, *J. Am. Chem. Soc.,* 1983, **105,** 6555.

49. R. Zhao, X. Ji, S. Jiang, L. Liu, B. L. Weeks, Z. Zhang, *Green. Chem* 2011, **13**, 1891

PHOTOVOLTAIC AND NONLINEAR OPTICAL APPLICATIONS OF CONJUGATED POLYMERS

In this chapter, the photovoltaic and third-order nonlinear optical applications of π-conjugated conducting polymers are discussed. The third-order nonlinear absorption coefficient (β), imaginary part of the nonlinear susceptibility (Im $\chi^{(3)}$) and optical limiting threshold of the polymers were evaluated. Phenylene vinylene based polymers showed saturable absorption type graph with negative nonlinear absorption coefficient. Bithiophene and phenothiazine based copolymers showed positive nonlinear absorption coefficient and showed superior optical limiting property. The photovoltaic performance of some of the polymers were evaluated by fabricating inverted and conventional solar cells using polymers blended with PCBM as active layer. Inverted solar cell constructed using the device structure ITO/ZnO/polymer: PCBM/Ag gave better power conversion efficiency.

5.1 Introduction

Conjugated polymers are attracting much research interest for industrial applications because of their attractive combination of donor-acceptor units, low band gaps, suitable energy levels, high charge carrier mobility and low-cost of fabrication.[1-5] Using the quantum mechanical calculation, the band gap of the polymers can be tuned by adding appropriate donor and acceptor moieties. The conducting polymers with donor-acceptor groups have been investigated by many research groups owing to their potential applications in a wide variety of optoelectronic and photonic devices.[6-8] However, there have been only a few reports on the third-order nonlinear optical properties of the polymers. Nonlinear optical properties (NLO) of materials have been recognized for several years, with inorganic materials such as lithium niobate.[9] Recently, researchers have been exploring nonlinear optical properties in other classes of materials, such as organic polymers. Organic polymers show large and fast nonlinearities, fast response time and processability of donor-acceptor groups and often much better NLO properties than those observed in inorganics.[10] The NLO materials can exhibit one or more nonlinear optical mechanisms: two-photon absorption (TPA), excited state absorption (ESA), free carrier absorption, thermal defocusing and scattering, photorefraction, nonlinear refraction and induced scattering.[11] Two photon absorption (TPA) has considerable interest due to its potential application in two photon fluorescence imaging,[12,13] optical data storage[14,15] and optical power limiting.[16-20] The large nonlinear optical properties of donor-acceptor copolymers are due to their two photon absorption.

After the development of conducting polymers, as a new class of semiconducting materials, it has received considerable interest in the organic photovoltaic (OPV) technology. Organic polymers have shown high absorption coefficients, lightweight, large-area solution processing, and flexibility which allow organic solar cells to be efficient in thin films and under low sunlight irradiation.[21,22] Π-conjugated low band gap polymers can produce photons at longer wavelength which improve the efficiency of polymer solar cells due to the better overlap of the absorption spectrum.[10, 23,24]

The present chapter discusses the third-order nonlinear optical and the photovoltaic properties of the synthesised conjugated polymers.

5.2 Nonlinear optics

Nonlinear optics is the area of optics that deals with the interaction of light with matter under the circumstances where the linear superposition principle is violated. Since the advent of the laser in the 1960's, the field of nonlinear optics was developed.[25] In the presence of non-laser sources, the superposition principle holds true in this regime, and light waves can pass through materials and interfaces without interacting with each other. Whereas, laser sources can provide sufficiently high light intensities to modify the optical properties of materials. In the presence of laser sources, light waves interact with each other, exchanging momentum and energy, and the superposition principle is no longer valid. This nonlinear optical interaction of light wave results in harmonic generation, sum- and difference- frequency signals, the intensity dependence of the complex refractive index, stimulated light scattering and light-by-light scattering.[26] These processes lead to applications including optical switching, optical power limiting and image processing.

There are various techniques available for the determination of third-order optical nonlinearities such as degenerate four-wave mixing, nearly degenerate three-wave mixing, Z-scan technique, optical Kerr effect, ellipse rotation, interferometric methods, two beam coupling, beam self-bending and third harmonic generation.[27] All these methods are considered to be more sensitive techniques, but they are complex. Among the accessible techniques, Z-scan technique offers simplicity as well as very high sensitivity in measuring the nonlinear optical properties of materials. Therefore, in the present research work, single beam Z-scan technique was chosen for evaluating the third-order optical nonlinearity of the conducting polymers.

5.2.1 Z-scan technique

Z-scan technique was used to determine the magnitude of nonlinear absorption and the sign and magnitude of nonlinear refraction simultaneously. It was originally proposed by Sheik-Bahae *et al*. and applied to the study of third-order optical nonlinearity.[28-31] In this experiment, the sample under analysis was moved along the tightly focused laser beam. When the sample was moved, the intensity of the laser beam was changed and the sample experienced different intensities, depending on the position of the sample relative to focus (z=0). In the present work, NLO measurements were performed with nanosecond laser system with 532 nm wavelength. The laser beam was focused using a focal length of 200 mm. The beam waist can be calculated using the formula,

$$\omega_0 = \frac{1.22\lambda f}{d}$$ .... (5.1)

where λ is the wavelength of laser, f is the focal length of the lens and d is the diameter of laser beam. The other parameter known as Rayleigh length

is defined as, the distance along the propagation direction of a laser beam from the waist to the place where the area of cross section is doubled. It is estimated to be using the formula,

$$z_0 = \frac{\pi \omega_0^2}{\lambda}$$ ....(5.2)

To determine $\chi^{(3)}$, two parameters are needed, i.e., nonlinear refractive index (n_2) and nonlinear absorption coefficient (β). 'n_2' can be determined by performing closed aperture Z-scan and 'β' can be determined by performing open aperture Z-scan experiments. In the present study, focus was mainly on the measurement of nonlinear absorption coefficient and thereby to calculate imaginary part of the nonlinear susceptibility (Im $\chi^{(3)}$) of the polymers. Nonlinear absorption of a material are of two types, one is saturable absorption (SA) and the other is reverse saturable absorption (RSA). When the polymer sample approached the focus, the measured transmittance in the detector was either decreased or increased, forming a valley or peak at the focus. The process in which the transmittance decreases, forms a valley at the focus is known as reverse saturable absorption and is also known as positive type of absorption nonlinearity. In saturable absorption, transmittance increases, forms a peak at the focus and is known as negative type of absorption nonlinearity. The coefficient of nonlinear absorption is related to the imaginary part of the third-order nonlinear susceptibility $\chi^{(3)}$,[32] i.e., it could be due to TPA, free carrier absorption (FCA), RSA, self-focusing, self-defocusing or induced scattering.[33] In the case of polymers, both TPA and FCA show higher order nonlinear process and contribute to induced absorption. Compared to TPA, FCA is weak and hence the corresponding contribution in the Z-scan curves is relatively less.[34] The standard open

aperture Z-scan is expressed by using the nonlinear transmission equation (5.3).[28,29]

$$T_{(Z)} = \frac{c}{q_0\sqrt{\pi}} \int_{-\infty}^{\infty} \ln(1 + q_0\, e^{-t^2})dt \dots\dots\dots\dots\dots\dots\dots (5.3)$$

Where, $q_0(z,r,t) = \beta I_0\, L_{eff}$, with β being the NLA coefficient. I_0 is the incident irradiance at the beam focus (z=0). The effective sample thickness, L_{eff}, is given by[29]

$$L_{eff} = \frac{1 - e^{-\alpha l}}{\alpha} \dots\dots\dots\dots\dots\dots\dots\dots\dots\dots\dots (5.4)$$

Where, α is the linear absorption coefficient, and 'I_0' is the irradiance at focus

The experimental data were fitted with the theoretical curve obtained from the two photon absorption theory and calculated the effective nonlinear absorption coefficient. The imaginary part of the third-order nonlinear susceptibility was calculated using the equation (5.5).[29]

$$\text{Im}\, \chi^{(3)} = \frac{n_0^2 c^2 \beta}{240\pi^2 \omega} \dots\dots\dots\dots\dots\dots\dots\dots\dots (5.5)$$

where n_0 is the linear refractive index of the polymer in chloroform solution, c is the velocity of light in vacuum, ω is the angular frequency of radiation which is obtained from the equation $\omega = 2\pi c/\lambda$, where $\lambda = 532$ nm. .

The low band gap copolymers showed strong optical nonlinearity which was mainly due to the donor-acceptor scheme.

5.2.2 Optical power limiting

The nonlinear optical process in which the transmittance of a material decreases as the input fluence increases due to enhanced absorption from the excited state or multiphoton absorption or both is called optical limiting process. The optical limiting properties of the polymers are studied by measuring the nonlinear transmission as a function of input intensity. Optical limiters are transparent at low input fluences, but become opaque at high inputs.[35,36] Recently, the development of powerful and wide wavelength range laser sources has made it necessary the protection of sensors, optical components and human eyes against the high intensity. An ideal optical limiter is the one which exhibits a linear transmission below the optical limiting threshold value and above that, the transmitted power attains a steady value, it clamps the output to a constant value protecting the sensors.

Optical limiting property of a material is mainly due to third-order nonlinear absorption, which corresponds to the imaginary part of nonlinear susceptibility. The minimum criteria required for a good optical limiter are low limiting threshold, high linear transmittance throughout the sensor band width, stability, broad band spectral response, optical clarity and robustness etc.[37] Currently, donor- acceptor polymers have received much attention as optical limiters and used for protection of eyes and sensors from high intensity laser. The optical nonlinearity of the conjugated polymeric materials is the result of an optimum combination of various factors such as π-delocalization length, donor-acceptor groups, dimensionality, conformation, and orientation for a given molecular structure. Optical limiting experiment

was done at 532 nm using OA Z-scan technique. The optical limiting curves were plotted using the equation (5.6)

$$I_z = \frac{E}{\pi(1+\left(\frac{z}{z_0}\right)^2)\tau\omega_0^2} \quad \dots\dots\dots\dots\dots\dots\dots\dots\dots\dots\dots\dots (5.6)$$

Where, $\tau = 7\times 10^{-9}$ s, $\omega_0 = 42.56\times10^{-6}$ m, E= 79 μJ, the z_0 value was obtained by the equation

$$z_0 = \pi\omega_0^2/\lambda.$$

5.3 Photovoltaics

The research on photovoltaic devices began in 1950's, when a number of organic dyes, particularly chlorophyll were studied.[38] Recently, the investigation on less expensive type solar cells such as polymer solar cell has increased. One of the important factors which depends on the efficiency of the solar cell is its device architecture. Different photovoltaic device structures have been developed in order to assist efficient photon to charge conversion. The charge separation occurs between two layers in which donor material must be in contact with higher work function electrode while the acceptor material with the lower work-function electrode. Commonly used device architectures are single layer, bilayer and bulk heterojunction. The present study mainly focuses on the bilayer and bulk heterojunction device architecture.

5.3.1 Bilayer device

The bilayer heterojunction device is constructed with sandwich structure, in which p-n type semiconductors are stacked on top of each

other. The organic polymer was used as the active layer and was located between the higher work function electrode ITO and the metal electrode. The donor-acceptor polymer was coated on the top of ITO as layer by layer structure. Finally, lower work-function metal electrode was coated by vacuum evaporation technique. In the presence of an external light source, the donor-acceptor material absorbs light and excitons are generated. These excited species diffuse towards the donor-acceptor interface.[39] At the interface, they get dissociated to free charges. Finally, the free charges move towards the respective electrodes with the help of internal electric field. The layer by layer structure of donor-acceptor material results in a small interfacial area limiting the amount of absorbers which can actually contribute to the photocurrent. Generally, the diffusion length of exciton will be much less than the optical absorption length, which limits the quantum efficiency of such devices. Sariciftci *et al*.[40] constructed the first bilayer OSC device to use conjugated polymer where the hole transport material was poly[2-methoxy-5-(2'-ethylhexyloxy)-1,4-phenylene vinylene] (MEH-PPV) and the electron transport material was C60. The bilayer device showed PCE of 0.04 % which was obtained under monochromatic light of 514.5 nm. This showed improved device performance compared to single layer device.

5.3.2 Bulk heterojunction (BHJ) device

To improve the efficiency of bilayer heterojunction devices, the bulk heterojunction architecture was introduced with increased interfacial area between the donor and acceptor. [22,41-42] In BHJ device, a thin film comprised of a mixture of donor and acceptor materials was sandwiched between a pair of asymmetric electrodes. Organic polymers or small molecules were used

as the donor material and formed a hole-transporting path to the anode. Fullerene derivatives were used as the acceptor material and formed the electron-transporting path to the cathode. Conjugated donor-acceptor materials produced bound electron-hole pairs or excitons in the excited state which diffused between the domains of the donor and acceptor materials. The excitons got dissociated to form positive and negative charge carriers at the interface. The charge carriers moved towards their respective electrodes through the continuous donor and acceptor pathways.[43] The electron will be transported towards the material with large electron affinity and the hole will be transported towards the material with the lower ionisation potential which results in different potential energy which is larger than the exciton binding energy.[44-46] The bulk heterojunction is currently the most acceptable device structure for organic solar cells due to the efficient photo-induced electron transfer achieved from conjugated polymer to the fullerene derivatives. The advantages of BHJ over bilayer heterojunction is that excitons can be dissociated anywhere in the donor-acceptor interface, active layer and the interface distance should be in the order of the exciton diffusion length. Polymer that was initially utilized in bulk heterojunction structure was MDMO-PPV.[47]

5.3.3 Conventional photovoltaic devices

Two main classes of bulk heterojunction device geometries presently in use are the conventional and the inverted organic solar cells.[48,49] The fundamental component in organic solar cells is a transparent conductive oxide layer (TCO). Indium tin oxide (ITO) which has the work function of 4.5 to 4.7 eV is commonly used as transparent conductive oxide. ITO has the ability to collect both holes and electrons.[50,51]

The conventional geometry comprises of a substrate covered with a transparent conductive oxide followed by an electron blocking layer (poly(3,4-ethylenedioxy thiophene):poly(styrene sulfonate) (PEDOT:PSS)), a photoactive layer, in some cases electron transport layer (e.g., lithium fluoride or calcium or $CsCO_3$) and finally, a low work function metal electrode (the cathode). The photoactive bulk-heterojunction layer is coated between the hole and electron blocking layers with domains of acceptor material dispersed in a donor matrix. Below the ambient conditions, the low work function metal electrode typically form non-conductive oxides leading to a rapid degradation of the solar cell performance.[52,53] Hence, encapsulation of these devices using costly packaging materials with very low oxygen and water permeation has become necessary.

Tao *et al*. constructed conventional bulk heterojunction photovoltaic device in the configuration ITO/PEDOT:PSS (40 nm)/PTB7:PC71BM/Al (100 nm). The power conversion efficiency of PTB7: PC71BM polymer solar cells were improved to 9.1% by treatment with methanol followed by a water- and alcohol-soluble conjugated polyelectrolyte cathode interface layer.[54]

5.3.4 Inverted photovoltaic devices

In the inverted type geometry, the order of the layers is reversed i.e., the hole blocking layer is inserted between the transparent electrode and the photoactive layer. The top metal electrode now being the hole-collecting anode with high work-function, air-stable material like silver or gold is used. TiO_2, ZnO and In_2S_3 are the most widely studied electron transport materials to be inserted between ITO and the active layer of

inverted PSCs. [55-57] Different types of metal electrodes are used in conventional and inverted device geometry. Low work function metals such as aluminum and/or calcium are typically used as back electrodes in the conventional cells, while higher work function metals such as silver are used in the inverted cells. Different arrangements of the layers in the two geometries create interfaces with various surface interactions, which may affect the photovoltaic performances. Remarkably, the inverted geometry devices tend to be much more stable than the conventional one, which are intended as durable devices in the view point of life-time issue.[58] Shirakawa *et al.* fabricated the first inverted organic solar cell applying a compact ZnO hole blocking layer and a gold layer as top electrode.[59] Sungho *et al.* constructed inverted photovoltaic device in which ZnO was coated as electron collective layer between ITO and blended PTB7-Th:PC71BM photoactive layer and the device gave maximum power conversion efficiency of 9.57 %.[60]

5.3.5 J-V Characteristics of photovoltaic devices

The current density-voltage characteristics of a solar cell in the dark and under illumination are shown in Figure 5.1. In the dark, there is no current flowing, until the contacts start to inject at forward bias for voltages larger than the open circuit voltage. Under illumination, in the fourth quadrant, the device generates power. At some point on the J-V curve, maximum power point (P_{max}) i.e., the product of current and voltage ($J \times V$) is the largest, that the cell can deliver to an external load.
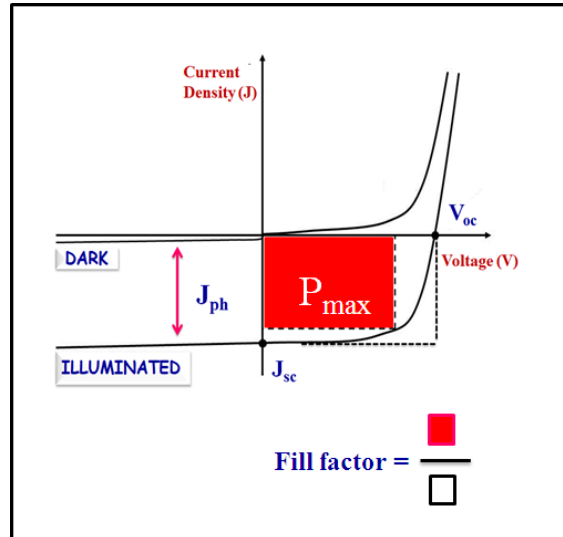
Figure 5.1: J-V curve for bulk heterojunction organic solar cell device under both dark and illumination conditions

The power conversion efficiency is the percentage of input power from light source that is converted to the output power at the operating point where the maximum power is produced by the device. The power conversion efficiency (PCE) is determined by the following equation (5.7): [61]

$$\text{PCE} = \eta = \frac{P_{max}}{P_{in}} = \frac{V_{oc} \times I_{sc} \times FF}{P_{in}} \quad\text{...} (5.7)$$

Where $P_{max} = J_{max} \times V_{max}$ i.e., is the maximum power a device can produce and $P_{in} = 100$ mW/cm^2 is the standard power input. The ratio of P_{max} to the product of short-circuit current density (J_{sc}) and open circuit voltage (V_{oc}) is called the fill factor (FF). FF is given by the following equation,

$$\text{FF} = \frac{V_{max} \times I_{max}}{V_{OC} \times I_{sc}} \quad\text{..} (5.8)$$

Where, V_{max} and J_{max} are the maximum voltage and maximum current density respectively.

5.3.5.1 Open circuit voltage (V_{oc})

The open-circuit voltage, V_{oc}, is the maximum voltage available from a photovoltaic cell under illumination and this occurs at zero current. Open-circuit voltage is a measure of the amount of recombination in the device. It is the difference of electrical potential between the two terminals of an organic solar cell. 'V_{oc}' depends linearly on the energy difference between the highest occupied molecular orbital (HOMO) of the donor materials and the lowest unoccupied molecular orbital (LUMO) of the acceptor materials.[62]

5.3.5.2 Short circuit current (I_{sc})

The short circuit current, I_{sc}, is the current that flows through the external circuit when the electrodes of the solar cell are short circuited. The short circuit current is due to the formation and collection of light-generated charge carriers. For an ideal organic solar cell with moderate resistive loss, I_{sc} and the light-generated current are identical. The maximum current that the solar cell can deliver strongly depends on the area of the solar cell, the number of photons (i.e., the power of the incident light source), the spectrum of the incident light, the optical properties (absorption and reflection) and the collection probability of the solar cell.

5.3.5.3 Fill factor

The fill factor is the ratio between the maximum power generated by a solar cell and the product of V_{oc} with J_{sc}.

5.4 Results and discussion

5.4.1 Open aperture (OA) Z-scan measurements of the polymers

The third-order nonlinear susceptibility ($\chi^{(3)}$) of the copolymers in chloroform was evaluated using Z-scan technique, designed and developed by Sheik Bahae *et al.*[28-31] Nonlinear optical properties of the copolymers were measured using simple and single beam Z-scan technique with nanosecond laser performed with a Q-switched Nd:YAG laser system (Spectra Physics LAB −1760) with pulse width of 7 ns at 10 Hz repetition rate and 532 nm wavelength. In the experiment, a Gaussian laser beam was focused to a narrow waist; its radius (ω_o) was calculated to be 42.56 μm. The sample was moved in the direction of light incidence near the focal spot of the lens with a focal length of 200 mm. The Rayleigh length was estimated to be 10.69 mm, which was much larger than the thickness of either the sample cuvette (1 mm) or the self-assembled films, which is an essential requirement for the validity of the Z-scan theory. CS_2 was used as the standard to calibrate the Z-scan system. The transmitted beam energy, reference beam energy and their ratios were measured simultaneously by an energy ratiometer (REj7620, Laser Probe Corp.) having two identical pyroelectric detector heads (Rjp 735). The effects of fluctuations of laser power was reduced by dividing the transmitted power by the power attained at the reference detector; both being measured using identical photo detectors. The data were analysed according to the procedure described by Bahae *et al.*[28] The nonlinear absorption coefficient was measured by fitting the experimental Z-scan plot with the theoretical plots.

Optical power limiting measurements were also carried out to investigate the optical limiting response of the polymer samples. To study the optical

limiting property of the polymers, the nonlinear transmission was measured as a function of input intensity.

5.4.1.1 Phenylene vinylene based copolymers

The open-aperture (OA) Z-scan traces for the four copolymers MD-CA-PPV, MD-FL-PPV, MD-PT-PPV and MD-AN-PPV in $CHCl_3$ are presented in Figure 5.2. The polymers showed saturable absorption at a wavelength of 532 nm. The open aperture curve exhibited a normalised peak type graph with a negative nonlinear absorption coefficient.
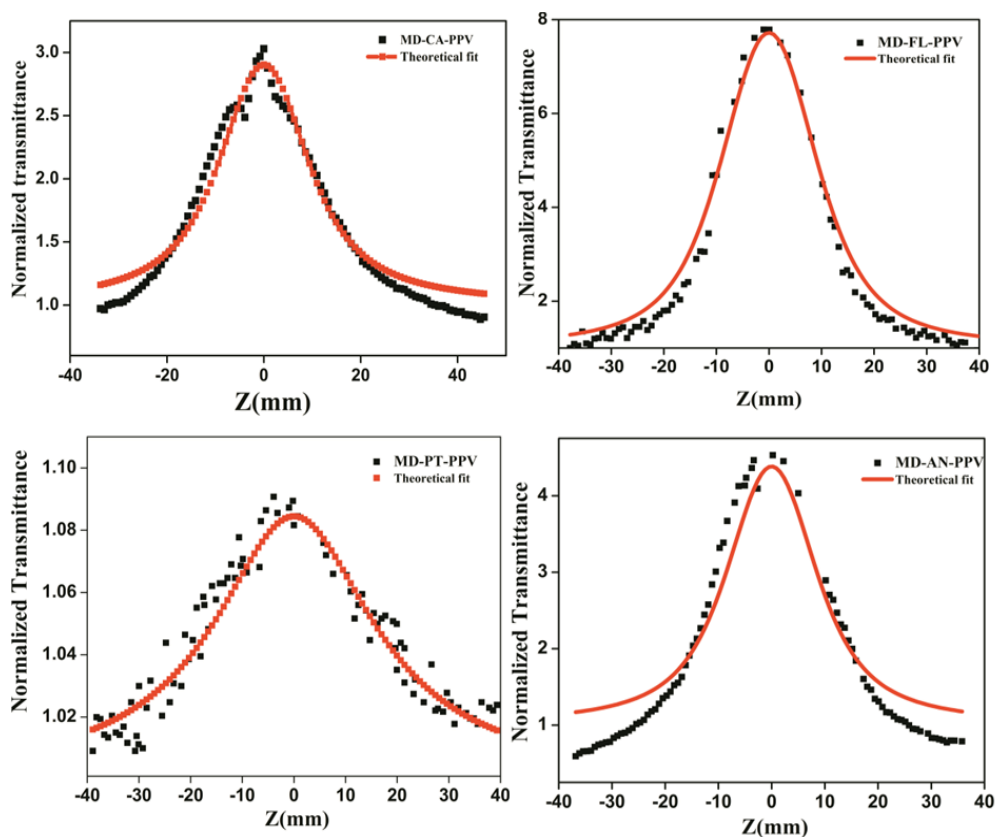

Figure 5.2: Open aperture (OA) Z-scan traces of (a) MD-CA-PPV (b) MD-FL-PPV (c) MD-PT-PPV and (d) MD-AN-PPV in $CHCl_3$ at 79 μJ

It is clear from the figure that the nonlinear absorption traces of the copolymers fitted well with the graph derived from the two photon absorption (TPA) theory. This concludes that TPA is the basic mechanism involved in the nonlinear absorption process. The PPV based polymers showed switch over from Reverse Saturable Absorption (RSA) to Saturable Absorption (SA). This could be attributed to ground state band bleaching of phenylene vinylene copolymers in solution,[63] i.e., the excited state absorption and free carrier absorption result in ground state band bleaching. The calculated value of nonlinear absorption coefficient (β, m/W) and the third-order nonlinear susceptibility ($\chi^{(3)}$, esu) are listed in Table 5.1. MD-CA-PPV, MD-FL-PPV, MD-PT-PPV and MD-AN-PPV could not be used as optical limiters because they showed enhanced transmittance at the focus.

Table 5.1: Calculated values of nonlinear absorption coefficient and imaginary part of nonlinear susceptibility of (a) MD-CA-PPV (b) MD-FL-PPV (c) MD-PT-PPV and (d) MD-AN-PPV at 532 nm

Copolymer	Nonlinear absorption coefficient (β, m/W)	Imaginary part of Nonlinear Susceptibility (Im $\chi^{(3)}$, esu)
MD-CA-PPV	-0.17×10^{-10}	-0.03×10^{-11}
MD-FL-PPV	-2.06×10^{-10}	-0.45×10^{-11}
MD-PT-PPV	-0.63×10^{-10}	-0.14×10^{-11}
MD-AN-PPV	-2.83×10^{-10}	-0.59×10^{-11}

The third-order nonlinear absorption coefficient values of the PPV copolymers were found to be in the order of 10^{-10} m/W which showed that the band gap of each polymer was in the semiconducting range and it was already confirmed theoretically and experimentally. Saturable absorption polymers have been used widely in short pulsed laser generations as crucial

passive mode-locking, Q-switching elements and for designing novel photonic devices.[64]

5.4.1.2 Bithiophene based copolymers

a) P(BT-PH) and P(BT-CZ)

The open-aperture (OA) Z-scan plots of the two copolymers P(BT-PH) and P(BT-CZ) in CHCl$_3$ are presented in Figure 5.3.
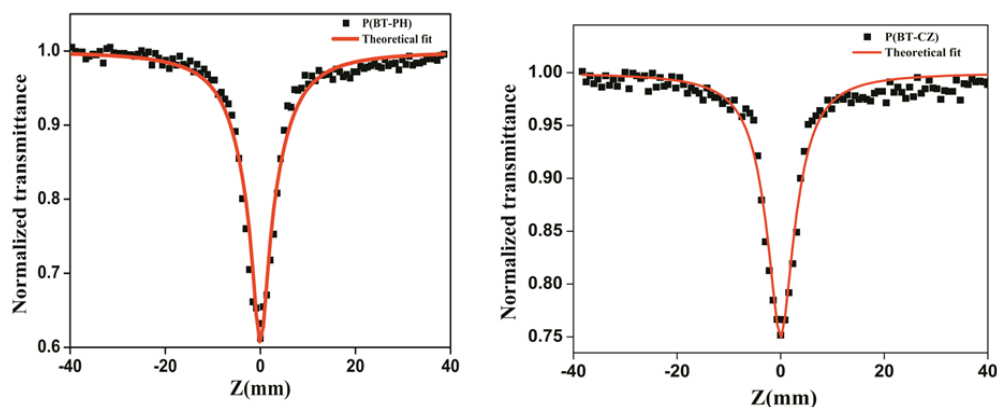
Figure 5.3: Open aperture (OA) Z-scan traces of P(BT-PH) and P(BT-CZ) in CHCl$_3$ at 79 μJ

Both the copolymers showed a normalized transmittance valley type graph with positive nonlinear absorption coefficient. It could be seen from the figure that the experimental curve fitted well with the graph derived from two photon absorption theory (TPA). The copolymers, P(BT-PH) and P(BT-CZ) showed reverse saturable absorption type graph. The third-order nonlinear absorption coefficient (β) and imaginary part of the nonlinear susceptibility (Im χ$^{(3)}$) were determined by Z-scan technique under an open aperture configuration (Table 5.2). The nonlinear absorption coefficient, β was obtained by fitting the experimental scan plot of the OA measurement

to equation (5.3), given in section 5.2.1. Also, the imaginary part of the third-order susceptibility ($\text{Im}\chi^{(3)}$) of copolymers was determined by equation (5.5), given in section 5.2.1. The experimentally determined values of β and $\text{Im }\chi^{(3)}$ were found to be in the order of 10^{-10} m/W and 10^{-11} esu respectively. The values implied that, the band gap of the donor-acceptor copolymers P(BT-PH) and P(BT-CZ) were in the semiconducting range. The charge transfer from donor to the acceptor units resulted in strong nonlinearity for the copolymers.

Table 5.2: Calculated values of nonlinear absorption coefficient and imaginary part of nonlinear susceptibility of P(BT-PH) and P(BT-CZ) at 532 nm

Copolymer	Nonlinear absorption Coefficient (β, m/W)	Imaginary part of Nonlinear Susceptibility ($\text{Im }\chi^{(3)}$, esu)
P(BT-PH)	3.85×10^{-10}	0.81×10^{-11}
P(BT-CZ)	2.87×10^{-10}	0.62×10^{-11}

The nonlinear absorption coefficient was obtained to be 3.85×10^{-10} and 2.87×10^{-10} m/W for P(BT-PH) and P(BT-CZ) respectively. There was slight increase in the β value of P(BT-PH) compared to P(BT-CZ). In addition, the $\chi^{(3)}$ value was also found to be increased for P(BT-PH). The large optical nonlinearity of P(BT-PH) compared to P(BT-CZ) was due to the more acceptor strength of PH than the CZ unit. In the case of D-A copolymers, nonlinearity is generally due to the charge transfer from donor to acceptor unit, i.e., due to strong delocalization of π electrons.

Optical power limiting

The optical limiting process occurs mainly due to the nonlinear absorption; it is the result of extent of conjugation, donor-acceptor groups,

dimensionality, conformation and orientation. The optical limiting properties of the copolymers P(BT-PH) and P(BT-CZ) were investigated by OA Z-scan technique at 532 nm. Figure 5.4 presents the transmitted energy of bithiophene based polymers as a function of input intensity. At low input fluence the output varies linearly with input energy i.e., polymers obey Beer's law. When the input power reaches optical limiting threshold, the transmitted energy starts to deviate and show optical limiting effect.
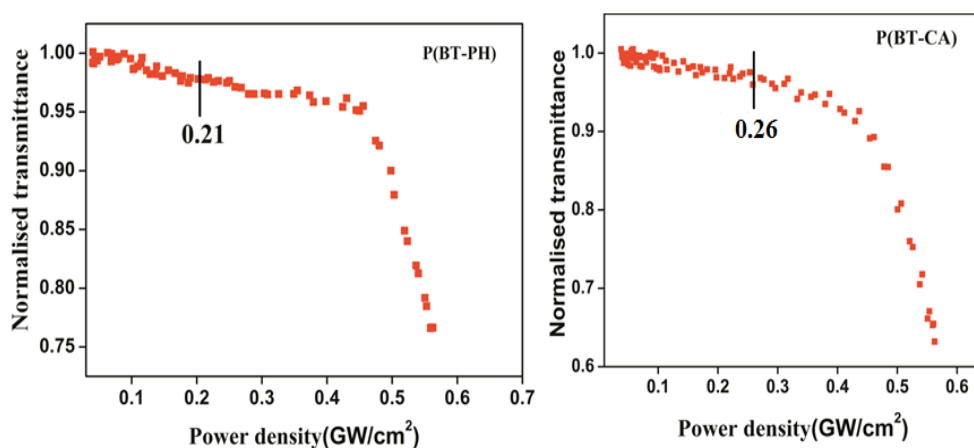
Figure 5.4: Optical limiting curves of P(BT-PH) and P(BT-CZ)

Optical limiting threshold is determined to be 0.21 and 0.26 GW/cm^2 for P(BT-PH) and P(BT-CZ), respectively. The polymer with low value of optical limiting threshold is a good optical limiter. Both the copolymers exhibited superior optical limiting response which was due to the donor-acceptor scheme. The P(BT-PH) showed slightly better optical limiting response than P(BT-CZ). Both the copolymers exhibited large optical nonlinearity due to the strong delocalisation of π-electrons.

b)   P(BT-FLN) and P(BT-TPA)

To study the third-order NLO parameters of bithiophene based copolymers, P(BT-FLN) and P(BT-TPA) the open aperture (OA) Z-scan technique was conducted at 532 nm. The OA plots of the copolymers in CHCl$_3$ are shown in Fig. 5.5.
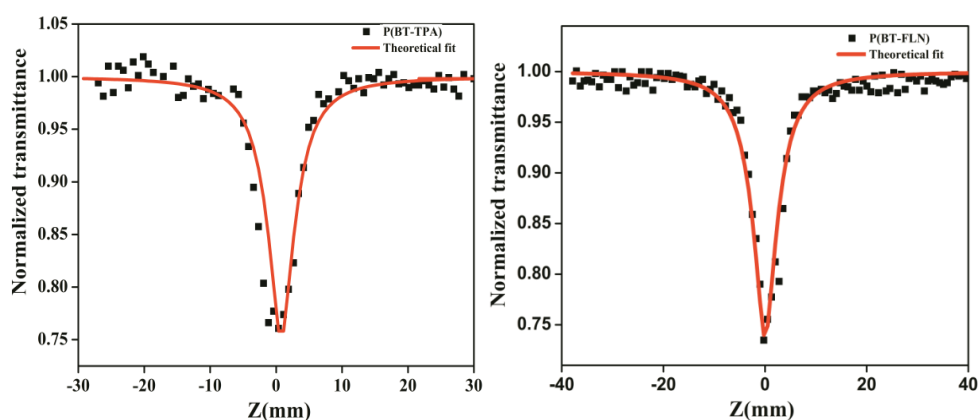
Figure 5.5: Open aperture (OA) Z-scan traces of P(BT-FLN) and P(BT-TPA) in CHCl$_3$ at 79 μJ

In solution phase, both the copolymers exhibited a normalized transmittance valley type graph, indicating the reverse saturable absorption (RSA) with a positive NLO absorption coefficient. The third-order nonlinear absorption coefficient, imaginary part of the nonlinear susceptibility values were calculated and are given in the Table 5.3. The nonlinear absorption coefficient, β was obtained by fitting the experimental scan plot of the OA measurement to equation (5.3), given in section 5.2.1. Also the imaginary part of the third-order susceptibility (Imχ$^{(3)}$) of copolymers was determined by equation (5.4), given in section 5.2.1. Here also, the values of absorption coefficient and imaginary value of the nonlinear susceptibility were found to be

in the range of 10^{-10} m/W and 10^{-11} esu respectively. It revealed that the band gap of the copolymers P(BT-FLN) and P(BT-TPA) were in the semiconductor range which was already proved theoretically and experimentally.

Table 5.3 Calculated values of nonlinear absorption coefficient and imaginary part of nonlinear susceptibility P(BT-FLN) and P(BT-TPA) at 532 nm

Copolymer	Nonlinear absorption Coefficient (β, m/W)	Imaginary part of Nonlinear Susceptibility (Im $\chi^{(3)}$, esu)
P(BT-FLN)	2.99×10^{-10}	0.67×10^{-11}
P(BT-TPA)	3.01×10^{-10}	0.65×10^{-11}

Optical power limiting

The optical limiting property of the copolymers, P(BT-FLN) and P(BT-TPA) were investigated at 532 nm in CHCl$_3$ solution by open aperture Z-scan technique. Fig. 5.6 shows the transmitted energy of P(BT-FLN) and P(BT-TPA) as a function of input intensity.
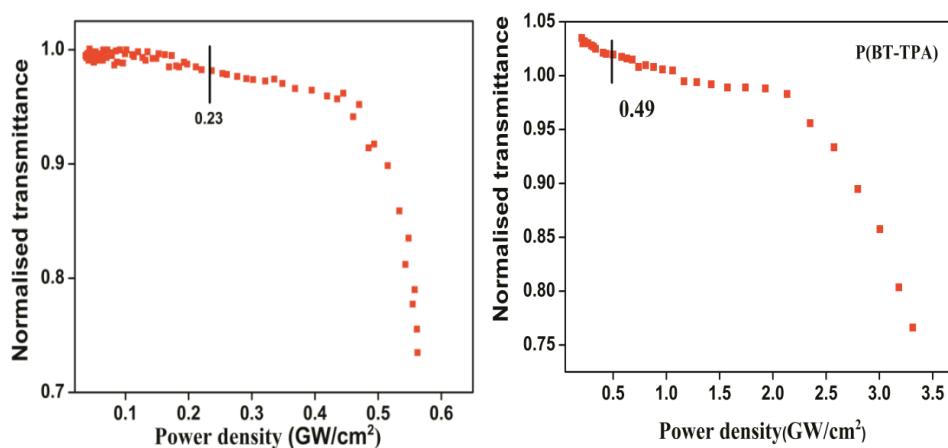

Figure 5.6: Optical limiting curves of P(BT-FLN) and P(BT-TPA)

At lower input fluence, polymer obeys Beer's law. Optical limiting threshold was noted as the deviation from linearity. Optical limiting threshold was determined to be 0.23 and 0.49 GW/cm^2 for P(BT-FLN) and P(BT-TPA) respectively. The low value of optical limiting threshold implied that the polymers could act as good optical limiter.

5.4.1.3 Phenothiazine based copolymers

The open aperture Z-scan technique was used to measure the NLO properties of phenothiazine based copolymers. The OA Z-scan traces of the copolymers P(PHENO-TPA) and P(PHENO-MeTH) are shown in the figure 5.7.
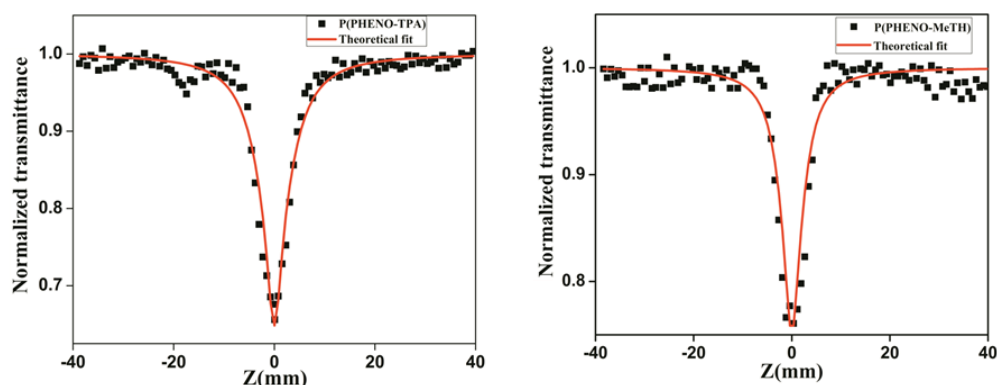
Figure 5.7: Open aperture (OA) Z-scan traces of P(PHENO-TPA) and P(PHENO-MeTH) in CHCl$_3$ at 79 µJ

The copolymers showed reverse saturable absorption and presented a normalized valley type graph with a positive NLO absorption coefficient. The nonlinear absorption traces of the copolymers were fitted well with the graph derived from two photon absorption theory. In the copolymers, P(PHENO-TPA) and P(PHENO-MeTH), PHENO acted as acceptor and TPA and MeTH acted as donors which was confirmed theoretically. The

donor-acceptor scheme was responsible for the strong optical nonlinearity of the copolymers. The nonlinear absorption coefficient (β) and third-order susceptibility ($Im\chi^{(3)}$) values were measured and are summarised in the Table 5.4. The 'β' was obtained by fitting the experimental scan plot of the OA measurement to equation (5.3), given in section 5.2.1. Also $Im\chi^{(3)}$ of copolymers was determined by equation (5.5), given in section 5.2.1.

Table 5.4: Calculated values of nonlinear absorption coefficient and imaginary part of nonlinear susceptibility of P(PHENO-TPA) and P(PHENO-MeTH) at 532 nm.

Copolymer	Nonlinear absorption Coefficient (β, m/W)	Imaginary part of Nonlinear Susceptibility ($Im\ \chi^{(3)}$, esu)
P(PHENO-TPA)	3.64×10^{-10}	0.79×10^{-11}
P(PHENO-MeTH)	3.01×10^{-10}	0.64×10^{-11}

From the table, it could be seen that the β and $Im\ \chi^{(3)}$ values were in the range of 10^{-10} m/W and 10^{-11} esu respectively which indicated that the band gap of the polymer was in the semiconductor range which was already confirmed theoretically and experimentally.

Optical power limiting

To probe the optical limiting behaviour of P(PHENO-TPA) and P(PHENO-MeTH) copolymers, the nonlinear transmission was measured as a function of input intensity under open aperture Z-scan configuration at 532 nm. The input fluence exceeded optical limiting threshold of the polymer it became opaque and it could be developed as a device which could protect human eye and high sensitive instruments from laser induced

damages. The optical limiting performance of copolymers P(PHENO-TPA) and P(PHENO-MeTH) exhibiting RSA behaviour is revealed in Fig. 5.8. The input intensity at which the normalized transmission begins to deviate from linearity is called optical limiting threshold and they were obtained to be 0.32 and 0.60 GW/cm^2 for P(PHENO-TPA) and P(PHENO-MeTH) respectively.
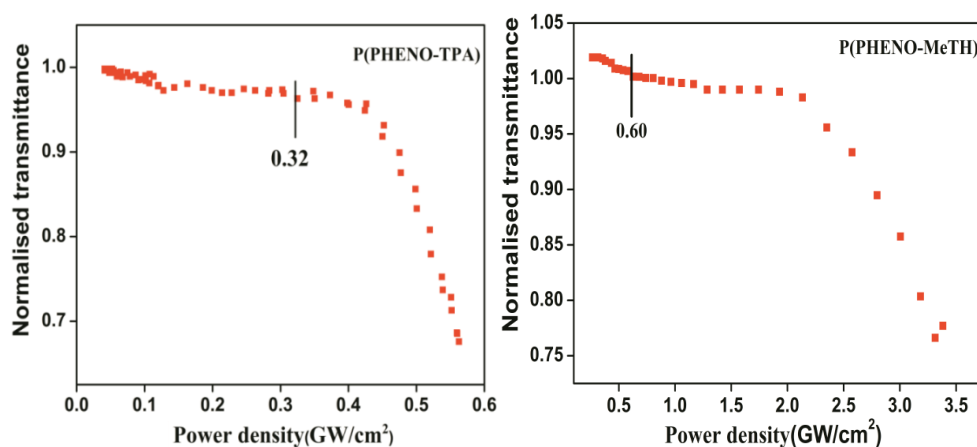
Figure 5.8: Optical limiting curve of P(PHENO-TPA) and P(PHENO-MeTH)

5.4.2 Photovoltaic device

The photovoltaic performance of some of the synthesized polymers were evaluated by constructing both conventional and inverted bulk heterojunction device. A layer of polymer: PCBM blend in the ratio 1:1 was used as the photoactive layer in conventional solar cell. The device configuration was ITO/MoO$_3$/POLYMER:PCBM/LiF/Al. Conventional device architecture employed a patterned indium tin oxide (ITO) glass which was precleaned in an ultrasonic bath with deionized water, acetone and isopropanol (each for 20 min). A thin layer of MoO$_3$, which acted as anode buffer layer, was

deposited onto the ITO glass by vacuum evaporation technique. Polymer: PCBM mixture (1:1 ratio) in chlorobenzene, which was a blend of the donor and acceptor materials, was spin-coated on the anode buffer layer to form a photosensitive layer. LiF, which acted as cathode buffer layer, was deposited by vacuum evaporation. The device was completed by evaporating a low work function metal electrode (Al or Ca/Al) over the active layer. Figure 5.9 shows the schematic representation of the conventional solar cell.
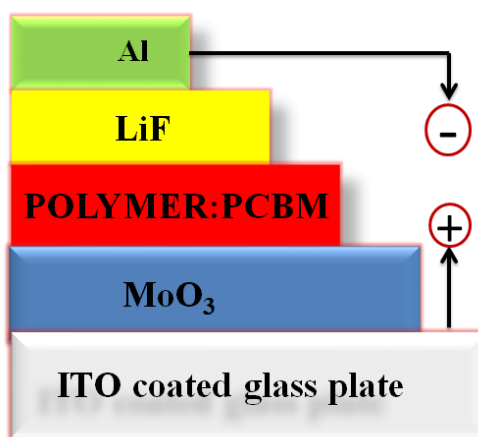
Figure 5.9: Schematic diagram of the conventional solar cell

Polymer solar cells with a conventional configuration were also constructed using Tris (8-hydroxyquinolinato)aluminium (Alq_3) as cathode buffer layer and MoO_3 as anode buffer layer in the configuraton ITO/MoO_3/POLYMER: PCBM/Alq_3/ Al and another one with poly(3,4-ethylenedioxythiophene): poly(styrenesulfonate) (PEDOT:PSS) as anode buffer layer and LiF, as cathode buffer layer in the architecture, ITO/PEDOT:PSS /POLYMER:PCBM/LiF/Al. In both the cases, the open circuit voltage and short circuit current were obtained to be very low. The poor efficiency and stability arises due to the corrosive nature of PEDOT: PSS and oxidative nature of metal cathode.[64, 65]

Therefore, to avoid the ITO/PEDOT: PSS interface and the use of low work function cathode, inverted bulk-heterojunction solar cell was constructed. In inverted device architecture, the nature of charge collection was reversed, i.e., an opposite layer sequence was used having the hole blocking layer between the transparent electrode and the photoactive layer to effectively collect electrons. The top contact used a high work function electrode, such as air-stable material like silver or gold, which was used at the top to collect holes. The most commonly used hole blocking layer is ZnO, TiO_2 or In_2S_3 thin film which can be processed from solution.

In the present study, a simple inverted bulk heterojunction solar cell was constructed using a blend of polymer with [6,6] phenyl C61 butyric acid methyl ester (PCBM) as the active layer, and spray deposited ZnO as the electron selective layer. The device configuration was ITO/ZnO/polymer:PCBM/Ag. ZnO was deposited onto the ITO glass by simple and non-vacuum chemical spray pyrolysis (CSP) technique. Blend of polymer and PCBM (99 % purity; Osscila), (1:1 ratio) was dissolved in chlorobenzene to form a solution and was spin coated to serve as the active region. Finally, Ag electrode was deposited by vacuum evaporation. Except the deposition of Ag electrode, the overall device fabrication was performed under ordinary atmospheric conditions. J-V characteristics were measured using a source measure unit NI PXI-1033 and illumination was done using class AAA solar simulator [PET, USA]. Figure 5.10 shows the schematic representation of the inverted solar cell.
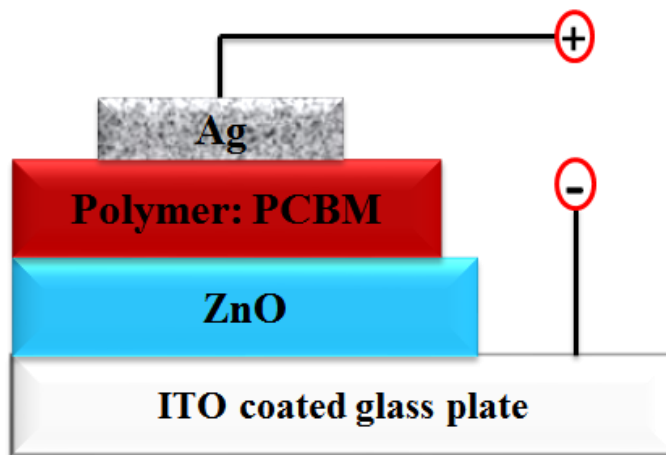
Figure 5.10: Schematic diagram of the inverted solar cell

5.4.2.1 Photovoltaic performance of conventional solar cell constructed using synthesized polymers

From the theoretical as well as experimental data, it was found that the phenylene vinylene based copolymers showed low band gap which was very much suitable for photovoltaic application. This was confirmed by fabricating a conventional and inverted bulk heterojunction device using the PPV polymers.

5.4.2.1.1 MD-AN-PPV: PCBM blend in 1:1 as photoactive layer

The current density-voltage (J-V) characteristics of the conventional heterojunction under illumination and in the dark are shown in the Figure 5.11. The device configuration was ITO/MoO$_3$/MD-AN-PPV: PCBM/LiF/Al. Here, MD-AN-PPV: PCBM blend in the 1:1 ratio was used as the photoactive layer. The conventional solar cell under illumination gave an open circuit voltage (Voc) of 564 mV and short circuit current density (Jsc) of 0.57 mA/cm^2

and fill factor was found to be 21 %. The maximum Power Conversion Efficiency (PCE) achieved by the solar cell was 0.007 %.

Figure 5.11: J-V curve of conventional solar cell with configuration ITO/MoO₃/ MD-AN-PPV: PCBM/LiF/Al under dark and under illumination

5.4.2.1.2 MD-CA-PPV: PCBM blend in 1:1 as photoactive layer

The polymer, MD-CA-PPV and PCBM blend in 1:1 ratio was also used as photoactive layer in the conventional device architecture and the configuration was ITO/MoO₃/MD-CA-PPV: PCBM/LiF/Al. The J-V characteristics of the conventional solar cell under dark and illumination are shown in the Figure 5.12. Under white light illumination, the device exhibited a short circuit current density (J_{sc}) of 0.20 mA/cm^2 and an open circuit voltage (V_{oc}) of 832 mV. The fill factor (FF) and PCE were obtained to be 24 % and 0.04 % respectively. In both cases, MD-CA-PPV and MD-AN-PPV acted as the electron donor and PCBM as the electron acceptor, with the conventional device structure ITO/MoO₃/polymer:PCBM/LiF/Al.

The above results proved the capability of these polymers in solar cell fabrication.

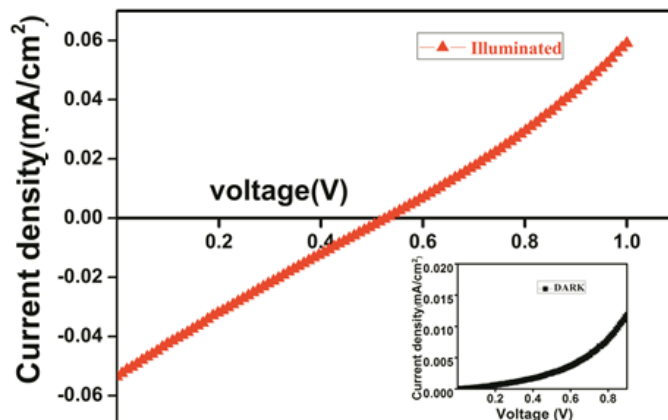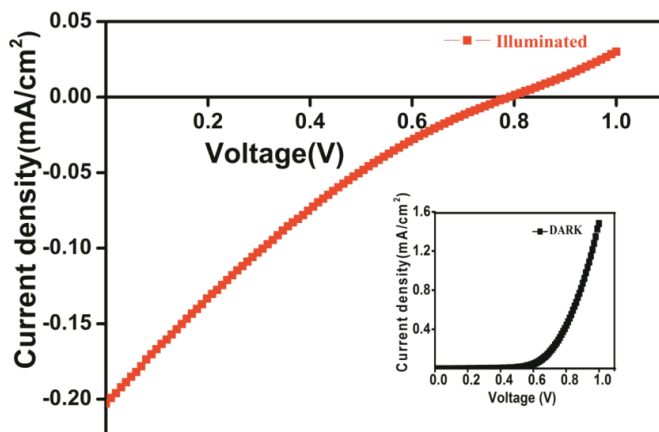**Figure 5.12:** J-V curve of conventional solar cell with configuration ITO/MoO₃/MD-CA-PPV: PCBM/LiF/Al under dark and under illumination

5.4.2.2 Photovoltaic performance of inverted solar cell constructed using synthesized polymers

The suitability of the PPV polymers for active layer in photovoltaic device was verified by constructing heterojunction device using the polymers and the semiconductor ZnO. The photovoltaic performance of the polymers, MD-CA-PPV and MD-FL-PPV were checked by fabricating the inverted solar cell. The theoretical as well as experimental data revealed that both polymer showed very low band gap and they were suitable for photovoltaic application.

5.4.2.2.1 MD-CA-PPV: PCBM blend in 1:1 as photoactive layer

Figure 5.12 shows the J-V characteristics of the heterojunction in the configuration ITO/ZnO/Polymer:PCBM/Ag under illumination and in the dark. Blend of MD-CA-PPV: PCBM (1:1 ratio) was spin coated to serve as the photosensitive layer. The electron collecting layer ZnO, with high resistivity of $\sim 10^2$ Ω cm was deposited by chemical spray pyrolysis (CSP) technique over ITO plate. From the Figure 5.13 it could be seen that, the device exhibited rectifying behaviour in the dark which may be due to the barrier formed at the ZnO/polymer interface. Under white light illumination (100 mW/cm^2), the device, ITO/ZnO/MD-CA-PPV:PCBM/Ag heterojunction exhibited an efficiency of 0.43 %. It has short circuit current density (J_{sc}) of 0.77 mA/cm^2 and an open circuit voltage (V_{oc}) of 1030 mV and fill factor was found to be 54 %.

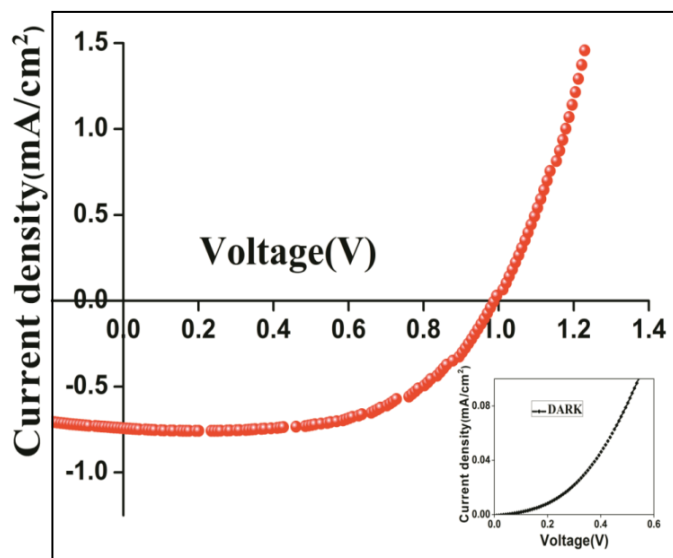**Figure 5.13:** J-V curve of inverted solar cell with configuration ITO/ZnO/ MD-CA-PPV:PCBM/Ag under dark and illumination

MD-CA-PPV: PCBM in (1:1) ratio was used as the photoactive layer in both conventional and inverted solar cell in the configuration ITO/MoO$_3$/MD-CA-PPV/PCBM/LiF/Al and ITO/ZnO/MD-CA-PPV:PCBM/Ag. On changing the architecture from conventional to inverted, a significant improvement in the fill factor of the device was observed which was increased from 24 to 54 %. J$_{sc}$ also showed a progress on changing the configuration i.e., increased from 0.20 to 0.77 mA/cm^2. Increase in J$_{sc}$ and fill factor has led to an enhancement in efficiency of the device. The efficiency increased from 0.04 % to 0.43 % on changing the device configuration from conventional to inverted solar cell.

Inverted solar cell showed better collection of charge carriers which resulted in the better J$_{sc}$ values than the other. Fill factor of the device is the key parameter that determines the quality of the device and the calculated values revealed the better device quality for inverted structure.

5.4.2.2.2 MD-FL-PPV as photoactive layer

The applicability of MD-FL-PPV for photovoltaic device was verified by fabricating a bilayer heterojunction device with the structure ITO/ ZnO/ MD-FL-PPV /Ag. Figure 5.14 shows the J-V characteristics of the hetrojunction under illumination and dark. Under white light illumination (100 mW/cm^2), the device exhibited a short circuit current density (J$_{sc}$) of 0.86 mA/cm^2 and an open circuit voltage (V$_{oc}$) of 1194 mV for MD-FL-PPV. The fill factor (FF) and efficiency were calculated to be 50 % and 0.51 % respectively.
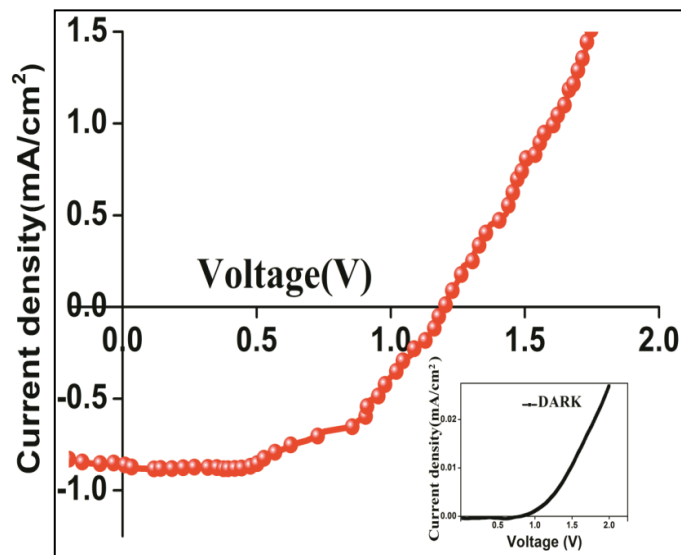
Figure 5.14: J-V curve of inverted solar cell with configuration ITO/ZnO/ MD-FL-PPV /Ag under dark and illumination

A graphical representation of energy diagram for ZnO/ MD-FL-PPV device with Ag and ITO electrodes before the materials are placed in contact is shown in Figure 5.15.
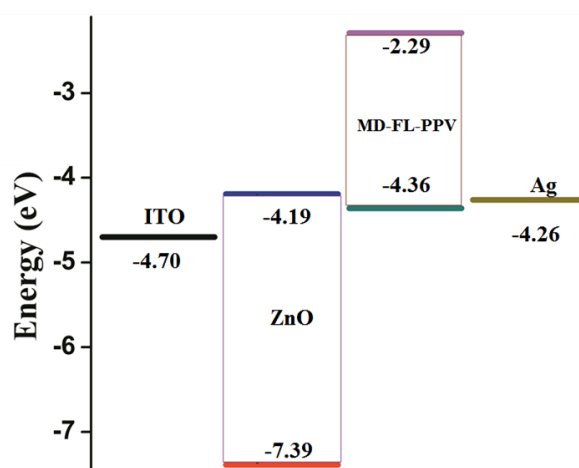
Figure 5.15: Energy level diagram of ITO/ ZnO/ MD-FL-PPV /Ag photovoltaic devices

The energies of the conduction band (CB) and valence band (VB) edges for ZnO are -4.19 eV and -7.39 eV respectively, whereas the LUMO and HOMO levels of MD-FL-PPV are -2.29 eV and -4.36 eV respectively. The work functions of Ag and ITO electrodes are taken to be about -4.26 eV and -4.7 eV, respectively.

The device principle can be explained as follows: donor polymer absorbs the incident radiation and the excitons are generated in MD-FL-PPV which get diffused to the ZnO/ MD-FL-PPV interface. Since the LUMO of MD-FL-PPV lies above the conduction band edge of ZnO, the excitons are expected to efficiently dissociate by electron transfer to ZnO. In the same manner, a photoinduced hole transfer from ZnO to MD-FL-PPV is expected. Since electrons are carried to one contact by ZnO, and holes are transported by the MD-FL-PPV layer to the opposite contact, the paths of oppositely charged carriers are separated and recombination would be suppressed.

5.4.2.2.3 MD-FL-PPV: PCBM blend as photoactive layer

The phenylene vinylene polymer based inverted bulk-heterojunction solar cells were fabricated using a blend of MD-FL-PPV and PCBM as the active layer, and spray deposited ZnO as the electron selective layer. The cell configuration was ITO/ZnO/PL:PCBM/Ag. In order to get an efficient device, the dimensions of the donor and acceptor phases in the active layer should be of the order of exciton diffusion length. Every exciton photogenerated within the blend should reach the interface and get dissociated. There should be a solid pathway in both phases in order to enable the collection of either electrons or holes. Several factors control

morphology of the active layer, one of which being the ratio between donor and acceptor materials.

Fig. 5.16 shows the current density-voltage (J-V) characteristics of inverted bulk-heterojunction device with varying ratios of donor (MD-FL-PPV) to acceptor (PCBM). The photoactive layer of the device was cast from a chlorobenzene solution containing MD-FL-PPV and PCBM. The ratio of the polymer: PCBM blend was varied by changing the weight ratio of PCBM in the solution from 0.5 to 1.5.
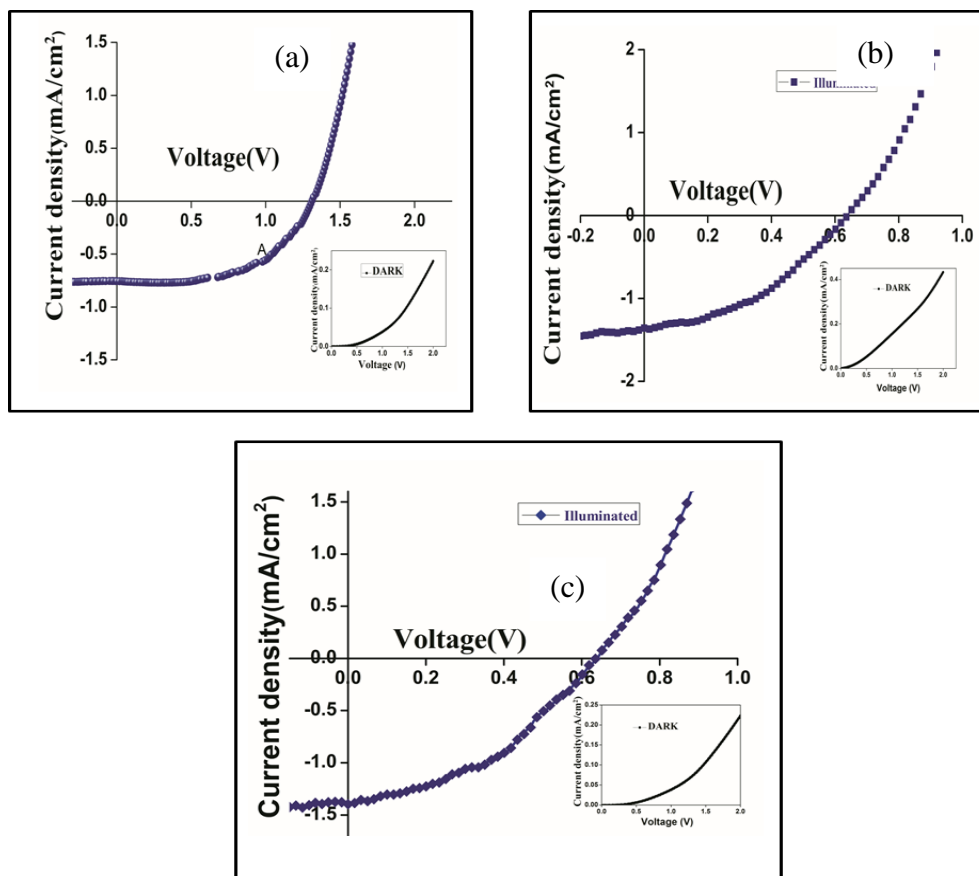

Figure 5.16: J–V characteristics of bulk-heterojunction for different MD-FL-PPV: PCBM ratios at 100 mW/cm^2 illumination

Table 5.5: Photovoltaic parameters of the devices for different MD-FL-PPV: PCBM ratios

MD-FL-PPV:PCBM ratio	V_{oc} (mV)	J_{sc} (mA/cm^2)	FF (%)	Efficiency (%)
1:0.5	1362	0.59	75	0.60
1:1	644	1.35	42	0.36
1:1.5	633	1.42	41	0.37

It was clear that, on increasing the PCBM content, short circuit current density (J_{sc}) was increased; it might be due to an increase in photogenerated carriers and the formation of PCBM rich domains, facilitating electron transport to the cathode. At the same time, the open circuit voltage (V_{oc}) showed a continuous decrease with increase in PCBM content and it could be due to the generation of shunts as a result of the increase in electron pathways between the two electrodes with increase in PCBM concentration.[66] Generally, at low amount of PCBM, poor electron transport due to the formation of incomplete pathways to the electrode results, whereas, with high concentration of PCBM, poor hole transport because of the formation of isolated polymer phases results.[67] The balance of electron and hole ratio affect the efficiency of solar cell performance. The fill factor is the key parameter which measures the balance between hole and electron transport in the active layer. The maximum fill factor (75%) was obtained for the ratio 1:0.5. The most favourable donor to acceptor ratio was found to be 1:0.5. The solar cell processed from chlorobenzene under illumination gave open circuit voltage of 1362 mV and short circuit current density (Jsc) of 0.59 mA/cm^2. The best device has an efficiency of 0.60 % and fill factor was 75% at an illumination of 100 mW/cm^2.

For MD-FL-PPV: PCBM blend in 1:1 ratio, the device exhibited a short circuit current density (J_{sc}) of 1.35 mA/cm^2 and an open circuit voltage (V_{oc}) of 644 mV. The fill factor (FF) and efficiency were calculated to be 42 % and 0.36 % respectively. The device showed a short circuit current density (J_{sc}) of 1.42 mA/cm^2, open circuit voltage (V_{oc}) of 633 mV and fill factor of 41% at the polymer: PCBM ratio of 1:1.5. The maximum power conversion efficiency achieved by this photovoltaic device was 0.37 %.

5.5 Conclusion

The third-order nonlinear optical properties of the synthesized π-conjugated polymers have been investigated by Z-scan technique. The nonlinear absorption coefficient (β), the third-order nonlinear susceptibility ($\chi^{(3)}$) and the optical limiting threshold of the polymers were determined in CHCl$_3$ solution using 7ns laser pulses at 532 nm. The polymers MD-CA-PPV, MD-FL-PPV, MD-PT-PPV and MD-AN-PPV showed normalised transmittance peak type graph with negative nonlinear absorption coefficient. The switch over from RSA to SA is due to the ground state band bleaching of polymers in chloroform solution. The other synthesized polymers, such as bithiophene and phenothiazine based polymers showed normalised transmittance valley type graph with positive nonlinear absorption coefficient. It was found that nonlinear absorption was due to effective two photon absorption process. The nonlinear absorption coefficient and the third-order nonlinear susceptibility of polymers were in the order of 10^{-10} m/W and 10^{-11} esu, respectively. Except PPV polymers, the other polymers showed superior optical power limiting behaviour due to donor-acceptor scheme at 532 nm. Hence the polymers examined seem to be promising

candidates for future optoelectronic and photonic applications. The photovoltaic performance of some of the polymers was evaluated by constructing conventional and inverted heterojunction device using polymer: PCBM blend as active layer. MD-CA-PPV: PCBM blend was used as active layer in both conventional and inverted solar cell. The conventional solar cell gave a power conversion efficiency of 0.04 % and inverted solar cell gave 0.43 % efficiency. The bilayer inverted solar cell constructed using MD-FL-PPV as active layer and gave a power conversion efficiency of 0.51 %. MD-FL-PPV: PCBM blend was used as active layer with varying ratio of PCBM to study the most favourable donor to acceptor ratio. The inverted solar cell was fabricated in the configuration ITO/ZnO/PL: PCBM/Ag. The maximum power conversion efficiency was obtained in the ratio 1:0.5 was 0.60 %. The device developed with both the structures, exhibited better photovoltaic performance for inverted architecture. The maximum fill factor was obtained for inverted structure which confirmed the quality of the inverted structure. A further improvement in the device can be achieved by optimizing the device parameters.

References

1.   M. Liu, Y. Gao, Y. Zhang, Z. Liu, L. Zhao, *Polym. Chem.,* 2017, **8**, 4613.

2.   S. Zhang, L. Ye, W. Zhao, B. Yang, Q. Wang, J. Hou, *Sci. China. Chem.,* 2015, **58**,.2

3.   J. Kim, C. E. Song, I. Kang, W. S. Shin, Z. G. Zhang, Y. Li, D. H. Hwang, *Bull. Korean Chem. Soc.,* 2014, **35,** 5.

4.   D. A. Mengistie, M. A. Ibrahem, P. C. Wang, C. W. Chu, *ACS Appl. Mater. Interfaces.,* 2014, **6,** 2292.

5. G. Marzano, C. V. Ciasca, F. Babudri, G. Bianchi, A. Pellegrino, R. Po, G. M. Farinola , *Eur. J. Org. Chem.,* 2014, **30**, 6583

6. T. T. Steckler, P. Henriksson, S. Mollinger, A. Lundin, A. Salleo, M. R. Andersson, *J. Am. Chem. Soc.,* 2014, **136**, 1190.

7. H. Luo, Z. Liu, D. Zhang, *Polym. J.*, 2018, **50**, 21.

8. D. Khlaifia, F. Massuyeau, C. P. Ewels, J. L. Duvail, E. Faulques, K. Alimi, *Chemistry Select.*, 2017, **2**, 10082.

9. T.Verbiest, A. Persoons, *Macromol. Symp.*, 1996, **102**,347.

10. E. Bundagaard, F. C. Krebs, *Sol. Energ. Mater. Sol. Cells.,* 2007, **91**, 954.

11. R. L. Sutherland, *Handbook of Nonlinear Optics*, 1st edition New York, Dekker, 1996.

12. W. Denk, J. H. Strickler, W. W. Webb, *Science,* 1990, **248**, 73

13. C. Xu, W. Zipfel, J. B .Shear, R. M. Williams, W. W. Webb, *Proc. Natl. Acad, Sci USA.,*1996, **93,**10763.

14. C. C. Corredor, Z. L. Huang, K. D. Belfield, A. R. Morales, M. V. Bondar, *Chem. Mater.,* 2007, **19,** 5165.

15. D. A. Parthenopoulos, P. M. Rentzepis, *Science,* 1989, **245,** 843.

16. C. Tang, Q. Zheng, H. Zhu, L. Wang, S. C. Chen, E. Ma, X. Chen, *J. Mater. Chem. C.,* 2013, **1**, 1771.

17. J. M. Hales, S. Zheng, S. Barlow, S. R. Marder, J. W. Perry, *J. Am. Chem. Soc.,* 2006, **128**, 11362.

18. R. Zieba, C. Desroches, F. Chaput, M. Carlsson, B. Eliasson, C. Lopes, M. Lindgren, S. Parola, *Adv. Funct. Mater.,* 2009, **19**, 235.

19. T. C. Lin, Y. F. Chen, C. L. Hu, C. S. Hsu, *J. Mater. Chem.,* 2009, **19**, 7075.

20. T. C. Lin, G. S. He, P. N. Prasad, L. S. Tan, *J. Mater. Chem.,* 2004, **14**, 982.

21. H.Y. Chen, J. H. Hou, S. Q. Zhang, Y. Liang, G. W. Yang, Y. Yang, L. P. Yu, Y. Wu, G. Li, *Nat. Photonics* 2009, **3**, 649.

22. G. Yu, J. Gao, J. C. Hummelen, F. Wudl, A. Heeger, *Science* 1995, **270**, 1789.

23. W. H. Lee, S. K. Lee, W. S. Shin, S. J. Moon, M. J. Park, S. H. Lee, *Sol. Energ. Mater. Sol. Cells,* 2014, **122**, 190.

24. R. R. Sondergaard, M. Hosel, F. C. Krebs, *J. Polym. Sci. Part B. Polym. Phys.,* 2013, **51**, 16.

25. P.A. Franken, A. E. Hill, C. W. Peters, G. Weinreich, *Phys. Rev. Lett.,* 1961, **7**, 118.

26. K. Rottwitt, P. T. Lichtenberg, *Nonlinear Optics Part A: Basic Principles and Materials*, CRC Press, 2014.

27. R. L. Sutherland, *Hand book of Nonlinear Optics*, 2nd edition, Marcel Dekker Inc, 2003.

28. M. S. Bahae, A. A. Said, E. W. Van Stryland, *Opt. Lett.,* 1989, **14,** 955.

29. M. S. Bahae, A. A. Said, T. H. Wei, D. J. Hagan, E. W. Van Stryland, *IEEE. J. Quantum Elect.,* 1990, **26**, 760.

30. J. Wang, M. S. Bahae, A. A. Said, D. J. Hagen, E. W. V. Stryland, *J. Opt. Soc. Am. B.,*1994, **11**, 1009.

31. A. A. Said, M. S. Bahae, D. J. Hagan, T. H. Wei, J. Wang, J. Young, E. W. V. Stryland, *J. Opt. Soc. Am. B*., 1992, **9,** 405.

32. S. Mathew, A. D. Saran, S. A. Joseph, B. S. Bhardwaj, D. Punj, P. Radhakrishnan, V. P. N. Nampoori, C. P. G. Vallabhan, J. R. Bellare, *J. Mater Sci: Mater Electron*, 2012, **23**, 739.

33. V. Kumari,V. Kumar, B. P. Malik, R. M. Mehra, D. Mohan, *Opt. Commun.,* 2012, **285**, 2182.

34. M. J. Soileau, W. E. Williams, E. W. V. Stryland, *IEEE J. Quant. Electron.,* 1983, **19,** 731.

35. G. S. He, G. C. Xu, P. N. Prasad, B. A. Reinhardt, J. C. Bhatt, A. G. Dillard, *Opt. Lett.*, 1995, **20**, 35.

36. N. K. M. N. Srinivas, S. V. Rao, D. N. Rao, *J. Opt. Soc. Am. B,* 2003, **20**, 2470.

37. N. K. M. N. Srinivas, S. V. Rao, D. N. Rao, B. K. Kimball, M. Nakahima, B. S. Decristofano, D. Narayanan Rao, *J. Porphyr. Phthalocyanines*, 2001, **5**, 549.

38. H. Spanggaard, F. C. Krebs, *Sol. Energy. Mater. Sol. Cells,* 2004, **83**, 125.

39. M. Kim, *Understanding Organic Photovoltaic Cells: Electrode. Nanostructure, Reliability, and Performance*, Ph. D Thesis, 2009.

40. N. S. Sariciftci, L. Smilowitz, A. J. Heeger, F. Wudl, *Science*, 1992, **258**, 1474.

41. S. Gunes, H. S. Neugebauer, N. S. Sariciftci, *Chem. Rev.,* 2007, **107,** 1324.

42. K.Coakley, M. D. McGehee, *Chem. Mater.,* 2004, **16**, 4533.

43. X. He, S. Mukherjee, S. Watkins, M. Chen, T. Qin, L. Thomsen, H. Ade, and C. R. McNeill, *J. Phys. Chem. C.,* 2014, **118**, 9918.

44   S. E. Shaheen, R. Radspinner, N. Peyghambarian, G. E. Jabbour, *Appl. Phys. Lett.,* 2001, **79**, 2996.

45. J. J. M. Halls, C. A. Walsh, N. C. Greenham, E. A. Marseglia, R. H. Friend, S. C. Moratti, A. B. Holmes, *Nature,*1995, **376**, 498.

46. C. J. Brabec, N. S. Sariciftci, J. C. Hummelen, *Adv. Funct. Mater.,* 2011, **11**, 15

47. M. Kaushik, B. Kaushik. *Int. J. Eng. Sci.*, 2013, **7,** 64742.

48. H. L. Yip, A. K. Y. Jen, *Energy Environ. Sci.,*2012, **5,** 5994.

49. L. M. Chen, Z. Hong, G. Li, Y. Yang, *Adv. Mater.,* 2009, **21**, 1434.

50. Y. Long, *Appl. Phy. Lett.,* 2009, **95**, 193301

51. T. W. Ng, M. F. Lo, Z. T. Liu, F. L. Wong, S. L. Lai, M. K. Fung, C. S. Lee, S. T. Lee, *J. Appl. Phys.,* 2009, **106,**114501

52. M.O. Reese, M.S. White, G. Rumbles, D.S. Ginley, S.E. Shaheen, *Appl. Phys. Lett.,*2008*,* **92,** 053307.

53. M. T. Llyod, D. C. Olson, P. Lu, E. Fang, D.L. Moore, M.S. White, M.O. Reese, D. S. Ginley, J. W. P. Hsu, *J. Mater. Chem.,*2009, **19**, 7638.

54. Y. Tao, D. Yang, X. Zhu, L. Zhou, J. Zhang, G. Tu, C. Li, *RSC Adv.,* 2014, **4**, 50988.

55.	C. P. Chen, Y. D. Chen, S. C. Chuang, C. P. Chen, Y.D. Chen, S.C. Chuang, *Adv. Mater.,* 2011, **23,** 3859.

56.	G. Li, C. W. Chu, V. Shrotriya, J. Huang, Y. Yang. *Appl. Phys. Lett.,* 2006, **93**, 221107.

57.	C. Waldauf, M. Morana, P. Denk, P. Schilinsky, K. Coakley, S. A. Choulis, C. Brabec, *J. Appl. Phys. Lett.,* 2006, **89**, 233517.

58.	S.K. Hau, H.L. Yip, H. Ma, A.K.Y. Jen, *Appl. Phys. Lett.,* 2008, **93**, 233304.

59.	T. Shirakawa, T. Umeda, Y. Hhashimoto, A. Fujii, K. Yoshino, *J. Phys. D.,*2004, **37**, 847.

60.	N. Sungho, J. Seo, S. Woo, W. H. Kim, H. Kim, D. D. C. Bradley, Y. Kimb, *Nat Commun.,* 2015, **6**, 8929.

61.	H. Hoppe, N. S. Sariciftci, *J. Mater. Chem.,* 2004, **19**, 1924.

62.	C. J. Brabec, A. Cravino, D. Messiner, N. S. Sariciftci, T. Fromhertz, M. Minse, L. Sanchez, J. C. Hummelen, *Adv. Funct. Mater.,* 2001, **11**, 374.

63.	A. Thankappan, S. Thomas, V. P. N. Nampoori, *Opt. Laser. Technol.,* 2014, **58**, 63.

64.	M. Zhang,G. Hu,G. Hu, R. C. Howe, L.Chen, Z. Zheng,T. Hasan, *Sci. Rep.,* 2015,**14,** 17482.

65.	K. W. Wong, H. L. Yip, Y. Luo, K. Y. Wong, W. M. Lau, K. H. Low, H. F. Chow, Z. Q. Gao, W. L. Yeung, C. C. Chang, *Appl. Phys. Lett.,* 2002, **80,** 2788.

66.	M. P. De Jong, L. J. Van zendoorn, M. J. A. de Voigt, *Appl. Phys. Lett.,* 2000, 77, 2255.

67.	M. R. Rajesh Menon, M. V. Maheshkumar, K. Sreekumar, C. Sudha Kartha, K. P. Vijayakumar, *Photovoltaic Specialists Conference*, 38th IEEE, Austin, Texas, USA, 2012.

Chapter 6

SUMMARY

The present thesis has outlined the synthesis of theoretically designed low band gap conjugated polymers using various synthetic strategies, which are suitable in optoelectronics. This chapter précises the major achievements in the overall research work done. Designed copolymers were synthesized via Gilch polymerization, Direct arylation and Suzuki coupling reactions. The nonlinear optical properties and the photovoltaic performance of the synthesized polymers were evaluated. Solvatochromic correlations were used to estimate the ground state (μ_g) and excited state (μ_e) dipole moments of some of the copolymers. Scope of the future work is also outlined here.

6.1 Summary of the work

The major target of the thesis was to design and synthesize conjugated polymers for optoelectronic applications. To develop D-A low band gap copolymers, computational design combined with chemical intuition was used to predict the electronic properties of the polymers. An attempt was

made to obtain the D-A copolymer with desired properties by varying the donor-acceptor combinations through the conjugated backbone. In the present study, eleven low band gap conjugated copolymers were designed and synthesized. A DFT calculation prior to synthesis is a simple and economic way to screen out the less effective materials before synthesis. Monomers and oligomer units were optimized using DFT/B3LYP/6-31G formalism. This calculation was extended to determine the band gap, oscillator strength, vertical excitation energies using Time Dependent Density Functional Theory (TD-DFT). The band gap and energy levels of the conjugated copolymers were calculated by applying PBC/DFT methods. The designed conjugated copolymers were synthesized using various synthetic methods like Gilch polymerization, direct arylation and Suzuki coupling reaction. The synthesized copolymers were characterized by different spectroscopic and analytical techniques. The electrochemical behavior of the polymers were measured using Cyclic voltammetry and the HOMO and LUMO energy levels were measured according to the equation proposed by Bredas. From the onset absorption of the polymers, the optical band gap of the polymers were determined using Tauc's equation. The optical and electrochemical band gap supported the theoretical prediction. There was significant difference between the electrochemical band gap and the theoretical and optical band gaps. Possible explanations were provided in the respective chapters.

Table 6.1: Theoretical and experimental band gap of copolymers

Polymer	E_g (theoretical) eV	E_g (Electrochemical) eV	E_g (Optical) eV
MD-CA-PPV	1.98	1.50	1.96
MD-FL-PPV	2.07	1.44	2.03
MD-PT-PPV	2.31	1.22	2.01
MD-AN-PPV	1.99	1.04	1.98
P(BT-PH)	2.52	1.55	2.09
P(BT-CZ)	2.68	1.87	2.14
P(BT-FLN)	2.48	1.25	2.12
P(BT-ANT)	2.94	1.36	2.15
P(BT-TPA)	2.24	1.50	2.11
P(PHENO-TPA)	2.51	1.63	2.15
P(PHENO-MeTH)	2.67	1.68	2.06

The electrochemical band gaps were not in good agreement with the optical band gap as well as the theoretically predicted band gap. The theoretical band gaps were actually obtained for the isolated gas phase chains and the difference in the mechanism of optical excitation and electrochemical oxidation/reduction processes in the system under study has led to this mismatch.

The third-order optical nonlinearity of the copolymers was measured using Z-scan technique, which was distinguished for its simplicity and sensitivity. The open aperture Z-scan plot of PPV based copolymers showed saturable absorption type graph with negative nonlinear absorption coefficient. Bithiophene and phenothiazine based Donor-Acceptor copolymers showed reverse saturable absorption type graph with positive

nonlinear absorption coefficient. The OA traces of the copolymers fitted well with the plot derived from the two photon absorption (TPA) theory. Nonlinear absorption coefficient (β, m/W) and imaginary value of third-order nonlinear susceptibility (Im $\chi^{(3)}$) (esu) of the synthesized polymers were calculated and are given in table 6.2.

Table 6.2: Nonlinear absorption coefficient (β), imaginary value of third-order nonlinear susceptibility (Im $\chi^{(3)}$) and optical limiting threshold of copolymers

Polymer	β 10^{-10} (m/W)	Im $\chi^{(3)}$ 10^{-11} (esu)	Optical limiting threshold (GW/cm^2)
MD-CA-PPV	-0.17×10^{-10}	-0.03×10^{-11}	-
MD-FL-PPV	-2.06×10^{-10}	-0.45×10^{-11}	-
MD-PT-PPV	-0.63×10^{-10}	-0.14×10^{-11}	-
MD-AN-PPV	-2.83×10^{-10}	-0.59×10^{-11}	-
P(BT-PH)	3.85×10^{-10}	0.81×10^{-11}	0.26
P(BT-CZ)	2.87×10^{-10}	0.62×10^{-11}	0.21
P(BT-FLN)	2.99×10^{-10}	0.67×10^{-11}	0.23
P(BT-TPA)	3.10×10^{-10}	0.69×10^{-11}	0.49
P(PHENO-TPA)	3.64×10^{-10}	0.79×10^{-11}	0.32
P(PHENO-MeTH)	3.01×10^{-10}	0.64×10^{-11}	0.60

The third-order nonlinear absorption coefficient (β) and the imaginary part of third-order nonlinear susceptibility parameter (Im $\chi^{(3)}$) were found to be in the order of 10^{-10} (m/W) and 10^{-11} (esu), which meant that the polymers exhibited strong optical nonlinearity due to donor-π-acceptor scheme. In D-A copolymers, the intramolecular charge transfer from donor to acceptor units and delocalization of π electrons resulted in optical

nonlinearity and could be used as ideal candidates in nonlinear optical applications. Except PPV copolymers, all the other polymers showed superior optical limiting property at 532 nm wavelength due to two photon absorption (TPA) process.

The solvent effect and the change in dipole moments of the fluorescent copolymers in toluene / acetonitrile mixtures of varying polarity were investigated. Using the theory of solvatochromism, the difference in the excited state (μ_e) and ground state (μ_g) dipole moments were determined from Bakhshiev and Kawski–Chamma–Viallet equations for MD-CA-PPV, MD-FL-PPV, MD-PT-PPV, MD-AN-PPV and P(BT-CZ). These equations are based on the variation of Stokes shift with solvent's relative permittivity and refractive index. Further, the change in dipole moment value ($\Delta\mu$) was also calculated using the variation of Stokes shift with the molecular microscopic empirical solvent polarity parameter (E_T^N). The Onsager cavity radius, ground and excited state dipole moment values of some of the copolymers are summarized in Table 6.3.

It is clear from the table that all the polymers possessed higher dipole moment values in the excited state than in the ground-state i.e., excited state was more polarized than the ground state, and, therefore, was more sensitive to solvent effects. The reason for the discrepancy in the results of $\Delta\mu$ values is mainly due to the various assumptions and simplifications made in the evolution of the solvatochromic methods.

Table 6.3: Cavity radius, Ground and excited state dipole moments of (a) MD-CA-PPV, (b) MD-FL-PPV, (c) MD-PT-PPV, (d) MD-AN-PPV and (e) P(BT-CZ) in toluene/acetonitrile mixtures of varying polarity

Polymer	a^1 (Å)	$\mu_g{}^2$ (D)	$\mu_e{}^3$ (D)	$\Delta\mu^4$ (D)	$\Delta\mu^5$ (D)
MD-CA-PPV	6.8	4.7	17.9	13.2	8.83
MD-FL-PPV	6.78	15	26.5	11.5	5.72
MD-PT-PPV	6.40	37.9	41.8	3.9	2.19
MD-AN-PPV	6.27	13.5	18.2	4.7	5.92
P(BT-CZ)	6.13	7.02	13.36	6.34	4.44

[1]Calulated from equation 2.9
[2]The ground state dipole moment calculated using Eq. 2.10.
[3]The excited state dipole moment calculated from Eq. 2.11.
[4] The change in dipole moment for μ_g and μ_e
[5]The change in dipole moment calculated from Eq. 2.15.

Photovoltaic performances of some of the copolymers were evaluated by fabricating both conventional and inverted bulk heterojunction solar cells and inverted bilayer heterojunction solar cells. The conventional solar cell was constructed using polymer: PCBM blend in 1:1 ratio as active layer and the cell configuration adopted was ITO/MoO$_3$/MD-CA-PPV:PCBM/LiF/Al. The maximum power conversion efficiency was obtained to be 0.04 %. Inverted solar cell constructed in the configuration ITO/ZnO/polymer: PCBM/Ag using MD-CA-PPV:PCBM blend in 1:1 ratio was used as photoactive layer and gave a power conversion efficiency of 0.43 %. ITO/ZnO/MD-FL-PPV: PCBM/Ag inverted bulk heterojunction device was fabricated using varying amount of PCBM and the effect of donor to acceptor ratio on the performance of the device was studied. The most favorable donor to acceptor ratio was found to be 1:0.5 which gave a power conversion efficiency of 0.60 %. Bilayer heterojunction device with

device structure ITO/ZnO/MD-FL-PPV/Ag was fabricated, which gave a power conversion efficiency of 0.51 %.

Table 6.4: Photovoltaic performances of synthesized polymers

Device configuration	V_{oc} (mV)	J_{sc} (mA/cm^2)	FF (%)	Efficiency (%)
MD-AN-PPV in chlorobenzene ITO/MoO$_3$/PL:PCBM/LiF/Al	564	0.57	21	0.007
MD-CA-PPV in chlorobenzene ITO/MoO$_3$/PL:PCBM/LiF/Al	832	0.20	24	0.04
MD-CA-PPV in chlorobenzene ITO/ZnO/PL:PCBM/Ag	1030	0.77	54	0.43
MD-FL-PPV in chlorobenzene ITO/ZnO/PL/Ag	1194	0.86	50	0.51
MD-FL-PPV in chlorobenzene ITO/ZnO/PL:PCBM/Ag (Ratio 1:0.5)	1362	0.59	75	0.60
MD-FL-PPV in chlorobenzene ITO/ZnO/PL:PCBM/Ag (Ratio 1:1)	644	1.35	42	0.36
MD-FL-PPV in chlorobenzene ITO/ZnO/PL:PCBM/Ag (Ratio 1:1.5)	633	1.42	41	0.37

6.2 Major Achievements

- Designed and synthesized eleven conjugated copolymers for photovoltaic and NLO applications.

- The change in the dipole moment ($\Delta\mu$) was calculated both from solvatochromic shift method and on the basis of microscopic empirical solvent polarity parameter (E_T^N) and values are compared.

- The synthesised copolymers showed strong third-order optical nonlinearity.

- The D-A copolymers presented good optical power limiting behaviour at 532 nm.

- Photovoltaic performances of the copolymers were confirmed by constructing both conventional and inverted organic solar cell using some of the polymers in different cell configurations.

- Inverted bulk heterojunction solar cell constructed using MD-FL-PPV:PCBM in 1:0.5 ratio as active layer with a device structure ITO/ZnO/ MD-FL-PPV:PCBM/Ag processed from chlorobenzene gave a maximum power conversion efficiency of 0.60 %.

6.3 Future Outlook

Out of the eleven polymers synthesized, only three polymers were used to study photovoltaic activity to measure the suitability in organic solar cell device. Other polymers could be subjected to more detailed studies to explore the suitability of these copolymers in optoelectronic device applications.

▌▌▌ List of Publications ▌▌▌

[1] **Sowmya Xavier** and K. Sreekumar, *Solvatochromic studies of newly synthesized PPV based copolymer PME-FL via Gilch Polymerisation route.* ISBN No: 978-81-930558-1-6, 2015.

[2] **Sowmya Xavier** and K. Sreekumar, *Synthesis and Characterisation of PPV Based Copolymer PME-PH via Glich Polymerisation Route.* ISBN No: 978-93-80095-738, 2016.

[3] **Sowmya Xavier** and K. Sreekumar, *Synthesis and Solvatochromic Properties of Poly (p-phenylene vinylene) Based Co-polymers: PMECA, PMEPH and PMEAN.* ISBN No: 978-81-930558-2-3, 2017.

[4] Sona Narayanan, Anshad Abbas, Anjali C.P., **Sowmya Xavier**, C. Sudha Kartha, K. S. Devaky, K. Sreekumar, Rani Joseph, *Low Band Gap Donor-Acceptor Phenothiazine Copolymer with Triazine Segment: Design, Synthesis and Application for Optical Limiting Devices,* Journal of Luminescence. (In press)

[5] **Sowmya Xavier,** R. Geethu, Sona Narayanan, K. P. Vijayakumar and K. Sreekumar, *Theoretical Design and Third-Order Nonlinear Optical Properties of Four Newly Synthesized PPV Derivatives and their Applications in Photovoltaic Devices,* Polymers for Advanced Technologies (Under Review)

Papers presented in conferences

[1] **Sowmya Xavier,** C.P Anjali and K. Sreekumar, *Third Order Nonlinear Optical Properties of Newly Synthesized PPV Based Copolymer Via Gilch Polymerisation Route, "* in the National Conference on Recent Trends in Bio-inorganic & Organometallic Chemistry (NCBOC- 2015) held at SSIET, Coimbatore, 2015.

[2] **Sowmya Xavier** and K. Sreekumar, *Design And Synthesis Of A Low Band Gap Conjugated Copolymer 3,4- Ethylenedioxy Thiophene / Phenothiazine For Bulk Heterojunctions Photovoltaic Cell*, in the International Conference on Advances in Applied Mathematics, Materials Science and Nanotechnology for Engineering and Industrial Applications (ICMMN 2K16) held at FISAT, Angamaly , Kerala, 2016.

[3] **Sowmya Xavier** and K. Sreekumar, *Synthesis and solvatochromic properties of poly(p-phenylene vinylene) based copolymer : PMEFL* in the National Conference on Current Trends in Chemistry (CTriC-2017) held at CUSAT, Kalamassery, Kerala, 2017.

****